





# **DEVELOPMENT AND OPTIMISATION OF ADHESION MECHANISMS BETWEEN RUBBER AND THERMOPLASTIC MATERIALS FOR 2K INJECTION MOULDING**

Brittany LAING

Supervisor:

Prof. dr. ir. A. Van Bael

Co-supervisors:

Prof. dr. ir. J. De Keyzer

Prof. dr. ir. D. Seveno

Members of the Examination Committee:

Prof. dr. G. Langie, chair

Prof. dr. B. Goderis, assessor

Dr. K. Metten (Hercorub NV.), assessor

Prof. dr. A. Ginzburg, secretary

Prof. dr. ing. T. Lucyshyn (Montanuniversität Leoben)

Dissertation presented in  
partial fulfilment of the  
requirements for the  
degree of Doctor of  
Engineering Technology (PhD)

November 2021

© 2021 KU LEUVEN, Faculty of Engineering Technology  
Uitgegeven in eigen beheer, BRITTANY LAING, DIEPENBEEK

Alle rechten voorbehouden. Niets uit deze uitgave mag worden vermenigvuldigd en/of openbaar gemaakt worden door middel van druk, fotokopie, microfilm, elektronisch of op welke andere wijze ook zonder voorafgaandelijke schriftelijke toestemming van de uitgever.

All rights reserved. No part of the publication may be reproduced in any form by print, photoprint, microfilm, electronic or any other means without written permission from the publisher.

---

# Voorwoord

---

*“Be brave, be curious, be determined, overcome the odds. It can be done”*

-Stephen Hawking, Brief Answers to the Big Questions

Iedere uitdaging die je start lijkt initieel onmogelijk. Echter dankzij doorzettingsvermogen, vastberadenheid en steun is de finish vaak sneller in zicht dan je je voor mogelijk achtte. Zo is mijn doctoraat en bijbehorende thesis een nieuwe mijlpaal die ik hier met trots aan u voorstel. Graag zou ik dan ook de mensen rondom mij willen bedanken om dit mee mogelijk te maken.

Eerst en vooral betreft dit mijn promotor prof. dr. ir. Jozefien De Keyzer. Zij was mijn go-to persoon op professioneel en persoonlijk vlak. Onze gesprekken tilde mijn onderzoek tot een hoger niveau en het zorgde ervoor dat ik zelfzekerder werd als persoon en onderzoeker. Daarnaast wil ik promotoren prof. dr. ir. Albert Van Bael en prof. dr. ir. David Seveno bedanken voor hun input, advies, begeleiding en interessante gesprekken. Dit verbeterde mijn kritisch vermogen en zorgde vaak voor nieuwe inzichten. Bovendien zou mijn doctoraat niet mogelijk geweest zijn zonder de ondersteuning van dr. Kris Metten van Hercorub N.V. betreffende de rubbercomposities. Graag bedank ik hem en prof. dr. Bart Goderis voor hun bijdrage als assessor in mijn begeleidingscommissie. Mijn dank gaat ook uit naar prof. dr. Greet Langie, prof. dr. Anton Ginzburg en prof. dr. Ing. Thomas Lucyshyn om te zetelen in mijn examencommissie en voor het evalueren van mijn proefschrift.

Als doctoraatsonderzoeker van ‘Cel Kunststoffen’ werd ik omringd door collega’s met een achtergrond in elektromechanica, materiaalkunde en chemie. Dit zorgde voor een zeer rijke omgeving die ook steeds evolueerde. Ik wil hen allemaal bedanken voor de leuke interacties en samenwerking. Aangezien mijn onderzoek voortvloeide uit een voorafgaand doctoraat, wil ik specifiek Gert-Jan bedanken om mij initieel op gang te helpen en voor het overbrengen van zijn kennis.

Dit onderzoek zou uiteraard niet mogelijk geweest zijn zonder financiële steun. Graag bedank ik het Fonds Wetenschappelijk Onderzoek voor het toekennen van mijn SB PhD Fellowship (1SB0319N, 1SB0321N). Daarnaast wil ik Hercorub N.V. bedanken voor het voorzien van alle rubbermaterialen. Ook kon ik beroep doen op een deel hulpvolle onderzoekers zoals Bernard Nysten (UCL) voor AFM metingen, Tom Van der Donck en Sofie Sannen (Kaneka) voor SEM-EDX, Imran Aslam voor Raman spectroscopie, Nahn Vo voor Confocale microscopie, en Leen Thomassen omtrent de interfase reactiemechanismen.

Uiteindelijk zijn we dan aangekomen bij de belangrijkste personen uit mijn leven, mijn familie en partner Jo. Mijn ouders, broer en zus zijn al heel mijn leven mijn grootste supporters en ze stimuleerden mij steeds om het beste uit mijzelf te halen. Daarnaast is Jo mijn eeuwige steun en toeverlaat, mijn thuis. Afgelopen jaren stonden niet enkel in teken van mijn doctoraat maar ook in teken van de bouw van ons huis in Riemst. Onze dagen bestonden hoofdzakelijk uit werken en bouwwerken. Dit heeft bloed, zweet en tranen gekost maar uiteindelijk valt nu alles in zijn plooi met onze recente verhuizing naar

onze nieuwbouw en het afronden van mijn doctoraat. Nu is het tijd om te genieten van al ons hard werk.

---

## Abstract

---

Successful two-component (2K) injection moulding of multi-material products requires an efficient production process and an optimal material combination. Specifically for thermoset rubbers with thermoplastics, this is challenging as during injection moulding these materials have opposite temperature requirements. Therefore, a novel process with a mould containing thermally separated heat cavities was developed by Bex et al. [1]. Available research mainly concerned process optimisation aspects, but little research has focused on material optimisation in such two-component injection moulding. Furthermore, knowledge concerning the adhesion mechanism is scarce. Therefore, a study of the influence of material composition and the accompanying adhesion mechanisms was deemed necessary to optimise the process and to improve the economic feasibility.

Ethylene-propylene-diene rubber (EPDM) adhered to thermoplastics is ideal for two-component sealing applications thanks to its resistance to compression, chemical environment and high temperatures. Therefore, the EPDM composition was studied to enhance the adhesion with thermoplastics. The rubber curing system appears to enable adhesion mechanism like interdiffusion and/or co-vulcanisation. The most efficient curing system composition is found to depend on the rubber-thermoplastic material combination. Furthermore, adhesion benefits from a rubber molecular structure with high accessibility to reaction sites and a high number of rubber monomer units which are also present in the molecular structure of the thermoplastic. The adhesion can be improved as well with higher contents of paraffinic oil enhancing mobility of molecular chains at the interface. The choice of filler mainly depends on the desired rubber product properties.

Adhesion between a thermoset rubber and a thermoplastic is a complex phenomenon consisting of multiple adhesion mechanisms induced during the injection moulding process. For adhesion to occur at a polymer interface, intimate contact is a prerequisite. Therefore, a more sophisticated contact angle methodology, closer-to-processing-conditions, is presented to evaluate wettability. The developed technique indicated that wetting does not directly control the amount of adhesion, possibly due to the high pressures used during 2K injection moulding forcing contact between the rubber and thermoplastic. Furthermore, the occurrence of co-vulcanisation can be predicted with a newly developed reactive wetting methodology. During co-vulcanisation several reactions may occur between the thermoplastic and EPDM. Therefore, possible chemical reaction mechanisms are clarified and discussed. Finally, interfacial characterisation suggests that the interdiffusion width is limited to maximum a few micrometres. Presumably, entanglements contribute highly to a strong adhesion.

Eventually, when formulating the rubber composition, adhesion needs to be optimised within product property requirements and minimal cycle time. Therefore, material selection guidelines in terms of radar charts are provided. Additionally, a detailed materials selection grade map is provided for EPDM with polypropylene as this material combination has the highest industrial relevance, e.g. sealing applications in electrical vehicles. This selection map was validated with an industrial case study emphasising the

required synergy between product properties and optimal adhesion. Furthermore, even though good adhesion complicates recyclability, end-of-life potential was found by recycling low concentrations of 2K granulates in thermoplastic vulcanisates.

---

## Samenvatting

---

Succesvol twee-component (2K) spuitgieten van kunststoffen vereist een efficiënte productie en een optimale materiaalcombinatie. Voor de combinatie van een thermohardend rubber met een thermoplast is dit uitdagend gezien het verschil in temperatuurvereisten tijdens de verwerking. Om dit op te lossen ontwikkelde Bex et al. [1] een nieuw proces bestaande uit een matrijs met thermisch gescheiden vormholtes. Onderzoek omtrent twee-component spuitgieten is voornamelijk gefocust op procesoptimalisatie, maar diepgaand onderzoek naar de invloed van materiaalcomposities ontbreekt. Ook kennis over het hechtingsmechanisme tijdens dit proces ontbreekt nog in de wetenschappelijk literatuur. Daarom is een studie omtrent de invloed van de materiaalcompositie en bijbehorende hechtingsmechanismen nodig geacht om het proces te optimaliseren en om de economische haalbaarheid te verbeteren.

Hechting tussen ethyleen-propyleen-dieen rubber (EPDM) en een thermoplast is ideaal voor twee-component afdichtingstoepassingen dankzij de goede weerstand tegen compressie, een chemische omgeving en hoge temperatuur. Daarom werd de EPDM compositie onderzocht om de hechting met thermoplasten te verbeteren. Het rubbervulkanisatiesysteem maakt interdiffusie en/of co-vulkanisatie mogelijk en de efficiëntie van deze mechanismen is afhankelijk van de specifieke materiaalcombinatie. Daarbij vergemakkelijkt een rubberketenstructuur met toegankelijke bindingsplaatsen aan de interfase de hechting. Monomeerunits in rubber die ook aanwezig zijn in de ketenstructuur van de thermoplast verbeteren ook hechting, mogelijk door een betere compatibiliteit. Een toevoeging van olie als weekmaker verhoogt ook de ketenmobiliteit aan de interfase. De keuze in type vulstof blijkt dan weer voornamelijk af te hangen van de gewenste producteigenschappen.

Tijdens het twee-component spuitgieten is de hechting tussen rubbers en thermoplasten een complex fenomeen. Om een goede hechting te induceren is optimaal contact tussen beide materialen nodig. Daarom werd een geavanceerde contacthoektechniek onderzocht die beter de condities van het effectieve hechtingsproces nabootst. Deze techniek toonde aan dat de bevochtiging niet direct gerelateerd kan worden aan de hechtingssterkte. Tijdens het spuitgieten wordt contact tussen beide materialen namelijk gedwongen waardoor interdiffusie en/of co-vulkanisatie domineren. Om deze co-vulkanisatie aan te tonen werd een methodologie ontwikkeld waarbij een onderscheid gemaakt kon worden tussen reactieve en fysische bevochtiging. Tijdens de co-vulkanisatie kunnen verschillende chemische reacties plaatsvinden tussen EPDM en de thermoplast. Daarom werden de bijhorende chemische reacties verduidelijkt. Bovendien werd aan de hand van interfasekarakterisatietechnieken een interdiffusiezone gevonden van maximum enkele micrometers. Mogelijks dragen de ketenverstrengelingen dus erg bij tot een sterke adhesie.

Bij de hechtingsoptimalisatie moet een rubbercompositie gekozen worden binnen de productvereisten waarbij de cyclustijd minimaal is. Daarom werden materiaalselectierichtlijnen opgesteld. Voor EPDM met polypropyleen werd een gedetailleerdere selectiemap voorzien gezien de hoge industriële relevantie ervan, vb. voor afdichtingstoepassing in elektrische auto's. Een validatie bevestigde het belang van

een synergie tussen goede hechting en vereiste producteigenschappen. Bovendien is ondanks de goede hechting een recyclage mogelijk aan het einde van de levensduur door hergebruik in thermoplastische vulkanizaten.

---

# Contents

---

Voorwoord .....	I
Abstract .....	III
Samenvatting .....	V
Contents .....	VII
List of Symbols .....	XI
List of Figures.....	XV
List of Tables .....	XXI
<b>Chapter 1 Introduction.....</b>	<b>1</b>
1.1 Motivation and problem statement .....	1
1.2 Objectives.....	2
1.3 Thesis outline.....	3
<b>Chapter 2 Rubber-thermoplastic adhesion: state of the art.....</b>	<b>5</b>
2.1 Introduction.....	5
2.2 Adhesion mechanisms .....	5
2.2.1 Fundamental adhesion theories .....	6
2.2.2 Adhesion failure mechanism .....	14
2.2.3 Surface and interface characterisation.....	15
2.3 Thermoset rubber composition and adhesion.....	21
2.3.1 EPDM composition.....	21
2.3.2 Crosslinking methods .....	25
2.3.3 Rubber characteristics.....	33
2.4 Adhesion in rubber-thermoplastic injection moulding .....	36
2.4.1 Process development.....	37
2.4.2 Process simulation.....	39
2.5 Conclusion .....	40
<b>Chapter 3 Optimisation of the EPDM curing system for adhesion with thermoplastics .....</b>	<b>41</b>
3.1 Introduction.....	41
3.2 Methodology.....	42
3.2.1 Thermoplastic grades.....	42
3.2.2 2K injection moulding: sample preparation.....	42
3.2.3 Cure characteristics.....	44
3.2.4 Crosslink density.....	44
3.2.5 Physico-mechanical properties .....	45
3.2.6 Compatibility measurements .....	45

3.2.7	Adhesion measurement .....	46
3.2.8	Statistics .....	47
3.3	Peroxide curing system .....	47
3.3.1	Co-agent type and concentration.....	47
3.3.2	Dicumylperoxide concentration.....	58
3.4	Sulphur curing system.....	66
3.4.1	Materials and processing .....	66
3.4.2	Results and discussion .....	67
3.5	Conclusion .....	71
<b>Chapter 4 Optimisation of the EPDM composition for adhesion with thermoplastics .....</b>		<b>75</b>
4.1	Introduction.....	75
4.2	EPDM macromolecular structure.....	75
4.2.1	Materials and methods.....	76
4.2.2	Results and discussion .....	79
4.3	Additives: fillers and plasticisers.....	89
4.3.1	Materials and methods.....	89
4.3.2	Results and discussion .....	94
4.4	Conclusion .....	102
<b>Chapter 5 Adhesion mechanism analysis .....</b>		<b>103</b>
5.1	Introduction.....	103
5.2	Wetting.....	103
5.2.1	Drop and surface analysis: set-up .....	104
5.2.2	Thermoplastic melt properties .....	105
5.2.3	Wetting of thermoplastic melt on rubber substrate .....	108
5.2.4	Relation between adhesion percentage and work of adhesion.....	111
5.3	Chemical bonding.....	112
5.3.1	EPDM-Thermoplastic co-vulcanisation: reaction mechanism.....	112
5.3.2	Prediction of EPDM-thermoplastic co-vulcanisation.....	115
5.4	Interdiffusion.....	123
5.4.1	Rubber-thermoplastic immersion in cyclohexane .....	123
5.4.2	Material interaction.....	125
5.4.3	SEM-EDX.....	128
5.4.4	Nano-mechanical analysis by AFM.....	130
5.5	Conclusion .....	133
<b>Chapter 6 Material selection guidelines, case-study and end-of-life.....</b>		<b>135</b>
6.1	Introduction.....	135
6.2	Material selection guidelines.....	135
6.2.1	EPDM – PP.....	136
6.2.2	EPDM – PE.....	139
6.2.3	EPDM – polar thermoplastics .....	141
6.2.4	Material selection map .....	142
6.3	Economic evaluation.....	145
6.3.1	Product cost optimisation: Thermoplastic-rubber 2K seal.....	145
6.3.2	Industrial relevance of 2K injection moulding of PP with EPDM .....	148

6.4	Case study: EPDM-PP 2K automotive sealing applications .....	149
6.4.1	Materials and methods .....	151
6.4.2	Results and discussion .....	155
6.5	End-of-life of PP-EPDM 2K products .....	158
6.5.1	Methodology.....	159
6.5.2	Results and discussion .....	161
<b>Chapter 7</b>	<b>Conclusions and outlook .....</b>	<b>167</b>
7.1	Introduction.....	167
7.2	Conclusions.....	167
7.3	Outlook.....	169
<b>Appendix A</b> .....		<b>171</b>
<b>Bibliography</b> .....		<b>179</b>
<b>List of Publications</b> .....		<b>189</b>
<b>Curriculum Vitae</b> .....		<b>191</b>



---

## List of Symbols

---

### Arabic symbols

<i>Symbol</i>	<i>Description</i>	<i>Unit</i>
a	Molecular aggregation number	-
B	Dimensionless constant equal to 277	-
$d_{\infty}$	Interface thickness	Mm
$D_n$	Needle diameter	mm
$E_{\text{coh}}$	Cohesive energy	J/mol
F	Force	N
$F_t, F_p$	Total and polar molar attraction function	$(\text{J cm}^3)^{1/2}/\text{mol}$
G	Fracture energy	N/mm
$G_m$	Gibbs free energy of mixing	J/mol
$h_c$	Specific enthalpy of fusion	J/g
$H_m$	Enthalpy of mixing	J/mol
$H_{\text{vap}}$	Enthalpy of vaporisation	J/mol
M	Molmass	g/mol
$m_0$	Dried weight after swelling	g
$m_{\text{max}}$	Equilibrium swelling weight	g
$M_w$	Molecular weight	g/mol
$M_{w,c}$	Critical entanglement molecular weight	g/mol
n	Number of repeating units per polymer chain segment	-
P	Peel force per unit width	N/mm
R	Gas constant	J/K mol
$R_1$ and $R_2$	Principle radii of curvature	mm
$R_a$	Average roughness	$\mu\text{m}$
S	Spreading coefficient	$\text{mJ}/\text{m}^2$
$S'$	Torque	dNm
$S_m$	Entropy of mixing	J/K mol
T	Absolute temperature	K
t	Time	s
$t_{10}, t_{90}$	Time at vulcanisation degree of 10% and 90%	Min
$T_b$	Boiling temperature	K
$T_c$	Crystallisation peak temperature	$^{\circ}\text{C}$

---

<i>Symbol</i>	<i>Description</i>	<i>Unit</i>
$T_{co}$	Onset crystallisation temperature	$^{\circ}C$
$T_{cr}$	Critical temperature	K
$T_g$	Glass transition temperature	$^{\circ}C$
$T_m$	Melting peak temperature	$^{\circ}C$
$T_{mo}$	Onset melting temperature	$^{\circ}C$
$ts_1, ts_2$	Scorch time at a torque increase of 1 dNm or 2 dNm	min
$v_0$	Reference volume	$cm^3/mol$
$V_d$	Droplet volume	$\mu l$
$v_m$	Molar volume	$cm^3/mol$
$V_r$	Volume fraction of rubber in the equilibrium swollen vulcanised sample	-
$V_s$	Molar volume of the swelling solvent	$ml/mol$
$W_0$	Worthington number	-
$W_a$	Work of adhesion	$J/m^2$
$x$	Weight percentage of polypropylene	-
$Y_1, Y_0$	Shear force conditioned and of control	N
$\Delta h_c$	Enthalpy of fusion of 100% crystalline polymer	$J/g$
$\Delta H_m$	Melting enthalpy	$J/g$
$\Delta P$	Laplace pressure	Pa
$\Delta_T$	Lydersen correction for polymer non-ideality	-

### Greek symbols

<i>Symbol</i>	<i>Description</i>	<i>Unit</i>
$\rho_e$	Elastomer density	$g/cm^3$
$\rho_s$	Solvent density	$g/cm^3$
$\sigma_a$	Adhesion strength	MPa
$\sigma_t$	Total bulk strength	MPa
$\gamma^-$	Lifshitz-Van der Waals component	$J/m^2$
$\gamma^+$	Acid surface energy component	$J/m^2$
$\gamma_L$	Surface tension of the liquid	$J/m^2$
$\gamma^{LW}$	Base surface energy component	$J/m^2$
$\gamma_S$	Surface tension of the solid	$J/m^2$
$\gamma_{SL}$	Surface tension of the solid-liquid interface	$J/m^2$
$\delta_h$	Hydrogen solubility component	$MPa^{1/2}$
$\delta_d$	Dispersive solubility component	$MPa^{1/2}$
$\delta_p$	Polar solubility component	$MPa^{1/2}$

<i>Symbol</i>	<i>Description</i>	<i>Unit</i>
$\rho_d$	Density of drop phase	g/cm <sup>3</sup>
$\tau_R$	Reptation relaxation time	s
$\alpha$	Crystallinity	%
$\delta$	Solubility parameter	MPa <sup>1/2</sup>
$\theta$	Equilibrium contact angle	°
$\nu$	Crosslink density	mol/cm <sup>3</sup>
$\rho$	Density	g/cm <sup>3</sup>
$\Phi$	Volume fraction	-
$\chi$	Flory-Huggins interaction parameter	-
$\gamma$	Surface tension	J/m <sup>2</sup>

### Abbreviations

<i>Symbol</i>	<i>Description</i>	<i>Unit</i>
2K	Two-component	-
ABS	Acrylonitrile butadiene styrene	-
ACN	Acrylonitrile content	-
AFM	Atomic force microscopy	-
ATR-FTIR	Attenuated total reflectance Fourier transform infrared spectroscopy	-
BSE	Backscattered electrons	-
BET	Brunauer, Emmett and Teller theory for specific surface area	m <sup>2</sup> /g
C	Carbon	-
CED	Cohesive energy density	J/ml
CRI	Cure rate index	min <sup>-1</sup>
EDX	Energy Dispersive X-ray Spectroscopy	-
ENB	5-ethylidene-2-norbornene	-
EPDM	Ethylene propylene diene monomer rubber	-
HDPE	High-density polyethylene	-
HNBR	Hydrogenated acrylonitrile-butadiene rubber	-
LSR	Liquid silicone rubber	-
MAPP	Maleic anhydride-grafted polypropylene	-
MWD	Molecular weight distribution	-
PA	Polyamide	-
PC	Polycarbonate	-
PE	Polyethylene	-
PP	Polypropylene	-
PPE	Pol(oxy-2,6-dimethyl-1,4-phenylene)	-

<i>Symbol</i>	<i>Description</i>	<i>Unit</i>
PUR	Polyurethane	-
PVDF	Polyvinylidene fluoride	-
RFL	Resorcinol-formaldehyde-latex	-
SE	Secondary electrons	-
SEM	Secondary electron microscopy	-
TAIC	Triallyl isocyanurate	-
TMPT	Trimethylolpropane trimethacrylate	-
ToF-SIMS	Time-of-flight ion mass spectrometry	-
TPE	Thermoplastic elastomer	-
TPE-S	Styrene based thermoplastic elastomer	-
XPS	X-ray photoelectron spectroscopy	-

---

## List of Figures

---

Figure 1: Mechanism of mechanical interlocking between a liquid and a substrate.....	6
Figure 2: Schematic representation of the electrostatic theory.....	7
Figure 3: Intermolecular interactions at solid-liquid interface (a) profile of sessile drop on a planar solid surface (b).....	7
Figure 4: Interdiffusion mechanism between two polymers in contact.....	9
Figure 5: Chemical bonding at a polymer-polymer interface.....	12
Figure 6: Weak boundary layer theory according to Bikerman [31]. .....	13
Figure 7: Bond failure modes: cohesive failure (left) and adhesive failure (right) between polymer A and polymer B. ....	14
Figure 8: Drop shape analysis of polymer melt on a solid substrate as pendant drop (a), necking drop (b), sessile drop (c).....	19
Figure 9: EPDM structure containing an ethylene, propylene and diene unit. ....	22
Figure 10: Structure of 5-ethylidene-2-norbornene (ENB).....	22
Figure 11: Carbon black primary particle (a), aggregate (b), agglomerate (c) [78]. ....	24
Figure 12: Crosslinked rubber network structure. ....	26
Figure 13: Peroxide carbon-carbon crosslink between carbon atoms of each elastomer chain, and monosulphidic crosslink and polysulphidic crosslink where a single or multiple sulphur atoms is linked to two elastomer chains respectively. ....	26
Figure 14: Dicumylperoxide decomposition mechanism [88], [91]......	28
Figure 15: Mechanism for peroxide crosslinking of EPDM [59].....	29
Figure 16: Side reactions of PP unit in EPDM: $\beta$ -scission and disproportionation [88]. ....	30
Figure 17: Peroxide crosslinked network of the rubber matrix in the presence of co-agents with crosslinks originating from (A) polymer radicals, (B) co-agent forming crosslink, (C) thermoset domains of co-agents grafted to rubber chains, (D) interpenetrating network of homopolymerised co-agents covalently bonded to the rubber [89].....	31
Figure 18: Reaction mechanism of accelerated sulphur vulcanisation of EPDM (x= accelerator residue) [108]. ....	33
Figure 19: Rheometer vulcanisation curve after [88]......	34
Figure 20: Vulcanisate properties as a function of crosslink density [75], [89]. ....	36
Figure 21: Temperature profile across the versatile 2K mould with the rubber cavity set at 180°C and the thermoplastic cavity temperature of 70°C [3]. ....	38
Figure 22: Thermoset rubber-thermoplastic sample with interdiffusion (left) and chemical bonding (right) at the interface. ....	41
Figure 23: 2K specimen dimensions are represented (a). The thickness of both the rubber and thermoplastic part is 2 mm and the blue dotted line represents the location for tensile testing samples. Hardness was measured at the interface (blue dots) and in the bulk (orange dots) to determine vulcanisation degree (b). ....	43

Figure 24: High temperature contact angle measurement chamber with thermoplastic granule on EPDM substrate.....	46
Figure 25: EPDM-thermoplastic sample with (a) EPDM composition with co-agents (red), (b) thermoplastic composition, and (c) adhesion mechanism at the interface, i.e. interdiffusion and chemical bonding (red).....	48
Figure 26: Torque-time curves at 180°C of EPDM compound with varying concentrations TMPT (a) and TAC (b). Control sample without co-agent (C0) is represented in both figures.....	50
Figure 27: Mechanical properties in function of co-agent concentration for EPDM with TMPT and TAC: tensile strength (a), elongation at break (b), Shore A hardness (c) and compression set (d). Error bars represent 95 % confidence intervals.....	51
Figure 28: Tensile strength (a) and Shore A hardness (b) of unaged and aged samples. A significant difference ( $p < 0.05$ ) between mean values of aged and unaged samples of each compound is indicated with *. Error bars represent 95 % confidence intervals.....	52
Figure 29: Crosslink density of control sample C0, and EPDM with varying concentrations of TAC and TMPT. Error bars represent 95 % confidence intervals. ....	53
Figure 30: Contact angles of thermoplastic melts (PE at 180°C, PP at 200°C and PC at 230°C) during spreading on EPDM without co-agent (C0), with 12 phr TMPT (TMPT12) and with 12 phr TAC (TAC12). The error bars represent 95 % confidence intervals. ....	54
Figure 31: ATR-FTIR spectra of EPDM without co-agent (C0), with 12 phr TMPT (TMPT12) and with 12 phr TAC (TAC12). ....	55
Figure 32: Adhesion strength in function of co-agent concentration for PP, PE, PC and ABS. The error bars represent 95 % confidence intervals. The microscopic images show a circular zone (2 mm radius) of the fracture surfaces at the thermoplastic side. Black indicates the rubber and white the thermoplastic. For PC with TMPT12, no rubber is visible, the PC itself is transparent resulting in a darker image.....	55
Figure 33: Adhesion percentage (adhesion strength divided by total strength) in function of co-agent concentration for PP, PE, PC and ABS. The error bars represent 95 % confidence intervals. The microscopic images show a circular zone (2 mm radius) of the fracture surfaces at the thermoplastic side. Black indicates the rubber and white the thermoplastic. ....	57
Figure 34: Vulcanisation times $t_{90}$ (a) and scorch times $t_{s1}$ (b) at 140°C, 160°C and 180°C for EPDM with 2 phr DCP (DCP2), 4 phr DCP (DCP4), 6 phr DCP (DCP6) and 8 phr DCP (DCP8).60	
Figure 35: Crosslink density obtained from swelling measurements in function of DCP concentration. The dotted line represent a linear fit, which is accompanied by the linear equation and the correlation coefficient $R^2$ . Error bars represent 95 % confidence intervals.60	
Figure 36: Mechanical properties of EPDM in function of DCP concentration: tensile strength (a), compression set (b), Shore A hardness (c), and elongation at break (d). Error bars represent 95 % confidence interval.....	61
Figure 37: Tensile strength (a) and hardness (b) of unaged and aged samples. A significant difference ( $p < 0.05$ ) between mean values of aged and unaged samples of each compound is indicated with *. Error bars represent 95 % confidence intervals.....	61
Figure 38: Contact angle measurements of thermoplastic melts of PE (180°C), PP (200°C) and PC (230°C) during spreading on EPDM with 2 phr DCP (DCP2), 4 phr DCP (DCP4), 6 phr DCP (DCP6) and 8 phr DCP (DCP8). Error bars represent 95 % confidence interval.....	62
Figure 39: ATR-FTIR spectra of vulcanised EPDM substrates: DCP2 (2 phr DCP), DCP4 (4 phr DCP), DCP6 (6 phr DCP) and DCP8 (8 phr DCP) (a), and a magnification of the spectra between 3100 and 3600 $\text{cm}^{-1}$ (b). ....	63

Figure 40: Adhesion strength in function of DCP concentration between EPDM and PE, PP, ABS and PC. EPDM strength ( $\sigma_t$ ) is represented as comparison. Error bars indicate 95 % confidence intervals. ....	63
Figure 41: Adhesion percentage in function of DCP concentration for PP, PE, PC and ABS. The error bars represent 95 % confidence intervals. The microscopic images show a circular zone (2 mm radius) of the fracture surfaces at the thermoplastic side. Black indicates the rubber and white the thermoplastic. For PC - 4 phr DCP, no rubber is visible and for PE - 6 phr DCP only rubber is visible. ....	64
Figure 42: Scorch time ( $t_{s1}$ ) and vulcanisation time ( $t_{90}$ ) for all EPDM compounds at 140°C (a), 160°C (b) and 180°C (c), and cure rate index (CRI) for all EPDM compounds at 140°C, 160°C and 180°C (c).....	68
Figure 43: Adhesion strength between PE or PP and EPDM containing different curing systems, and total EPDM strength ( $\sigma_t$ ) of all EPDM samples. The numbers indicate differences in EPDM strength between samples (ANOVA, Tukey, $p < 0.05$ ). Significant differences in adhesion strength between EPDM samples S1-S5 and PE are given in capital letters, and between EPDM samples S1-S5 and PP in lower case letter (ANOVA, Tukey, $p < 0.05$ ). Error bars represent 95 % confidence intervals. ....	69
Figure 44: EPDM-PE Adhesion strength in function of curing time ( $t_{90}$ ) (a), scorch time ( $t_{s1}$ ) (b), cure rate index (CRI) (c) and the interfacial vulcanisation degree. Error bars represent 95 % confidence intervals. ....	70
Figure 45: Contact angle measurements of thermoplastic melts of PE (180°C) on S4 and S5. Error bars represent 95 % confidence interval. ....	71
Figure 46: CRI of EPDM with high diene content (4640, 4.9 wt% ENB) and low diene content (3640, 1.8 wt% ENB) with a sulphur curing system (a) and a peroxide curing system (b). ....	80
Figure 47: Physico-mechanical properties of peroxide and sulphur-cured EPDM grades: tensile strength (a) crosslink density (b). Error bars represent 95 % confidence intervals. Grouping information from the Tukey method is given by a upper case letter for sulphur curing and by lower case letters for peroxide curing.....	82
Figure 48: Adhesion percentage between sulphur-cured EPDM containing 1.8 or 4.9 wt% ENB (3640 and 4640 respectively) and PP. Error bars represent 95 % confidence intervals. The microscopic images show a circular zone (2 mm radius) of the fracture surfaces at the thermoplastic side. Black indicates the rubber and white the thermoplastic. ....	82
Figure 49: Main effect plots for Mooney viscosity and ethylene content for sulphur-cured EPDM-PP (a) and peroxide-cured EPDM-PP (c), the interaction between Mooney viscosity and ethylene content for sulphur-cured EPDM-PP (b) and peroxide-cured EPDM-PP (d). ....	84
Figure 50: Residual plots for adhesion percentage between sulphur-cured EPDM and PP. ....	84
Figure 51: Residual plots for adhesion percentage between peroxide cured EPDM and PP. ....	85
Figure 52: Adhesion percentages between sulphur-based EPDM-PP and peroxide-based EPDM-PP with varying ethylene content and Mooney viscosity. The error bars represent 95 % confidence intervals. The microscopic images show a circular zone (2 mm radius) of the fracture surfaces at the thermoplastic side. Black indicates the rubber and white the thermoplastic. ....	88
Figure 53: 2K product consisting of a thermoplastic internal wheel surrounded by an EPDM seal (a). 1K product of the EPDM seal (b). ....	90
Figure 54: Peel test sample preparation. 2K thermoplastic internal wheel partially covered with aluminium tape (a) and positioning of 2K sample during testing (b). ....	92
Figure 55: Set-up of custom-made shear test. ....	93

Figure 56: Cure characteristics of EPDM at 160°C with varying filler and oil concentration: torque in function of time (a) and scorch time ( $t_{s1}$ ), vulcanisation time ( $t_{90}$ ) and CRI (b). .....	94
Figure 57: Vulcanisation curve of injection moulded K-O30 based on hardness measurements. The dashed line represents 90 % vulcanisation degree. Error bars represent 95 % confidence intervals. ....	96
Figure 58: Mechanical properties of EPDM with varying oil and filler concentrations: tensile strength (a), compression set (b), Shore A hardness (c), and elongation at break (d). Error bars represent 95 % confidence interval. Grouping information from a one-way ANOVA is given by lower case letters. ....	97
Figure 59: Peel test results between PP or PC and EPDM with varying oil an filler content: adhesion force (a), and equivalent adhesion width (b). The error bars represent 95 % confidence intervals. Grouping information from a one-way ANOVA is given by lower case letters for PP and by upper case letters for PC. ....	98
Figure 60: Contact angles of PP (at 200°C) on EPDM without oils and fillers (UNF), on EPDM with 30 phr oil and 110 phr calcined kaolin (K-O30), and on EPDM with 30 phr oil and 70 phr N550 carbon black (R-O30) (a); PC (at 230°C) on UNF, on EPDM without oil and 110 phr calcined kaolin (K-O30) on EPDM with 30 phr oil and 110 phr calcined kaolin (K-O30) (b). The error bars represent 95 % confidence intervals. ....	99
Figure 61: Cohesive failure between K-O30 and PP after a peel test. ....	100
Figure 62: Shear test: (a) shear force between PP and K-O30, R-O30 and UNF over a shear distance, and (b) 2K sample during and after testing. ....	101
Figure 63: Environmental control chamber with heated needle device for analysis of polymer melts (pendant drop) and wetting on solid substrate. ....	104
Figure 64: PVT properties of PE (a) and PP (b). ....	105
Figure 65: Viscosity in function of shear rate for PP at 240°C and PE at 160°C. ....	107
Figure 66: Pendant droplet of PP at 240°C (a), and of PE at 160°C (b). ....	107
Figure 67: Temperature dependency of surface tension of PP. 95 % confidence intervals are reported. ....	108
Figure 68: Deposition of PP droplet at 240°C on EPDM_TAC3 substrate: droplet necking (a), contact between droplet and substrate (b), filament formation (c), rupture of filament (d), and droplet spreading (e) and (f). ....	109
Figure 69: Contact angles of PP melt on EPDM substrates TAC3, TAC12, S1 and S5, and on an NBR substrate at 240°C. ....	109
Figure 70: Contact angles of PP melt on EPDM_TAC12 at 240°C and PE melt on EPDM_TAC12 at 160°C. ....	110
Figure 71: Adhesion percentage in function of work of adhesion ( $W_a$ ) between EPDM types TAC3, TAC12, S1 and S5 or NBR and polyolefins PP and PE. ....	111
Figure 72: Hydrogen abstraction from EPDM, PE, PP and ABS chain by methyl radicals from DCP. The brackets indicate repeating units in each polymer, but these are removed in the reaction mechanism to give a clearer view. ....	113
Figure 73: Co-vulcanisation reactions between EPDM and PE, PP or ABS. For EPDM with PP or PE, two combination and one addition reactions result in three types of crosslinks. For EPDM with ABS four combination and four addition reactions result in a total of eight crosslink types. ....	114
Figure 74: Reactive wetting between thermoplastic melt (liquid) and EPDM substrate (solid) (a) and thermodynamic wetting of thermoplastic melt on EPDM substrate (b). ....	115

Figure 75: Ellipse fitting of PE droplets on an unvulcanised DCP8 substrate after 5 min (a), after 30 min (b) and on a vulcanised DCP8 substrate after 3 min (c), after 30 min (d). The baseline represents the contact between the PE droplet and EPDM substrate which is slightly higher than the EPDM substrate surface (in c and d) due to a reflection of the droplet on the surface. .... 117

Figure 76: Microscopic images of DCP2 substrate surface after 30 min at (a) 150°C, (b) 160°C and of DCP 8 at (c) 160°C. In (c) the image represents a side view of the complete DCP8 substrate (10 x 10 x 2 mm) to illustrate the surface topography. (d) 3D image of a gas bubble from the DCP8 substrate. .... 118

Figure 77: Vulcanisation degree in function of time for S1, DCP2 and DCP8. The dashed line indicates the measuring time of 30 min of the contact angle measurements. .... 118

Figure 78: Spreading of PE granule on DCP2 (a) and DCP8 (b) at 150°C. At 0 min the PE granule is in solid state. ‘UNV’ refers to unvulcanised and ‘VULC’ refers to vulcanised. .... 119

Figure 79: Spreading of PE granule on S1 at 150°C. At 0 min the PE granule is in solid state. ‘UNV’ refers to unvulcanised and ‘VULC’ refers to vulcanised. .... 120

Figure 80: Contact angle measurements of PE melt (150°C) on DCP2, DCP8 and S1. Error bars represent 95 % confidence interval. .... 120

Figure 81: ATR-FTIR spectra of vulcanised and unvulcanised DCP2 (a) and DCP8 (b). .... 121

Figure 82: Contact angle measurements of PE melt (150°C) on vulcanising and vulcanised EPDM with 50 wt% ethylene content (4570) and 70 wt% ethylene content (4770). EPDM was sulphur-based (S) or peroxide-based (P). Error bars represent 95 % confidence intervals. .... 122

Figure 83: Microscopic images of EPDM-PP samples after swelling in cyclohexane and drying: PP-P4520 (a) and PP-S4520 (b). .... 124

Figure 84: SEM imaging of EPDM-PE interface region in BSE mode (a), and corresponding EDX elemental mapping of carbon (b), nitrogen (c), oxygen (d), silicon (e), sulphur (f), calcium (g), and zinc (h). .... 129

Figure 85: Relative sulphur amount (S/C) along the line scan going from PE to EPDM. The possible interphase region is confined by the dotted line. .... 130

Figure 86: AFM images of PE-EPDM topography and DMT modulus for a surface area of 50 x 50  $\mu\text{m}^2$  (a), 15 x 15  $\mu\text{m}^2$  (b), and 5 x 5  $\mu\text{m}^2$  (c). .... 132

Figure 87: Radar chart illustrating adhesion strength and rubber properties of peroxide-based EPDM-PP with varying peroxide and co-agent concentrations. .... 136

Figure 88: Radar chart illustrating adhesion strength and rubber properties of peroxide-based EPDM-PP with varying EPDM macromolecular structures. Compression set results are based on the EPDM NORDEL™ grade datasheet as listed in Appendix A. .... 137

Figure 89: Radar chart illustrating adhesion strength and rubber properties of peroxide-based EPDM-PP with varying oil and filler content. .... 137

Figure 90: Radar charts illustrating adhesion strength and rubber properties of sulphur-based EPDM-PP with varying sulphur system composition. .... 138

Figure 91: Radar charts illustrating adhesion strength and rubber properties of sulphur-based EPDM-PP with varying EPDM macromolecular structure. Compression set results are based on the EPDM NORDEL™ grade datasheet as listed in Appendix A. .... 139

Figure 92: Radar charts illustrating adhesion strength and rubber properties of EPDM-PE with varying peroxide system composition. .... 140

Figure 93: Radar charts illustrating adhesion strength and rubber properties of EPDM-PE with varying sulphur system composition. .... 140

Figure 94: Radar charts illustrating the influence of peroxide curing on adhesion strength and rubber properties (a) EPDM-PC, and (b) EPDM-ABS. .... 141

Figure 95: Radar charts illustrating the influence of fillers and oils on adhesion strength and rubber properties of EPDM-PC. .... 142

Figure 96: Material selection grade map of EPDM-PP. .... 144

Figure 97: Product price of a PE-EPDM, ABS-NBR, PP-EPDM and PC-EPDM 2K seal for a batch size of 50000 products in case of the manual 1K process (a), and the semi 2K process (b). .... 147

Figure 98: Total product cost based on material cost, mould cost and production cost. .... 147

Figure 99: Optimal product price of a PE-EPDM, ABS-NBR, PP-EPDM and PC-EPDM 2K seal for a batch size of 50000 products in case of the manual 1K process (a), and the semi 2K process (b). .... 148

Figure 100: Optimal product cost of PP-EPDM for manual 1K at 180°C or 170°C and semi 2K. .... 149

Figure 101: Plug & seal connector for electrical vehicle cooling system [152]. .... 150

Figure 102: Vulcanisation degree of EPDM.c. The dashed line represents 90 % vulcanisation degree. Error bars represent 95 % confidence intervals. .... 155

Figure 103: Tensile strength of EPDM.c at 23°C, 40°C, 55°C, 70°C, and 85°C. The retention indicates the decrease in strength compared to the strength at 23°C. Error bars represent 95 % confidence interval for the tensile strength. .... 156

Figure 104: Adhesion force of EPDM.c-PP (control) and after immersion in H<sub>2</sub>O, coolant, brake fluid and heat aging at 100°C. The retention indicates the decrease in adhesion force compared to the control sample. Error bars represent 95 % confidence interval for the tensile strength. .... 157

Figure 105: Adhesion force of EPDM.c-PP at 23°C, 40°C, 55°C, 70°C, and 85°C. The retention indicates the decrease in adhesion force compared to the sample at 23°C. Error bars represent 95 % confidence interval for the adhesion force. .... 158

Figure 106: Geometry of ISO 527-2/1B tensile bars with dimensions. The sample thickness is 4 mm [158]. .... 160

Figure 107: Microscopic image with related grain diameter distribution for EPDM (a) and PP (b). A fitted Weibull distribution is shown in each graph. .... 162

Figure 108: Mechanical properties of virgin PP/recycled EPDM/recycled PP blends: tensile strength (a), elongation at break (b), Young's modulus (c), and hardness and impacts strength (d). Error bars represent 95 % confidence intervals. Grouping information from a one-way ANOVA is given by lower case letters and by upper case letters for impact strength. .... 163

Figure 109: Mechanical properties of TPV/recycled EPDM/recycled PP blends: hardness (a), and tensile strength and elongation at break (b). Error bars represent 95 % confidence intervals. Grouping information from a one-way ANOVA is given by lower case letters and by upper case letters for elongation at break. .... 165

---

## List of Tables

---

Table 1: Adhesion mechanisms [11].	6
Table 2: Elastomers and blends that can or cannot be to cured with peroxides [88], [90], [91].	27
Table 3: Thermoplastic-thermoset rubber material combinations.	37
Table 4: Process parameters for individual components.	43
Table 5: Chemical names and structure of the peroxide curing system components.	48
Table 6: Composition of EPDM compounds containing varying co-agent type and concentration (phr).	49
Table 7: Mould temperatures for thermoplastic and rubber cavity with the accompanying interface temperature and curing times for thermoplastic – peroxide-based EPDM.	49
Table 8: Vulcanisation time ( $t_{90}$ ) and scorch time ( $t_{s1}$ ) of EPDM compounds with varying concentrations TMPT and TAC and of a control sample without co-agent (C0) at 140°C, 160°C and 180°C.	50
Table 9: EPDM compositions with varying DCP concentrations.	59
Table 10: Cure characteristics of the EPDM compounds with varying DCP concentration.	59
Table 11: Sulphur curing system composition	66
Table 12: Mould temperatures for thermoplastic and rubber cavity with the accompanying interface temperature and curing times for thermoplastic – sulphur-based EPDM	67
Table 13: EPDM compound order, ranging from high to low, for cure time ( $t_{90}$ ), scorch time ( $t_{s1}$ ), cure rate index (CRI) and interfacial vulcanisation degree in 2K sample.	68
Table 14: Characteristics of NORDEL™ EPDM grades.	76
Table 15: Curing system formulation for EPDM with macromolecular changes.	77
Table 16: Factors and factor levels for the full factorial design.	78
Table 17: Cure characteristics of all EPDM NORDEL™ grades at 180°C and 160°C.	79
Table 18: Melting enthalpy and crystallinity calculated from DSC curves for each EPDM NORDEL™ grade with sulphur or peroxide curing.	81
Table 19: Analysis of variance results of adhesion percentages of sulphur-cured EPDM-PP (DF: Degree of freedom, Adj SS: Adjusted sum of squares, Adj MS: Adjusted mean of squares, S: Standard deviation).	86
Table 20: Analysis of variance results of adhesion percentages of peroxide-cured EPDM-PP (DF: Degree of freedom, Adj SS: Adjusted sum of squares, Adj MS: Adjusted mean of squares, S: Standard deviation)	87
Table 21: Rubber compositions with varying oil and filler concentrations.	90
Table 22: Individual injection moulding parameters for the 2K sealing product	91
Table 23: Cure characteristics of EPDM compounds with varying filler and oil concentration at 180°C and 160°C.	94
Table 24: Density of PE (M80064, Sabic) at 160°C, 180°C, 200°C, and 220°C.	105
Table 25: Density of PP (400-GA05, Ineos) at 200°C, 220°C, 240°C, and 260°C.	105

Table 26: Mass swell percentage of PP-P4520 and PP-S4520 after immersion in cyclohexane. .	124
Table 27: Interaction parameter at room temperature for co-agents TAC and TMPT, and curing agent DCP with polymers EPDM, PP, PE, ABS and PC.....	127
Table 28: Interaction parameter at room temperature between thermoset rubbers and thermoplastics. ....	128
Table 29: Material cost of rubber and thermoplastic part in a 2K seal.....	146
Table 30: Rubber vulcanisation time of a PP-EPDM, PE-EPDM, PC-EPDM or ABS-NBR 2K seal when applying a 2K or 1K injection moulding process. ....	146
Table 31: Rubber composition requirement for EPDM-PP connector. ....	151
Table 32: Injection moulding parameters of PP and EPDM.c for production of a 2K seal.....	152
Table 33: EPDM.c-PP sample and shear test conditioning. ....	154
Table 34: EPDM.c vulcanisate mechanical properties. ....	155
Table 35: Compressive stress at 25 % deformation at 23°C, 40°C and 85°C. ....	156
Table 36: Injection moulding parameters for tensile bars of PP-recycled EPDM/PP and TPV-recycled EPDM/PP.....	160
Table 37: DSC parameters of blend compositions Virgin PP/ recycled EPDM/ recycled PP...	162
Table 38: DSC parameters of blend compositions TPV/ recycled EPDM/ recycled PP.....	164

---

# Chapter 1 Introduction

---

## 1.1 Motivation and problem statement

Two component (2K) injection moulding adheres two different polymers together to manufacture an end-product in a single manufacturing process, eliminating an additional assembly step [2]. Strong adhesion at the interface between both materials during this 2K injection moulding process is an important aspect. When combining thermoplastics with thermoset rubbers novel material combinations arise which can be ideal for applications exposed to high temperature, harsh chemical environment and/or mechanical strain. Usually, thermoplastic elastomers (TPEs) are used as soft component in 2K injection moulding, but TPEs tend to fail under these harsh conditions. Instead, ethylene-propylene-diene rubber (EPDM) as soft component offers excellent dynamic and heat aging properties together with resistance to polar solvents. Consequently, it is an ideal rubber for sealing applications. These seals are often incorporated and fitted mechanically or with an adhesive onto thermoplastics parts. A 2K process combining EPDM with thermoplastics would improve product reliability, quality and offers perspectives for reducing material cost thanks to a re-design [3]. Combining thermoset rubbers like EPDM with common thermoplastics like polyethylene (PE), polypropylene (PP), acrylonitrile-butadiene-styrene (ABS) and polycarbonate (PC) requires dealing with the opposite processing requirements of both polymer materials. In particular, thermoplastics require an injection at a high temperature (190-300 °C) into a cooled mould (20-100 °C), while thermoset rubbers require an injection at low temperature (80-100 °C) into a heated mould (160-200 °C) to ensure that vulcanisation takes place in the mould [2]. Therefore, 2K injection moulding is currently limited to combining high temperature resistant plastics with thermoset rubbers, e.g. polyamide (PA) with hydrogenated acrylonitrile-butadiene-styrene rubber (HNBR) [4]. However, in sealing applications, rubber combined with commodity plastics, like polypropylene (PP), would be more beneficial due to their lower cost and use in high volumes compared to high performance plastics [3].

Therefore, Bex et al. [1], [5] developed a mould with thermally separated heat cavities and optimised the process to induce a thermoset rubber-thermoplastic adhesion. During this process, the temperature of the rubber cavity is set sufficiently high to vulcanise the product, while the thermoplastic part is sufficiently cooled. This leads to an intermediate temperature at the interface. For semi-crystalline thermoplastics, this temperature is around the melting point but below the temperature at which small voids at the interface form, causing a small/narrow melted zone of the thermoplastic material. For amorphous materials, the interface temperature is set above the glass transition temperature to initiate movement of the polymer chains but it is limited by the temperature at which excessive

deformation of the thermoplastic part occurs. As a result, adhesion can be realised at the interface between both materials.

Despite the development of this 2K technique enabling rubber-thermoplastic adhesion, novel challenges arise related to the adhesion at the interface. Currently, EPDM with a sulphur vulcanising system can adhere to high density polyethylene (HDPE) and to PP, but each of these combinations has specific limitations. EPDM with HDPE requires a low interface temperature due to its low melting temperature (130°C), leading to high processing times (1000 s) necessary to completely cure the 2K product. For EPDM with PP, only a low adhesion strength can be achieved at the interface (2.5 MPa compared to 8 MPa bulk strength), even though PP shows good compatibility, or wetting, with sulphur-based EPDM [6]. Furthermore, adhesion of EPDM with more polar thermoplastics, such as ABS or PC, was not yet achieved.

In 2K injection moulding studies, the focus has so far mainly been on the influence of process parameters on the adhesion strength. However, adhesion between two polymer surfaces is a complex phenomenon related to intermolecular interactions. Dispersive forces are always present, but depending on the specific material composition, acid-base interactions, interdiffusion (leading to intermingling or/and entanglement), and/or chemical bonding can be realised as well [7], [8]. Varying the rubber formulation could influence these molecular interactions. In addition, an in depth study of the adhesion mechanisms is currently lacking. Thus, the rubber-thermoplastic material combination, which is ideal for products exposed to high temperatures, harsh chemical environments or mechanical strains, require further understanding of the adhesion mechanisms and the influence of material composition aimed at optimisation of adhesion strength and processing time. With such knowledge, a well-reasoned choice of suitable material combinations can be made while taking into account product requirements.

## 1.2 Objectives

**The main objectives of this PhD are threefold: (1) to provide insight into the adhesion mechanisms between rubbers and thermoplastics; (2) to optimise the adhesion strength at the thermoset rubber-thermoplastic interface by focussing on rubber formulation; (3) to increase economic feasibility of 2K injection moulding by reducing processing times.**

To accomplish these objectives, the study is divided into scientific and technological categories.

**The scientific objectives** are to gain fundamental insights into the effects of EPDM compound formulation on the adhesion strength with thermoplastics and on the adhesion mechanism at the interface in 2K injection moulding. More specifically, the following sub-goals were defined:

- (1) Studying the influence of sulphur or peroxide-based curing systems and the accompanying curing efficiency on the adhesion with thermoplastics;
- (2) Studying the influence of composition of the primary rubber polymer and additives (e.g. plasticisers and fillers) on the adhesion with thermoplastics;
- (3) Clarifying the adhesion mechanisms at the rubber-thermoplastics interface, in particular, co-vulcanisation, interdiffusion and wettability.

**The technological objectives** are the following:

- (1) Development of an experimental procedure to predict the compatibility between a rubber and a thermoplastic based on wettability measurements at high temperature;
- (2) Development of an experimental procedure to define/predict chemical bonding between a rubber and a thermoplastic;
- (3) Production of economically feasible 2K products combining commodity plastics with special purpose rubbers;
- (4) Development of guidelines for material selection to define the rubber formulation for optimal adhesion while meeting product requirements.

### 1.3 Thesis outline

This thesis consists of seven chapters each focussing on a particular domain of the work concerning thermoset rubber-thermoplastic adhesion in 2K injection moulding. In this first chapter (Chapter 1) the motivation and problem statement was described together with the objectives and general outline of the thesis. Afterwards, following chapters are discussed:

Chapter 2 - A state of the art is given on rubber-thermoplastic adhesion. This includes adhesion mechanism theories and their applicability for polymer-polymer adhesion, with a particular focus on thermoset rubber-thermoplastic adhesion. Furthermore, the thermoset rubber composition and its relation to adhesion is discussed. Finally, the rubber-thermoplastic adhesion in 2K injection moulding is addressed by comparing different hard-soft material combinations and discussing the process and simulation of thermoset rubber-thermoplastics adhesion.

Chapter 3 – An optimisation of the rubber curing system on the adhesion with thermoplastics is presented. First, the influence of peroxide curing systems is studied with the specific focus on co-agents and the peroxide curing agent dicumylperoxide. Second, the sulphur curing system is analysed by varying the sulphur accelerator composition which creates differences in curing efficiency and which allows optimisation of processing time.

Chapter 4 – In this chapter components in the rubber composition, beside the curing system, are optimised for good adhesion. First, the macromolecular structure of EPDM is varied and afterwards, the influence of filler and plasticiser in the EPDM formulation on adhesion with thermoplastics is analysed.

Chapter 5 – The adhesion mechanisms are evaluated, discussed and characterised with the specific focus on wetting, chemical bonding and interdiffusion.

Chapter 6 – Based on results of the previous chapter materials selection guidelines are presented by means of radar charts. Furthermore, an economic evaluation provides insight in the feasibility of the proposed material combinations. Afterwards, a case study is elaborated with the focus of 2K sealing applications. Finally, end-of-life aspects of rubber-thermoplastic products are evaluated.

Chapter 7 – The thesis is finalised with the main conclusions and suggestions for further research.

---

# Chapter 2 Rubber-thermoplastic adhesion: state of the art

---

## 2.1 Introduction

This chapter provides a state of the art concerning rubber-thermoplastic adhesion. First, the different types of adhesion mechanisms are addressed and relevant literature is discussed (Section 2.2). This entails the fundamental adhesion theories, possible adhesion failure mechanisms, and relevant interface and characterisation techniques. Second, the rubber composition is elaborated (Section 2.3) with the focus on how changes in composition can affect the adhesion. As the focus of the current study is on EPDM adhesion with thermoplastics, the EPDM composition is explained. In addition, the rubber curing system creates a certain degree of crosslinking in the rubber part which might diminish or promote adhesion with thermoplastics or change product properties. Therefore, peroxide and sulphur curing and main rubber characteristics are addressed. Finally, the previously developed 2K injection moulding process which enables adhesion between thermoset rubbers and thermoplastics is explained together with the developed simulation model for adhesion prediction (Section 2.4).

## 2.2 Adhesion mechanisms

Adhesion phenomena are based on interatomic and intermolecular interactions at the interface between two materials. The mechanisms related to the adhesion phenomena are known to be dependent on surface characteristics of the combining materials. Over time, the subject of adhesion has been receiving increasing interest due to its application in many technologies with polymer materials. Furthermore, for adhesion in multicomponent materials the product performance depends greatly on the strength of the interface. Specifically for polymer adhesion, automobile and aerospace industries have been the driving force for understanding adhesion mechanisms to find alternatives for metal-metal components. In addition, applications of sealing materials have been of major interest for industries like building, engineering and biomedical [8]–[10].

The adhesion mechanisms were traditionally classified as mechanical interlocking, electrostatic, diffusion, and adsorption. However, these mechanisms were expanded to mechanical interlocking, electrostatic, diffusion, wetting, chemical bonding and weak boundary layer as shown in Table 1 [11]. Literature indicates that a combination of different mechanisms is expected to be responsible for adhering materials together. The numerous proposed models originate from a variety of approaches due to the interdisciplinary aspect of adhesion phenomena. The validity of each mechanism depends on the nature of the materials in contact and how the system is bonded [10]–[13].

Table 1: Adhesion mechanisms [11].

Traditional	Current
Mechanical interlocking	Mechanical interlocking
Electrostatic	Electrostatic
Diffusion	Diffusion
Adsorption	Wetting
	Chemical bonding
	Weak boundary layer

The presented theories are individually or in combination able to realise the adhesion occurring at an interface between two materials. As indicated by Rezaeian et al. [14], for rubber adhesion to solid substrates, adhesion is dominated by interfacial interactions, rubber chain entanglements and crosslinking.

## 2.2.1 Fundamental adhesion theories

### 2.2.1.1 Mechanical interlocking

The mechanical theory can be traced back to McBain and Hopkins describing mechanical interlocking to porous or rough substrates [14]. The theory describes the penetration of adhesives into surface irregularities, e.g. pores or cavities, on the substrates' surface as shown in Figure 1 [11]. Generally, when surface roughness plays an essential role in adhesion, the mechanical interlocking theory applies. However, it is debated whether mechanical interlocking provides higher adhesion strength or whether increasing surface area enhances other mechanisms such as interdiffusion or chemical bonding [8], [11].

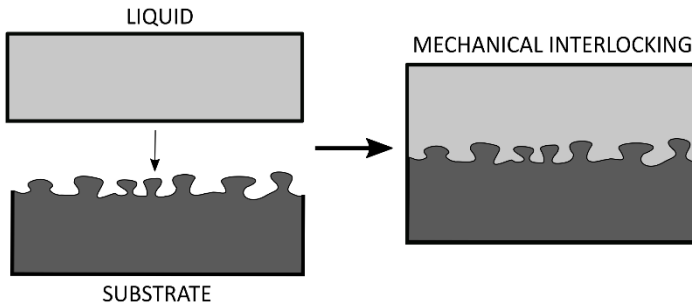


Figure 1: Mechanism of mechanical interlocking between a liquid and a substrate.

### 2.2.1.2 Electrostatic theory

The electrostatic theory was first proposed by Deryaguin and colleagues in 1948 [10]. In this physical model, the molecules of the different adhering materials can be represented by two plates of an electrical capacitor causing a double electrical layer at the interface. The adhesive strength is then created by attractive electrostatic forces across the double layer. These forces can originate from dispersion forces or the interaction of permanent dipoles. When pulling apart the materials in contact, an electrical discharge can be measured as the bond ruptures [10], [14]. A schematic representation is given in

Figure 2 which represents an electropositive material donating charges to the electronegative materials, creating a double electrical layer at the interface. The electrostatic mechanism has merit in polymer-metal systems. However, its contribution to non-metallic adhesion systems is limited when comparing it to chemical bonding [11], [15].

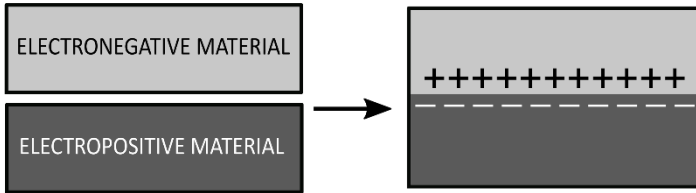


Figure 2: Schematic representation of the electrostatic theory.

### 2.2.1.3 Adsorption theory (wetting)

For adhesion to occur at a polymer interface, intimate contact is a prerequisite. Most commonly, contact between a liquid and a solid results from interfacial forces on a molecular scale. This continuous contact between solid and liquid is defined as ‘wetting’ [11]. Interfacial forces acting during wetting are a result of van der Waals and Lewis acid-base interactions and are referred to as secondary interactions. Hydrogen bonds, ionic bonds and ion-dipole interactions are examples of electron donor-acceptor Lewis acid-base interactions, while forces resulting from molecular dipoles, i.e. Keesom orientation forces, Debye inductions forces and London dispersion forces, are van de Waals forces. The London forces are less dependent on the chemical structure and act between all atomic and molecular species. The magnitude of secondary interactions does not exceed 50 kJ/mol [13].

The forces acting at the surface can be related to the surface free energies of the liquid and solid. In a liquid, mechanical equilibrium exists in the bulk as molecules are pulled equally in all directions by neighbouring molecules. However, at the vapour-liquid interface, there are no neighbouring molecules, which causes the molecules to be pulled inwards creating an internal pressure. Consequently, the surface area is contracted to a droplet shape by internal forces, as shown in Figure 3a, which is called surface tension [10], [16].

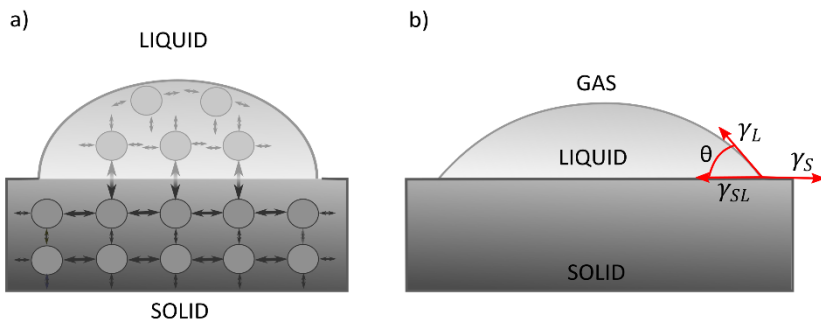


Figure 3: Intermolecular interactions at solid-liquid interface (a) profile of sessile drop on a planar solid surface (b).

In a solid-liquid-vapor system, Young's equation can be applied to evaluate wetting equilibrium. Figure 3b represents the profile of a sessile drop on a planar solid surface with a three-phase contact point. The relationship between surface tensions and equilibrium contact angle  $\theta$  in this system is then given by Young's equation (Eq. (1)) [10].

$$\gamma_S = \gamma_{SL} + \gamma_L \cos \theta \quad (1)$$

where  $\gamma_S$ ,  $\gamma_L$  and  $\gamma_{SL}$  are the surface tensions of the solid-vapor, liquid-vapor and at the solid-liquid interface respectively. The wettability of the liquid on the solid substrate is characterised by the contact angle measured at the contact line:  $\theta=0^\circ$ , complete wetting;  $\theta<90^\circ$ , good wetting;  $90^\circ<\theta<180^\circ$ , low wetting;  $\theta=180^\circ$ , non-wetting [17]. Furthermore, the work required to separate the solid-liquid interface is referred to as the work of adhesion ( $W_a$ ). This work of adhesion is the work required to create liquid-vapor and solid-vapor from a solid-liquid interface and can be defined by the Dupré equation (Eq.(2)). Higher interfacial interactions will lead to a greater work of adhesion. Thus, smaller contact angles indicate better wetting and therefore a greater work of adhesion. When combining Young's equation with Dupré's equation, the Young-Dupré equation can be derived as Eq. (3). Furthermore, wetting can also be evaluated with the spreading coefficient  $S$  (Eq. (4)). Partial wetting, e.g.  $0<\theta<90^\circ$ , results in a negative  $S$  and a lower  $\theta$  will cause a negative  $S$  closer to zero. Similar to  $W_a$ ,  $S$  can be recalculated as shown in Eq. (5) [10], [13], [17]:

$$W_a = \gamma_S + \gamma_L - \gamma_{SL} \quad (2)$$

$$W_a = \gamma_L (1 + \cos \theta) \quad (3)$$

$$S = \gamma_S - (\gamma_L + \gamma_{SL}) \quad (4)$$

$$S = \gamma_L (\cos \theta - 1) \quad (5)$$

Regardless of the adhesion mechanisms, intimate contact between two polymer surfaces is a prerequisite, i.e. wetting must be ensured. When a liquid wets a solid substrate, spreading occurs through physical interactions leading to an increase of the liquid coverage area in time after droplet deposition. When topographic heterogeneity applies, it is important that the molten polymer is able to fully wet the rough surface as this increases contact area promoting further physical or chemical adhesion mechanisms [18]–[21].

Specifically for wetting of molten polymers, studies have been done on glass substrates, bulk metallic glasses, tool steel surfaces, coatings and vulcanised rubbers by direct contact angle measurements to understand wetting behaviour close-to-processing conditions [6], [18], [22]–[24]. This is addressed in more detail in Section 2.2.3.5 Contact angle analysis.

#### 2.2.1.4 Interdiffusion

When polymers are brought into contact, mutual adhesion can be caused by interdiffusion of macromolecules, i.e. long-chain molecules, across the interface, creating

an interphase [10]. This mechanism, as originally proposed by Voyutskii, is based on the mobility and mutual solubility of macromolecular chains or chain segments [14]. A schematic representation of interdiffusion at a polymer-polymer interface is given in Figure 4. When the two materials are soluble, an interphase is formed in which properties of material A gradually change in properties of material B. This diffusive bond does not cause a discontinuity in properties or stress concentrations. However, more commonly a mismatch in properties of both materials does occur with accompanying insolubility of both materials [15].

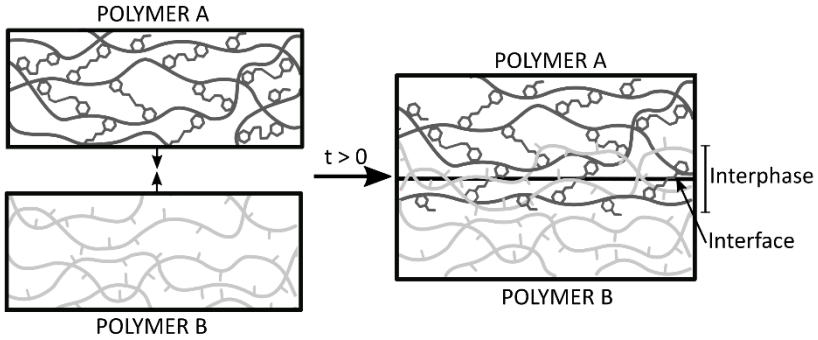


Figure 4: Interdiffusion mechanism between two polymers in contact.

From the thermodynamic perspective, mutual solubility, or compatibility, results from a negative Gibbs free energy of mixing ( $\Delta G_m$ ). The Gibbs free energy of mixing is related to enthalpy of mixing ( $\Delta H_m$ ) and the entropy of mixing ( $\Delta S_m$ ) as represented in Eq. (6):

$$\Delta G_m = \Delta H_m - T\Delta S_m \quad (6)$$

Upon mixing an increasing disorder is usually created, leading to a positive  $\Delta S_m$  and thus a negative  $-T\Delta S_m$  term. However, polymers are long-chain molecules with high molecular weight which cause a considerable smaller entropy gain compared to low molecular weight materials. This is due to the limited number of possible configurational states of high molecular weight polymers [13], [15]. Thus, to induce a negative  $\Delta G_m$  with accompanying miscibility,  $\Delta H_m$  would have to be negative or only slightly positive. This would require attractive molecular interactions between the components [4].

To determine the entropy and enthalpy changes, the Flory-Huggins theory can be applied. This theory starts from a lattice with identical unit cells in which chain segments may be distributed in a certain number of ways [13]. The interaction between the mixing polymers can be described by the Flory-Huggins interaction parameter  $\chi_{AB}$  which can be derived from the free enthalpy of mixing per volume unit (Eq. (9)):

$$\Delta S_m = -R \left( \frac{\Phi_A}{v_A} \ln \Phi_A + \frac{\Phi_B}{v_B} \ln \Phi_B \right) \quad (7)$$

$$\Delta H_m = RT \frac{\chi_{AB}}{v_0} \Phi_A \Phi_B \quad (8)$$

and hence:

$$\Delta G_m = RT \left( \frac{\Phi_A}{v_A} \ln \Phi_A + \frac{\Phi_B}{v_B} \ln \Phi_B + \frac{\chi_{AB}}{v_0} \Phi_A \Phi_B \right) \quad (9)$$

In Eq. (9),  $v_A$  and  $v_B$  are the molar volumes of the individual components,  $v_0$  is a reference volume ( $= \sqrt{v_A v_B}$ ),  $\Phi_A$  and  $\Phi_B$  are the volume fractions of each component,  $R$  is the gas constant, and  $T$  is the absolute temperature. The first two terms between brackets represent the entropy of mixing of polymer A and B. This is also indicated in Eq. (7). The last term in Eq. (9) represents the interactions between the mixed monomer units (enthalpy) as also indicated in Eq. (8). A further derivation of the enthalpy of mixing was presented by Hildebrand [15]. This derivation also addresses mutual solubility, but now based on cohesive energy of materials ( $E_{coh}$ ). The cohesive energy indicates how strongly the atoms or molecules in a solid or liquid are attracted to each other and can be defined by Eq. (10):

$$E_{coh} = \Delta H_{vap} - RT \quad (10)$$

where  $\Delta H_{vap}$  is the enthalpy of vaporisation. The relation between the enthalpy change due to vaporisation and cohesive energy is representative for the magnitude of intermolecular forces. The cohesive energy density (CED) can be defined as the relation between  $E_{coh}$  and the molar volume ( $v_m$ ) (Eq. (11)). Then, for the solubility theory, a solubility parameter ( $\delta$ ) was defined according to Eq. (12) in such way that  $\delta^2$  equals the cohesive energy density [15].

$$CED = \frac{E_{coh}}{v_m} \quad (11)$$

$$\delta = \sqrt{\frac{E_{coh}}{v_m}} \quad (12)$$

Hildebrandt then defined the enthalpy of a solution (or mixture) based on the solubility parameters of two materials, i.e.  $\delta_A$  and  $\delta_B$  (Eq.(13)). When solubility parameters are equal, maximum polymer bond strength can be reached [4], [13], [15]. No exothermic mixture can be reached as the enthalpy of mixing can only be positive or zero. In this case, the possibility of chemical interactions is excluded. As polar interaction and hydrogen bonds are not addressed in the above equations, a further extension was made by Hansen's solubility parameters: the dispersive component ( $\delta_d$ ), the polar component ( $\delta_p$ ), and the hydrogen component ( $\delta_h$ ). Introducing these components in Eq.(13) results in Eq.(14). These three-dimensional solubility parameters can be determined based on group contribution procedures as developed by Hoftyzer, van Krevelen, Hoy or Barton [25], [26].

$$\Delta H_m = (\delta_A - \delta_B)^2 \Phi_A \Phi_B \quad (13)$$

$$\Delta H_m = [(\delta_{d,A} - \delta_{d,B})^2 + (\delta_{p,A} - \delta_{p,B})^2 + (\delta_{h,A} - \delta_{h,B})^2] \Phi_A \Phi_B \quad (14)$$

Eventually, the relationship between the interaction parameter and the solubility parameters can be found by combining Eq. (9) and Eq. (14) resulting in Eq. (15) [4].

$$\chi_{AB} = [(\delta_{d,A} - \delta_{d,B})^2 + (\delta_{p,A} - \delta_{p,B})^2 + (\delta_{h,A} - \delta_{h,B})^2] \frac{v_0}{RT} \quad (15)$$

The interaction parameter  $\chi_{AB}$  is dimensionless and temperature dependent. The proposed Eq. (15) does not allow negative values for the interaction parameter. In this case, literature states that to have mutual miscibility  $\chi_{AB}$  needs to reach low values, i.e. below 0.00277 for polymers and below 2.77 for low molecular weight materials [4], [13], [25]. However, polymers usually have significantly higher  $\chi_{AB}$ , rendering them only partially miscible or completely immiscible according to the Flory-Huggins theory. For example, even polyethylene and polypropylene are incompatible at 140°C with  $\chi_{AB}$  being 0.011 [13]. Thus, mutual solubility is rarely reached for polymers. Even though this thermodynamic incompatibility exists, there is still a statistical probability of polymer A chains diffusing in polymer B because, as indicated by da Silva et al. [13], “an atomically sharp interface between two such polymers will not be stable”. Thus, a small entropy gain is created which reduces the Gibbs free energy. The extent of interdiffusion will depend on the value of the interaction parameter, with smaller  $\chi_{AB}$  resulting in a higher interdiffusion probability. The interface strength is expected to increase with higher interpenetration of the chains and the fracture energy  $G$  is argued to be proportional to the square of the interface thickness  $d_\infty$  which also corresponds to an inverse relationship with  $\chi_{AB}$  according to Wool (Eq.(16)) [13], [27]. Furthermore, based on studies of molecular dynamics, the interdiffusion region appears to be strongly dependent on temperature, contact time and molecular weight as well [4]. This will be addressed more specifically in the Section ‘Polymer entanglement’.

$$G \sim d_\infty^2 \sim \frac{1}{\chi} \quad (16)$$

Elastomers and thermoplastics differentiate in properties which also requires consideration when addressing interdiffusion. Non-cross-linked elastomers can adhere through tack which is caused by dispersive forces across the interface and long chains diffusing. For amorphous or semi-crystalline polymers heating above the glass transition temperature is required to activate interdiffusion. This phenomenon is referred to as welding or crack-healing [9]. However, when an elastomer containing a crosslinking agent is adhered to a thermoplastic, interdiffusion and crosslinking enter into competition. During adhesion, molecular chains diffuse and this process is slowed down by the formation of crosslinks. If crosslinking occurs too fast, adhesion will be limited as the chains are immobilised [28].

### Polymer entanglement

Strong adhesion between polymers can be reached due to physical crosslinking. Entanglements are physical crosslinks created by the interpenetration of molecular chains and subsequently determine rheological, dynamic and fracture properties [27]. Even low interpenetration, with modest ‘intermingling’, can cause a significant adhesion increase.

The proposed interdiffusion phenomenon of chain entanglements is controlled by polymer chain dynamics. A theoretical approach for the molecular dynamics of polymers was given by De Gennes and this was extended by Doi and Edwards, and Graessley [10], [13]. This approach considers a polymer chain in concentrated solutions and melts as being constrained in a tube. The polymer molecule is represented as a chain with a random coil formation which is trapped in an environment of fixed obstacles [10]. The entrapped molecule moves out of the tube by wriggling in a snake-like manner and therefore this motion was named ‘reptation’. When 70% of the chain has moved out of the tube, the reptation relaxation time is reached. The interphase region created during this relaxation time increases in width with time [13]. Furthermore, the reptation relaxation time was found to vary with molecular weight ( $M_w$ ) as  $M_w^3$  [10].

The reptation model is only valid for long chains which are able to entangle. In practice, this corresponds to polymers with  $M_w \gg M_{w,c}$ . Here,  $M_{w,c}$  refers to the critical entanglement molecular weight, i.e. molecular weight at which entanglement occurs [10], [13]. Below  $M_{w,c}$  no entanglements are possible which will lead to low practical adhesion ( $\sim 1 \text{ J/m}^2$ ) [10].

For EPDM, Ruch et al. [29] found that the elastomer chains diffuse much slower than expected during autohesion. Normally, at the interface between similar elastomers, chains diffuse very rapidly at temperatures needed for crosslinking, generally above  $120^\circ\text{C}$ , causing complete healing of the interface before immobilising the chain by crosslinking. However, slow diffusion for EPDM at curing temperatures was found which was believed to be caused by the high degree of entanglements due to branched chains within EPDM.

### 2.2.1.5 Chemical Bonding

Chemical bonding entails intermolecular forces acting at the surface between polymers. These chemical bonds are classified as primary bonds, whereas physical interactions, e.g. van der Waals, are secondary force interactions [10]. The difference between primary and secondary interactions stems from the bond energy of each type. Covalent bonds have a strength ranging from 100 to 1000 kJ/mol. For example, carbon-carbon (C-C) bonds have a bonding energy of 352 kJ/mol. However, van der Waals interactions and hydrogen bonds do not exceed 50 kJ/mol [10]. In Figure 5, chemical bonding is represented at a polymer-polymer interface. These chemical bonds do not necessarily concentrate at the interface, but may also occur after molecular chain penetration, i.e. located in the polymer interphase region.

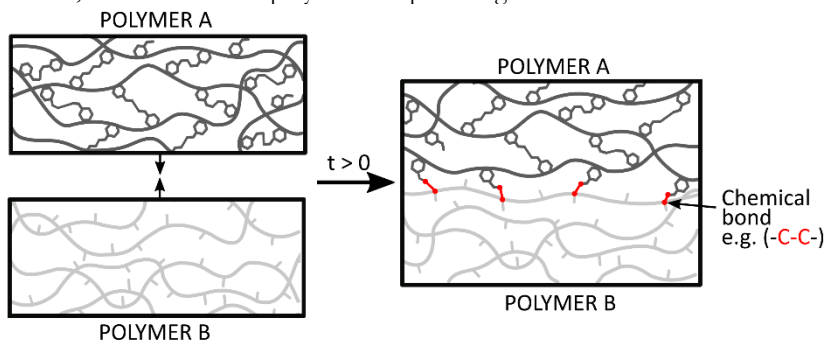


Figure 5: Chemical bonding at a polymer-polymer interface.

Primary bonds can consist of covalent or ionic bonds. These bonds are well reported in literature and their contribution to the adhesive strength has been proven to be significant [10]. Gent and Ahagon [10] even evidenced a linear relationship between intrinsic peel energy and the surface concentration of silane coupling agents leading to more interfacial covalent bonding between a glass substrate and a cross-linked elastomer which improved the adhesive strength severely. Similarly, the interfacial strength between two cross-linked polyethylene sheets, containing dicumylperoxide (DCP) as curing agent, showed a linear relationship with the number of bonds per unit interfacial area as long as this did not exceed  $1 \times 10^{13}$  bonds/cm<sup>2</sup> [10]. It is also reported in literature that a maximum adhesion strength is reached when increasing the number of bonds at the interface and when this maximum is surpassed adhesion strength decreases due to a concentration of mechanical stresses at the interface [8]. For adhesion at EPDM joints, Ruch et al. [29] indicated that when crosslinking at high temperature of both EPDM phases occurs, interdiffusion and co-crosslinking proceed simultaneously and are competitive.

Specifically for the thermoset rubber-thermoplastics combination, studies have shown that chemical bonding can be established at the interface due to the crosslinking process which is often referred to as co-vulcanisation. Mutsuda and Komada investigated pol(oxy-2,6-dimethyl-1,4-phenylene) (PPE) adhesion to rubbers and reported peroxide radicals in the rubber causing hydrogen abstraction on the thermoplastic creating interfacial chemical C-C bonds due to a recombination of polymer radicals [30]. Thus [4] also indicated co-vulcanisation by C-C bonding between HNBR and polyamide 6.6 (PA6.6) due to the presence of peroxide crosslinking agents.

#### 2.2.1.6 Weak boundary layer

Bikerman first described the weak boundary layer theory with ‘weak boundary’ referring to a cohesive weak layer in the interfacial region [15]. This weak layer causes an interface which fails at low stress or with a low fracture energy. This phenomenon can originate from the adhesive, the adherent, the environment, or a combination of these three factors. A specific representation of the types of weak boundary layers according to Bikerman is given in Figure 6 and contains following classes: air pores, impurities at the interface, reactions between component and medium. This can result in a lower cohesive strength at the interface and subsequently, can cause a lower adhesive bond than expected [11], [13], [15].

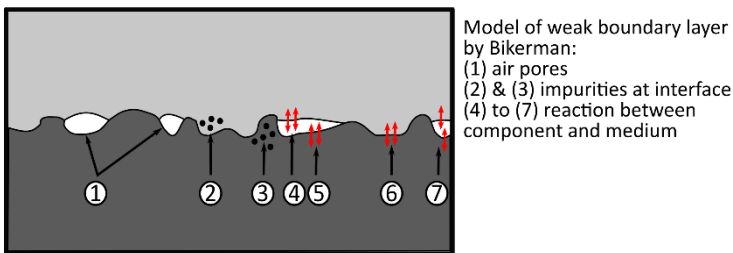


Figure 6: Weak boundary layer theory according to Bikerman [31].

Polymers often contain a range of additives like antioxidants, processing aids, plasticisers and fillers. Especially, elastomers consist of complex formulations. As discussed, polymers tend to be incompatible due to a positive free energy of mixing. Similarly, for polymers containing additives, the entropy term will be low and the enthalpy will likely be positive, rendering the system thermodynamically unstable. This might cause the additive to migrate out of the polymer or to localise at the interface [13]. Generally, all low molecular weight components, i.e. additives or fractions of the polymer itself, might concentrate at the interface and this usually occurs during solidification processes. For example, polyethylene contains low molecular weight constituents which may cause a weak boundary layer at the interface creating low adhesion strength [11].

### 2.2.2 Adhesion failure mechanism

Polymers which are adhered through an adhesion mechanism or a combination of adhesion mechanisms can fail in two ways upon separation. First, adhesive failure between two polymers can occur at the interface between both materials due to an interfacial bond failure. Second, a cohesive failure indicates a failure in the bulk of one of the adhering polymers, e.g. in polymer A. Upon failure, a layer of polymer A remains on the surface of polymer B. In Figure 7, a schematic of these bond failure modes is represented. Ideally, 100% cohesive failure is created as this indicates a failure strength equal to the polymer bulk strength [11], [32]. However, often only partial cohesive failure is reached, leading to only a percentage in coverage of the surface of polymer B. Furthermore, when a weak boundary is present at the interface, for example due to voids at the interface, the actual adhesion mechanism between the two considered materials could be concealed. Therefore, complete wetting (intimate contact) and avoidance of a weak boundary layer is important for a precise adhesion failure mechanism evaluation [15].

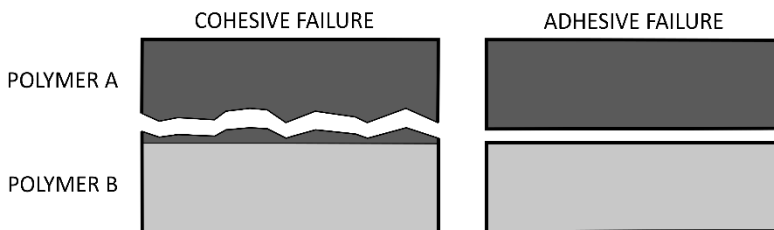


Figure 7: Bond failure modes: cohesive failure (left) and adhesive failure (right) between polymer A and polymer B.

Despite the possibility of evaluating the failure mode, defining the interfacial strength is still a more adequate criterion. Furthermore, in case of interdiffusion, the fracture strength depends on the length of interdiffused chains at the interface. When only short chain lengths are involved, i.e. low molecular weight ( $M_w < M_{w,c}$ ), chain pull-out is most likely to occur. The interface is then accompanied by a weak interface which can also be described as a two sides being “nailed” together. The fracture energy during chain pullout can be influenced by surface roughness, inter- and intramolecular interaction, e.g. Van der Waals forces. When entanglements at the interface between two polymers are enabled, fracture can occur through chain pull-out or disentanglement. This entails an intermediate molecular weight that is involved in interdiffusion ( $M_w > M_{w,c}$ ). However,

at a molecular weight  $M^*$ , the chain molecules can become too large to disentangle. Thus, for high molecular weight ( $M_w > M^*$ ), bond rupture, or chain scission, is the dominant mechanism of fracture [13]. Chain scission is also the prevailing mechanism when two polymers are chemically bonded at the interface, irrespective of the molecular weight [10].

For polymer-polymer welding, Da Silva et al. [13] describe the initial interdiffusion as being rapid over a short length, i.e. low molecular weight has diffused, making chain pull-out the dominant fracture mechanism. However, for diffusion over long times during welding, bond rupture dominates, indicating a fully healed weld.

### 2.2.3 Surface and interface characterisation

To acquire a full understanding of the polymer-polymer adhesion mechanism, supporting surface characterisation is often performed. Possible techniques include time-of-flight ion mass spectrometry (ToF-SIMS), X-ray photoelectron spectroscopy (XPS), atomic force microscopy (AFM), scanning electron microscopy (SEM), Raman spectroscopy, attenuated total reflectance Fourier transform infrared spectroscopy (ATR-FTIR) and optical contact angle analysis. Numerous studies have applied these techniques to analyse surface properties like roughness, chemical composition and surface free energy [8]. However, depending on the applications and research question, different approaches in terms of characterisation are needed. Based on available literature and the focus on EPDM-thermoplastic adhesion in 2K injection moulding the following techniques are addressed in more detail: SEM coupled with Energy Dispersive X-ray spectroscopy (EDX), Raman spectroscopy, ATR-FTIR, AFM and contact angle analysis.

#### 2.2.3.1 SEM-EDX

SEM is a well-known technique used to investigate conductive surfaces by electron scattering. For polymers, the surface is made conductive by applying a coating. A focused electron beam scans the sample surface and this electron bombardment leads to the emission of secondary electrons (SE), backscattered electrons (BSE), element specific X-Rays and Auger electrons. Depending on the specific detector, characterisation of the surface topography, morphology or chemical composition can be given [33], [34].

The SE and BSE signals are usually analysed to image the sample, with SE providing information of sample morphology and topography, and BSE indicating contrasts in multiphase systems (due to a contrast in atomic numbers). However, for polymers the resolution in BSE signals is low as the atomic numbers are low and there are no large differences among polymer types. With Energy dispersive X-ray spectroscopy (EDX), X-rays emitted from the surface can be coupled to SEM analysis to get information about the chemical composition of a material. During measurement, the electrons of a sample are excited by an electron beam, which causes emission of X-rays with a specific energy. The energy of the emitted X-ray is element specific making a quantitative and qualitative analysis possible. For polymer materials a thin conductive coating is necessary for successful electron imaging [33], [35]. SEM is normally performed under high vacuum to eliminate air molecules which interfere during measurement. However, low vacuum SEM enables analysis of non-conductive materials such as polymers as residual gas molecules are ionized within the chamber, neutralising the negative charge which forms on non-conductive samples [36]. This low vacuum SEM-EDX technique was applied by Enganati et al. [37] for polymer adhesion analysis. The authors performed line scan

measurements along the interphase region to analyse sulphur diffusion from the rubber matrix to a resorcinol-formaldehyde-latex (RFL) adhesive. The sulphur counts from the line scan indicated a significant higher sulphur content in the RFL phase than in the rubber phase which only arose after the curing process, evidencing a sulphur migration during curing. Results gave a better understanding of the chemistry in the interphase region and possibility of interdiffusion of rubber components towards the adhesive.

### 2.2.3.2 Raman spectroscopy

Raman spectroscopy is a vibration spectroscopic technique. With a strong monochromatic laser source, the sample can be excited which causes light to be re-emitted or inelastically scattered from the excited molecules [34]. Thus, photons interact with a molecule which elevates it to a higher energy state. When the molecule relaxes from this high energy state to a vibrational energy level different from its original state a difference in energy is created. The energy difference between the incident photon and the scattered photon is called the Raman shift. Two types of scattering can occur: (1) Stokes scattering or (2) anti-Stokes scattering.

- (1) Stokes scattering indicates a scattered photon having a higher vibrational energy than the incident photon;
- (2) anti-Stokes scattering indicates a final energy state which is lower than that of the incident photon.

Thus, Raman spectroscopy focusses on changes in molecular bond polarisability due to specific energy transition. This enables analysis of bonds between homonuclear atoms like carbon-carbon or sulphur-sulphur which cannot be detected by FTIR [34], [38].

Bruckmoser et al. [39] investigated the potential of Raman spectroscopy to detect interdiffusion in 2K injection moulded parts. The material combinations of interest were thermoplastic with thermoplastic and thermoplastic with styrene based thermoplastic elastomer (TPE-S). Line scans were performed perpendicular to the interface over a distance of  $\pm 5 \mu\text{m}$  and a step size of  $1 \mu\text{m}$ . Depending on the material combination, interdiffusion lengths of  $1 \mu\text{m}$  to  $3 \mu\text{m}$  were found. However, the spatial resolution limit of  $1 \mu\text{m}$  disabled characterisation of the interdiffusion below the micrometer range.

### 2.2.3.3 ATR-FTIR

ATR-FTIR is, like Raman spectroscopy, a vibration spectroscopic technique. However, in contrast to Raman, IR is sensitive to changes in dipole moment instead of changes in polarisability. ATR-FTIR is used as surface characterisation technique which is sensitive to functional groups. Thus, this can provide information about the curing reactions in elastomer samples, but also about the chemical composition at the sample surface, e.g. to analyse sample degradation [40]. Especially when modifications are made to the sample composition or surface, ATR can be of interest. With ATR, the sample is put in contact with a crystal, e.g. diamond, zinc selenide or germanium, and the absorption of the evanescent wave is measured. Specifically, an IR beam is directed on a crystal with a high refractive index which causes a reflection of the IR beam on the internal surface of the crystal, i.e. where it is in contact with the sample, creating an evanescent wave orthogonally into the sample. The wave only protrudes by a couple of microns (0.5-5) into the sample and the sample can absorb energy causing an attenuated wave. Afterwards, the attenuated energy of each wave is retrieved in the original infrared beam which returns to the detector [32], [34], [41].

### 2.2.3.4 AFM

Atomic force microscopy (AFM) is a characterisation technique consisting of a microcantilever probe enabling measurement of interactions with the specimen surface. Consequently, micromechanical properties are analysed. A specific AFM technique is force modulation microscopy. This technique monitors the cantilever oscillation and accompanying damping due to energy dissipation. Thus, hard/soft surfaces can be analysed because a hard surface causes weak damping while a soft surface provides strong damping. When the stiffness of the cantilever is known, specimen stiffness can be determined as well [34].

Mutsuda et al. [30] used viscoelastic atomic force microscopy at the interface between thermoplastic PPE and thermoset rubbers styrene butadiene rubber (SBR) and EPDM. By AFM, a layer could be observed containing a viscoelasticity between that of PPE and SBR or EPDM. The thickness of this layer was related to the interdiffusion layer between PPE and the thermoset rubber. Thus, AFM can be used to characterise the diffusion width at a thermoset rubber-thermoplastic interface.

### 2.2.3.5 Contact angle analysis

Contact angle analysis during wetting has been extensively studied and reviewed in literature with regards to static and dynamic spreading, solid surface tension and surface heterogeneities [16], [20], [42]–[45]. Several studies have investigated the relationship between surface energies, calculated from wetting theories, and the strength of polymer joints [6], [18], [46]. For example, the Van Oss model, as wetting theory, divides the surface tension in Lifshitz-van der Waals (LW) (i.e. London dispersive forces), acid (+) and base (-) components which can be derived from measurements with reference fluids with known surface energies, e.g. water, ethylene glycol, and diiodmethane, at room temperature [47]. Then, the interface tension between two combining polymers can be defined by (Eq. (17)) and this parameter indicates the work required to increase a unit of area between two surfaces in contact. Thus, a lower interface tension enables better wetting.

$$\gamma_{SL} = \left( \sqrt{\gamma_S^{LW}} - \sqrt{\gamma_L^{LW}} \right)^2 + 2 \left( \sqrt{\gamma_S^+} - \sqrt{\gamma_L^+} \right) \left( \sqrt{\gamma_S^-} - \sqrt{\gamma_L^-} \right) \quad (17)$$

However, for interface characterisation, it is important to perform contact angle analysis in close-to-processing conditions. For example, the surface energy components of a polymer melt are temperature dependent. For 2K injection moulding, this entails evaluating wetting at high temperature, i.e. spreading of a polymer melt on solid substrate in a heated chamber. Then, the contact angle can be a direct measure for wetting which can be referred to as direct contact angle measurements. Bex et al. [6] compared two wetting methodologies: (1) direct contact angle measurements of molten thermoplastics on rubber substrates, and (2) calculation of wetting parameters (Van Oss model) from surface energy components for both materials in solid state (i.e. room temperature). The direct contact angle measurements indicated good wetting of EPDM by PP and PE, while NBR was best wetted by PC. Injection moulding also induced adhesion for these material combinations. However, wetting parameters were not in agreement with injection moulding results as good wetting behaviour was calculated for PP on both EPDM and

NBR. This was attributed to the low surface energy of PP [6]. Furthermore, no equilibrium contact angles were reached. Hence, no minimum contact angles could be defined to ensure in-process adhesion.

To determine the wetting parameters at high temperature, pendant drop shape analysis can be executed on a polymer melt droplet pending from a syringe. Pendant drop is a drop shape analysis as shown in Figure 8a. At equilibrium, the Young-Laplace equation (Eq.(18)) can be applied to calculate the surface tension of the polymer melt.

$$\gamma \left( \frac{1}{R_1} + \frac{1}{R_2} \right) = \Delta P \equiv \Delta P_0 - \Delta \rho g z \quad (18)$$

where  $R_1$  and  $R_2$  are the principal radii of curvature at a point P, with  $R_1$  measured in a drop cross-section that includes the z-axis and  $R_2$  measured in a plane perpendicular to the former (x-z) [48].  $\Delta P$  is the Laplace pressure across the interface, and  $\Delta \rho$  is the density difference between the drop phase  $\rho_d$  and the continuous phase  $\rho$ . The Laplace pressure can be rewritten as the difference between a reference pressure  $\Delta P_0$  at  $z = 0$  and the hydrostatic pressure  $\Delta \rho g z$  [49]. To define a good fitting accuracy during pendant drop analysis, Berry et al. [49] defined the Worthington number ( $W_o$ ) which is a non-dimensional quantity, scaled 0 to 1 and calculated according to Eq. (19):

$$W_o = \frac{\Delta \rho g V_d}{\pi \gamma D_n} \quad (19)$$

The  $W_o$  takes the effect of the droplet volume into account. When a droplet is close to the point of detaching from the needle, it is close to its critical volume. Then, the most accurate pendant drop shape analysis can be retrieved as  $W_o \sim 1$  [49]. Based on Eq. (19)  $W_o$  can be defined with  $V_d$  as the droplet volume and  $D_n$  the needle diameter. For polymer melts, after reaching the critical droplet volume, gravitational effects will become too large, causing necking as shown in Figure 8b. The droplet will elongate until contact with the solid substrate is reached. Then, after detachment a sessile droplet forms from which equilibrium contact angles can be determined as shown in Figure 8c. Eventually, the final contact angle and polymer melt surface tension enable calculation of  $W_d$  and S according to Eq. (11) and Eq. (13).

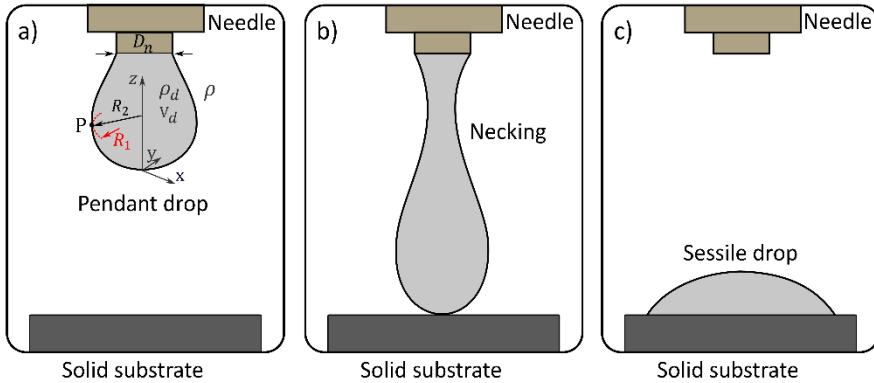


Figure 8: Drop shape analysis of polymer melt on a solid substrate as pendant drop (a), necking drop (b), sessile drop (c).

Zhang et al. [23] elaborated the spreading dynamics of molten polymer drops on glass substrates by subsequent pendant drop, droplet deposition and monitoring the sessile droplet. Furthermore, Fuentes et al. [18] calculated the work of adhesion and the spreading coefficient of glass and polymers PP, polyvinylidene fluoride (PVDF) and maleic anhydride-grafted polypropylene (MAPP) at room temperature and in molten state. A good correlation was found between  $W_a$  and practical adhesion at room temperature for PP and PVDF glass fibre systems. For the polymer melts on glass substrates, wetting parameters ( $W_a$  and  $S$ ) only marginally corresponded with the accompanying practical adhesion values due to other factors playing a role like chemical bonding, hydrogen bonding, entanglements and polymer matrix strength. While PVDF seemed to be the best choice at room temperature, at high temperature PVDF gave the most negative spreading coefficient, i.e. spontaneous wetting on the glass substrates is unlikely. The difference in results at room temperature and high temperature was ascribed to the fact that surface energies of the polymers in processing condition attribute to wetting, but the surface properties in solid state contribute to interfacial strength. Vera et al. [50] evaluated the work of adhesion between melted polymers PP, ABS and PC on coated and uncoated steel mould surfaces. Regardless of the substrate, PP gave higher values than PC and ABS. Due to the good wettability with PP, the authors recommended this polymer for good impregnation of the mould cavity.

When a liquid wets a solid substrate, spreading usually occurs through a physical process leading to an increase of the liquid coverage area in time after droplet deposition [20]. This process is referred to as non-reactive wetting as no reaction between the liquid and substrates occurs. However, chemical reactions between the liquid and solid substrate can also alter the solid/liquid interface and consequently the wetting process [20], [51]. Reactive wetting is well reported in metal-metal joining processes like brazing and soldering, or in metal-ceramic processes [52]–[54]. In contrast, information about reactive wetting triggered by a polymer melt is limited in literature. In studies by Grundke et al. [7], [55], the wetting kinetics of unmodified and chemically modified polypropylene melts on untreated and aminosilane-treated glass fibers were characterised, evidencing the role of physical or chemical interactions at the interface [55]. Furthermore, an interfacial chemical reaction was created between a maleic anhydride copolymer melt and

poly(aminosiloxane) surface during wetting which acted as an additional driving force for the spreading process [7]. Similarly, Fuentes et al. [18] observed a reduction in static contact angles with increasing maleic anhydride (MA) content in molten MAPP/PP blends which was explained by covalent bonding between the MA groups and the glass substrate.

#### 2.2.3.6 Mechanical testing

After inducing adhesion at the polymer-polymer interface, direct adhesion measurements can be executed to evaluate the practical adhesion strength. Several methods are discussed in literature [8], [11], [15], but for 2K injection moulding tensile tests, peel tests, and shear tests are the most common [3], [4], [56]–[58]. The applicability of a certain adhesion strength test depends on the specific design and geometry of the 2K specimen. For the presented thesis, specimen geometries are created using the moulds developed by Bex et al. [3] which reduces tests of interest to tensile testing (1), peel testing (2), and shear testing (3):

- (1) Tensile testing entails an evaluation of adhesion strength by applying a load perpendicular to the bond line and in centre of the bond area. The stress is then obtained by dividing the load by the loaded area [13]. The disadvantage of this type of test is that the average stress at failure is reported, but the actual stress distribution at the interface is non-uniform, especially for hard-soft combinations. These material combinations exhibit a mismatch of stiffness and Poisson ratio which enables debonding near the edges. Thus, during testing the soft component narrows near the interface. Specifically, higher tensile stresses are reached near the edges than in the centre of the specimen [15]. Consequently, fracture almost always occurs near the interface, either cohesively or adhesively, and the resulting adhesion strength is not an intrinsic property. However, adhesion strength can still be evaluated with tensile tests per specific geometry for comparative tests as it is a property of a specific system [3].
- (2) Peel testing consists of a procedure during which a flexible adherent is peeled of a rigid adherent at a fixed rate and constant angle. Standard measurements involve a peel angle of 90° or 180° with measurements starting at the open end of the bond and a progressive peeling along the length of the rigid adherent [34]. The peel strength is usually reported as peel force per unit of width. Results from peels test depend on the thickness of the components, their elastic properties and the peel rate. Therefore, testing conditions need to be reported at all times.
- (3) Shear testing can be executed under tensile or compression loading. Often, samples for shear test most resemble the geometry of adhesive bonds in practical applications. Shear testing involves several possible specimen geometries with each having a standardised testing procedure. The shear test of interest for this thesis is ISO 10123 which describes a specimen with a pin geometry being bonded inside a collar. During testing, the pin is pressed through the collar which rests on a support cylinder. Results of this shear test procedure are reported in force required to initiate failure divided by the bond area [10].

## 2.3 Thermoset rubber composition and adhesion

Thermoset rubbers are vulcanised elastomers with the ability to be reversibly deformed, which is referred to as elasticity. In contrast to thermoplastics, thermoset rubbers contain crosslinks which are induced by a vulcanisation process. These rubbers are used under conditions above their glass transition temperature ( $T_g$ ), and this  $T_g$  for rubbers is far below room temperature. The vulcanisation process causes a random elastomer chain configuration to become three-dimensional due the formation of junctions, i.e. crosslinks. Then, during deformation, a reduction in entropy is created due to fewer available conformational states and no chain slippage can occur as the polymer chains are linked. Afterwards, when the deformation force is removed, the polymer chains return to their equilibrium state with high entropy [59], [60].

Elastomers find their origin in a natural substance from the tree *Hevea Braziliensis*. However, from the early 20<sup>th</sup> century the development of synthetic rubbers started. Based on their performance and price, rubbers can be classified in three groups ranging from low to high performance and cost as following: general purpose rubbers, special purpose rubbers and specialty rubbers. Furthermore, hydrocarbon-based rubbers have low oil resistance and depending on the number of unsaturations in the polymer chain heat resistance can be defined, i.e. low amount of unsaturations gives higher temperature resistance. With regard to the envisaged applications which require resistance to high temperatures, chemical environments and/or mechanical strains, special purpose rubbers are of interest. Examples of special purpose rubbers are nitrile rubber (NBR) and EPDM. NBR offers oil resistance, while EPDM is more suited for exposure to polar chemical environments. Furthermore, EPDM has higher heat resistance as it has no double bonds in the polymer backbone, providing also good resistance to oxygen, ozone and UV [61].

Rubber compounding entails selecting various ingredients at a specific quantity, i.e. a formulation, mixed into a compound which needs to abide to the following requirements: suitable for processing, good final properties, and competitive pricing [61]. Furthermore, health, safety and environment are becoming important considerations as well. Ingredients in rubber formulations are quantified by the unit ‘parts per hundred parts of rubber’ (phr) with hundred parts of rubber referring to the raw rubber. The ingredients within the formulation can be classified as raw gum polymer, filler system, plasticiser system and curing system. Often stabilisers are added as well to avoid degradation. The main ingredients and their importance in rubber adhesion, specifically for EPDM, are addressed in more detail.

### 2.3.1 EPDM composition

EPDM is the most widely used special purpose rubber and has worldwide production of approximately 1,150 kilotons [62]. It is an olefin based copolymer of ethylene and propylene. This copolymer exhibits strength, flexibility, and elasticity which enables it to be classified as an elastomer [61]. To improve reactivity, a third unsaturated monomer, e.g. ethylidene norbornene (ENB), is added which results in the terpolymer ethylene-propylene-diene monomer. In Figure 9, the structure of EPDM is represented (ChemDraw Prime, PerkinElmer). Based on the weight percentages of the three units in EPDM, grades are defined. An EPDM grade is usually selected based on the required properties for an application. Besides the EPDM grade, additives like fillers and plasticisers are added to the EPDM composition. Fillers with reinforcing capabilities are required in EPDM as it lacks raw elastomer strength. Plasticisers are added to reduce

compound viscosity and/or to improve processing. Depending on the requirements, an EPDM grade, filler and plasticiser need to be selected, which can influence the adhesion with thermoplastics during 2K injection moulding. Therefore, these three components are discussed in further detail.

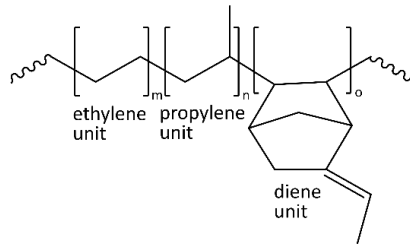


Figure 9: EPDM structure containing an ethylene, propylene and diene unit.

### 2.3.1.1 Macromolecular structure

The properties of EPDM strongly depend on the specific structure of this terpolymer (Figure 9), including ethylene/propylene ratio, diene content and the molecular weight, creating a high range of applications [59]. In EPDM, non-conjugated dienes are incorporated as third monomer to add unsaturations to the polymer. The most commonly used diene is 5-ethylidene-2-norbornene (ENB), as it provides fast cure rates, and the diene level can range from 0.5 to 12 wt% [59], [63], [64]. In Figure 9, ENB is shown as diene unit in EPDM. The diene offers one double bond for copolymerisation with ethylene and propylene, while reserving the other double bond for vulcanisation in the EPDM side chain, enabling sulphur vulcanisation. The ENB structure with the two dienes and allylic hydrogen atoms which are easily abstractable is presented in Figure 10 (ChemDraw Prime, PerkinElmer). For peroxide curing, the dienes can increase crosslinking efficiency [59]. Orza [59] stated that increasing the ENB level increases the contribution of addition during chemical crosslinking. Furthermore, Naskar et al. [65] reported in-situ compatibilisation of PP and ENB-EPDM due to occurrence of PP-ENB EPDM graft-links. Thus, co-vulcanisation at the EPDM-thermoplastic interface during 2K injection moulding may be influenced by ENB content as well.

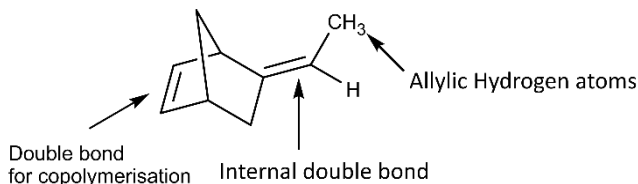


Figure 10: Structure of 5-ethylidene-2-norbornene (ENB).

Ethylene contents in EPDM grades can range from 40 to more than 75 wt%. Below 55 wt% ethylene, the copolymer has an amorphous morphology, while ethylene contents above 60 wt% show crystalline domains due to the long ethylene sequences. These partially crystalline domains can influence the elastomer's mechanical strength due to formation of reversible physical crosslinks [59], [64]. Furthermore, high ethylene content can increase crosslinking efficiency and reduce chain scission as there are less tertiary hydrogen atoms from propyl groups [63]. Avalos et al. [66] studied the effect of ethylene

content on the properties of PP/EPDM blends. Higher crosslink densities were found with higher ethylene content. Al-Juhani et al. [67] found a compatibilising effect by EPDMs with different structures and PP/LDPE blends as the ethylene and propylene blocks in EPDM might enhance miscibility with PP or PE. A certain degree of miscibility between EPDM and PP was also denoted by Xiao et al. [68] due to an interpenetration between the non-crystalline part of PP and the interface of EPDM. Ma et al. [69] reports strain induced crystallisation of the polyethylene segments in organoclay/EPDM nanocomposites with high ethylene contents. Linova et al. [70] studied the structure of the interfacial interaction zone in EPDM/NBR. They found that EPDM with high ethylene content caused the most crosslinks in the interfacial layer. Additionally, the influence of increasing the ethylene content and ENB level on elastomer curing and mechanical properties is well reported in literature and by EPDM raw polymer producers. [59], [61], [63], [71]–[73]. With high ethylene content, better temperature stability is provided and higher tensile and tear strengths, and hardness is reached. A higher ENB content results in higher modulus, lower compression set and better oil resistance [63].

Molecular weight ( $M_w$ ) and molecular weight distribution (MWD) are important measures of rheology of an EPDM. Crowther [74] indicates improved interdiffusion between rubbers as molecular weight decreases. Furthermore, Thust [4] studied the adhesion between HNBR and PA6.6. During the overmoulding process, interdiffusion was presumed dominant at the interface and a lower molecular weight HNBR, with accompanying higher chain mobility, appeared to promote adhesion. Furthermore, differences in raw polymer macromolecular structure, i.e. higher acrylonitrile content (ACN), caused a lower crosslinking efficiency and crosslink density due to the electron withdrawing effect of ACN. This low crosslink density improved mobility of HBNR molecules and subsequent interdiffusion of the polymer chains into PA6.6.

### 2.3.1.2 Rubber fillers

EPDM is a rubber which can be highly loaded with reinforcing fillers, e.g. clays, silicas and carbon black. With these fillers, high tensile and tear properties can be achieved. Reinforcing fillers in rubbers are characterised, in contrast to plastic reinforcement, by the ability to improve two antagonistic properties, i.e. modulus and deformation at break [61], [75].

One of the most widely used and efficient fillers is carbon black. Filling elastomers with carbon black also reduces cost and changes electrical and optical properties. Carbon black consists of aggregates which are composed of primary particles. These primary particles are composed of stacks of graphene sheets [76]. Aggregates that are clustered together form an agglomerate which are held together by Van der Waals forces. The different carbon black morphologies are shown in Figure 11. However, these agglomerates usually break up during mixing. Furthermore, the reinforcing properties of carbon black are mainly determined by particle size, i.e. specific surface area, and degree of aggregation, i.e. structure. When particle size decreases, dispersion within the rubber is improved and better reinforcement is created. Based on ASTM D 1765, carbon blacks are characterised by a letter 'N', i.e. normal curing, or 'S', i.e. slow curing, followed by a three digit suffix. The first number refers to particle size and two other numbers are randomly selected, e.g. N772 [75], [77]. The particle size defines the surface area. This is a morphological characteristic that defines the interaction possibility between elastomer

and filler surface. Furthermore, the structure of carbon black refers to the irregularities in shape of aggregates and a higher structure leads to a better dispersion [75], [77].

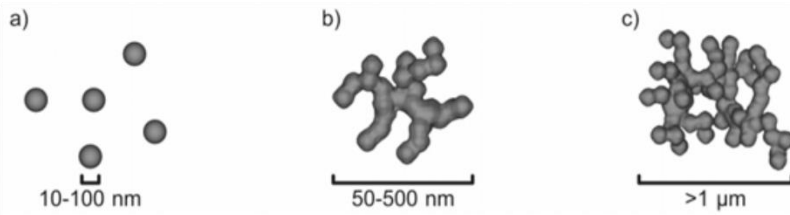


Figure 11: Carbon black primary particle (a), aggregate (b), agglomerate (c) [78].

In the filled elastomer matrix, entanglement of rubber molecules on the carbon black plays an important role at the rubber-carbon black interface. For EPDM, chain molecules can physically adsorb on the surface of carbon black and the higher EPDM-carbon black interfacial area improves the reinforcement. Zhang and Chen [79], explained the entanglement of rubber chains in voids of carbon black aggregates, with elastomer chains becoming immobilised and forming a shell surrounding the carbon black. These covered carbon black particles are considered as physical crosslinks limiting chain mobility and retaining the rubber deformation. Furthermore, a higher carbon black surface area increases entanglements with rubber chains. Rubber can also chemically bond with functional groups present on carbon blacks, e.g. sulphur, increasing the amount of chemical crosslinks. According to different sources, carbon black can both positively (1) or negatively (2) affect adhesion or properties at interfaces: (1) A study on carbon black reinforcement of natural rubber-based adhesives and sealants indicated that cohesion forces are enhanced by higher specific surface area carbon blacks due to network entanglements or mechanical interlocking forces [80]. (2) For the adhesion of 2K polyurethane (PUR) and ABS, addition of carbon black had a negative effect and higher volume contents in PUR led to further adhesion reduction with ABS because intermolecular H-bonding in PUR competes with interfacial H-bonding [81]. Furthermore, Chookaew et al. [82] investigated weldline strength in injection moulded rubber parts and found that natural rubber had reduced weldline strength due to differences in curing properties and a decreased tack when adding carbon black.

Kaolin clay, or hydrous aluminum silicate  $[Al_2Si_2O_5(OH)_4]$ , is another widely used filler type for all types of rubber compounds as it provides good reinforcement at a moderate cost and good processability. Clay fillers are usually added between 20 to 150 phr [61]. Compared to carbon black, kaolin filler is also much safer in terms of health and environment. Furthermore, kaolin provides a smooth finished surface, high thermal stability, good compression set, and high resistance to chemical environments and weathering [83]. When heat treating kaolin, eliminating water in the kaolin clay, calcined kaolin consisting of smaller particles is created. Calcined clay offers very good compression set in compositions without carbon black. A finer particle size of kaolin is preferred for reinforcement of physical properties. Sheikh et al. [84] found that kaolin filler acted as highly reinforcing for EPDM, but optimum cure time and cure rate were adversely affected. This reinforcing affect could influence the interfacial strength during multi-component injection moulding as well. Furthermore, the lower cure rates might promote the interdiffusion mechanism.

### 2.3.1.3 Rubber plasticisers

Plasticisers like oils and esters are added to reduce compound viscosity and/or to improve processing. Oils are added to non-polar rubber while ester plasticisers are more suited for polar rubbers due to their mutual compatibility. The largest consumer of ester plasticisers are NBR rubbers, while EPDM favours oils. When oils are added to the rubber compounds, they are referred to as process oils. Oils added to the rubber main polymer are called extender oils. The three main oil categories are: paraffinic, naphthenic, and aromatic. Good compatibility with the rubber compound is of high importance to avoid migration out of the compounds, e.g. to the substrate surface, which may cause loss of physical properties or deterioration of multicomponent systems. Whether good compatibility between the polymer system and oil can be reached depends on oil properties such as viscosity, molecular weight, and molecular composition. Often, there is a trade-off between filler content and oil content. For example, to maintain hardness within a rubber sample 1.3 phr process oil is needed with the addition of 1 phr carbon black which has reinforcing properties; with less reinforcing carbon black, addition of 0.7 phr may suffice [61], [74], [75], [85].

Plasticisers like oil can reduce the entanglement density in rubber due to a diluting effect. This may facilitate diffusion across the interface but also might induce more easily disentanglement upon deformation. Litvinov [86] found that EPDM/PP thermoplastic vulcanisates (TPV) network density decreased with increasing content of extended oil due to disentanglement of the polymer chains. Furthermore, studies on the distribution of processing oil in TPV have also been performed [87]. EPDM and PP both have good miscibility with paraffinic processing oils. For EPDM/isotactic PP (iPP), oil amounts were proportional to the EPDM and iPP volume fractions. During cooling and iPP crystallisation, oil tended to migrate out of the iPP phase, creating a semi-crystalline iPP phase, and amorphous iPP/oil phase and EPDM/oil phase in solid state.

### 2.3.2 Crosslinking methods

Elastomers in amorphous, un-crosslinked state exhibit a resistance to deformation which is directly proportional to the macromolecular entanglements. These entanglements are not permanent and therefore vulcanisation, also called curing or crosslinking, methods are used to reach dimensional stability within the rubber [88]. During crosslinking, chemical bonds are formed between the polymer macromolecular chains creating a three-dimensional network. Consequently, the rubber consists of a stable network which can be submitted to prolonged deformations [88], [89]. In the rubber vulcanisate network, besides chemical crosslinks, also physical crosslinks are present, such as hydrogen bonds, polar and dispersion forces between polymer chains, and intra and intermolecular entanglements as shown in Figure 12.

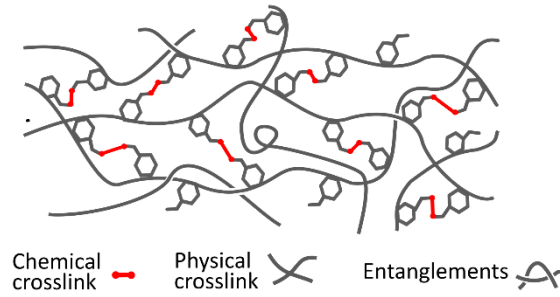


Figure 12: Crosslinked rubber network structure.

Several systems have been developed to cure elastomers, but currently the most common methods are peroxide and sulphur curing. Sulphur curing is used for crosslinking unsaturated elastomers by forming sulphidic crosslinks, while peroxides can cure both saturated and unsaturated elastomers by creating C-C bonds. Peroxide curing offers better heat stability due to the formation of these C-C bonds. These C-C bonds have a higher dissociation energy ( $\sim 352$  kJ/mol) than the sulphidic bonds formed during sulphur curing, giving them thermal stability and good resistance to thermo-oxidative aging. For sulphur curing, several sulphidic bonds may form, depending on sulphur curing composition, with bonding energies in increasing order: polysulphidic C-S<sub>x</sub>-C ( $x=3-6$ , 252 kJ/mol), disulphidic C-S<sub>2</sub>-C (268 kJ/mol), and monosulphidic C-S-C (285 kJ/mol) [88], [89]. Peroxide and sulphur crosslink types (ChemDraw Prime, PerkinElmer) are shown in Figure 13. Despite their lower heat resistance, sulphidic bonds have better physico-mechanical and dynamic properties and good resistance to dynamic fatigue than C-C crosslinks. This is due to their higher chain flexibility and ability to dissipate external stress by rearrangement. Specifically, during deformation sulphidic crosslinks are disrupted faster than C-C bonds which induces the formation of macroradicals. These macroradicals can create new crosslinks in regions with lower stress. Thus, a less stressed and stronger network is formed which enables good stress relaxation [89].

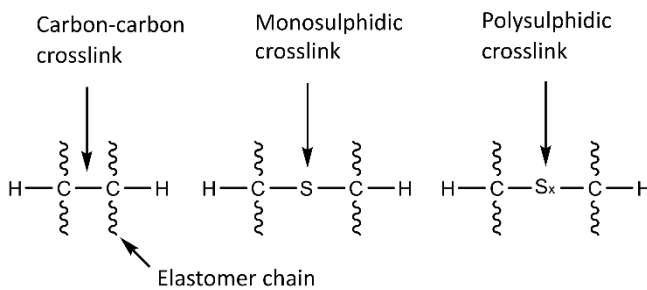


Figure 13: Peroxide carbon-carbon crosslink between carbon atoms of each elastomer chain, and monosulphidic crosslink and polysulphidic crosslink where a single or multiple sulphur atoms is linked to two elastomer chains respectively.

### 2.3.2.1 Peroxide crosslinking

Peroxide vulcanisation is a radical process initiated by peroxide decomposition causing further rubber crosslinking. Even though peroxide can cure both saturated and unsaturated elastomers, not all elastomers can be crosslinked with peroxides. In Table 2 rubbers and blends that can or cannot be cured with peroxides are listed [88], [90], [91]. Polymers that cannot be cured with peroxides exhibit degradation upon exposure to peroxide radicals as these radical can initiate a chain scission reaction.

Table 2: Elastomers and blends that can or cannot be to cured with peroxides [88], [90], [91].

Possible		Not possible
Polymers	Blends	Polymers
NR (natural rubber)	NBR/EPDM	ACM (polyacrylate rubber)
IR (polyisoprene rubber)	SBR/EPDM	IIR (butyl rubber)
BR (butadiene rubber)	PE/EPDM	CIIR (chlorobutyl rubber)
CR (chloroprene rubber)	PE/EVA	CO (epichlorohydrin rubber)
SBR (styrene butadiene rubber)	NBR/EVA	PP (polypropylene)
Q (silicone rubbers)		PB (polybutene-1)
NBR (nitrile rubber)		
HNBR (hydrogenated acrylonitrile-butadiene rubber)		
U (urethane rubbers)		
EPM (ethylene-propylene-monomer)		
EPDM (ethylene-propylene-diene terpolymer)		
PE (polyethylene)		
T (polysulphide rubber)		
CM (chlorinated polyethylene)		
CSM (chlorosulphonated polyethylene)		
EVA (ethylene-vinylacetate-copolymer)		
ABS (acrylonitrile-butadiene-styrene)		
AEM (Ethylene acrylic rubber)		
EBA (ethylene-butylacrylate)		
FKM (fluorelastomers)		

### Peroxide curing agent

Organic peroxides contain one or more oxygen-oxygen (R-OO-R) bonds with R referring to other chemical groups. Several categories of peroxide exist based on their chemical composition, e.g. dicumylperoxide (DCP) is a diaralkyl peroxide [88], [91]. Peroxides offer improved thermal resistance and lower compression set, ideal for sealing applications [92]. When exposed to heat, these peroxides will undergo homolytic cleavage by breaking the oxygen-oxygen bond yielding two radicals. In the case of DCP, as shown in Figure 14, the cumyloxy radicals can undergo further  $\beta$ -scission to form acetophenone, as by-product, and methyl radicals. This methyl radical is less sterically hindered than the cumyloxy radical which may improve reaction efficiency during crosslinking.  $\beta$ -scission entails cleavage of the weakest C-C bond with tertiary carbon being weaker than secondary and primary carbons. The peroxide decomposition follows first order reaction kinetics which make the dissociation of the peroxide molecule proportional to the peroxide concentration [88].

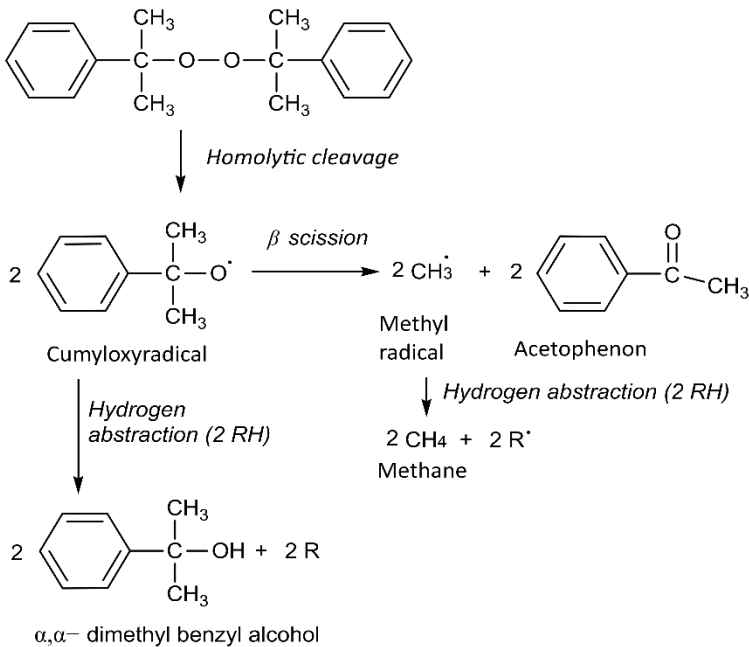


Figure 14: Dicumylperoxide decomposition mechanism [88], [91].

The radicals, created after homolytic cleavage, can then initiate hydrogen abstraction from the polymer chain, or addition can take place to the double bond of unsaturated polymers creating a polymer radical. The ability to abstract a hydrogen atom depends on the structure of the hydrogen donor. For example, due to resonance stabilisation, allylic and benzylic structures are favoured. Addition is more likely when terminal double bonds or double bonds at the end of a side-chain groups (vinyl) are present. Finally, two radicals will recombine to form a carbon-carbon crosslink, i.e. a combination reaction [88], [91].

For EPDM, Orza et al. [59] elaborated the curing mechanism (Figure 15) which proceeds by hydrogen abstraction and addition reactions. For the specific application of ENB as termonomer, hydrogen abstraction is favoured. H-atoms can be abstracted from the secondary  $\text{CH}_2$  and tertiary  $\text{CH}$  units of the EPDM backbone, and at the allylic position ENB, yielding alkyl and allyl macro-radicals. Then, an EPDM macro-radical can attach to a carbon atom from the double bonds of an EPDM chain through addition which is followed by hydrogen abstraction to yield an allyl/alkene crosslink or alkyl/alkene crosslink. For ENB, the diene conversion is  $\sim 25\%$  [88]. For the combination reaction, two radicals recombine to form a covalent C-C bond. This causes  $\sim 25\%$  alkyl/alkyl,  $\sim 25\%$  allyl/allyl, and  $\sim 50\%$  allyl/alkyl combination crosslinks.

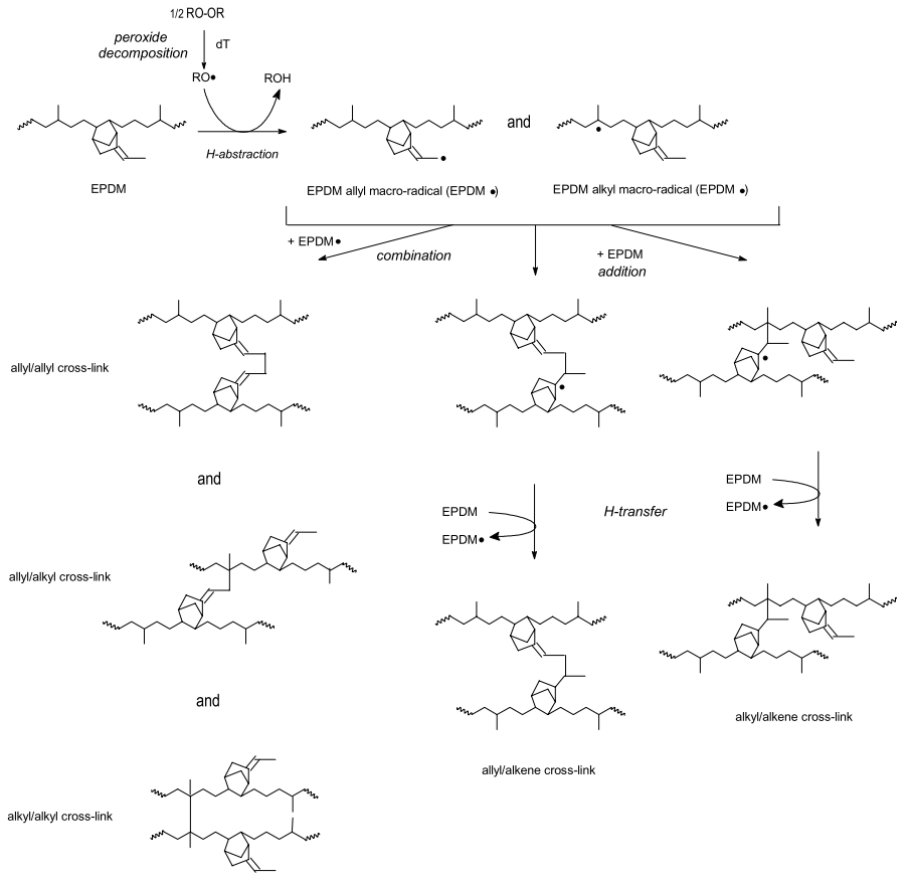


Figure 15: Mechanism for peroxide crosslinking of EPDM [59].

Besides formation of crosslinks, undesirable side reactions may occur like  $\beta$ -scission or disproportionation of the elastomer main chain. For EPDM, main chain scission, or  $\beta$ -scission, is likely to occur at the tertiary radical of the propylene unit. This causes the elastomer to break and form a double bond and a radical due to electron rearrangement as shown in Figure 16 [88], [91]. Furthermore, disproportionation is a side reaction which is also promoted by tertiary radicals. Allylic radicals terminate through combination due to the presence of the double bond but tertiary alkyl radicals may prefer disproportionation as shown in Figure 16. This reaction does not reduce molecular weight of the elastomer, but reactive radical sites are reduced decreasing the efficiency of the peroxide as no C-C crosslink is created.

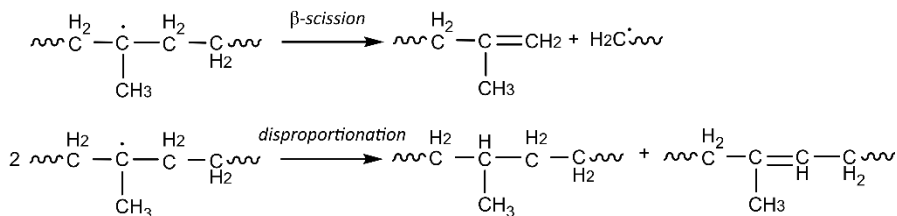


Figure 16: Side reactions of PP unit in EPDM:  $\beta$ -scission and disproportionation [88].

Several studies have shown a significant influence of peroxide vulcanisation on the crosslink density and general properties of vulcanised rubbers [40], [93], [94]. Consequently, an influence of the peroxide curing agent on the adhesion at the interface can be expected as well. Furthermore, peroxides could induce a co-vulcanisation reaction between EPDM and thermoplastics as unsaturations are not required. Thus [4] studied the possibility of co-vulcanisation between HNBR-PA6.6 and found that direct contact was required between the peroxides and PA6.6 during 2K injection moulding. However, interdiffusion was still deemed dominant, but this was due to the better miscibility of peroxides in HNBR. Overall, Thus [4] indicated the occurrence of both interdiffusion and chemical bonding at an HNBR-PA6.6 interface. For PE, crosslinking is often employed with peroxides when used in thermoplastic vulcanisate blends or to create crosslinked PE (XPE) to increase durability or heat resistance [91], [95], [96]. It is known that DCP has a good efficiency to cure PE as the alkoxy radicals from DCP are prone to abstract hydrogen from PE and the extent of crosslinking is dependent on the peroxide amount [95], [97]. However, when organic peroxides are brought into contact with PP, there is general risk of polymer degradation, as besides crosslinking also chain scission can occur due to the tertiary radicals that form. Overall, crosslinking is energetically less favorable than chain scission [98], [99]. For PP, it is important to use a co-agent assisted peroxide curing system to minimise degradation [98], [100]. Studies of PP/EPDM thermoplastic vulcanisates (TPVs) have shown that DCP is less prone to degrade PP compared to other peroxides like di(2-tert butyl peroxy isopropyl)benzene or tert-butyl cumyl peroxide, but overall the peroxide concentration needs to be limited [92], [101]. Furthermore, peroxides can cure ABS which could lead to co-vulcanisation with EPDM [91]. Peroxides may also migrate to the surface at higher concentrations causing a change in compatibility with polar and non-polar thermoplastics [4]. Overall, literature clearly shows the importance of peroxide concentration and its influence in blends, at interfaces and the general properties of polymers.

### Co-agents

Co-agents are multifunctional organic molecules that are used to improve crosslinking with peroxides. Co-agents can prevent side reactions that consume free radicals, like chain scission and disproportionation, creating a better peroxide curing efficiency [88]. This improved crosslinking efficiency is created because the co-agent creates additional crosslinks thanks to the formation of co-agent bridges. Hence, crosslinking performance is improved and crosslink density increased. For EPDM, this entails a reaction between the co-agent and labile tertiary radical suppressing side reactions. Physico-mechanical properties benefit from the addition of co-agents as tensile and tear strength, modulus, heat aging, hardness, compression, abrasion resistance, and adhesion to polar substrates are improved. By introducing these co-agents, less peroxide

is needed to reach equal crosslink density. There are two types of co-agents that can be classified based on their effect on the curing process [88], [102]:

- (1) Type I co-agents: Type I co-agents are polar multi-functional organics. These co-agents include acrylates, methacrylates and bismaleimides which contain easily accessible unsaturations. Therefore, they mainly react through addition reactions forming highly reactive radicals. These co-agents can increase the cure rate and crosslinking density.
- (2) Type II co-agents: Type II co-agents are less polar molecules which form more stable radicals. This group includes cyanurates, phthalates and isocyanurates which contain readily accessible unsaturation sites and easily abstractable allylic hydrogen atoms. These co-agents mainly react through addition, but hydrogen abstraction is possible as well. Their presence in the rubber only causes an increase in crosslinking density.

Based on the co-agent type, the crosslinked network structure of the rubber matrix can be influenced. The peroxide crosslinked network of the rubber matrix in presence of co-agents was discussed by Kruzalak et al. [103], [104] and Henning et al. [105] and is represented in Figure 17. While type I co-agents homopolymerise and/or graft to macroradicals through addition reactions, type II co-agents can participate in intermolecular propagation and intramolecular cyclisation reactions. The polar molecules of type I have low solubility in the rubber matrix due to their polarity and therefore they tend to phase separate and homopolymerise. These homopolymerised domains can co-crosslink with the rubber matrix and behave as filler particles.

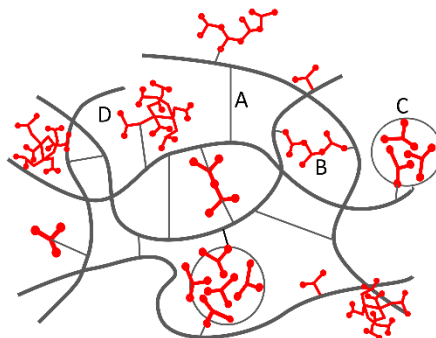


Figure 17: Peroxide crosslinked network of the rubber matrix in the presence of co-agents with crosslinks originating from (A) polymer radicals, (B) co-agent forming crosslink, (C) thermoset domains of co-agents grafted to rubber chains, (D) interpenetrating network of homopolymerised co-agents covalently bonded to the rubber [89].

The principle of interfacial chemical bonding due to the presence of peroxides in rubber and the influence of co-agents to improve this crosslinking reaction are reported in several studies. For thermoplastic vulcanisate blends (TPVs), studies have shown that methacrylate co-agents help minimising degradation of PP, while improving EPDM crosslinking [98], [99], [106]. These TPVs exhibited improved mechanical properties and lower compression sets. For PE, allylic type co-agents are indicated as most suitable as they do not readily homopolymerise compared to acrylic types when using a strong hydrogen abstracting peroxide like DCP [61]. More specifically for multi-component injection moulding, direct bonding was achieved between PPE and EPDM with radicals

[30]. This EPDM consisted of a peroxide curing agent and trimethylolpropane trimethacrylate (TMPT) as co-agent. It was indicated that the bonding mechanism was possibly caused by radical reactions such as hydrogen abstraction reactions due to the presence of peroxides. Specifically for 2K injection moulding of thermally stable PA 6.6 with HNBR, it was stated that a stronger adhesion was obtained due to the presence of co-agents like triallyl isocyanurate (TAIC) or TMPT. These co-agents show better compatibility with PA 6.6, leading to co-agent enrichment at the interface. This caused a co-vulcanisation reaction at the interface. Regardless of the type of co-agent and peroxide, higher co-agent concentrations led to an increase in adhesion strength. The authors ascribed this to an increase of radical yield, higher crosslink density and reactivity at the interface [4].

### 2.3.2.2 Sulphur crosslinking

Sulphur vulcanisation is the most applied curing system in the industry and is relatively inexpensive. It is mainly used in general purpose rubbers as these contain unsaturations which is a requirement for successful crosslinking. Vulcanisation with solely elementary sulphur as curing agents proceeds extremely slow. Elementary sulphur consists of a cyclic structure with eight atoms ( $S_8$ ). Therefore, accelerators and activators are employed as well. Consequently, vulcanisation kinetics are improved [61], [89].

Accelerators are organic molecules, usually containing nitrogen and sulphur atoms. They can increase the reaction rate, reduce vulcanisation time, and reduce the required vulcanisation temperature. Accelerators can be classified as primary and secondary accelerators [61], [107]:

- (1) Primary accelerators: they provide good processing safety due to the scorch delay, and medium to fast cure. Primary accelerators include thiazoles and sulphenamides. They are usually dosed between 0.5 and 1.5 phr in the rubber compound.
- (2) Secondary accelerators: they activate the primary accelerators and produce fast cures at the expense of scorch safety. Secondary accelerators include guanidines, thiurams and dithiocarbamates. However, for EPDM, thiurams are primary accelerators due to the low amount of double bonds in EPDM. They are dosed between 0.05-0.5 phr, which usually corresponds to 10-40% of the primary accelerator.

Activators are organic and inorganic chemicals. Usually, zinc oxide is used as inorganic activator and stearic acid, i.e. a fatty acid, as organic activator. During the vulcanisation reaction (Figure 18), zinc oxide and stearic acid form a salt, which together with accelerators creates an intermediate complex. This complex can activate sulphur providing an efficient cure. Due to its complexity a detailed sulphur vulcanisation mechanism is not yet clear. However, Van Duin [108] proposed a reaction mechanism of EPDM with accelerator sulphur vulcanisation. In EPDM, the allylic hydrogen is substituted by accelerator residues through sulphur bridges, yielding a crosslinking precursor. The ENB unsaturation is not consumed, but is needed to activate the allylic hydrogen positions. Afterwards the actual sulphur crosslinks are formed consisting of 1 to 5 sulphur atoms, i.e. polysulphidic crosslinks. Due to the high temperature, desulphuration then occurs, resulting in shorter sulphur bridges, i.e. mono and disulphidic crosslinks. Above 300°C, devulcanisation can be initiated as well in the presence of diarylsulphide.

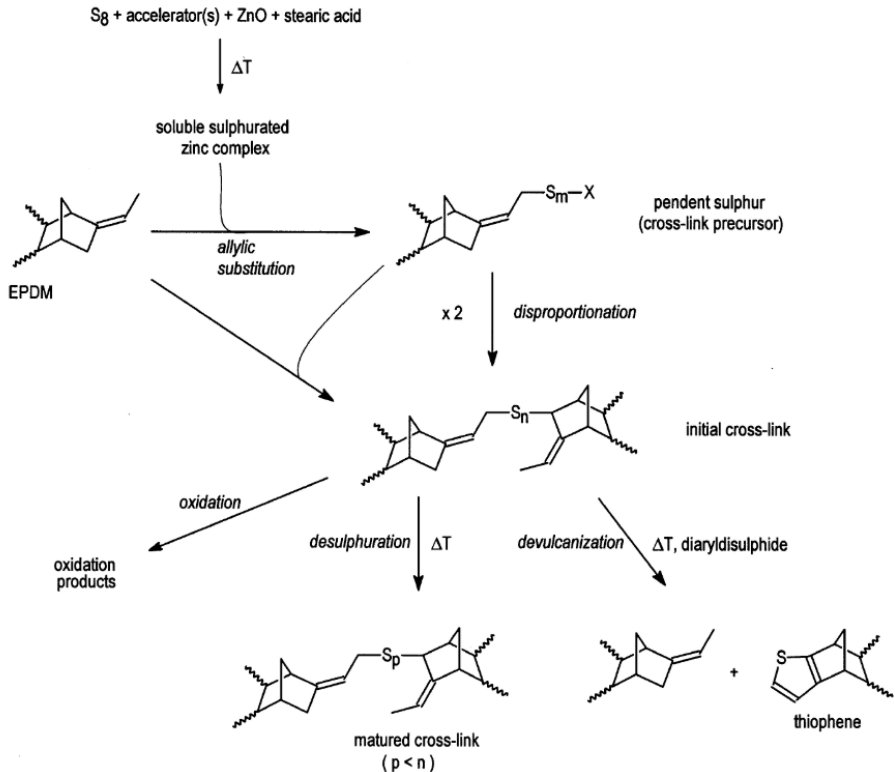


Figure 18: Reaction mechanism of accelerated sulphur vulcanisation of EPDM (x= accelerator residue) [108].

Adjusting the accelerator composition, i.e. primary and secondary, in the sulphur curing system will alter curing kinetics. This might not only influence processing time, but the adhesion of thermoset-thermoplastic as well. Voleppe et al [109] evaluated the adhesion mechanism between poly(ether sulfone) thermoplastic and a high density thermosetting epoxy network. The authors found that a competition occurred between the interdiffusion at the thermoplastic-thermoset interface and the curing reaction in the epoxy network. Diffusion seemed to be thermally favoured during the early stages of curing.

### 2.3.3 Rubber characteristics

#### 2.3.3.1 Vulcanisation characterisation

When characterising the vulcanisation process, properties like onset of vulcanisation, vulcanisation rate and the extent of vulcanisation are of interest. During vulcanisation, the rubber is exposed to a high temperature (150-190 °C). Initially, the high temperature causes a decrease in viscosity. However, upon start of vulcanisation, the viscosity increases again. The time at which an abrupt increase in viscosity occurs, is referred to as scorch time. For injection moulding, sufficient delay or scorch resistance is needed to permit flow into the mould before vulcanisation. Afterwards rapid vulcanisation, or

crosslinking, follows leading to a certain extent of crosslinking [75]. In Figure 19, a typical vulcanisation curve is shown. Such a curve can be registered by a moving die rheometer (MDR) [89]. This device consists of an upper die which is fixed and a lower die that oscillates (e.g. oscillation frequency of 1.7 Hz at a deformation angle of 0.5°). Upon measurement, the torque  $S'$  is plotted against time at a constant temperature. In an MDR both a viscous torque and an elastic torque are measured, but the elastic torque indicates the cure state [61]. Thus, the torque in Figure 19 is proportional to the low-strain elasticity modulus and the increase in torque is proportional to the number of crosslinks formed per unit of volume of rubber. Besides chemical crosslinks, physical crosslinks may influence torque as well, e.g. entanglement of polymer chains with carbon black [79].

The cure curve kinetics can be divided in three different stages [61], [75], [89]:

- (1) **Scorch time** ( $ts_1$ ,  $ts_2$ ,  $t_{10}$ ): scorch time is defined as the time  $ts_1$  until one torque unit rise above the minimum is reached when 0.5-1° arc strain is applied, or time  $ts_2$  until two torque unit rise above the minimum is achieved at 3° or 5° arc strain. Scorch can also be defined as time until 10% state-of-cure is reached ( $t_{10}$ ).
- (2) **Crosslinking**: the crosslinking stage is confined by scorch time and cure time. Cure time  $t_{90}$  is the time at which 90% vulcanisation degree (Eq. (20)) is reached which corresponds to the time needed to achieve optimal properties of the final vulcanisate. Based on the cure time and scorch time the cure rate index (CRI) can be defined according to Eq. (21) which is a measure of the rate of vulcanisation.

$$\text{Vulcanisation degree} = \frac{S' - S'_{\min}}{S'_{\max} - S'_{\min}} \quad (20)$$

$$\text{CRI} = \frac{100}{\text{cure time} - \text{scorch time}} \quad (21)$$

- (3) **Over crosslinking**: in the third stage, the elastomer chain can be modified and crosslinks restructured due to too long exposure to a constant high temperature. Ideally, a plateau is reached indicating a stable structure without any further changes. However, the number of crosslinks might decrease which is referred to as reversion. Thus, a deterioration of the vulcanisate properties occurs which softens the rubber. When torque keeps increasing, marching modulus, or stiffening, occurs.

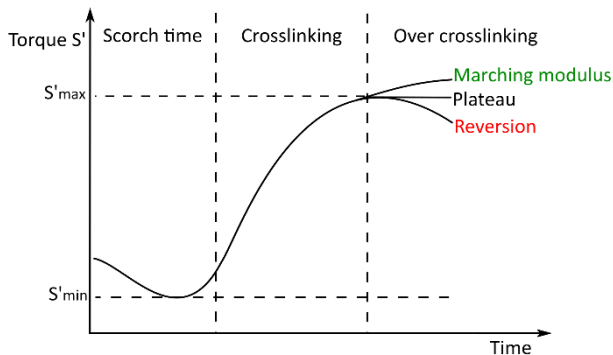


Figure 19: Rheometer vulcanisation curve after [88].

## 2.3.3.2 Network crosslink density

A rubber network contains numerous crosslinks. An important characteristic for this network is crosslink density  $\nu$  ( $\text{mol cm}^{-3}$ ) which is the concentration of elastically-effective network chains [89]. A common method to determine the crosslink density is an equilibrium swelling measurement. The vulcanisate will swell until an equilibrium swelling degree is reached and based on the volume of solvent absorbed by the vulcanisate, the crosslink density can be calculated with the Flory-Rehner equation (Eq. (22)) for tetrafunctional networks:

$$\nu = -\frac{1}{2} \frac{\ln(1 - V_r) + V_r + \chi V_r^2}{V_s \left( V_r^{\frac{1}{3}} - 0.5V_r \right)} \quad (22)$$

where  $V_s$  is the molar volume of the swelling solvent,  $\chi$  is the Huggins polymer-solvent interaction parameter and  $V_r$  is the volume fraction of rubber in the equilibrium swollen vulcanisate. Other methodologies for crosslink density characterisation are the Mooney-Rivlin method for deformation measurements and high-resolution solid-state NMR. In a vulcanisate network, besides chemical crosslinks connecting several elastomer chains, temporary and trapped chain entanglements are present as well [59], [110]. Schlögl et al. [110] indicated that swelling experiments reflect the crosslink contribution which possibly also contains the trapped entanglement fraction.

The extent of vulcanisation greatly affects mechanical properties as shown in Figure 20. When the crosslink density increases, tensile strength increases up to the optimal vulcanisation degree after which it reduces again. Formation of crosslinks also reduces hysteresis, which is the ratio of viscous component to the elastic component of deformation resistance. The hysteresis represents the heat released when going from loading to unloading of the rubber. Thus, the work needed to stretch a rubber is higher than the work for returning to its original shape as stretching requires more energy. The difference in energy is converted into heat and is caused by viscous damping of the rubber. More heat corresponds to lower rubber elasticity. Similarly, elongation at break and compression set decrease with increasing crosslink density. Fatigue life, tear strength and toughness are improved at relatively low crosslink densities but they decrease with further formation of crosslinks. These properties are related to the energy to break and this increases with higher number of network chains and hysteresis. The hysteresis decreases as more network chains are created, causing a maximum in energy of fracture properties. The presented properties are not solely dependent on crosslink density, but the type of crosslink, polymer type, and type and amount of filler also play a major role [75], [89].

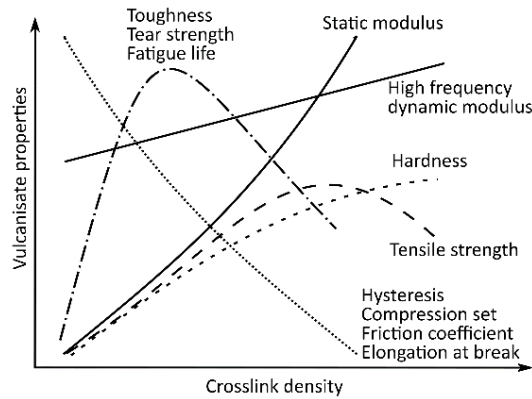


Figure 20: Vulcanisate properties as a function of crosslink density [75], [89].

During crosslinking, long rubber molecules with high molecular weight become linked. The average molecular weight between the crosslinks is related to the tensile strength of the vulcanisate. Un-crosslinked rubber chains tend to slide over each other and disentangle upon deformation. Fracture will occur due to viscous flow at low stress without breaking chemical bonds. However, vulcanisation increases molecular weight of a chain, creating a branched molecule and broader MWD. Thus, disentanglement becomes more difficult causing higher rubber tensile strength. Ideally, within the rubber, the crosslink density is high enough to prevent fracture due to viscous flow but low enough to avoid brittle fracture [75], [107].

## 2.4 Adhesion in rubber-thermoplastic injection moulding

In 2K injection moulding, several hard-soft combinations can be made. However, depending on the specific choice of soft component advantages and disadvantages arise. Besides thermoset rubbers, liquid silicone rubber (LSR) or TPE can be selected as soft component. However, with the specific focus on sealing applications where high chemical and temperature resistance is required and products are exposed to mechanical strains, these materials tend to fail:

- (1) **TPE:** TPEs generally exhibit low temperature resistance. Furthermore, they have low chemical or oil resistance, depending on the chemical composition of the TPE, and are accompanied by high compression sets [111].
- (2) **LSR:** Even though LSR shows good temperature resistance and compressions set, their oil or chemical resistance are below requirements. For example, they degrade when exposed to acidic and basic environments. Furthermore, LSR's are expensive and when combined with thermoplastics, the addition of organofunctional silanes or a surface treatment is needed [111].

Thus, combining thermoplastics with thermoset rubbers would be highly innovative. The envisaged markets are automotive, medical, chemical, electronics, construction, and applications can range from energy absorbing devices to sealing applications, e.g. pump housing, valves, wheels or medical syringes. These applications benefit from the mechanical strength and stiffness of the thermoplastic, while the rubber provides mechanical and chemical properties for sealing, damping and friction.

Throughout studies on adhesion in 2K injection moulding, the main focus has been on the influence of processing conditions [112]–[115]. Furthermore, for adhesion with thermoset rubbers, literature has been limited to thermally stable thermoplastics, e.g. PA6.6. When defining proper material combinations, literature clearly highlights the importance of the right curing system as this influences the adhesion mechanism. Table 3 shows material combinations found in literature with the specific focus on thermoset rubbers with thermoplastics together with curing system of use. When combining PPE with peroxide curing EPDM a radicalisation reaction can induce co-vulcanisation at the interface as indicated by Mutsuda et al. [30]. For PA with XNBR a combination of C-C bonds at the interface can be found together with crosslinks created through amides, i.e. condensation of the PA amino groups with carboxyl groups of XNBR [4].

Table 3: Thermoplastic-thermoset rubber material combinations.

Thermoplastic	Thermoset rubber	Curing system	Source
PPE	SBR, NR/SBR, NBR/SBR, EPDM/SBR, EPDM	Sulphur Peroxide	[116], [30], [117]
PA6.12	XNBR, HNBR, AEM, FKM	Peroxide Bisphenol Amine	[116], [117]
PA blend	HNBR, AEM, FKM	Peroxide Bisphenol Amine	[116], [117]
PA6.6	HNBR	Peroxide	[4]
PBT	EPDM, MVQ/FMVQ	Peroxide	[117]

A detailed study on the influence of material parameters was also presented by Thust [4]. By changing the HNBR formulation, the adhesion with PA6.6 was optimised as already addressed in the previous sections. Results showed that the co-vulcanisation at the interface, even though possible, was limited. To increase the interfacial bonding efficiency, high peroxide concentration and/or co-agents concentrations were needed in the interface region. Furthermore, a low molecular weight and lower crosslink density appeared to improve the interdiffusion process. Eventually, it was postulated that the amount of adhesion, on the material level, was dominated by the concentration and the functionality of the co-agents together with its compatibility with the rubber and thermoplastic. The influence of these co-agents was already addressed in the section ‘Co-agents’. The study by Thust [4] clearly indicates the importance of selecting the right rubber formulation.

#### 2.4.1 Process development

2K injection moulding of thermoplastics with thermoset rubbers creates opportunities for novel material combinations. Specifically, products combining special purpose rubbers like EPDM with commodity plastics like PP are ideal for applications exposed to relatively high temperatures, harsh chemical environment and/or mechanical strains which can be important for 2K sealing applications [118]. Creating successful products with these materials required the development of a new process as

thermoplastics and rubbers have opposite temperature processing requirements. Therefore, Bex et al.[1] implemented a versatile mould with thermally separated heat cavities to enable adhesion between thermoset rubbers and thermoplastics.

During the injection moulding process, thermoplastic parts are produced separately (1K) by placing a metal inert in the rubber cavity. After production of multiple thermoplastic products, the metal insert is removed and the rubber component is injected. The temperature of the rubber cavity is set sufficiently high to vulcanise the product, while the thermoplastic part is cooled. This leads to an intermediate temperature at the interface. For semi-crystalline thermoplastics, this temperature is around the melting point and below the temperature at which small voids at the interface form, causing a small/narrow melted zone of the thermoplastic material. For amorphous materials, the interface temperature is set above the glass transition temperature to initiate movement of the polymer chains but it is limited by the temperature at which deformation of the thermoplastic part occurs. As a result, adhesion can be created at the interface between both materials. Figure 21 shows the temperature profile in the 2K mould with a rubber cavity at high temperature (180°C) and a thermoplastic cavity at 70°C which creates an interface temperature of 135°C, i.e. around the melting point of PE. The cavity temperatures are externally controlled by separate temperature control units and maintained throughout the vulcanisation process. Afterwards, the rubber part is cooled to solidify the molten thermoplastic interface. This is done with a rapid heat cycling system [1], [3].

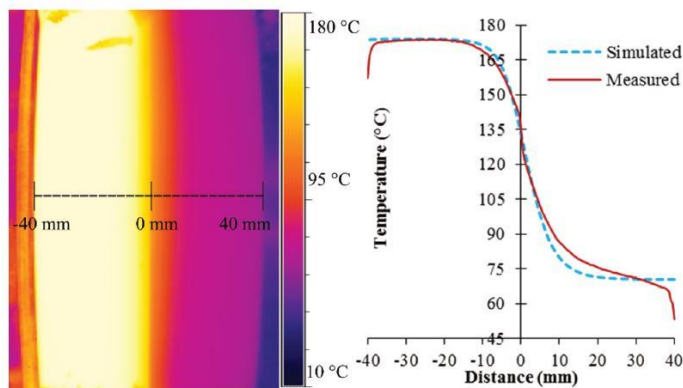


Figure 21: Temperature profile across the versatile 2K mould with the rubber cavity set at 180°C and the thermoplastic cavity temperature of 70°C [3].

Bex et al. [119] also investigated relevant process parameters which influence adhesion between thermoset rubbers and thermoplastics. The main parameter for good adhesion appeared to be the interface temperature, which is determined by the mould temperature. A higher interface temperature, improves the adhesion strength. However, as mentioned before, this interface temperature is limited by the formation of voids for semi-crystalline thermoplastics or deformation for amorphous thermoplastics. Other parameters like injection temperature, injection speed, holding pressure or interface roughness had only a small or a non-significant effect on the adhesion. By process optimisation, an interface strength close the bulk tensile strength of the rubber could be reached for EPDM-HDPE and NBR-ABS. However, due to the low interface temperatures ( $\sim 135^\circ\text{C}$ ) for these materials long vulcanisation times are required. This

leads to undesirably long processing times. For material combinations EPDM-PP and NBR-PC, low adhesion strength was reached irrespective of the optimal processing conditions. This was ascribed to two possibly causes: (1) the higher interface temperature leading to too high cure rates which limits the adhesion mechanism, (2) the unfavourable mould temperature profile, e.g. 180°C in the rubber cavity and 140°C in the thermoplastic cavity for EPDM-PP, leading to a low temperature drop next to the interface going from EPDM to the PP part. Thus, a trade-off has to be made between processing time and adhesion strength [3].

In terms of industrial relevance, Bex et al. [3] found that a higher product cost arises from the 2K process compared to a 1K process. However, 2K injection moulding offers advantages like high adhesion strength, secured positioning with accurate dimensions, and material savings. Therefore, high quality products seem to be more suited for the proposed 2K injection moulding process.

#### 2.4.2 Process simulation

Besides the influence of processing, research has focused on the development of a simulation method for rubber-thermoplastic 2K injection moulding. A model was developed by Six et al. [120], [121] to predict the adhesion strength between the thermoset rubber and thermoplastic. The proposed model is only valid for material combinations with interdiffusion as adhesion mechanism as it is based on the Brownian motion of polymer chains.

Bex et al. [5] indicated that the adhesion strength is mainly influenced by the interface temperature in the 2K mould and mentioned interdiffusion as possible adhesion mechanism between sulphur cured EPDM and PE. Therefore, Six et al. [121] applied the polymer reptation model of De Gennes [122] for rubber-thermoplastic overmoulding modelling. The reptation model accounts for the interface healing at high temperature as there is a probability of polymer chain movement across the interface. This is generally used to predict the interdiffusion at polymer-polymer interfaces. When the polymer molecular chains start crossing the interface, the adhesion strength increases and this is described by the degree of healing. For semi-crystalline materials healing can occur in the melt state. Therefore, the authors used the melting behaviour measured with differential scanning calorimetry (DSC) to predict the interfacial strength. By combining results of the melting behaviour with the predicted interface temperature, from numerical simulations, the degree of melting could be predicted. Besides the degree of melting, the rubber curing degree was incorporated in the model by Six et al. [121] as well because curing will decrease the ability of chain movement. The interdiffused thermoplastic chains can then be locked in place. Therefore, the Kamal model [121] was applied to define the degree of cure of the thermoset rubber near the interface. This degree of cure is linearly correlated to the local rubber strength. Eventually, the local interface strength was defined by the simulated degree of healing and the local rubber strength.

Six et al. [120] investigated the material combination of EPDM with HDPE. In particular, adhesion between a semi-crystalline thermoplastic and a sulphur cured EPDM. Six and co-workers concluded that the proposed model is thought to be valid as well for other combinations of thermoset rubbers with thermoplastic. However, this requires further investigation because Six et al. [120] solely focused on processing influence on the adhesion, i.e. interface temperature defining the adhesion strength. Results from the study by Bex et al. [3] indicated a lack of good adhesion between PP and EPDM even though optimal processing parameters were implemented. Furthermore, variations in

rubber material composition were not evaluated. Only the degree of cure of the rubber was defined for the simulation model. Information of the influence of polymer molecular structure, rubber compound formulation, rubber-thermoplastic compatibility, rubber crosslink density is currently lacking. Therefore, these aspects require an in depth study.

## **2.5 Conclusion**

It can be concluded that the adhesion between two polymer materials can be induced by several adhesion mechanisms. Characterising the adhesion at the interface can provide a better insight in these mechanisms. Furthermore, the rubber formulation consists of a variety of components, each having a specific function. Literature indicates that each of these components, e.g. curing agents, fillers, oils, and polymer macromolecular chain, could severely influence polymer-polymer interactions. However, for the current 2K injection moulding process, combining thermoset rubbers with thermoplastics, material composition influences are unknown. Optimising the rubber composition and accompanying adhesion mechanism could broaden the possible material combinations for 2K injection moulding.

---

## Chapter 3 Optimisation of the EPDM curing system for adhesion with thermoplastics

---

### 3.1 Introduction

For the current 2K injection moulding process, combining thermoplastics with thermoset rubbers that have opposite temperature processing requirements, little is known about the influences of the rubber curing system on the adhesion. For the development of the 2K injection moulding process for thermoset rubbers with thermoplastic, Bex et al. [1], [3], [5] solely applied sulphur-based EPDM, while peroxide curing could have many advantages. Differences in adhesion mechanism might be induced with regard to interdiffusion and chemical bonding as shown in Figure 22. Furthermore, changing the curing system could influence curing kinetics and consequently processing times. Therefore, in this chapter the influence of peroxide curing (Section 3.3), is investigated with regard to co-agent type and concentration and peroxide curing agent concentration in EPDM to optimise the adhesion with thermoplastic. Furthermore, the sulphur curing system is studied (Section 3.4) to analyse whether the accelerator composition can be optimised to reduce processing time without lowering the adhesion strength.

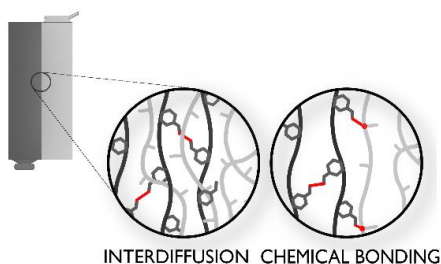


Figure 22: Thermoset rubber-thermoplastic sample with interdiffusion (left) and chemical bonding (right) at the interface.

Results of the influence of the peroxide curing system have been published in two journal papers in the Journal of Applied Polymer Science [123], [124]:

- (1) [B. Laing](#), J. De Keyzer, D. Seveno, and A. Van Bael, “Effect of co-agents on adhesion between peroxide cured ethylene–propylene–diene monomer and thermoplastics in two-component injection molding,” *J. Appl. Polym. Sci.*, vol. 48414, p. 48414, 2019

- (2) B. Laing, J. De Keyzer, D. Seveno, and A. Van Bael, "Adhesion between ethylene-propylene-diene monomer and thermoplastics in two-component injection molding: Effect of dicumylperoxide as curing agent," *J. Appl. Polym. Sci.*, p. 49233, Mar. 2020.

Furthermore, results were presented and published in proceedings of the International Conference on Polymers and Mould Innovations 2018 (PMI2018) and the International Rubber Conference 2019 (IRC2019) [125], [126]:

- (1) B. Laing, G.-J. Bex, J. De Keyzer, D. Seveno, and A. Van Bael, "Influence of peroxide curing on adhesion between thermoplastics and thermoset rubbers in two-component injection moulding," in *8th Bi-annual International Conference on Polymer and Mould Innovations*, 2018, p. 111.
- (2) B. Laing, J. De Keyzer, D. Seveno, and A. Van Bael, "Effect of co-agents on the adhesion between peroxide cured EPDM and thermoplastics in two-component injection moulding," in *Book of papers of International Rubber Conference*, 2019.

## 3.2 Methodology

### 3.2.1 Thermoplastic grades

Four fixed thermoplastic grades are used to create 2K samples with EPDM. These are the following:

- (1) PP grade 400-GA05 from Ineos with a melting temperature of 164°C and a yield stress of 25 MPa;
- (2) PE grade M80064 from Sabic with a melting temperature of 135°C and a yield stress of 32 MPa;
- (3) PC grade Calibre 301-15 from Trinseo with a glass transition temperature of 150°C and a yield stress of 60 MPa;
- (4) ABS grade Novodur P2H-AT from Ineos, with a glass transition temperature of 110°C and a yield stress of 44 MPa.

Datasheets of all thermoplastics are provided in Appendix A. In this chapter, thermoplastic adhesion with varying EPDM curing system compositions is studied. First, variations are made in co-agent type and concentration in Section 3.3.1. Then, the peroxide concentration is varied in Section 3.3.2. Finally, the accelerator composition in the sulphur curing system is varied in Section 3.4. In each of these sections, the specific rubber composition is listed.

### 3.2.2 2K injection moulding: sample preparation

All samples were prepared according to the recently developed process described by Bex et al.[1], [5]. Injection moulding was executed on an Engel ES330H/80V/80HL-F equipped with a vertical rubber unit, horizontal thermoplastic injection unit and a clamping force of 1000 kN. The ratio of the screw length and the screw diameter (L/D) of the thermoplastic unit is 20 and the diameter of the screw is 35 mm. For the rubber unit, the L/D ratio is 16 and the screw has a diameter of 25 mm. First, all thermoplastics parts were produced separately in the thermoplastic cavity, while a metal insert was placed in the rubber cavity. Afterwards, the metal insert was removed from the rubber cavity. Then, a thermoplastic part was placed in the 2K mould and overmoulded with rubber,

leading to specimen dimensions as shown in Figure 23a with a thickness of 2 mm. In the bulk region of EPDM a uniform mould temperature is assured. The dotted blue line represents the sample location for tensile testing to determine the adhesion strength and how the force ( $F$ ) will be applied. The tensile bar dimensions are addressed in more detail in Section 3.2.7. In Figure 23b, locations for hardness measurements at the interface and in the bulk are indicated which enable calculating the vulcanisation degree at the interface. In Section 3.2.3, this is explained in more detail.

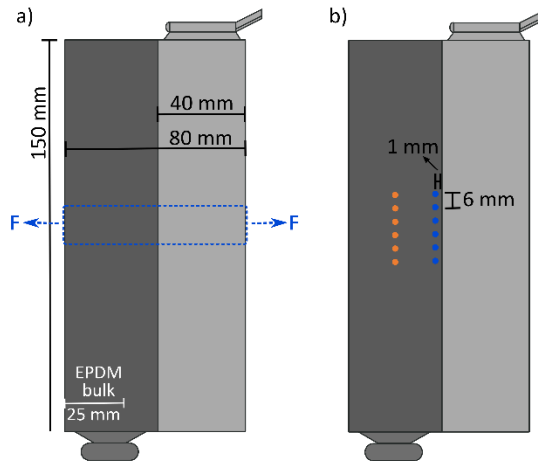


Figure 23: 2K specimen dimensions are represented (a). The thickness of both the rubber and thermoplastic part is 2 mm and the blue dotted line represents the location for tensile testing samples. Hardness was measured at the interface (blue dots) and in the bulk (orange dots) to determine vulcanisation degree (b).

The injection moulding parameters for the individual components, i.e. PP, PE, PC, ABS and EPDM are listed in Table 4. The injection and mould temperatures were recommended by the polymer suppliers. The injection rate was set high enough to ensure constant viscosity and a high holding pressure was selected, using an iterative procedure, to completely fill the product without causing flash [127].

Table 4: Process parameters for individual components.

Process parameters	PP	PE	PC	ABS	EPDM
Injection temperature (°C)	230	230	300	260	80
Mould temperature (°C)	20	20	80	70	180
Injection rate (cm <sup>3</sup> /s)	38	38	87	96	59
Holding pressure (bar)	494	790	494	494	248

During production of 2K samples, the rubber cavity was set at 180°C to ensure vulcanisation, while the thermoplastic cavity was set at a low temperature to achieve an optimal interface temperature for good adhesion as specified by Bex et al. [1], [5]. For each specific study the investigated materials combinations and thermoplastic mould temperature together with the accompanying interface temperature is listed. These will

be around the melting temperature of semi-crystalline thermoplastics or high enough above the glass transition temperature for amorphous thermoplastics.

### 3.2.3 Cure characteristics

Cure characteristics of the EPDM compounds were determined with a Monsanto moving die rheometer (MDR 2000E). Measurements of the vulcanisation degree were taken at 180°C to determine cure characteristics of EPDM bulk material. As temperatures during the actual 2K process are lower at the interface, depending on the material combination, vulcanisation degree was also measured at 160°C and 140°C. For each setting, the respective cure time ( $t_{90}$ ), scorch time ( $t_{s1}$ ), cure rate index (CRI) and delta torque ( $\Delta\text{torque}$ ) were obtained. The vulcanisation temperature in the rubber bulk (180°C) is higher than at the interface. Thus, there is a risk of reversion in the bulk during the long vulcanisation times for samples with low interface temperature, e.g. 140°C. Therefore, reversion of the EPDM bulk at 180°C which can occur during processing was determined based on Eq. (23) with  $S'_{max}$  and  $S'_R$  as the maximum torque and torque after the required processing time respectively:

$$\text{Reversion index (\%)} = \frac{S'_{max} - S'_R}{S'_{max}} \cdot 100 \quad (23)$$

The vulcanisation degree of the 2K injection moulded samples was monitored a posteriori to analyse whether 90 % vulcanisation degree was reached near the interface. As hardness relates linearly to the vulcanisation degree, Shore A hardness measurements were performed according to ISO 7619 with a measuring time of 15 s [1], [85], [128]. Five measurements were taken 1 mm from, and parallel with, the interface in the middle of the rubber part along the axial direction to determine the hardness near the interface as shown in Figure 23b. Hardness measurements were converted into vulcanisation degree according to Eq. (24), where  $x$  is the hardness at a specific point near the interface,  $x_{min}$  the hardness of unvulcanised rubber, and  $x_{max}$  the hardness of 100 % vulcanised rubber. As the vulcanisation degree is determined near the interface results will be reported as interfacial vulcanisation degrees.

$$\text{Vulcanisation degree} = \frac{x - x_{min}}{x_{max} - x_{min}} \quad (24)$$

### 3.2.4 Crosslink density

Crosslink density  $\nu$  was determined by equilibrium swelling measurements in cyclohexane. Three test pieces of each vulcanised compound were swollen for 72 h according to ISO 1817 at 23°C in 70 ml cyclohexane. Starting sample dimensions were 25 mm x 25 mm x 2 mm. After reaching equilibrium swelling, excessive solvent was removed with filter paper, samples were weighed ( $m_{max}$ ), dried in an oven at 60°C for 24 h to remove all the solvent and finally reweighed ( $m_0$ ). The volume fraction of rubber in the equilibrium swollen vulcanised sample ( $V_r$ ) was determined according to Eq. (25), where  $\rho_s$  and  $\rho_e$  are the densities of solvent and elastomer samples. Density of the elastomer was determined with a METTLER Toledo density kit.

$$V_r = \frac{m_0 \rho_s}{m_0(\rho_s - \rho_e) + m_{max} \rho_e} \quad (25)$$

Crosslink density  $\nu$  (mol/cm<sup>3</sup>) of each vulcanised compound was calculated according to Eq. (22) by applying the Flory-Rehner equation for tetrafunctional networks, where  $V_s$  of cyclohexane is 108.105 cm<sup>3</sup>/mol and  $\chi$  for EPDM-cyclohexane is 0.35 [26]. An average crosslink density was taken of three samples and 95 % confidence intervals are reported.

### 3.2.5 Physico-mechanical properties

For all physico-mechanical properties, measurements were done on the bulk of vulcanised EPDM after producing 2K samples with PP, which is the region shown in Figure 23a where a stable/uniform curing temperature of 180°C is established during injection moulding. The proposed series of tests were selected based on standard rubber testing and on important properties for the current material combinations, like good thermal resistance and mechanical strain, which are ideal for sealing applications. All samples were conditioned at 23 °C for 3 days. A Zwick Z050 equipped with a 1 kN load cell was used at room temperature, a crosshead speed of 200 mm/min and a gauge length of 13.5 mm to determine tensile properties. The hardness was measured using a CV Shore A hardness durometer according to ISO 7619. Compression set tests were performed at 23°C for 24 h according to ISO 815. Three rubber pieces were laminated to result in a sample thickness of 5.9 ± 0.1 mm. The sample diameter was 13 mm. Heat aging of all samples was tested by exposing vulcanised samples of each compound to 100 °C in an air circulated oven for 72 h (ISO 188). After heat aging, tensile strength and hardness were re-evaluated. Average values of three samples of each compound with their 95 % confidence intervals are reported.

### 3.2.6 Compatibility measurements

The compatibility of the thermoplastics with the vulcanised rubbers was assessed by contact angle measurements at high temperature as described by Bex et al. [6]. Vulcanised rubber substrates were taken from the EPDM bulk, where complete vulcanisation is assured. Consequently, physical interactions are enhanced between the rubber and thermoplastics as good wetting is a prerequisite for further adhesion mechanisms. A Dataphysics OCA 15 plus, equipped with a Dataphysics TEC 350 temperature control unit was used, which is the same set-up as used by Bex et al. [6] (Figure 24). The calculation of the contact angles was executed with Dataphysics SCA 202 analysis software.

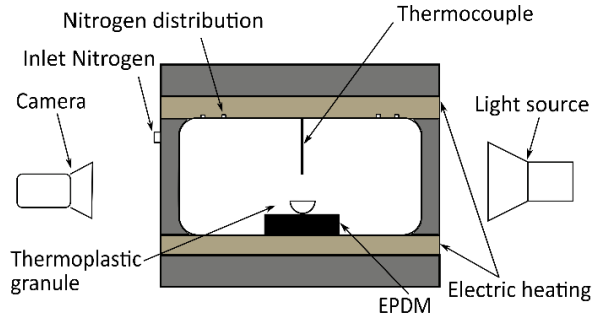


Figure 24: High temperature contact angle measurement chamber with thermoplastic granule on EPDM substrate.

Compatibility measurements were made on completely vulcanised rubber substrates to prevent further vulcanisation during contact angle measurements at high temperature. The average roughness values ( $R_a$ ) of the rubber substrate were measured with a Diavite Compact VHF on the surface in the middle of the rubber part. Each rubber sample was cleaned with isopropanol (99.5 %, Sigma-Aldrich). Square samples of 10 mm x 10 mm x 2 mm were cut out. For measurements with PC, a drying step pre-measurement was necessary according to supplier recommendations. Thermoplastic granules of cylindrical shape, e.g. PP, PE and PC, were cut along the symmetry axis to an equal volume to optimise the view in camera. The measurements started by placing a rubber substrate in the heated chamber under nitrogen environment for 5 minutes to heat up and stabilise. Then, a thermoplastic granulate was placed on the rubber substrate with the spherical side facing down. The temperature was set at 180 °C, 200 °C and 230 °C respectively for PP, PE and PC. ABS was not tested as degradation occurred too fast even under  $N_2$ -environment in the available heating chamber. Due to the elevated temperatures the thermoplastic then started to melt and after reaching a contact angle of 110°, contact angles were registered every minute during 15 min. During these 15 min stable measuring conditions could be assured, e.g. no polymer degradation. Three measurements were done for each combination of thermoplastic with EPDM rubber and average values with their 95 % confidence intervals are reported.

### 3.2.7 Adhesion measurement

Adhesion strength was evaluated by tensile testing. Similar to the analysis of maximum rubber strength, tensile tests were executed on a Zwick Z050 with a speed of 200 mm/min and a gauge length of 13.5 mm. However, here the adhesion strength was defined at the interface between the rubber and thermoplastic. For the material combinations of PP with EPDM and PE with EPDM, samples were punched out perpendicular to the interface, as shown in Figure 23, with a width of 10 mm, and the interface is located in the middle of the sample resulting in sample dimensions of 80 mm x 10 mm x 2 mm. For the material combinations of PC with EPDM and ABS with EPDM, it was not possible with the available machine to punch out samples without damaging the interface, as the material was too hard. Thus, rectangular samples with a width of 30 mm were prepared by sawing in thermoplastic part and cutting in the rubber part resulting in sample dimensions of 80 mm x 30 mm x 2 mm. Samples with this width

still fitted between the clamps of the tensile machine and enabled safe and stable usage of the band saw.

Beside adhesion strength, adhesion percentage was also calculated to compare the adhesion strength ( $\sigma_a$ ) to the total strength ( $\sigma_t$ ) of the rubber according to Eq. (26). Ideally, the adhesion percentage should reach 100 %, i.e. when the rubber bulk material is the weakest spot. However, it has to be taken into account that the rubber bulk is cured at 180°C, leading to higher crosslinking degrees compared to rubber near the interface, where curing temperatures are lower. Furthermore, due to the geometry of the 2K sample and the mismatch of stiffness and Poisson ratio of both materials, debonding occurs near the edges [3]. Consequently, fracture almost always occurs near the interface, either cohesively or adhesively

$$\text{Adhesion percentage (\%)} = \frac{\sigma_a}{\sigma_t} \cdot 100 \quad (26)$$

After fracture, the interface surface of the thermoplastic part was analysed visually with a Keyence VHX-500F digital microscope and a 50x magnification. Five adhesion measurements were performed for each material combination and 95 % confidence intervals are reported.

### 3.2.8 Statistics

Statistical analyses indicated throughout all chapters of this thesis were executed with Minitab 17. The significance of results was compared by a paired t-test (for two dependent groups) with 0.050 as significance level. A mean difference between two groups of zero was chosen as null hypothesis. Accordingly, a p-value smaller than 0.050 means the null hypothesis can be rejecting and a significant difference thus can be seen.

A one-way ANOVA was used to verify differences in mean values between different samples. Significance level was set at  $p < 0.05$ . Tukey's method was used, when equal variances were assumed, to indicate which groups differed significantly. Games-Howel was used when equal variances could not be assumed.

## 3.3 Peroxide curing system

### 3.3.1 Co-agent type and concentration

Type I co-agent TMPT is compared to type II co-agent TAC and variations in co-agent amount are evaluated while maintaining a constant dicumylperoxide level of 3.2 phr. Combinations are made with two non-polar thermoplastics, PE and PP, and two polar thermoplastics, ABS and PC. The considered co-agents could influence rubber compatibility with thermoplastics due to their polar characteristics and affect the adhesion mechanism at the interface. Figure 25 illustrates the material compositions and how the co-agents may affect or induce adhesion mechanism like interdiffusion or chemical bonding. The influence of co-agents in EPDM as shown Figure 25a was already discussed in Section 2.3.2.1. In Figure 25b, the thermoplastic polymer chains are illustrated. At the interface between the thermoplastic and EPDM, chemical bonding and interdiffusion can occur as discussed in Section 2.2.1.4 and 2.2.1.5. Furthermore, cure and swelling characteristics are determined and physico-mechanical properties, like

hardness, tensile properties, heat aging and compression set, of the rubbers obtained with different co-agent type and concentrations are characterised. Consequently, this study investigates whether the compositional changes improve or diminish product properties when exposed to high temperatures, a chemical environment and/or mechanical strains.

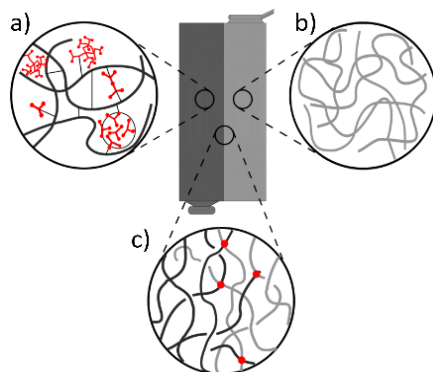


Figure 25: EPDM-thermoplastic sample with (a) EPDM composition with co-agents (red), (b) thermoplastic composition, and (c) adhesion mechanism at the interface, i.e. interdiffusion and chemical bonding (red).

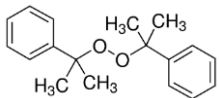
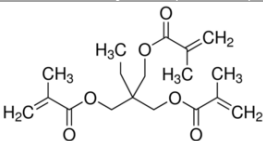
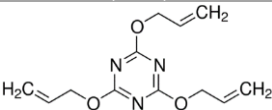
### 3.3.1.1 Materials and processing

All rubber materials were mixed and supplied by Hercorub, Belgium. An EPDM compound was produced and contained the following raw materials:

- (1) Raw gum EPDM (100 phr): Vistalon 2504N, Exxon Mobile with Mooney Viscosity ML 1+4, 125°C = 25 Mooney units (MU), ethylene content = 56.0 wt%, ethylene norbornene (ENB) content = 3.8 wt%);
- (2) Paraffinic oil (30 phr): Sunpar 2280, Petronas;
- (3) Silane treated calcined kaolin filler (110 phr): Polarite 103A, Imerys;
- (4) Zinc oxide (2.8 phr): MLCP International;
- (5) Zinc stearate (1 phr): Zinkstearat SMS, Bärlocher;
- (6) DCP (3.2 phr): Perkadox BC-40MB-gr, AzkoNobel, 40 % active peroxide content.

To analyse the influence of co-agent type and concentration, either Type I co-agent TMPT (Actigran 70, Kettlitz, 70 % active ingredient) or Type II co-agent TAC (50 % active ingredient) was added. The chemical name and structure of the peroxide curing system components were drawn in ChemDraw Prime (PerkinElmer) and are listed in Table 5.

Table 5: Chemical names and structure of the peroxide curing system components.

Dicumylperoxide (DCP)	Trimethylolpropane trimethacrylate (TMPT)	Triallyl cyanurate (TAC)
		

A control compound containing only DCP and no co-agents was included for comparison. The specific compositions are listed in Table 6. Concentrations of co-agents range between 0 and 12 phr. Each EPDM compound was then combined with PP, PE, ABS and PC.

Table 6: Composition of EPDM compounds containing varying co-agent type and concentration (phr).

Component (phr)	C0	TMPT1.5	TMPT3	TMPT6	TMPT9	TMPT12	TAC1.5	TAC3	TAC6	TAC9	TAC12
DCP <sup>a</sup>	3.2	3.2	3.2	3.2	3.2	3.2	3.2	3.2	3.2	3.2	3.2
TMPT <sup>a</sup>	-	1.5	3	6	9	12	-	-	-	-	-
TAC <sup>a</sup>	-	-	-	-	-	-	1.5	3	6	9	12

For the proposed material combinations, 2K samples were produced according to the process as described in 3.2.2. The specific mould temperatures of the rubber and thermoplastic cavity together with the accompanying interface temperature are listed in Table 7. This table also contains the vulcanisation times for all samples which were set high enough to ensure 90 % vulcanisation.

Table 7: Mould temperatures for thermoplastic and rubber cavity with the accompanying interface temperature and curing times for thermoplastic – peroxide-based EPDM.

Mould temperature (°C)	EPDM			
	PP	PE	PC	ABS
Thermoplastic cavity	140	80	155	90
Rubber cavity	180	180	180	180
Interface	161	139	166	143
Curing time (s)	1200	4000	800	4000

### 3.3.1.2 Results and discussion

#### Effect of co-agent type and concentration on rubber bulk properties

The cure curves and corresponding cure properties of the EPDM compounds with varying co-agent type and concentration are shown in Table 8 and Figure 26. When comparing co-agent TAC and TMPT in terms of torque, higher values are reached for TAC, which indicates an increased stiffness that could be caused by a higher crosslink density [40]. The higher torque values for TAC compared to TMPT can be attributed to the occurrence of intramolecular cyclisation and propagation reactions [129]. Higher co-agent concentrations also led to higher torque values because the efficiency of peroxide curing is promoted, causing an increase in crosslink density. 90 % vulcanisation time is

<sup>a</sup> Concentrations of DCP, TMPT and TAC are all calculated in phr of active ingredient. For example TMPT added to the mixture contains only 70 % active mass percentage of TMPT. The phr contents listed in this table only take into account the actual active amount.

significantly improved when adding co-agents compared to the control sample (C0). Both co-agents also reduce scorch safety/ts1 value.

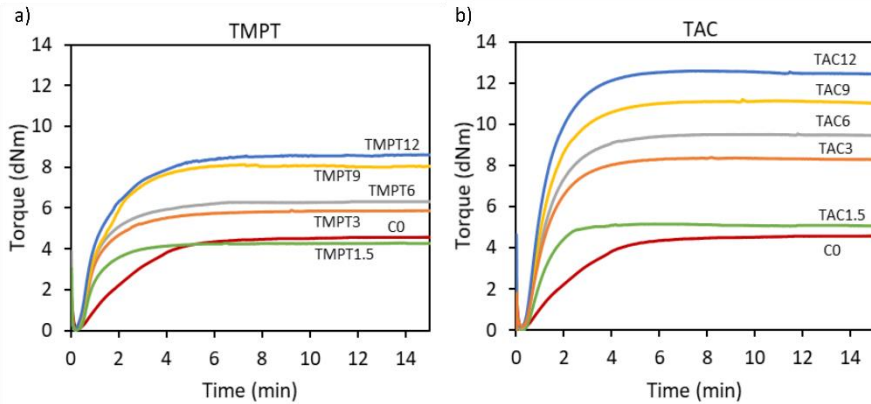


Figure 26: Torque-time curves at 180°C of EPDM compound with varying concentrations TMPT (a) and TAC (b). Control sample without co-agent (C0) is represented in both figures.

Based on the MDR results (Table 8,  $t_{90}$  at 160°C), necessary vulcanisation times for EPDM-PP and EPDM-PC could be set at 16 min when applying TAC or at 21 min when applying TMPT. However, a specific vulcanisation time was chosen for each rubber-thermoplastic combination for the injection moulding process, as mentioned in Table 7. To verify whether at least 90 % vulcanisation was reached during the injection moulding process, interfacial vulcanisation degrees were determined for all samples. For EPDM with PP, PE, ABS or PC at least 90 % vulcanisation degree was reached for all samples. As the vulcanisation time for samples combining EPDM with ABS or PE were set at 4000 s, reversion index at 180°C after 60 min was verified to check whether the EPDM material in the bulk did not degrade during these high vulcanisation times. Reversion was low for samples with 12 phr TAC or TMPT (2.62 and 2.41 respectively) and was 6.85 % for the control sample without co-agents (C0).

Table 8: Vulcanisation time ( $t_{90}$ ) and scorch time ( $t_{s1}$ ) of EPDM compounds with varying concentrations TMPT and TAC and of a control sample without co-agent (C0) at 140°C, 160°C and 180°C.

Sample	$t_{90}$ (min)			$t_{s1}$ (min)		
	140°C	160°C	180°C	140°C	160°C	180°C
C0	120.83	23.13	4.87	21.48	3.57	1.05
TMPT1.5	120.28	17.44	2.58	11.88	1.74	0.62
TMPT3	116.48	20.54	3.73	6.98	1.57	0.58
TMPT6	119.78	21.06	3.05	6.85	1.46	0.53
TMPT9	116.1	20.74	3.33	4.26	1.25	0.52
TMPT12	116.8	20.64	3.72	3.38	1.1	0.46
TAC1.5	106.66	12.88	2.19	13.02	2.12	0.67
TAC3	104.56	15.01	2.92	8.84	1.82	0.55
TAC6	105.93	15.91	3.05	9.66	1.79	0.55
TAC9	106.62	15.06	3.13	8	1.66	0.53
TAC12	106.8	15.88	2.84	7.7	1.49	0.50

Analysing the mechanical characteristics of EPDM (Figure 27), a noticeable increase in hardness and tensile strength is observed when adding higher concentrations of TMPT and TAC (hardness: by 11 °Sh A and 17° Sh A; tensile strength: by 41 % and 53 %, respectively). For elongation at break and compression set a relative decrease occurs when adding higher concentrations of TMPT and TAC (elongation at break: by 48 % and 80 %; compression set: by 31 % and 67 %, respectively). These trends can be ascribed to the general increase in crosslink density when co-agents are added to the peroxide curing system.[75] Thus, mobility of the macromolecular chains is restricted as co-agents can boost crosslinking efficiency and create co-agent bridges between rubber chains as extra crosslinks [89]. Furthermore, samples containing TAC showed an overall stronger increase or decrease in mechanical properties compared to TMPT due to the higher crosslink efficiency of TAC than TMPT at equal concentrations. TAC with its aromatic structure is likely to form co-agent domains, which can covalently bond to rubber and behave as filler particles, creating a more rigid structure.[90] In contrast, TMPT contains softer domains with higher flexibility due to its aliphatic structure. However, even though tear strength was not measured, samples containing higher concentrations than 3 phr of TAC tended to tear in the rubber part during adhesion testing, preventing good measurement of the adhesions strength, which suggests that tear strength is negatively influenced at TAC concentrations above 3 phr.

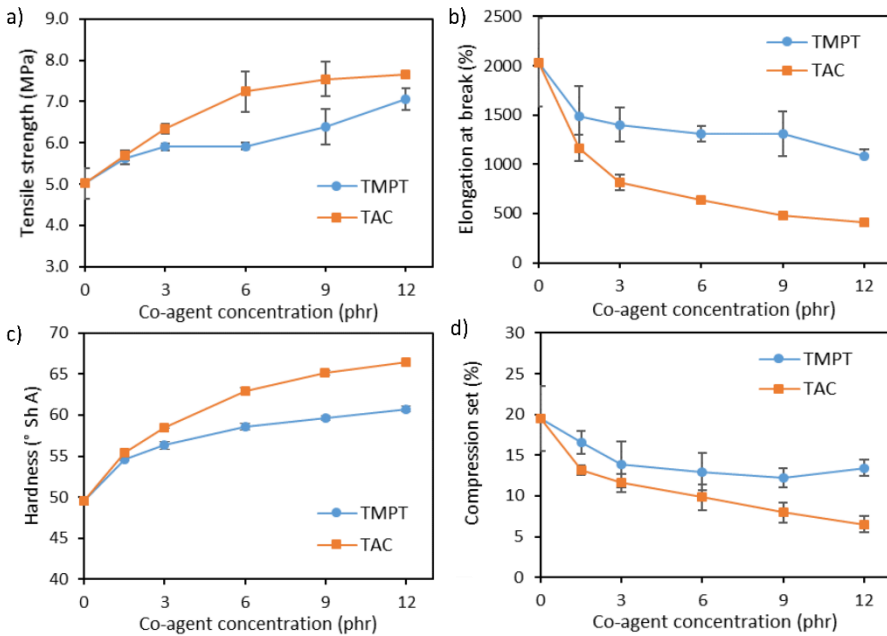


Figure 27: Mechanical properties in function of co-agent concentration for EPDM with TMPT and TAC: tensile strength (a), elongation at break (b), Shore A hardness (c) and compression set (d). Error bars represent 95 % confidence intervals.

After heat aging, tensile strength and hardness were determined again for all samples as shown in Figure 28 to evaluate the thermo-oxidation process. Heat aging is analysed as 2K products with the proposed material combinations could be applied in a thermal

environment in the industry. Thus, when selecting the optimal co-agent type and concentration, thermal aging should not negatively affect product properties.

Except for samples containing 3 phr TAC or TMPT, no significant ( $p > 0.05$ ) influence of thermal aging was detected in tensile strength. However, for aged samples containing TAC, deviations from mean values increased with higher TAC concentrations. This could be due to formation of heterogeneous networks, or co-agent domains, with concentrations of TAC exceeding necessary concentrations to efficiently vulcanise EPDM [59]. Consequently, excess unsaturation of these co-agents might be affected by the oxidation process, creating local deviations in crosslink density. All samples containing TAC also showed a significant ( $p < 0.05$ ) increase in hardness due to continued crosslinking during aging. This was only occasionally observed for TMPT (3 phr and 9 phr). Thus, samples containing TMPT seem to be less affected by aging than TAC. This is probably because there are fewer available double bonds as most of the double bonds were used during vulcanisation due to the dominance of addition reactions for the type I co-agents TMPT [88].

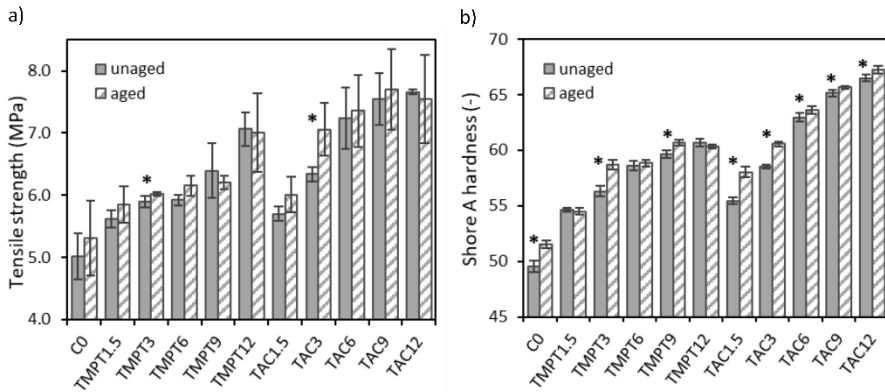


Figure 28: Tensile strength (a) and Shore A hardness (b) of unaged and aged samples. A significant difference ( $p < 0.05$ ) between mean values of aged and unaged samples of each compound is indicated with \*. Error bars represent 95 % confidence intervals.

All EPDM samples were swollen in cyclohexane to determine crosslink density. Results are shown in Figure 29. For the samples with co-agents, the lowest crosslink density was found for TMPT1.5. Both TMPT and TAC-based samples have crosslink densities which gradually increased with higher concentrations, but TAC reaches higher densities at equal concentration compared to TMPT. EPDM without co-agents (C0) had the lowest mean crosslink density and showed large deviations among different measurements. This is probably due to the varying peroxide efficiency in the absence of co-agents. Consequently, disproportionation and chain scission can occur, decreasing the number and consistency of crosslinks. Besides swelling in cyclohexane, water swelling was determined as well but the mass swelling degrees remained below 0.15 % for all samples. This indicates that increasing the co-agent concentration does not influence swelling in a polar fluid like water.

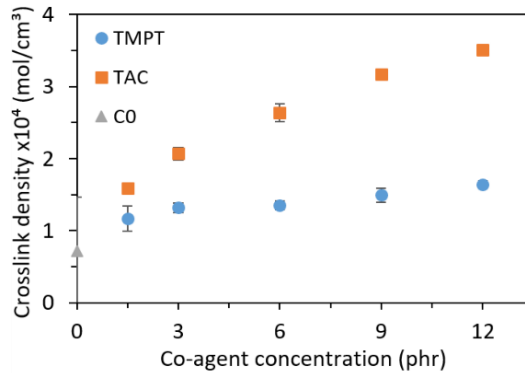


Figure 29: Crosslink density of control sample C0, and EPDM with varying concentrations of TAC and TMPT. Error bars represent 95 % confidence intervals.

Results of crosslink densities confirm the achieved mechanical properties from Figure 27 and torque values represented in Figure 26. Crosslink density increases with increasing co-agent concentration. In addition, Type II co-agent TAC has a higher crosslinking efficiency than TMPT, leading to higher densities at equal co-agent concentrations. Even though crosslink densities were measured in the rubber bulk material, at the interface (with lower vulcanisation temperature), higher co-agents concentrations will similarly lead to higher crosslink densities, which can affect the adhesion mechanism.

#### Effect of co-agent type and concentration on adhesion

To analyse the influence of co-agents in EPDM on compatibility with PP, PE, and PC, measurements were performed at high temperature on an EPDM substrate without co-agents (C0) and substrates containing the highest concentration (12 phr) of TMPT and TAC (compound TMPT12 and TAC12). Results are shown in Figure 30. To indicate whether the co-agents were indeed present at the surface of the rubber substrate, infrared (IR) spectra were acquired with a Perkin Elmer Spectrum 65 FTIR coupled to an attenuated total reflection (ATR) unit. Roughness values  $R_a$  were  $0.59 \pm 0.16 \mu\text{m}$  for C0,  $0.44 \pm 0.08 \mu\text{m}$  for TMPT12 and  $0.69 \pm 0.15 \mu\text{m}$  for TAC12. As the roughness values are low and comparable, the effect of the roughness on wetting is limited and is therefore not taken into account. Contact angles of PP, PE and PC cannot be compared as viscosity was not taken into account, however, this was not the goal of this study.

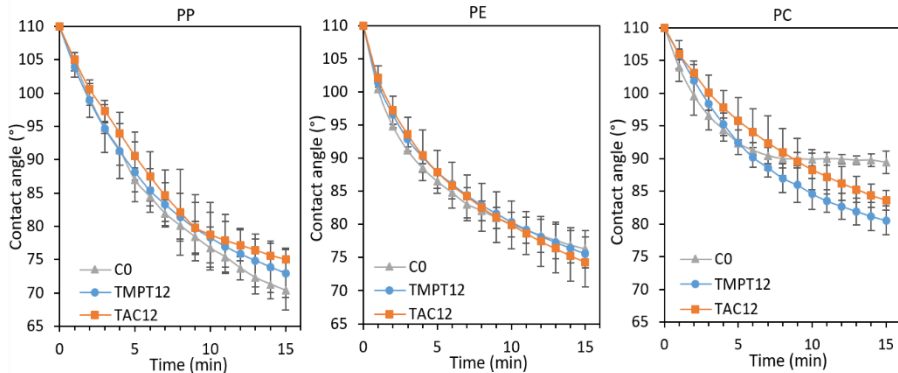


Figure 30: Contact angles of thermoplastic melts (PE at 180°C, PP at 200°C and PC at 230°C) during spreading on EPDM without co-agent (C0), with 12 phr TMPT (TMPT12) and with 12 phr TAC (TAC12). The error bars represent 95 % confidence intervals.

Compatibility measurements were performed on vulcanised rubber substrates. Consequently, the co-agents already participated in the vulcanisation process. During the actual adhesion in the 2K injection moulding process, co-agents can migrate to the surface due to their limiting affinity for EPDM [4]. Figure 31 confirms the presence of these co-agents at the surface of TAC12 and TMPT12 due to one characteristic peak at 1738  $\text{cm}^{-1}$  (C=O) for TMPT12 and three peaks at 1565  $\text{cm}^{-1}$  (conjugated cyclic -C=N groups of triazine), 1422  $\text{cm}^{-1}$  (=C-H) and 1338  $\text{cm}^{-1}$  (=C-H) for TAC12. In Figure 30, contact angles between PE and EPDM substrates indicate no significant difference in wetting behaviour whether co-agents are added or not. Thus, physical interactions at the interface are not affected when adding co-agents. For PP, similar results were found, but additionally, C0 does tend to go to slightly lower contact angles than TAC12 and TMPT12, probably due to the co-agent polarity. Interestingly, PC did show a significant difference in final contact angles between C0 and TAC12 or TMPT12. Thus, the presence of TAC or TMPT might influence the adhesion mechanism at the interface with PC, due to their possibility to migrate to the surface and to promote wettability. Based on these results, a higher adhesion strength is expected with higher co-agents concentrations for PC. Similar results were found in a study by Thust [4], where the interaction parameters (Eq.(15)) between co-agents and EPM and PA 6.6 were compared. He found that high interaction parameters were reached between co-agents and EPM, leading to segregation, while the interaction parameter with PA6.6 was much lower. Consequently, in PA6.6-EPM 2K samples co-agent enrichment occurred at the interface due to the higher affinity with PA6.6, promoting adhesion. Thus, similarly here, PC has higher polarity than EPDM due to the carbonyl groups and therefore the polar co-agents will have a higher affinity with PC resulting in a better compatibility. For a PC melt on a C0 substrate in Figure 30, angles stabilised to a constant value after 7 min, while on TAC12 and TMPT12 angles were still decreasing after 15 min.

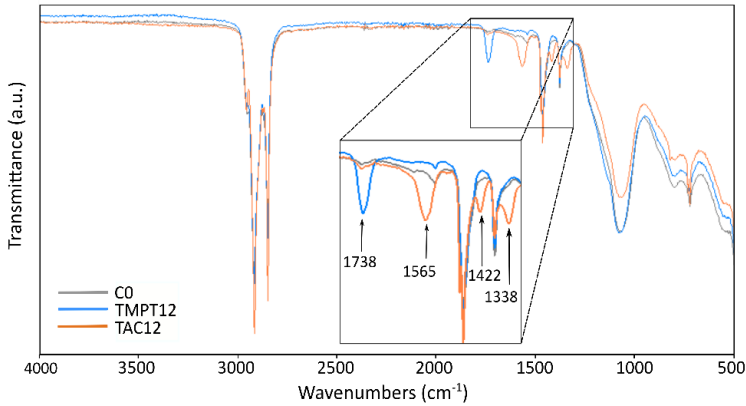


Figure 31: ATR-FTIR spectra of EPDM without co-agent (C0), with 12 phr TMPT (TMPT12) and with 12 phr TAC (TAC12).

To determine the actual adhesion strength at the interface, tensile tests were performed and results for these measurements in function of co-agent concentration are shown in Figure 32 for TAC and TMPT. Microscopic images are represented for each thermoplastic surface after fracture with EPDM without co-agents (C0) and the sample with the highest adhesion strength.

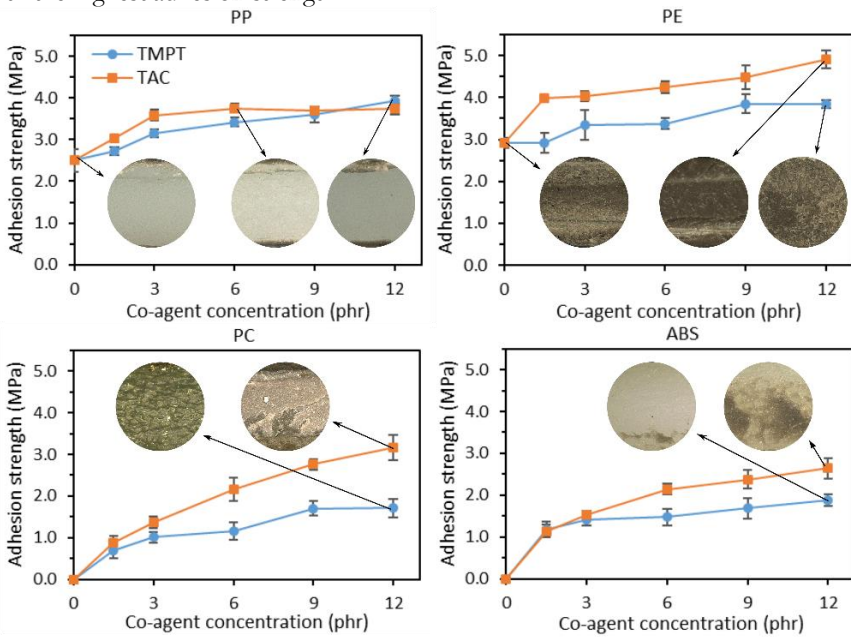


Figure 32: Adhesion strength in function of co-agent concentration for PP, PE, PC and ABS. The error bars represent 95 % confidence intervals. The microscopic images show a circular zone (2 mm radius) of the fracture surfaces at the thermoplastic side. Black indicates the rubber and white the thermoplastic. For PC with TMPT12, no rubber is visible, the PC itself is transparent resulting in a darker image.

First, for PP, an increase in adhesion strength was reached when co-agents were added. Initially, TAC leads to the highest strength at 6 phr with a significant adhesion improvement of 50 %. Further increase in concentration does not further improve the adhesion. TMPT shows a steadily increasing trend up to 12 phr by 57 % compared to EPDM without co-agents (0 phr). It is important to notice that even though co-agents increase the adhesion strength no fully cohesive failure was established, as can be seen in the microscopic images in Figure 32 (PP). The only visible improvement was observed at the edges of the sample, where more rubber is present. Possibly, co-agents improve chemical bonding via crosslinks with PP, but it is likely that the efficiency remains low. Second, PE shows a similar increase in adhesion with increasing co-agent concentration (by 31 % and 68 %, for TMPT and TAC respectively). TAC leads to overall better adhesion than TMPT. It is known that allylic type co-agents, such as TAC, are suitable for crosslinking PE as they do not readily homopolymerise like acrylic types (such as TMPT) do [61]. TAC tends to participate with hydrogen abstracting peroxides, like DCP, making it more efficient when crosslinking saturated polymers like PE [61]. It is expected that chemical bonds will form at the interface between EPDM and PE and results in Figure 32 confirm that TAC does improve the adhesion better than TMPT. Overall, results of PP and PE confirm findings of Thust [4] that the use of co-agents leads to a clear improvement in rubber-thermoplastic adhesion strength. Finally, for the polar PC and ABS, higher co-agent concentrations resulted in higher adhesion strengths. Without co-agents it was not possible to measure adhesion as samples fell apart upon opening of the mould. TAC also showed higher adhesion strengths than TMPT, up to even partial cohesive failure at 12 phr, as evidenced by the fracture surface images. Compatibility measurements already indicated that adding co-agents enhance wettability and thus physical interaction at the interface. Consequently, further adhesion mechanisms like interdiffusion can be promoted. Results in Figure 32 confirm these findings.

The adhesion strength was determined by tensile testing. However, the tensile strength of the rubber bulk materials, as shown in Figure 27a also increases with higher co-agent concentrations. Therefore, the adhesion strength is compared to the bulk strength by calculating a percentage of adhesion (Eq. (26)). In Figure 33, adhesion percentages are given in relation to co-agent concentration for PP, PE, PC and ABS.

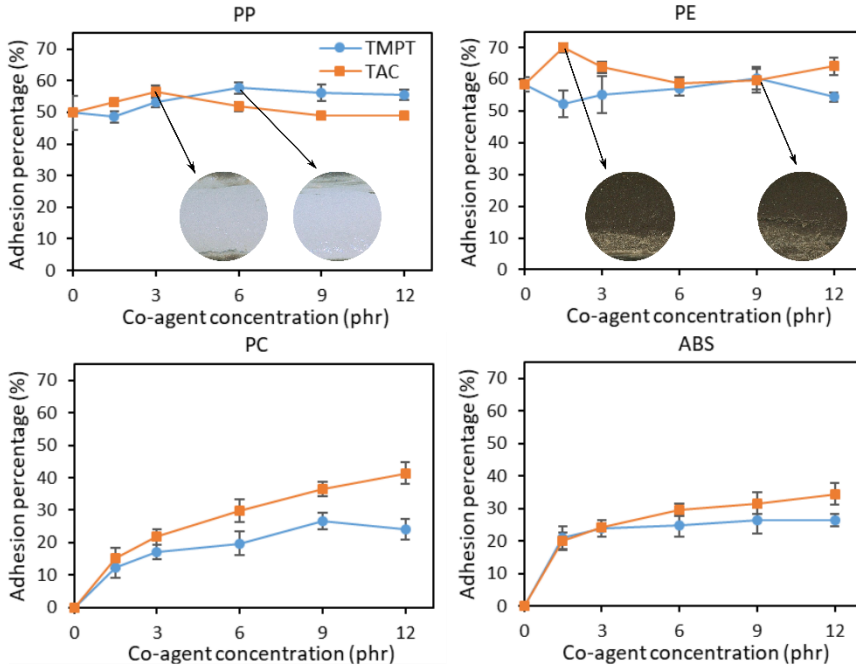


Figure 33: Adhesion percentage (adhesion strength divided by total strength) in function of co-agent concentration for PP, PE, PC and ABS. The error bars represent 95 % confidence intervals. The microscopic images show a circular zone (2 mm radius) of the fracture surfaces at the thermoplastic side. Black indicates the rubber and white the thermoplastic.

Based on the results represented in Figure 33, optimal co-agents concentrations can be determined specifically related to adhesion. As illustrated for PP and PE, TAC improves the adhesion when low concentrations are added. At these concentrations, radical yield increases, creating higher reactivity at the interface. Further increase in concentrations will lead to higher crosslink densities. Generally, a combination of chemical bonding and interdiffusion is expected, as was also stated in the study of Thust [4] when combining peroxide cured HNBR with PA 6.6. For chemical bonding, higher crosslink densities would be beneficial for improving interfacial bonding. However, for interdiffusion, high crosslink densities will restrict good chain mobility across the interface [4]. The combination of these mechanisms causes an optimum to occur here at a certain co-agent concentration. Furthermore, in the case of TAC, rigid co-agent domains can also form and side-reactions among co-agents can additionally reduce their overall positive effect on interfacial bonding. TMPT as co-agent requires higher concentrations for optimal adhesion compared to TAC. In the case of PP, optimal concentration for TAC in terms of adhesion percentage is 3 phr and 6 phr for TMPT. Although not significantly better than TAC, results of TMPT confirm findings of De Risi et al. [106] that improved properties can be reached when adding a methacrylate co-agent due to minimisation of PP degradation. For PE, 1.5 phr TAC increases the adhesion percentage by 70 %, while TMPT has almost no added value. As mentioned before, literature also indicates that TAC is more suitable for crosslinking PE [61]. Even though an optimum was found at 1.5 phr TAC for PE, a small increase can be seen again at high

TAC concentrations. At this concentration of 1.5 phr, TAC affects the adhesion stronger than the bulk strength. 12 phr TAC is not significantly different from 9 phr TAC. Furthermore, the non-polar PP and PE do not show similar trends as for PP there are the competing reactions of chain scission and crosslinking while PE normally has a good efficiency of crosslinking with peroxides. PP and PE also have a different polymer chain composition. Consequently, for PP diffusion will be more difficult as it has additional methyl group side chains compared to PE. Thus, this could affect the optimal co-agents concentrations. The trends of the polar PC and ABS are similar to the ones found in Figure 32. Thus, the effect of co-agent concentration on the adhesion strength is more pronounced than on the bulk strength. With higher co-agent concentrations, PC has the best adhesion with EPDM containing 12 phr TAC due to the better compatibility, further improving the adhesion.

### 3.3.2 Dicumylperoxide concentration

To investigate the influence of peroxide curing agent in EPDM on the adhesion with polar and non-polar thermoplastics, concentrations of DCP are varied while maintaining a fixed concentration of co-agent TMPT. The adhesion between EPDM and thermoplastics PE, PP, ABS and PC is evaluated by contact angle measurements at high temperature and tensile tests. Furthermore, cure characteristics and compound swelling are analysed to determine the state of cure and crosslink densities as this may influence the adhesion mechanism. General properties of all EPDM compositions are determined as well, in particular tensile properties, thermal resistance, compression set and hardness which are all important properties for sealing applications. Eventually, an assessment is made of the optimal DCP concentration for each EPDM-thermoplastic combination while taking into account the possible changes in rubber bulk properties.

#### 3.3.2.1 Materials and processing

All rubber materials were mixed and supplied by Hercorub, Belgium. An EPDM compound was produced which contains the following raw materials:

- (1) Raw gum EPDM (100 phr): Vistalon 2504N, Exxon Mobile with Mooney Viscosity ML 1+4, 125°C = 25 Mooney units (MU), ethylene content = 56.0 wt%, ethylene norbornene (ENB) content = 3.8 wt%);
- (2) Paraffinic oil (30 phr): Sunpar 2280, Petronas;
- (3) Silane treated calcined kaolin filler (110 phr): Polarite 103A, Imerys;
- (4) Zinc oxide (2.8 phr): MLCP International;
- (5) Zinc stearate (1 phr): Zinkstearat SMS, Bärlocher;
- (6) TMPT (2 phr): Actigran 70, Kettlitz, 70 % active ingredient.

To analyse the influence of peroxide curing agent concentration, formulations were made with 2, 4, 6, and 8 phr DCP (Perkadox BC-40MB-gr, AzkoNobel, 40 % active peroxide content). The EPDM sample names with respective DCP concentration are listed in Table 9. Each EPDM composition was then combined with PP, PE, ABS and PC.

Table 9: EPDM compositions with varying DCP concentrations.

Component (phr)	DCP2	DCP4	DCP6	DCP8
DCP <sup>a</sup>	2	4	6	8

For the proposed material combinations, 2K samples were produced according to the process as described in 3.2.2. The mould temperatures of each cavity and the accompanying interface temperatures and curing times are identical to the ones used in the study concerning co-agent type and concentration and can be found in Table 7.

### 3.3.2.2 Results and discussion

#### Effect of DCP concentration in EPDM on rubber bulk properties

MDR measurements were taken at 180°C for 20 min, at 160°C during 45 min and at 140°C during 160 min. Cure characteristics of all EPDM compounds are listed in Table 10. As DCP concentration increases, a clear increase in  $\Delta$ torque can be seen. This is due to the improved crosslinking efficiency as peroxide decomposition follows first order reaction kinetics [89], [93]. Measurements of crosslink density (Figure 35) confirm  $\Delta$ torque results indicating a linear correlation between crosslink density and DCP concentration. Furthermore, vulcanisation times ( $t_{90}$ ) at 180°C and 160°C do not differ much between different concentrations. However, at 140°C, higher concentrations do lead to better curing efficiency. Scorch time ( $t_{s1}$ ) tends to decrease with higher concentrations at every temperature. These trends in  $t_{90}$  and  $t_{s1}$  are also illustrated in Figure 34. Furthermore, reversion resistance was determined for each compound at 180 °C after 60 min according to Eq. (23), as the curing times for EPDM-PE and EPDM-ABS were set at 4000 s to ensure vulcanisation of the rubber near the interface leading to a long exposure to 180 °C in the bulk. Reversion in all compounds remains limited and reduces with higher peroxide concentration. However, it is recommended to use higher concentrations for EPDM-PE and EPDM-ABS to minimise reversion in the EPDM bulk. Furthermore, 90 % vulcanisation degree was reached at the interface of all 2K samples, indicating that the curing times listed in Table 7 sufficed.

Table 10: Cure characteristics of the EPDM compounds with varying DCP concentration.

Cure characteristics	DCP2	DCP4	DCP6	DCP8
$\Delta$ torque 180°C (dNm)	3.34	7.05	9.29	10.06
$t_{90}$ (min) at 180°C	2.65	2.49	2.65	2.14
at 160°C	17.96	16.79	18.47	17.07
at 140°C	118.38	117.16	106.45	102.46
$t_{s1}$ (min) at 180°C	0.86	0.52	0.46	0.41
at 160°C	2.45	1.42	1.06	0.89
at 140°C	17.18	11.70	7.02	6.39
Reversion index (%)	14.39	15.34	10.18	1.38

<sup>a</sup> Concentrations of DCP and TMPT are calculated in phr of active ingredient. For example TMPT added to the mixture contains only 70 % active mass percentage of TMPT. The phr contents listed in the table only take into account the actual active amount.

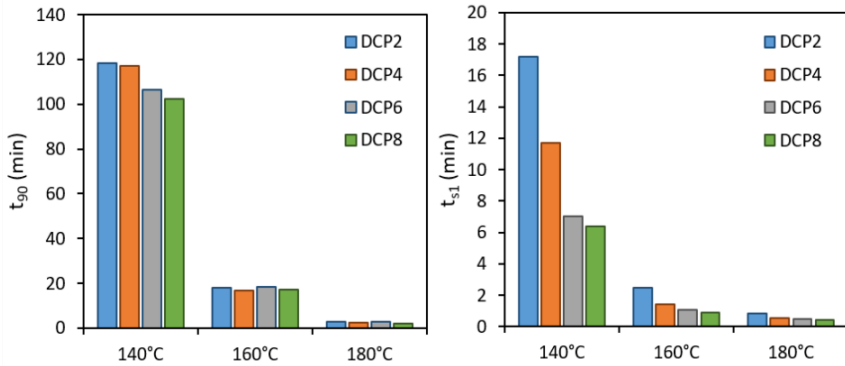


Figure 34: Vulcanisation times  $t_{90}$  (a) and scorch times  $t_{s1}$  (b) at 140°C, 160°C and 180°C for EPDM with 2 phr DCP (DCP2), 4 phr DCP (DCP4), 6 phr DCP (DCP6) and 8 phr DCP (DCP8).

Swelling measurements, followed by calculation of crosslink densities (Figure 35), indicate a linear relation between crosslink density and DCP concentration. This is due to an increasing amount of free radicals when adding higher concentrations of peroxides which cause an efficient formation of intermolecular bridges [130]. Even though these crosslink densities were determined in the EPDM bulk (cured at 180°C), a similar linear increase can be expected near the interface, which is cured at lower temperatures. Therefore, the increased crosslink densities have to be taken into account if both chemical bonding and/or interdiffusion occurs because higher crosslink densities may limit interdiffusion due to restriction of chain mobility, while interfacial bonding may be promoted due to increased reactivity at the interface [4], [123].

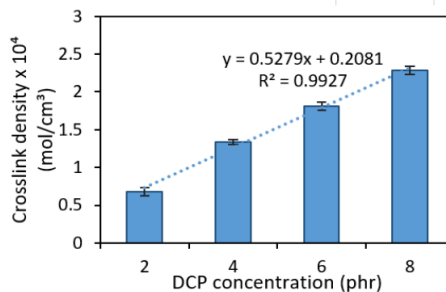


Figure 35: Crosslink density obtained from swelling measurements in function of DCP concentration. The dotted line represent a linear fit, which is accompanied by the linear equation and the correlation coefficient  $R^2$ . Error bars represent 95 % confidence intervals.

In Figure 36, mechanical properties are represented in function of DCP concentration. Adding higher concentrations of DCP clearly increases tensile strength and hardness (Figure 36a,c) respectively by 70 % and 22 %, when going from 2 phr to 8 phr DCP. For compression set and elongation at break (Figure 36b,d), an opposite trend was established with respective relative decreases of 77 % and 50 %. These results confirm literature findings and can be ascribed to the general increase in crosslink density and dense network formation of carbon-carbon crosslinks [40], [91]. Thus, requirements

in mechanical properties need to be taken into account when selecting the right peroxide concentration.

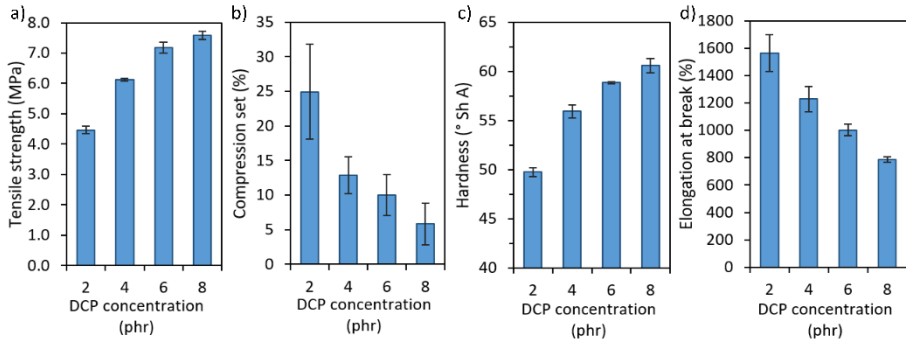


Figure 36: Mechanical properties of EPDM in function of DCP concentration: tensile strength (a), compression set (b), Shore A hardness (c), and elongation at break (d). Error bars represent 95 % confidence interval.

Heat aging was assessed by tensile and hardness measurements before and after exposure to 100°C during 72 h. The effect of this thermo-oxidation process in relation to DCP concentration is important as thermal resistance is required for sealing applications at high temperature. Results are shown in Figure 37. Paired t-tests of tensile strengths did not show a significant difference between aged and unaged samples ( $p < 0.05$ ) and the tensile strength was retained for all samples with at least 97 %. This high percentage of retention indicates good thermal stability. Thus, EPDM containing concentrations between 2 and 8 phr did not show any relative deterioration in time in terms of tensile strength. However, hardness was significantly affected resulting in an average increase in hardness and  $p$ -value  $< 0.050$  (2 phr DCP: by 2.4° Sh A,  $p = 0.000$ ; 4 phr DCP: by 1.3° Sh A,  $p = 0.001$ ; 6 phr: by 1.3° Sh A,  $p = 0.000$ ; 8 phr: by 1.44° Sh A,  $p = 0.001$ ). This change in hardness may be due to additional crosslinking or hardening caused by side reactions. For 2 phr DCP, hardness increased most from unaged to aged samples. The double bonds of EPDM are probably affected by oxidation due to the lower peroxide crosslinking efficiency at this low concentration, but overall the change in hardness remains limited.

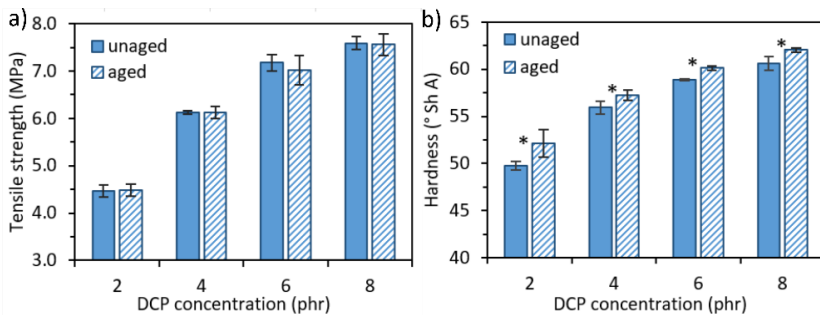


Figure 37: Tensile strength (a) and hardness (b) of unaged and aged samples. A significant difference ( $p < 0.05$ ) between mean values of aged and unaged samples of each compound is indicated with \*. Error bars represent 95 % confidence intervals.

### Effect of dicumylperoxide in EPDM on the adhesion

Results of the study on the effect of co-agents in the peroxide curing system showed that co-agents significantly promoted wetting with the polar thermoplastic PC. Therefore, wetting behaviour of molten PP, PE and PC was evaluated on EPDM substrates to analyse the influence of DCP concentration as well. Results of spreading of PE, PP and PC on each EPDM substrate (DCP2, DCP4, DCP6 and DCP8) are shown in Figure 38. Spreading dynamics cannot be compared directly between the different thermoplastics (PP, PE and PC) as viscosity values are not identical. This was, however, not the goal of these tests.

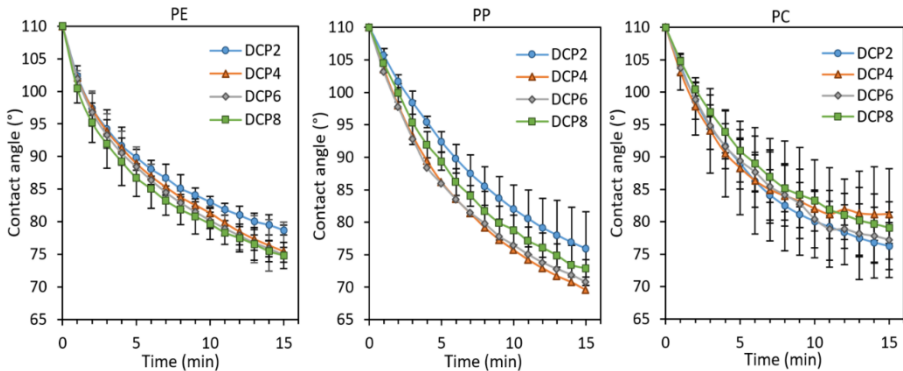


Figure 38: Contact angle measurements of thermoplastic melts of PE (180°C), PP (200°C) and PC (230°C) during spreading on EPDM with 2 phr DCP (DCP2), 4 phr DCP (DCP4), 6 phr DCP (DCP6) and 8 phr DCP (DCP8). Error bars represent 95 % confidence interval.

Contact angles of PP and PE on vulcanised substrates indicate better wetting, after 15 min, on the substrates with 4, 6 and 8 phr DCP (respectively DCP4, DCP6 and DCP8) compared to 2 phr DCP (DCP2) due to the presence of double bonds that were not consumed during curing. The slightly higher contact angles of DCP2 may be caused by oxidation of the DCP2 surface. The ATR-FTIR spectra showed a broad band between 3100 and 3600  $\text{cm}^{-1}$ , which was not observed for DCP4, 6 or 8 (Figure 39). Thus, polar hydroxyl groups were present on the surface of the DCP2 substrate. Similarly, for PC better wetting was reached on DCP2, which can be ascribed to the polar groups on the surface. Overall, between 4, 6 and 8 phr, no significant difference was found on polar or non-polar thermoplastics when increasing the DCP concentration. Furthermore, measurements were executed on fully vulcanised substrates, where DCP already participated in the vulcanisation process leading to likely decomposition products methane, acetophenone and 2-phenylpropanol-2 [88]. However, neither DCP, nor the decomposition products seem to significantly affect the surface composition of vulcanised EPDM with higher DCP concentrations which suggests that changes in surface free energies are limited. Thus, contrary to the study of co-agents, showing a significant influence of co-agent concentration on EPDM-thermoplastic compatibility, no compatibility differences in function of peroxide concentration were found. However, it might still be possible that shear induced enrichment of peroxides occurs at the interface during the injection moulding process as proposed by Thust [4].

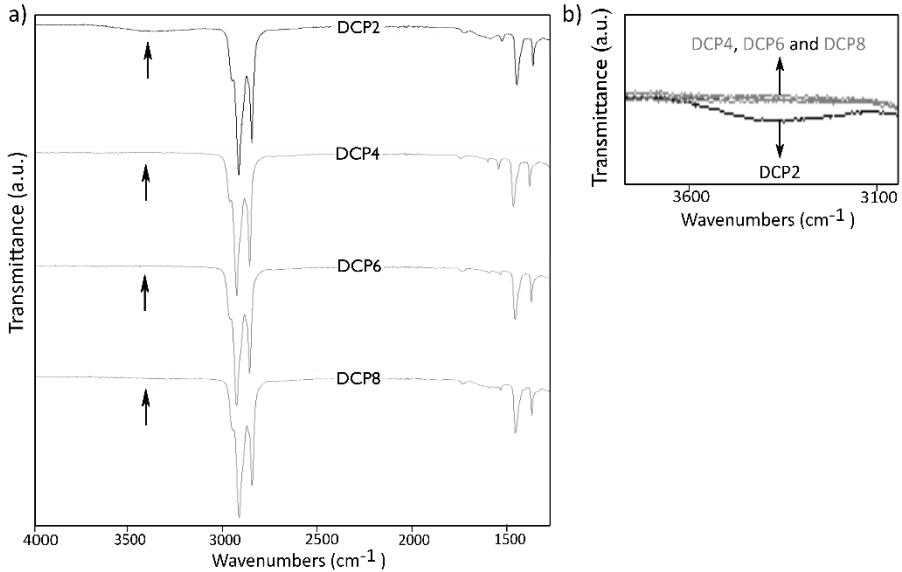


Figure 39: ATR-FTIR spectra of vulcanised EPDM substrates: DCP2 (2 phr DCP), DCP4 (4 phr DCP), DCP6 (6 phr DCP) and DCP8 (8 phr DCP) (a), and a magnification of the spectra between 3100 and 3600  $\text{cm}^{-1}$  (b).

The adhesion strength between EPDM and PE, PP, ABS or PC was determined by tensile testing. Results are represented in Figure 40. Besides the adhesion strength for the different material combinations, EPDM strength ( $\sigma_t$ ) is shown as well in function of DCP concentration.

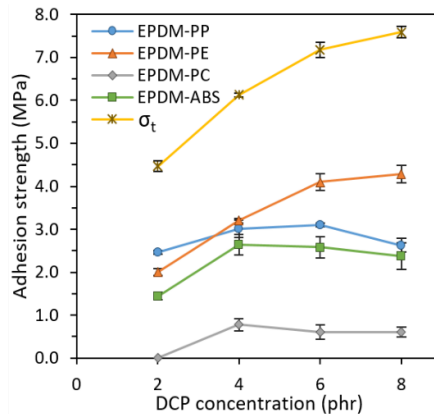


Figure 40: Adhesion strength in function of DCP concentration between EPDM and PE, PP, ABS and PC. EPDM strength ( $\sigma_t$ ) is represented as comparison. Error bars indicate 95 % confidence intervals.

Only the adhesion with PE increases significantly from 2 to 8 phr DCP. For PP adhesion strength increases to an optimum at 6 phr DCP but afterwards decreases significantly again to 8 phr DCP. For ABS and PC, the adhesion strength improves significantly up to a 4 phr DCP but afterwards no significant differences are established between 4, 6 or 8 phr DCP. Furthermore, the EPDM strength also increases with higher DCP concentrations. Thus, to analyse whether the adhesion strength does not merely improve due to the increased EPDM strength, values of adhesion strength were compared to the EPDM strength at each concentration by calculating an adhesion percentage (Eq.(26)), which is represented in Figure 41.

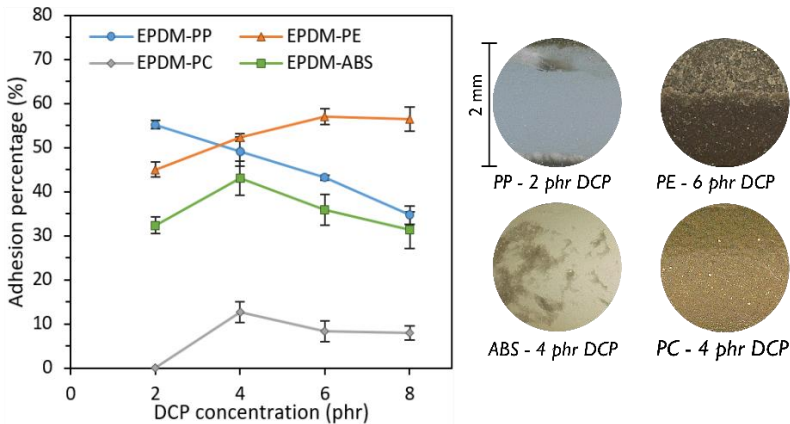


Figure 41: Adhesion percentage in function of DCP concentration for PP, PE, PC and ABS. The error bars represent 95 % confidence intervals. The microscopic images show a circular zone (2 mm radius) of the fracture surfaces at the thermoplastic side. Black indicates the rubber and white the thermoplastic. For PC - 4 phr DCP, no rubber is visible and for PE - 6 phr DCP only rubber is visible.

At the interface between EPDM and thermoplastics, adhesion mechanisms like chemical bonding or interdiffusion are expected. During injection moulding, the crosslinking reaction in the EPDM part may influence these adhesion mechanisms at the interface. Specifically, when interdiffusion is dominant, formation of crosslinks will limit chain mobility. However, the radicals created during curing can increase reactivity near the interface and improve co-vulcanisation which entails chemical bonding. When both adhesion mechanisms are plausible, a combination of both is expected as also stated by Thust [4].

In case of PP, scission reactions compete with crosslinking. Results of adhesion percentage indicate that increasing the DCP concentration drastically decreases the adhesion percentage (from 55 % at 2 phr to 35 % at 8 phr) in a linear manner ( $R^2 = 0.9921$ ). At the interface, both chemical bonding and interdiffusion could occur as adhesion mechanism, but it seems that both mechanisms are adversely affected by higher DCP concentrations. Interdiffusion is limited due to higher crosslink density in EPDM at the interface and probably degradation of PP prevails over crosslinking. This negative effect of higher peroxide concentrations was also seen in studies of EPDM/PP TPVs [92], [101]. In addition, as peroxide concentration increases, more scission may occur which reduces molecular weight of PP near the interface, therefore, the adhesion caused by interdiffusion may be limited due to a lack of entanglements [131]. Thus, for EPDM-

PP a low DCP concentration is recommended in combination with a higher co-agents concentration, as results in Section 3.3.1 showed that 6 phr TMPT could reduce PP degradation at 3.2 phr DCP.

The adhesion percentage between EPDM and PE gradually increases with higher peroxide concentration (by 12 % from 2 to 6 phr) up to a maximum at 6 phr DCP with a cohesive failure. At higher concentrations, i.e. 8 phr DCP, adhesion is not further improved, but merely adhesion strength increases due to an increase in EPDM strength (Figure 40). Literature also indicates the successful crosslinking of PE by DCP and confirms that increasing concentrations can lead to higher crosslink density of PE [95], [96]. However, Cespedes et al. [95] highlighted that improved properties are only reached up to certain DCP concentration in TPVs containing EPDM, HDPE and ground tire rubber because the thermoplastic phase may be affected by a thermo-oxidation (degradation) process. Thus, similarly in this study EPDM-PE adhesion improves up to 6 phr DCP, which can be mainly attributed to an increase in chemical bonding or formation of more carbon-carbon bonds between EPDM and PE. Chemical bonding dominates over interdiffusion because the higher crosslink density would normally limit chain mobility. Additionally, to improve the adhesion even more, co-agent triallyl cyanurate (TAC) would be recommended as this caused better adhesion at 1.5 phr TAC with 3.2 phr DCP, while TMPT did not enhance adhesion.

The adhesion of ABS only improves up to 4 phr DCP after which the adhesion percentage decreases again to 6 phr. Mean values decrease further to 8 phr, but the difference with 6 phr DCP is not significant. PC shows a similar trend. In case of ABS, crosslinks between EPDM and ABS chains are possible. However, degradation may occur as well. Therefore, crosslinking reactions may be promoted up to 4 phr, but higher concentration may limit interdiffusion and cause chain scission of ABS near the interface instead of promoting crosslinking. At 4 phr, the ABS surface showed occasional partial cohesive failure. For PC, no adhesion was reached with EPDM containing 2 phr DCP during injection moulding. In contrast, contact angle measurements indicated better wetting on 2 phr DCP, but FTIR measurements showed the presence of polar groups due to degradation. In unvulcanised EPDM with 2 phr DCP, these polar groups were not present yet at the interface and therefore did not affect adhesion during injection moulding. Probably, this low concentration did not suffice to induce an adhesion through interdiffusion, but at higher DCP concentrations, a low adhesion was possible. Similarly as for ABS, 4 phr DCP is optimal for adhesion with PC, but ABS reaches a higher adhesion percentage of 43 % compared to 13 % for PC as crosslinking may occur at the EPDM-ABS interface. Higher concentrations do not further improve adhesion with PC. This is in agreement with wetting measurements as compatibility was not affected by higher peroxide concentrations. The interdiffusion process will, however, be limited by higher crosslink density in EPDM causing a significant decrease in adhesion percentage from 4 phr to 6 phr. For polar thermoplastics, it would be recommended to implement a high TAC concentration to further improve adhesion.

The study by Thust [4] showed that adhesion between HNBR and PA6.6 was negatively affected by higher DCP concentration. In that study, co-vulcanisation was not promoted due to the high miscibility of DCP in HNBR and the higher interaction parameter of DCP with HNBR compared to PA6.6. Thust ascribed the decrease in adhesion to a decrease in interdiffusion due to the higher crosslink densities with higher DCP concentrations. This negative effect of DCP on the interdiffusion was also found here. Overall, results from the current study together with results from Thust [4] show

that selecting the optimal DCP concentration depends specifically on the 2K material combination and in particular on the dominant adhesion mechanism.

### 3.4 Sulphur curing system

According to the process developed by Bex et al. [1] sulphur-cured EPDM can adhere to PE. However, due to the low melting temperature of PE ( $\sim 135^\circ\text{C}$ ), high cycle times are required to ensure complete vulcanisation near the interface. Thus, with the current process, producing 2K EPDM-PE products is less economic compared to a manual connection of 1K products [3]. However, vulcanisation times, and consequently processing times, could be reduced by changing the composition of EPDM. For example, accelerators in the sulphur curing system are known to influence the kinetic parameters of vulcanisation. Accelerators can increase the reaction rate, reduce vulcanisation time, and reduce the required vulcanisation temperature [89]. Adjusting the accelerator composition, i.e. primary and secondary, in the sulphur curing system will alter curing kinetics. Therefore, the influence of cure rate on the adhesion was investigated to analyse whether processing time can be optimised without reducing the adhesion strength.

#### 3.4.1 Materials and processing

All rubber materials were mixed and supplied by Hercorub, Belgium. An EPDM compound was produced which contains the following raw materials:

- (1) Oil extended EPDM (200 phr): DUTRAL TER 6537, Eni Polimeri with Mooney Viscosity ML 1+4,  $125^\circ\text{C} = 43$  Mooney units (MU), propylene content = 32.0 wt%, ethylene norbornene (ENB) content = 8 wt%;
- (2) Paraffinic oil (56 phr): Sunpar 2280, Petronas;
- (3) Carbon black: N772 from Konimpex (76 phr) and N550 from Aditya Birla Group (56 phr);
- (4) Zinc oxide (5 phr): De Craene;
- (5) Stearic acid (1.1 phr): Baerocid SMS-1 A, Baerlocher GmbH;
- (6) Elemental sulphur (1 phr): Integrated Chemicals Specialties BV.

Following accelerators were used: dibenzothiazyl disulphide (MBTS, 80 % active ingredient, SAFIC ALCAN), tetramethylthiuram disulphide (TMTD, 80 % active ingredient, Avokal GmbH), zinc dialkyldithiophosphate (ZDDP, 67 % active ingredient, RheinChemie Additives), zinc-N-diethyl dithiocarbamate (ZDEC, 75 % active ingredient, Croxton+Garry Limited). Five different EPDM compositions were made with varying curing system compositions as shown in Table 11. Each EPDM composition was adhered to PP and PE.

Table 11: Sulphur curing system composition

Component (phr)	S1	S2	S3	S4	S5
MBTS	2	-	2	2	2
TMTD	0.88	0.88	-	0.88	0.88
ZDDP	2	2	2	-	-
ZDEC	-	-	-	-	2

S1 represents the control composition with S, two primary accelerators, i.e. MBTS and TMTD and one secondary accelerator, i.e. ZDDP. Then, in S2 and S3 primary

accelerators MBTS and TMDT were respectively left out of the formulation compared to S1. In S4, secondary accelerator ZDDP was left out of the formulation when comparing to S1. In composition S5, a different secondary accelerator, i.e. ZDEC was added compared to S1. Literature states that dithiocarbamates like ZDEC exhibit faster cure rates at low temperature, which may improve the cure rate near the EPDM-PE interface [85].

2K samples were produced according to the process as described in 3.2.2. The specific mould temperatures of the rubber and thermoplastic cavity together with the accompanying interface temperature are listed in Table 12. This table also contains the vulcanisation times for all samples.

Table 12: Mould temperatures for thermoplastic and rubber cavity with the accompanying interface temperature and curing times for thermoplastic – sulphur-based EPDM

Mould temperature (°C)	EPDM	
	PP	PE
Thermoplastic cavity	140	65
Rubber cavity	180	180
Interface	161	134
Curing time (s)	1000	1800

### 3.4.2 Results and discussion

#### 3.4.2.1 Effect of sulphur curing composition on EPDM cure characteristics

Cure characteristics were evaluated with an MDR at 180°C for 20 min, at 160°C for 45 min, and at 140°C during 80 min, except for S3 which was cured during 120 min. Figure 42 shows the results for all EPDM samples. Furthermore, in Table 13 an order is given for each cure property at each temperature. At 140°C, 160°C, and at 180°C results indicate that leaving out a primary accelerator like MBTS (S2) or TMTD (S3) significantly increases scorch and cure time compared to control composition S1. Consequently, these compositions exhibit a lower CRI. Especially, TMTD seems to be essential to reach good curing characteristics. At 140°C, when comparing S1 to S4, ZDDP seems to induce vulcanisation earlier ( $t_{s1}$  of S1 is lower than S4), but it does not improve the cure rate at this low temperature. However, at 180°C ZDDP does seem to boost curing as  $t_{90}$  and  $t_{s1}$  of S1 are lower than S4, and CRI of S1 is higher than S4. As expected, replacing secondary accelerator ZDDP by ZDEC improved the cure rate as CRI of S5 is much higher than S1 at both 140°C and 180°C. Interfacial vulcanisation degrees were determined as well which entails the EPDM vulcanisation degree near the interface in the injection moulded 2K samples calculated according to Eq. (24). For EPDM-PP samples the interface temperature is around 160°C and for EPDM-PE around 140°C. At these respective interfaces, the order in vulcanisation degree was determined based on a one-way ANOVA with Tukey's test. As expected, based on results of  $t_{90}$ , S5 has the highest vulcanisation degree and S2 and S3 have the lowest vulcanisation degrees at the interface.

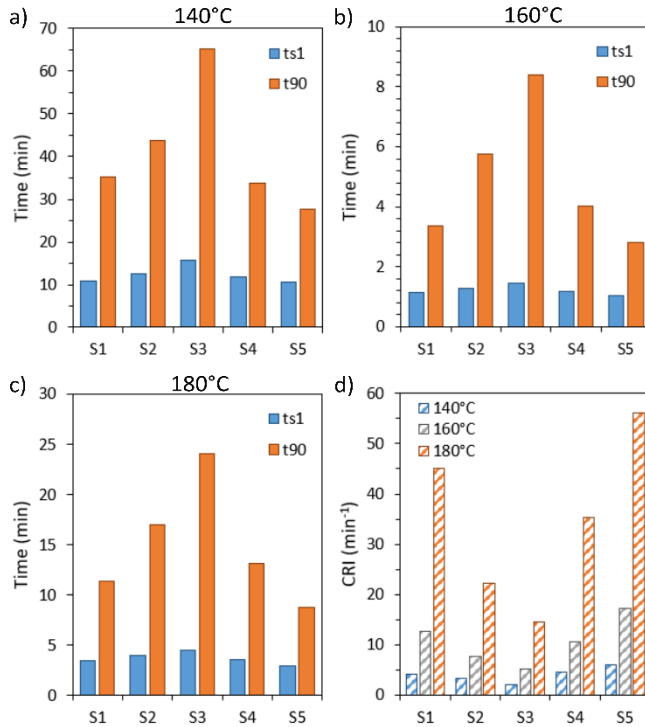


Figure 42: Scorch time ( $t_{s1}$ ) and vulcanisation time ( $t_{90}$ ) for all EPDM compounds at 140°C (a), 160°C (b) and 180°C (c), and cure rate index (CRI) for all EPDM compounds at 140°C, 160°C and 180°C (c).

Table 13: EPDM compound order, ranging from high to low, for cure time ( $t_{90}$ ), scorch time ( $t_{s1}$ ), cure rate index (CRI) and interfacial vulcanisation degree in 2K sample.

Cure characteristic	Temperature	Order
$t_{90}$ (min)	140°C	S5 < S4 < S1 < S2 < S3
	160°C	S5 < S1 < S4 < S2 < S3
	180°C	S5 < S1 < S4 < S2 < S3
$t_{s1}$ (min)	140°C	S5 < S1 < S4 < S2 < S3
	160°C	S5 < S1 < S4 < S2 < S3
	180°C	S5 < S1 < S4 < S3 < S2
CRI (min <sup>-1</sup> )	140°C	S5 > S4 > S1 > S2 > S3
	160°C	S5 > S1 > S4 > S2 > S3
	180°C	S5 > S1 > S4 > S2 > S3
Interfacial vulcanisation degree (%)	140°C	S5 > S4 = S1 > S2 > S3
	160°C	S5 ≥ S4 ≥ S1 ≥ S2 ≥ S3

### 3.4.2.2 Effect of cure properties on the adhesion

The adhesion strength of all sulphur-based EPDM compounds with PE or PP were determined and results are represented in Figure 43. Changes in the curing system composition did not cause significant differences in EPDM strength as  $\sigma_t$  of all samples belong to the same group based on Tukey's test. The adhesion strength with PE was

significantly affected. However, with PP no significant differences were observed. When comparing the adhesion percentages for S1, S1-PP reaches an adhesion percentage of  $17 \pm 1\%$  while S1-PE reaches  $62 \pm 1\%$ . This could be caused by the generally low adhesion strength which could be caused by the faster cure rate at the interface with PP ( $\sim 160^\circ\text{C}$ ) compared to PE ( $\sim 135^\circ\text{C}$ ) limiting sufficient interdiffusion. For PE, compared to S1, only S4 leads to a better adhesion. Thus, leaving out secondary accelerator ZDDP seems to be beneficial for the EPDM-PE adhesion. In contrast, S2, S3 and S5 caused a lower adhesion strength with PE than S1.

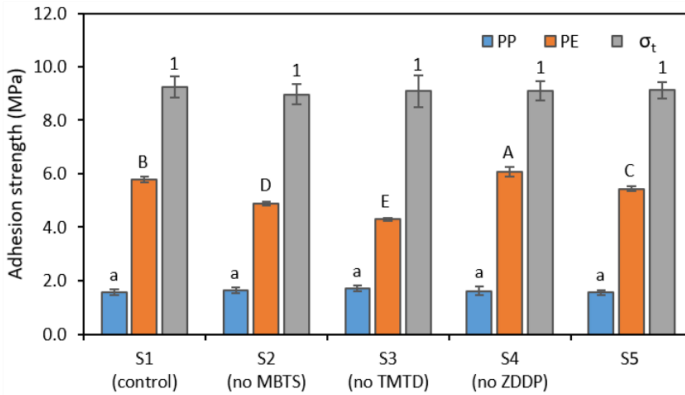


Figure 43: Adhesion strength between PE or PP and EPDM containing different curing systems, and total EPDM strength ( $\sigma_t$ ) of all EPDM samples. The numbers indicate differences in EPDM strength between samples (ANOVA, Tukey,  $p < 0.05$ ). Significant differences in adhesion strength between EPDM samples S1-S5 and PE are given in capital letters, and between EPDM samples S1-S5 and PP in lower case letter (ANOVA, Tukey,  $p < 0.05$ ). Error bars represent 95 % confidence intervals.

As shown in Figure 42, the accelerators caused significant differences in curing characteristics. Furthermore, Figure 43 indicates a clear influence of the accelerators, or curing system composition, on the adhesion with PE. Therefore, scorch time ( $t_{s1}$ ), cure time ( $t_{90}$ ), cure rate index (CRI) and interfacial vulcanisation degree were correlated with the adhesion strength of EPDM-PE as shown in Figure 44.

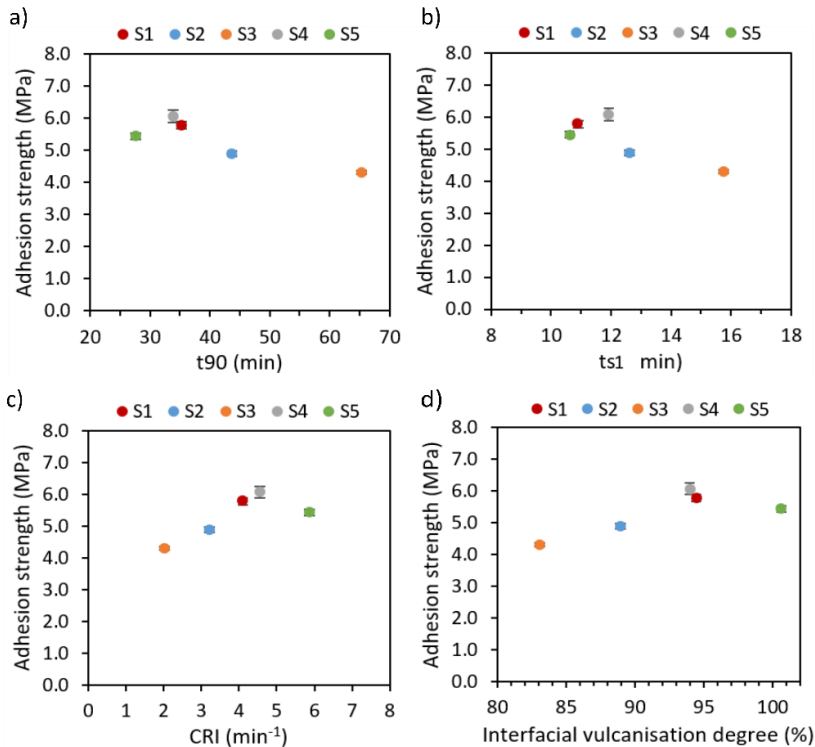


Figure 44: EPDM-PE Adhesion strength in function of curing time ( $t_{90}$ ) (a), scorch time ( $t_{s1}$ ) (b), cure rate index (CRI) (c) and the interfacial vulcanisation degree. Error bars represent 95 % confidence intervals.

When relating the adhesion strength to the  $t_{90}$  of all curing system compositions (Figure 44a), an increase in adhesion strength is found up to a maximum and afterwards the adhesion strength decreases again with higher  $t_{90}$ . Similarly, an optimum in  $t_{s1}$  (Figure 44b) can be seen as well. This results in an optimum value of CRI (Figure 44c) as CRI depends on  $t_{90}$  and  $t_{s1}$ . Thus, at a low cure rate, as is the case for S3 and S2, low adhesion is reached. However, these low values can be related to lower vulcanisation degrees near the interface. A fixed cure time was selected for all samples to explicitly create different vulcanisation degrees. Figure 44c confirms this as the interfacial vulcanisation degree of S2 and S3 is below 90 %. Thus, S2 and S3 will have a lower strength near the interface resulting in a weaker adhesion as also mentioned in a study by Six et al. [7]. Then, S1 and S4 show quite similar curing characteristics, but S4 has a higher scorch time compared to S1 (Table 13), while cure time  $t_{90}$  of S1 is slightly higher than S4. Literature states that diffusion can be thermally favoured during the early stages of curing [8]. Scorch time gradually increases from S5 to S1 and finally to S4 with adhesion strength respectively showing the same trend. Thus, interdiffusion may be promoted as the onset to vulcanisation is delayed. Specifically, for S5, even though high interfacial vulcanisation degree was reached, adhesion decreased. This could be due to the high cure rate preventing sufficient interdiffusion as crosslinking will dominate over the interdiffusion mechanism. Specifically, the adhesion mechanism may be promoted when crosslinks form at a slower rate, so that PE chains can diffuse across the interface, entanglements

can form and get locked into place due to continuing crosslinking. However, when the cure rate is too high the diffusion process may be limited as crosslinking rate is higher than the diffusion rate preventing sufficient entanglements [9]. To ensure that the decrease in adhesion strength going from S4 to S5 was not caused by a compatibility change, as ZDEC was added, a contact angle measurement (Figure 45) was executed at 180°C with a PE droplet. However, no differences in wetting kinetics or final contact angle after 15 min were observed.

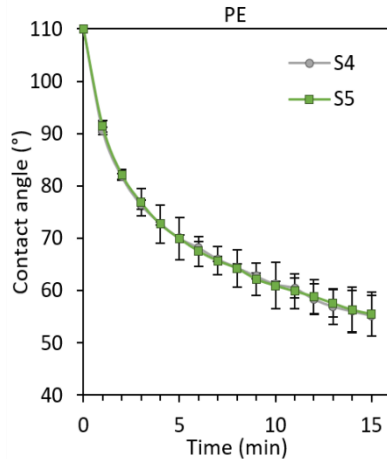


Figure 45: Contact angle measurements of thermoplastic melts of PE (180°C) on S4 and S5. Error bars represent 95 % confidence interval.

### 3.5 Conclusion

In this chapter, the influence of the EPDM curing system on the adhesion with thermoplastics was studied. This entailed a study of the peroxide curing system and sulphur curing system.

First, the effect of co-agents on adhesion between peroxide cured EPDM and thermoplastic materials was investigated. Specifically, TMPT was compared with TAC in EPDM and combinations were made with two non-polar (1) and two polar (2) thermoplastics:

- (1) Contact angle measurements showed that co-agents did not influence the compatibility with PP or PE. Thus, physical interactions are not affected by adding co-agents. However, the adhesion strength was significantly improved with both thermoplastics. Thus, co-agents in EPDM might increase reactivity at the interface and reduce side reactions causing crosslinking reactions with the non-polar PP and PE. For EPDM with PP, optimal adhesion was reached when adding 3 phr TAC or 6 phr TMPT. For EPDM with PE, successful bonding was reached at 1.5 phr TAC.
- (2) Compatibility results showed that both co-agents promote wettability and consequently facilitate adhesion with PC. This was confirmed by a significant increase in adhesion strength with polar thermoplastics (PC and ABS) at high concentrations. However, at high TAC concentrations EPDM has a tendency to tear due to the formation of a more rigid structure. TMPT in contrast preserved good properties but lower interfacial bonding was reached.

Second, the influence of DCP in EPDM on the adhesion with polar and non-polar thermoplastics was investigated. Even though compatibility with polar or non-polar thermoplastics did not change with higher DCP concentrations, adding higher concentrations of the peroxide curing agent did significantly affect the adhesion percentage between EPDM and PE, PP, ABS or PC. Consequently, differences in adhesion percentage can be mainly attributed to changes in adhesion mechanisms occurring after contact between both polymers. Depending on the dominant adhesion mechanism and specific material combination, optimal DCP concentrations were found:

- (1) For PE, higher DCP concentration improved the adhesion percentage up to 57 % at 6 phr showing a full cohesive failure. At this concentration, co-vulcanisation between EPDM and PE may be promoted.
- (2) PP tends to degrade when adding higher DCP concentrations inhibiting a proper adhesion. Therefore, a low DCP concentration is recommended with the addition of higher co-agent concentration to boost crosslinking which may also limit EPDM bulk degradation.
- (3) For the polar ABS and PC, 4 phr DCP caused respectively adhesion percentages of 43 % and 13 %. In case of EPDM with ABS, a combination of crosslinking and interdiffusion is expected leading to higher adhesion strength percentages than for EPDM with PC where interdiffusion is deemed dominant.

Depending on the material combination, changes in EPDM bulk properties need to be taken into account when defining the right co-agent type and peroxide concentration because optimal physico-mechanical properties and curing characteristics will be application dependent. Furthermore, compared with the previous work by Bex [3], a switch to peroxide curing can cause a clear improvement in adhesion with PP and even create a certain adhesion with polar thermoplastics. However, EPDM-ABS is still accompanied by high curing times making this economically less relevant compared to EPDM-PC.

Finally, the sulphur curing system was studied. Sulphur-cured EPDM can adhere to PE, but the low melting temperature of PE (135°C) causes high cycle times to ensure complete vulcanisation near the interface. Compared to peroxide curing it was found that sulphur curing provides a faster cure rate at this low temperature (e.g. 4000 s vs 1800 s respectively). Therefore, the effect of accelerators in the sulphur curing system was studied as they are known to influence the kinetic parameters of vulcanisation which could reduce processing times. An optimum in cure rate was found when relating the cure characteristics to the adhesion strength. After this optimum adhesion strength decreased again. Thus, strong adhesion between EPDM and PE during 2K injection moulding can only be reached at an optimal sulphur cure rate, which depends on the cure temperature near the interface as well. At that optimal cure rate, interdiffusion may be promoted while crosslinking occurs in the rubber part. Results showed that increasing the curing rate further reduced the adhesion. This implicates that a significant reduction in processing time by increasing the sulphur cure rate is not possible. Thus, reducing the process cycle time of EPDM-PE compared to results of Bex [3] is not possible without diminishing the adhesion. However, as Bex [3] indicated, sulphur-based EPDM-PE 2K products do offer advantages like high adhesion strength, secured positioning and dimensions, and material savings. Thus, 2K EPDM-PE products are ideal for high quality applications. For EPDM-PP, a variation in curing rate did not affect the adhesion strength and an average adhesion percentage of 17 % was reached for PP-S1. When comparing this to peroxide curing results, with 58 % adhesion percentage at optimal co-agent concentration, a significantly lower adhesion strength is created during sulphur

---

curing. For sulphur curing, only interdiffusion is likely and the low accompanying strength reinforces the idea of co-vulcanisation during peroxide curing at the EPDM-PP interface.



---

# Chapter 4 Optimisation of the EPDM composition for adhesion with thermoplastics

---

## 4.1 Introduction

In this chapter, a further optimisation of the EPDM composition is studied. In particular, in Section 4.2, the focus is put on the influence of the macromolecular structure of EPDM, i.e. ethylene content, ENB content and molecular weight, on the adhesion with PP. These are average molecular characteristics which may affect interdiffusion and/or chemical bonding at the interface. The previous Chapter 3 has shown the adhesion potential of EPDM with PP and together with the high range of applications and efficient cure at the interface, this material combination has a high industrial relevance. Therefore, EPDM-PP was selected in this adhesion study. Compared to PE, PP has higher temperature stability and better resistance to chemicals and organic solvents. EPDM with ABS or PC is not studied as the macromolecular structure does not change the polarity and for EPDM with ABS the peroxide curing efficiency is too low to make further adhesion optimisation (chemical bonding) economically relevant.

In the rubber composition, fillers are added as well for rubber reinforcement and plasticisers to reduce compound viscosity and/or to improve processing. Oils are low molecular weight components which are likely to migrate out of the rubber bulk upon exposure to high curing temperature and contact with the thermoplastic. This might induce a weak boundary layer at the rubber-thermoplastic interface, limiting interdiffusion or chemical bonding by changing the material compatibility and reducing the available EPDM chains at the interface. Furthermore, differences in filler type might influence the adhesion mechanism as well. Therefore, the influence of filler type and oil content on the adhesion of both EPDM-PP and EPDM-PC are studied as well in Section 4.3.

## 4.2 EPDM macromolecular structure

The influence of the macromolecular structure of EPDM, i.e. ethylene content, ENB content and average molecular weight, on the adhesion with PP is investigated. For a rubber grade, Mooney viscosity is used as practical indicator for the average molecular weight [63], [132]. EPDM compounds were cured with both a peroxide system and a sulphur system. EPDM compounds with a sulphur curing system facilitate interdiffusion with PP. EPDMs with a peroxide curing system, adhered to PP, may affect co-vulcanisation reactions at the interface. Vulcanisation behaviour of the EPDM bulk is characterised, together with the bulk crosslink density, tensile strength and crystallinity.

A factorial design of experiments is used to define the influence of ethylene content and Mooney viscosity of EPDM on the adhesion with PP. The influence of ENB on EPDM-thermoplastic adhesion is investigated at a fixed Mooney viscosity and ethylene content.

#### 4.2.1 Materials and methods

##### 4.2.1.1 Materials

Six NORDEL™ EPDM grades from DOW were selected according to their ethylene content, ENB content and molecular weight. The EPDM grades and their molecular characteristics are represented in Table 14. Mooney viscosity is represented as practical indicator of molecular weight. EPDM compounds with the selected EPDM grades were mixed and provided by Hercorub NV. Besides the EPDM grades, following raw materials were used:

- (1) Paraffinic oil (85 phr): Sunpar 2280, Petronas;
- (2) Carbon black: N772 from Konimpex (65 phr) and N550 from Aditya Birla Group (50 phr);
- (3) Zinc oxide (5 phr): De Craene;
- (4) Stearic acid (1 phr): Baerocid SMS-1 A, Baerlocher GmbH.

Then, either a peroxide curing system (P) or a sulphur curing system (S) was added to each compound, which resulted in the following twelve samples: S4520, S4570, S4770, S4725, S4640, S3640, P4520, P4570, P4770, P4725, P4640, P3640. The first number groups multiple ENB contents from low (e.g. 3) to higher (e.g. 4), the second number in these codes refers to the ethylene content, and the last two numbers to the Mooney viscosity. The peroxide curing system consisted of DCP (40 % active ingredient, Perkadox BC-40MB-gr, AzkoNobel) and co-agent TAC (50 % active ingredient) and the sulphur curing system consisted of accelerators MBTS (80 % active ingredient, SAFIC ALCAN), TMTD (80 % active ingredient, Avokal GmbH) and ZDDP (67 % active ingredient, RheinChemie Additives) and elemental sulphur (Integrated Chemicals Specialties BV). In Table 15, the curing system formulations are listed. All EPDM grades were combined with the PP grade specified in Section 3.2.1.

Table 14: Characteristics of NORDEL™ EPDM grades.

EPDM grades	Mooney Viscosity ML1+4, at 125°C <sup>a</sup>	Ethylene content (wt%) <sup>a,b</sup>	ENB content (wt%) <sup>a</sup>	Density (g/cm <sup>3</sup> )
4520	20	50	4.9	0.86
4570	70	50	4.9	0.86
4770 <sup>c</sup>	70	70	4.9	0.88
4725 <sup>b</sup>	25	70	4.9	0.88
4640	40	55	4.9	0.86
3640	40	55	1.8	0.86

<sup>a</sup> Supplied by the manufacturer

<sup>b</sup> The EPDM chain consists of a weight percentage ethylene, propylene and ENB

<sup>c</sup> Original product grades are 4770P and 4725P with P referring to pellet form

Table 15: Curing system formulation for EPDM with macromolecular changes.

Component (phr)	Sulphur curing (S)	Peroxide curing (P)
DCP <sup>a</sup>	-	3.2
TAC <sup>c</sup>	-	1.5
MBTSc	1.6	-
TMTD <sup>c</sup>	0.7	-
ZDDP <sup>c</sup>	1.3	-
S <sup>c</sup>	1	-

#### 4.2.1.2 Sample preparation

The 2K injection moulding process was applied as described in the previous chapter (section 3.2.2) with the individual injection moulding parameters mentioned in Table 4 resulting in rectangular specimens as shown in Figure 23. During the overmoulding step, the temperature in the rubber cavity was set at 180°C to cure EPDM. The interface temperature was 160°C. This temperature was experimentally determined with an infrared camera (OPTRIS PI400).

A 2<sup>2</sup> full factorial design was specified to determine the influence of Mooney viscosity and ethylene content for each material combination, i.e. sulphur-based EPDM with PP, and peroxide-based EPDM with PP. The type of curing system, i.e. sulphur and peroxide curing, was not added as a factor to the design to avoid interference during variation in EPDM grades while injection moulding. Furthermore, peroxide curing and sulphur curing affect the adhesion mechanisms differently, which is also the specific point of interest in this study. Therefore, the influence of Mooney viscosity and ethylene content was studied for EPDM with a peroxide curing and a sulphur curing system. The factors and factor levels are represented in Table 16. EPDM grades 4570, 4770, 4725 and 4520 were selected as corner points/settings for the factorial design. The 4520 and 4725 grades were selected for the low Mooney viscosity level of 20 MU as practical values at ML1+4, 125°C (Mooney MV 2000E at Hercorub) were respectively 20.4 MU and 24.1 MU for 4725. The range between low (20 MU) and high level (70 MU) was sufficiently large to make to deviation between 4725 and 4520 limited. After process stabilisation, five replicates were produced at each setting. Thus, in total two 2<sup>2</sup> factorial designs were executed, each containing twenty runs. Samples were produced in random order, but due to processing restrictions, replicates within each setting were not randomised. Eventually, main effect plots, two-factor interactions and results of the analysis of variance are determined by a factorial DOE on Minitab 17. Furthermore, normality of the response values were checked with an Anderson-Darling normality test on the standardised residuals and equality of variance was assessed.

As it was not possible to fit ENB content as a factor in the DOE, due to restrictions in available EPDM polymers, a comparison was made between a low and high ENB content, i.e. 1.8 wt% ENB and 4.9 wt% ENB, at a fixed Mooney viscosity (40 MU) and ethylene content (55 wt%). Thus, sulphur-based EPDM compounds and peroxide-based EPDM compounds with both ENB contents were combined with PP.

---

<sup>a</sup> Concentration is represented in phr of active amount

Table 16: Factors and factor levels for the full factorial design.

Factor	Low level	High level
Mooney viscosity (MU)	20	70
Ethylene content (wt%)	50	70

#### 4.2.1.2.1 Rubber characterisation

Cure characteristics of all EPDM compounds were evaluated with a Monsanto moving die rheometer (MDR2000E). During 2K injection moulding, curing temperature in the rubber bulk is 180°C. However, the temperature at the interface is lower (160°C). Therefore, cure time ( $t_{90}$ ), scorch time ( $t_{s1}$ ) and delta torque ( $\Delta\text{torque}$ ) and cure rate index (CRI) were obtained at 180°C and 160°C. Measuring times at these temperatures were 20 min for sulphur-based, and 45 min for peroxide-based compounds.

Heat flow analysis was executed with a Differential Scanning Calorimeter (DSC, 2920 TA). Unvulcanised EPDM samples from all mixed compounds (Table 2) were tested. Samples between 10-15 mg were cut from these starting materials. To eliminate the effects of thermal history, samples were heated to 100°C at 10°C/min and cooled to -60°C at 5°C/min. Afterwards, samples were heated from -60°C to 100°C at 10°C/min. All measurements were executed under nitrogen environment (30 mL/min). The degree of crystallinity of all samples was estimated from the peak area according to Eq. (27):

$$\alpha = \frac{\Delta h}{x \cdot 10^{-2} \Delta h_c} \cdot 100 \% \quad (27)$$

where  $x$  is the ethylene content (Table 14),  $\Delta h$  is the specific enthalpy of fusion (in J/g) retrieved from the peak area, and  $\Delta h_c$  is the enthalpy of fusion of 100 % crystalline polyethylene (290 J/g).

Tensile strength of the rubber bulk was determined according to the procedure in Section 3.2.5. Crosslink density  $\nu$  (mol/cm<sup>3</sup>) was determined according to the methodology as explained in Section 3.2.4 and calculated with the Flory-Rehner equation (Eq. (22)) for tetrafunctional networks. The densities of cyclohexane is 0.78 g/cm<sup>3</sup> and the elastomer densities are listed in Table 14. An average crosslink density was taken of three samples and 95 % confidence intervals are reported.

#### 4.2.1.3 Adhesion characterisation

The adhesion strength at the interface was analysed by tensile testing as explained in Section 3.2.7. Adhesion percentage is calculated according to Eq. (26). Five adhesion measurements were performed for each material combination and 95 % confidence intervals are reported. After fracture, the interface surface of the thermoplastic part was analysed visually with a Keyence VHX-500F digital microscope and a 50x magnification.

## 4.2.2 Results and discussion

### 4.2.2.1 Influence of macromolecular structure on EPDM cure characteristics

EPDM cure characteristics of EPDM grades with varying ENB content, Mooney viscosity and ethylene content were evaluated. In Table 17,  $\Delta S'$ , cure ( $t_{90}$ ) and scorch time ( $t_{s1}$ ) are represented.

Table 17: Cure characteristics of all EPDM NORDEL™ grades at 180°C and 160°C.

Characteristic Temperature	$\Delta S'$ (dNm) 180°C	$t_{90}$ (min)		$t_{s1}$ (min)		CRI ( $\text{min}^{-1}$ )	
		180°C	160°C	180°C	160°C	180°C	160°C
S3640	4.06	5.78	19.64	2.05	5.14	26.91	6.90
S4640	4.89	4.07	13.26	1.69	3.81	36.23	10.58
S4520	4.34	4.32	12.10	1.73	3.61	33.90	11.78
S4570	4.84	4.02	10.94	1.56	3.99	35.97	12.74
S4725	3.55	4.72	12.72	4.72	4.20	32.26	11.74
S4770	4.20	3.94	11.06	3.94	3.39	38.61	13.04
P3640	1.89	5.70	16.66	1.50	4.88	23.81	8.49
P4640	2.93	3.26	17.49	0.93	3.94	42.92	7.38
P4520	2.52	3.36	16.79	1.06	6.05	43.48	9.31
P4570	3.52	3.09	15.03	0.77	2.84	43.10	8.20
P4725	2.28	3.06	17.38	1.10	5.59	51.02	8.48
P4770	3.17	2.64	16.25	0.83	2.91	55.25	7.50

For sulphur-cured compounds, the diene content (S3640 and S4640) significantly influences the cure rate and scorch time at both 180°C and 160°C as shown in Figure 46. As the diene increases, sulphur cure rate increases which confirms literature findings [61], and this is accompanied by a higher crosslink density, as shown in Figure 46b. A similar result was found for the peroxide-cured samples at 180°C, with higher diene level (P4640) leading to increased curing efficiency as more crosslinks can form due to a higher amount of addition reactions [59]. This increase in addition is in agreement with literature [88] and a study by Orza [59], where at a high temperature of 175°C, increasing levels of ENB showed an increased contribution of addition to the total crosslink density. However, at 160°C, curing time of 1.8 wt% ENB (P3640: 16.66 min) was lower than 4.9 wt% ENB (P4640: 17.49 min), indicating that the influence of diene content on the curing efficiency at the interface of EPDM-PP samples might be limited. Whether crosslink density is affected as well at this temperature is unknown as crosslink densities were only determined in the EPDM bulk. The faster cure at low diene content (P3640) could indicate that crosslinking between EPDM and PP at the interface might proceed more efficiently through combination of a PP macro-radical with a macro-radical of EPDM instead of addition.

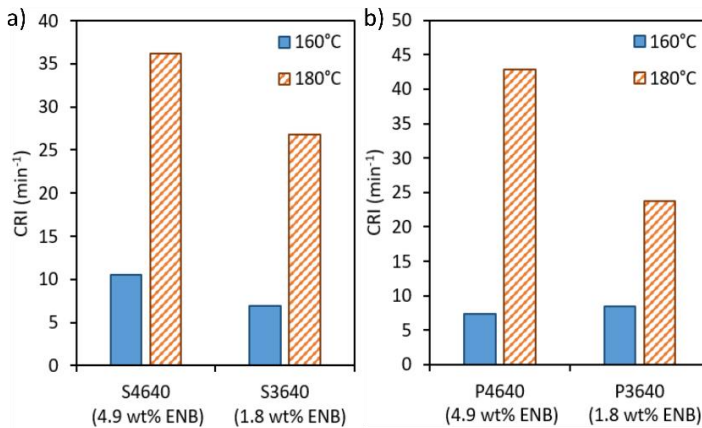


Figure 46: CRI of EPDM with high diene content (4640, 4.9 wt% ENB) and low diene content (3640, 1.8 wt% ENB) with a sulphur curing system (a) and a peroxide curing system (b).

Furthermore, Table 17 shows that sulphur-cured high Mooney viscosity grades (S4570 and S4770) provide faster cures than low Mooney viscosity grades (S4725 and S4520). At 160°C, high molecular weight peroxide-based compounds (P4570 and P4770), i.e. high Mooney viscosity, seem to reduce curing time ( $t_{90}$ ) compared to the low Mooney viscosity grades at equal ethylene content (P4520 and P4725 respectively).

For the peroxide-cured compounds, at 180°C, high ethylene content (P4725 vs P4520 and P4770 vs P4570) increases crosslinking efficiency as  $\beta$ -scission, i.e. scission of the weakest C-C bonds, is inhibited due to a lower amount of available propyl groups [63]. However, at 160°C, this beneficial effect of ethylene is less visible, which could indicate that at this temperature scission is less dominant over crosslinking. This confirms the literature statement of scission predominating at higher temperatures [88].

When comparing torque values of sulphur and peroxide-cured compounds, higher torques are reached with sulphur curing which can be attributed to a higher crosslink density.

#### 4.2.2.2 Influence of ethylene content on EPDM crystallinity

Heat flow analysis results are represented in Table 18. These curves were analysed to determine the crystallinity of all sulphur and peroxide-based EPDM compounds with different EPDM grades. Ethylene contents are indicated as well in Table 18. As the ethylene content increases, an increased EPDM crystallinity should be reached [61], [63]. For both sulphur and peroxide-based compounds an endothermic melting peak was found with a clear enthalpy of melting for samples containing 70 wt% ethylene (4725 and 4570). This resulted in a crystallinity degree of approximately 5 % in S4725, S4770, P4725 and P4770, while it was equal to or lower than 1% for the other compounds. Thus, at high ethylene content (70 wt%), EPDM is able to form crystalline domains creating thermally reversible physical crosslinks [59], [64]. At ethylene contents of 55 % and 50 % the EPDM grades (3640, 4640, 4520 and 4570) have a more amorphous character.

Table 18: Melting enthalpy and crystallinity calculated from DSC curves for each EPDM NORDEL™ grade with sulphur or peroxide curing.

Compound	Enthalpy (J/g)	Ethylene content (wt%)	Crystallinity (%)
S3640	1.8	55	1.1
S4640	1.7	55	1.1
S4520	0.9	50	0.7
S4570	1.0	50	0.7
S4725	10.3	70	5.1
S4770	10.6	70	5.2
P3640	2.0	55	1.2
P4640	1.8	55	1.1
P4520	0.8	50	0.6
P4570	0.9	50	0.6
P4725	10.3	70	5.1
P4770	10.4	70	5.1

#### 4.2.2.3 Influence of macromolecular structure on EPDM physico-mechanical properties

Tensile strength and crosslink density of the rubber bulk cured by either a sulphur or peroxide system were analysed for all samples and the results are represented in Figure 47. Other vulcanisate properties of all NORDEL grades are reported in the NORDEL™ EPDM product selection guide from Dow [133]. The tables comparing the properties of these EPDM grades are added in Appendix A.

Significant differences between samples were found by a one-way ANOVA. Equality of variances was assured (tensile strength:  $p = 0.198$  for sulphur curing,  $p = 0.054$  for peroxide curing; crosslink density:  $p = 0.546$  for sulphur curing,  $p = 0.117$  for peroxide curing). Both sulphur and peroxide-cured samples follow the same trend when comparing tensile strengths, with high ethylene contents (70 wt% in 4725 and 4770) leading to the highest tensile strength. The formed crystallites, created by the high number of ethylene groups, can act as a reinforcing agent and function as reversible crosslinks [75]. Furthermore, high molecular weight (4770 vs 4725 and 4570 vs 4520), i.e. high Mooney viscosity, caused higher tensile strength due the increase in crosslink density which may be related to the increase in physical entanglements and chemical crosslinks. In Figure 47b, a clear increase in crosslink density is seen going from low to high Mooney viscosity both at low ethylene content (4520 vs 4570) and high ethylene content (4725 vs 4770). Increasing the ENB content (4640 compared to 3640) caused increased tensile strength which can be related as well to an increase in crosslink density for both sulphur and peroxide curing in the EPDM bulk. When comparing crosslink density results of 4570 and 4725, higher crosslink density is reached for 4570. In contrast, tensile strength of 4725 is higher than 4570. This indicates that a strain-induced crystallisation of the ethylene segments may be occurring due to the high ethylene contents creating additional physical crosslinks during tensile testing [69].

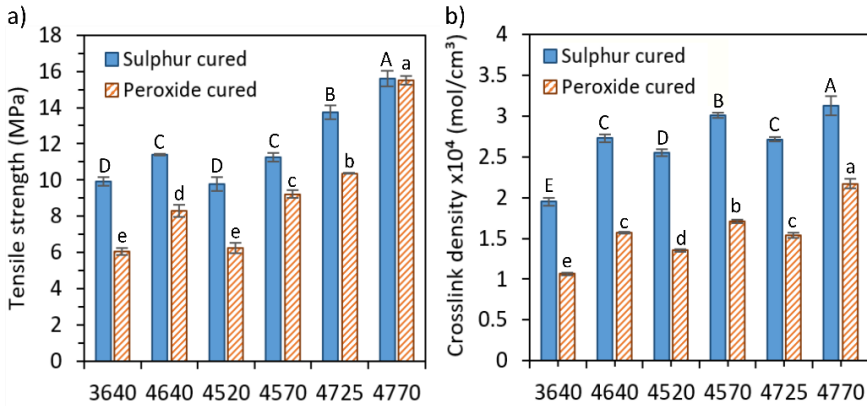


Figure 47: Physico-mechanical properties of peroxide and sulphur-cured EPDM grades: tensile strength (a) crosslink density (b). Error bars represent 95 % confidence intervals. Grouping information from the Tukey method is given by an upper case letter for sulphur curing and by a lower case letter for peroxide curing.

#### 4.2.2.4 Influence of ENB content on the adhesion between EPDM and PP

A comparison was made between a high and a low ENB level in sulphur-based and peroxide-based EPDM (with similar ethylene content and Mooney viscosity) when adhering to PP. Results of adhesion percentages between EPDM and PP are represented in Figure 48.

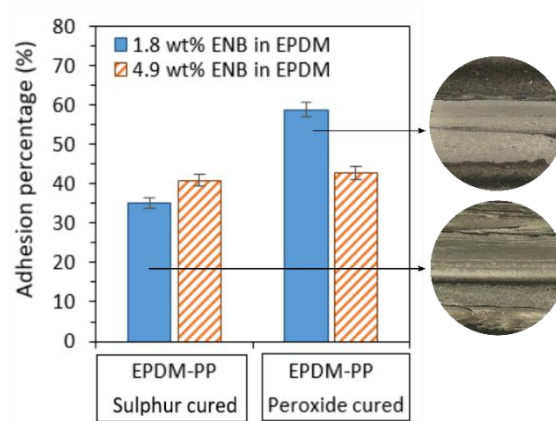


Figure 48: Adhesion percentage between sulphur-cured EPDM containing 1.8 or 4.9 wt% ENB (3640 and 4640 respectively) and PP. Error bars represent 95 % confidence intervals. The microscopic images show a circular zone (2 mm radius) of the fracture surfaces at the thermoplastic side. Black indicates the rubber and white the thermoplastic.

The ENB content significantly affects the adhesion percentage between sulphur-cured EPDM and PP ( $p = 0.000$ ). However, the increase in adhesion remains limited to 6 %. At the interface, interdiffusion is expected as adhesion mechanism when using sulphur as curing system [6], [123], [124]. Results indicate improved interdiffusion when

increasing ENB content (adhesion percentage:  $40.9 \pm 1.6$  % for 4.9 wt% ENB;  $35.1 \pm 1.3$  % for 1.8 wt% ENB). This is in disagreement with the expectation of high crosslink densities (cf. Figure 47b, 4640 vs. 3640) limiting interdiffusion. However, possibly, interdiffusion of the PP chains into the rubber network, or interdiffusion of the EPDM chains into the PP network proceeds simultaneously with the crosslinking process, as proposed by Ruch et al. [29]. Consequently, interdiffusion occurs in the initial stage and then a fixation of the diffused chains is required in the EPDM matrix to create entanglements. Due to the high diene content, more crosslinks are formed in the EPDM matrix which immobilise the PP chains by creating entanglements, leading to a stronger interdiffusion zone. Thus, a higher adhesion percentage is obtained, while with the lower diene samples a weaker diffusion zone is created.

Peroxide-based samples showed a higher adhesion percentage at lower ENB content. Curing results (Table 17), indicated a higher curing efficiency for P3640 (1.8 wt% ENB) compared to P4640 (4.9 wt% ENB) at 160°C, while at 180°C the opposite result was found. Thus, at the interface with a curing temperature of 160°C, crosslinking between EPDM chains and co-vulcanisation with PP might be influenced less by the unsaturation in ENB as combination reactions might proceed more efficiently than addition reactions. In contrast, in the bulk of the EPDM, a high amount of double bonds improves crosslinking efficiency and crosslink density which is presumably related to more addition reactions and entanglements [59], [88]. Wang et al. [134] found that the EPDM entanglement contribution to the crosslink density depends on the diene content at low peroxide concentration. These entanglements within EPDM might inhibit interdiffusion of PP at the interface. Furthermore, the bulky diene might limit crosslinking with PP at the interface due to the steric hindrance.

When comparing peroxide to sulphur curing, better adhesion is reached with peroxide curing due to the chemical adhesion associated with this curing system. At low ENB concentration, the images of the fractured PP surfaces (Figure 48) show a larger surface coverage by a thin EPDM layer, indicating better adhesion when chemical bonding is possible compared to solely interdiffusion. At 4.9 wt% ENB, there is no significant difference in adhesion between sulphur and peroxide curing.

#### 4.2.2.5 DOE to optimise Mooney viscosity and ethylene content in EPDM for adhesion with PP

The influence of Mooney viscosity and ethylene content on the adhesion percentage between peroxide or sulphur-cured EPDM and PP was assessed by two full factorial DOEs. Thus, all main effects and factor interactions were determined. Results for both sulphur and peroxide curing are represented in Figure 49.

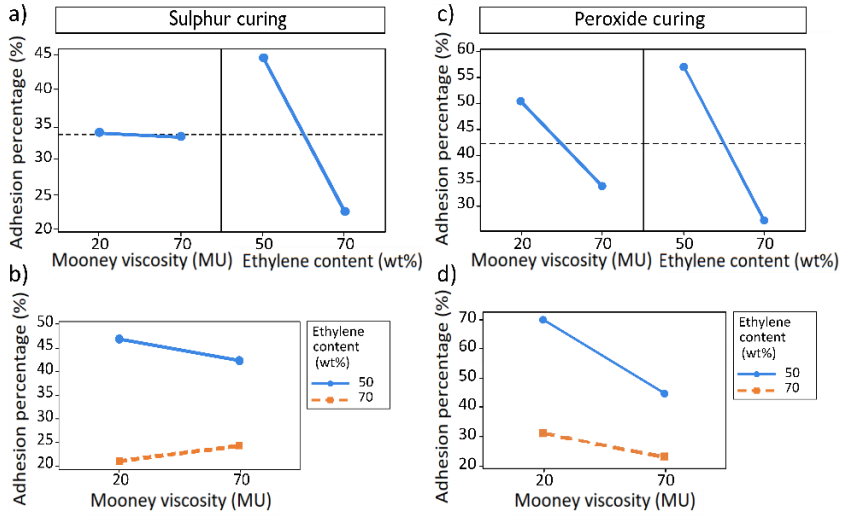


Figure 49: Main effect plots for Mooney viscosity and ethylene content for sulphur-cured EPDM-PP (a) and peroxide-cured EPDM-PP (c), the interaction between Mooney viscosity and ethylene content for sulphur-cured EPDM-PP (b) and peroxide-cured EPDM-PP (d).

The factorial regression analysis assumes that the observations are normally distributed, randomised, and of equal variance at all response levels. By using the analysis of residuals, these three requirements were confirmed (Figure 50 and Figure 51). The normality test of the standardised residuals indicated a p-value of 0.287 for sulphur-cured EPDM-PP and a p-value of 0.787 for peroxide-cured EPDM-PP which additionally proves the validity of the experimental design.

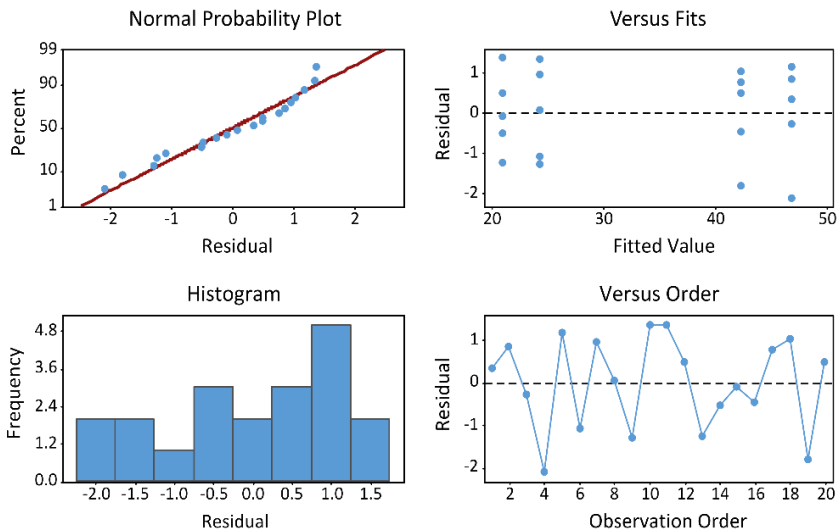


Figure 50: Residual plots for adhesion percentage between sulphur-cured EPDM and PP.

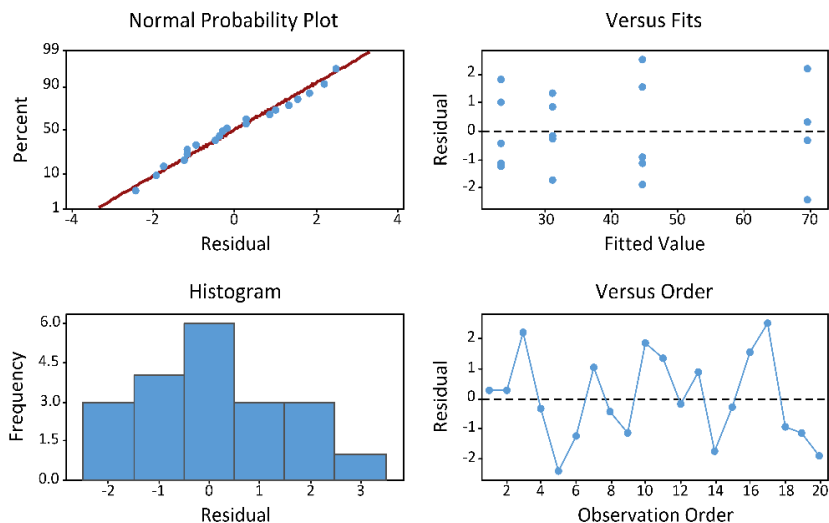


Figure 51: Residual plots for adhesion percentage between peroxide cured EPDM and PP.

For sulphur curing, results are represented in Figure 49a and Table 19. The  $R^2$  of the regression model was 99 %, indicating a good fit between the model and experimental data. Results demonstrate the significant main effect of ethylene content ( $p = 0.000$ ), while indicating the insignificant effect of Mooney viscosity ( $p = 0.257$ ). Ethylene content even accounted for 96 % of the total sum of squares. The main effect plot (Figure 49a) shows a large slope in function of ethylene content and the mean adhesion percentage between EPDM and PP decreased from 44.6 % to 22.8 %. This suggests that in the interface region, the high propylene content, i.e. low ethylene content, may improve compatibility and miscibility with PP and thus improves the interdiffusion process [67]. Figure 49a shows that Mooney viscosity, or molecular weight, does not play an active role during adhesion. A study by Ruch et al. [29] indicated that diffusion of EPDM chains occurs very slowly at an elastomer-elastomer interface even at a high temperature of 150°C which might indicate limited diffusability of EPDM in PP. The interaction between ethylene content and Mooney viscosity was found to be significant ( $p = 0.000$ ), but the influence remained weak as it only accounts for 3 % of the total sum of squares, i.e. 3 % of relative changes in adhesion percentage. From the interaction in Figure 49b, an opposite behaviour is seen from low to high Mooney viscosity at 50 wt% compared to 70 wt% ethylene content. Thus, at 50 wt% ethylene, better adhesion is reached at lower molecular weight because the EPDM chains have higher mobility which was also found in a study by Thust [4]. Furthermore, at higher Mooney viscosity, the cure rate increases which reduces the EPDM chain diffusion time as the chains are fixated more rapidly in the crosslinked matrix. However, at 70 wt% ethylene, adhesion increases going to high Mooney viscosity. This effect might be caused by differences in molecular weight distribution. Compounds 4570 (50 wt% ethylene, 70 MU), 4770 (70 wt% ethylene, 70 MU) and 4520 (50 wt% ethylene, 20 MU) have a medium molecular weight distribution while 4725 (70 wt% ethylene, 20 MU) has a broad distribution. Possibly, this broad distribution at 20 MU and 70 wt% ethylene interferes with the effect of Mooney viscosity. At the interface, a segregation of shorter chains might occur due to the high polydispersity and these shorter chains might limit the entanglement possibility after

diffusion [131]. This could also explain the insignificant effect of Mooney viscosity. However, this is currently speculated and needs further investigation.

Table 19: Analysis of variance results of adhesion percentages of sulphur-cured EPDM-PP (DF: Degree of freedom, Adj SS: Adjusted sum of squares, Adj MS: Adjusted mean of squares, S: Standard deviation).

Source	DF	Adj SS	Adj MS	F-value	P-value
Model	3	2505.67	835.22	615.96	0.000
Linear	2	2426.61	1213.30	894.79	0.000
Mooney viscosity (MU)	1	1.87	1.87	1.38	0.257
Ethylene content (wt%)	1	2424.73	2424.73	1788.20	0.000
2-Way Interactions	1	79.06	79.06	58.31	0.000
Mooney viscosity (MU) *	1	79.06	79.06	58.31	0.000
Ethylene content (wt%)					
Error	16	21.70	1.36		
Total	19	2527.36			
Model Summary	S	R <sup>2</sup>	R <sup>2</sup> (adj)	R <sup>2</sup> (predicted)	
	1.16446	99.14	98.98	98.66	

Table 20 and Figure 49c and d indicate a significant effect of ethylene content, Mooney viscosity and the interaction on the adhesion percentage between peroxide-cured EPDM and PP ( $p < 0.050$ ). As  $R^2$  for the regression model was 99 %, a good fit was established between the model and experimental data. When comparing the contributions to the total sum of squares, the main effects account for 94 % of changes in adhesion percentage (Mooney viscosity: 22 %, ethylene content: 72 %), and the interaction accounts for 6 %. Increasing the Mooney viscosity caused a decrease in mean adhesion percentage from 50.5 % to 33.9 %. An increase in ethylene content caused an even larger decrease from 57.3 % (at 50 wt% ethylene content) to 27.1 % (at 70 wt% ethylene content). Literature [91] states that high molecular weight, i.e. a high Mooney viscosity, is beneficial for crosslinking. Thus, crosslinking within EPDMs with high molecular weight (P4570 and P4770) might proceed more efficiently than the co-vulcanisation reaction with PP chains. A restriction in interdiffusion by the high molecular weight could also occur but as this was not evidenced for the sulphur curing system, the influence during peroxide curing is uncertain. Furthermore, higher ethylene content significantly lowers the adhesion percentage. Ruch et al. [29] already stressed the importance of interdiffusion at elastomer-elastomer joints for successful co-vulcanisation. Thus, at the peroxide curing EPDM-PP interface the polymer chains need to cross the interface in order to be covalently bonded to the opposite network. This may be prevented by the low compatibility between PP and EPDM with high ethylene content limiting the penetration of the chains at the interface and reducing the co-vulcanisation efficiency between EPDM and PP. Furthermore, curing results showed that at 160°C, ethylene content does not create a profound increase in curing efficiency as is the case at 180°C, suggesting less chain scission at this lower temperature. Therefore, at 160°C crosslinking with PP might still occur efficiently as crosslinking is promoted over chain scission. The highest adhesion percentage was reached when combining a low Mooney viscosity with a low ethylene content due to the mutual interaction, leading to 69.8 % adhesion between EPDM and PP.

Table 20: Analysis of variance results of adhesion percentages of peroxide-cured EPDM-PP (DF: Degree of freedom, Adj SS: Adjusted sum of squares, Adj MS: Adjusted mean of squares, S: Standard deviation)

Source	DF	Adj SS	Adj MS	F-value	P-value
<b>Model</b>	3	6274.27	2091.42	853.95	0.000
<b>Linear</b>	2	5904.89	2952.45	1205.52	0.000
Mooney viscosity (MU)	1	1364.87	1364.87	557.29	0.000
Ethylene content (wt%)	1	4540.02	4540.02	1853.74	0.000
<b>2-Way Interactions</b>	1	369.37	369.37	150.82	0.000
Mooney viscosity (MU) *	1	369.37	369.37	150.82	0.000
Ethylene content (wt%)					
<b>Error</b>	16	39.19	2.45		
<b>Total</b>	19	6313.45			
<b>Model Summary</b>	S	R <sup>2</sup>	R <sup>2</sup> (adj)	R <sup>2</sup> (predicted)	
	1.56496	99.38	99.26	99.03	

When comparing adhesion percentages of all material combinations, sulphur or peroxide-cured, in Figure 52, it can be concluded that EPDM 4520 provides the best adhesion with PP. The macromolecular structure of this compound promotes interdiffusion during peroxide and sulphur curing. PP with peroxide cured EPDM 4520 results in an adhesion strength of  $4.36 \pm 0.13$  MPa and PP with sulphur cured EPDM 4520 results in  $4.63 \pm 0.10$  MPa. Thus, in absolute strength, the sulphur curing system causes a slightly higher adhesion strength. However, when comparing these adhesion strengths to the total EPDM strength (Figure 47), a higher adhesion percentage is reached with peroxide curing (69.8 %) compared to sulphur curing (46.9 %). The strength between peroxide cured EPDM 4520 and PP comes closest to the bulk rubber tensile strength indicating a strong bond at the interface, probably due to chemical bonding at the interface. In Figure 52, macroscopic images of the PP fractured surface are represented of samples with the lowest and highest adhesion percentage for both peroxide and sulphur curing. S4725-PP and P4770-PP show the worst adhesion percentage and this resulted in nearly full adhesive failure. For S4520-PP and P4520-PP, an adhesive/cohesive failure was established and this was more pronounced for P4520-PP. Furthermore, when evaluating the curing results listed in Table 17, the optimal composition in terms of processing time would be S4570 as this had the lowest cure time of 10.94 min. However, clearly P4520 would be most suited for optimal adhesion. Thus, as already indicated in Chapter 3 in the study of the sulphur curing system, optimising the cycle time does not necessarily lead to the best adhesion. Again, a trade-off between both parameters is needed.

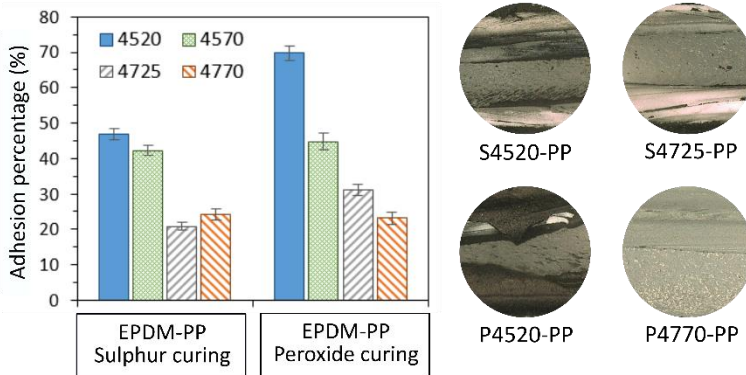


Figure 52: Adhesion percentages between sulphur-based EPDM-PP and peroxide-based EPDM-PP with varying ethylene content and Mooney viscosity. The error bars represent 95 % confidence intervals. The microscopic images show a circular zone (2 mm radius) of the fracture surfaces at the thermoplastic side. Black indicates the rubber and white the thermoplastic.

When comparing the current results with results reported by Bex [3], a clear improvement in adhesion with sulphur-based EPDM with PP can be reached by optimising the macromolecular structure. Bex [3] found an EPDM-PP adhesion strength of 2.5 MPa when optimising the processing parameters which corresponds to an adhesion percentage of 20 %. Bex indicated the high temperature, with high curing rate, and/or the temperature profile at the interface as possible negative factors for adhesion formation. Bex used an EPDM formulation similar to S1 as specified in section 3.4.1. For the combination of S1 with PP, an adhesion percentage of 17 % was reached. In S1, an EPDM was used with a Mooney viscosity of 43 MU (ML 1+4(125°C)), an ethylene content of 68 wt% and an ENB content of 8 wt%. It cannot be specified for this mixture whether solely the high ethylene content is responsible for the low adhesion percentage as the interaction with ENB content is unknown. However, from the current results it is clear that the interdiffusion with sulphur curing can be improved with PP but the high temperature, as indicated by Bex [3], might still inhibit full adhesion as a cohesive failure is still lacking.

Furthermore, the model for simulating the adhesion strength of Six et al. [121] is based on the interface temperature to define the degree of melt of the thermoplastic and the degree of cure of the rubber. However, rubber compounds S4570 and S4770 have a similar cure rate and 90 % vulcanisation time and these compounds were combined with PP GA05-400 from Ineos. Thus, in terms of adhesion strength, they should reach a similar adhesion strength after an equal processing time. However, the adhesion strength of PP-S4570 was  $4.76 \pm 0.16$  MPa and that of PP-S4770 was  $3.8 \text{ MPa} \pm 0.2 \text{ MPa}$ . This caused respective adhesion percentages of 42.3 % and 24.3 % which is significantly different. Therefore, an evaluation of the influence of differences in rubber composition on the proposed model is suggested. Possibly, this can be done by implementing a parameter for the compatibility between two materials in the model by Six. [120]. This model was developed by focussing on EPDM-HDPE simulation of the adhesion strength. Good compatibility between both materials was assumed based on wetting measurement results, but no intrinsic parameter for this is incorporated yet in the simulation [120].

### 4.3 Additives: fillers and plasticisers

In the rubber composition fillers are added for rubber reinforcement and plasticisers to reduce compound viscosity and/or to improve processing. For EPDM, oils are selected as plasticisers due to their mutual solubility. In this section, a paraffinic oil is added to the rubber mixture as, during peroxide curing with DCP, they tend to consume less alkoxy radical compared to naphthenic and aromatic oils [90]. The influence of process oil concentration is then investigated. Oils are low molecular weight components which are likely to migrate out of the rubber bulk upon exposure to high curing temperature and contact with the thermoplastic. This might induce a weak boundary layer at the rubber-thermoplastic interface, limiting interdiffusion or chemical bonding by changing the material compatibility and reducing the available EPDM chains at the interface. Furthermore, differences in filler type might influence the adhesion mechanism as well. Carbon black tends to interact with the polymer during vulcanisation creating a bound rubber phase or additional crosslinks which limit the chain mobility and might inhibit co-vulcanisation or interdiffusion with the thermoplastic. Therefore, a comparison is made with a calcined kaolin filler. This is a kaolin clay in which water has been eliminated by means of heat-treating/calcining. Calcined kaolin offers good compression set in non-black filled rubbers.

In this study, the influence of varying oil concentrations and filler type on cure characteristics, physico-mechanical properties and the adhesion with PP and PC is evaluated. Consequently, an optimisation of additives within the rubber compound can be achieved for good adhesion while providing good product properties.

#### 4.3.1 Materials and methods

##### 4.3.1.1 Materials

An EPDM rubber grade from Hercorub, Belgium was selected and changes were made to the oil and filler composition. Besides the filler and oil, the EPDM compound composition remained unchanged and contained the following raw materials:

- (1) Raw gum EPDM (100 phr): Vistalon 2504N, Exxon Mobile with Mooney Viscosity ML 1+4, 125°C = 25 Mooney units (MU), ethylene content = 56.0 wt%, ethylene norbornene (ENB) content = 3.8 wt%);
- (2) Zinc oxide (2.8 phr): MLCP International;
- (3) Zinc stearate (1 phr): Zinkstearat SMS, Bärlocher;
- (4) TMPT (2 phr): Actigran 70, Kettlitz, 70 % active ingredient;
- (5) DCP (3.2 phr): Perkadox BC-40MB-gr, AzkoNobel, 40 % active peroxide content.

Five different compounds were produced by varying the oil concentration and filler type as listed in Table 21. First, a control compound was produced without oils and fillers. Then, three compounds were produced with a calcined kaolin filler (PoleStar 200R, CCC International) and oil concentrations of 0, 15 or 30 phr. Finally, a carbon black-based compound was made by interchanging the kaolin filler by carbon black N550 (Aditya Birla Group) and adding 30 phr paraffinic oil. The calcined kaolin filler has a specific surface area (BET) of 8.5 m<sup>2</sup>/g while carbon black N550 has a specific surface area of 40 m<sup>2</sup>/g. The rubber compounds were peroxide cured. Each compound was combined with PP and PC (Section 3.2.1) as a high interface temperature can be reached during 2K injection moulding with accompanying efficient peroxide curing at the interface.

Table 21: Rubber compositions with varying oil and filler concentrations.

Component (phr)	UNF	K-O30	K-O15	K-O0	R-O30
Calcined kaolin	-	110	110	110	-
Carbon Black N550	-	-	-	-	70
Paraffinic oil	-	30	15	-	30

#### 4.3.1.2 2K injection moulding: 2K seal product

In contrast to the sample preparation for the previous investigations as described in 3.2.2, no rectangular 2K specimens were prepared. The internal cooling channels in the mould for rectangular shaped 2K specimens were corroded and the mould exhibited too much leakage. Instead, 2K seals were injection moulded as shown in Figure 53a. Figure 53b represents the EPDM seal as 1K product. The 2K mould for the presented product was developed by Bex et al. [3], [135]. Bex et al. [3] and Six et al. [120] provide information concerning the mould and product design. A fan gate was used for the rubber part, causing a weld line at the end of the flow length during injection moulding.

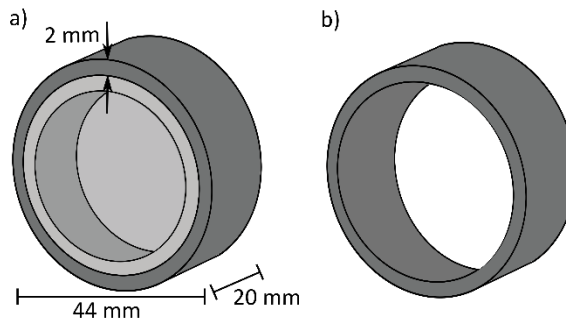


Figure 53: 2K product consisting of a thermoplastic internal wheel surrounded by an EPDM seal (a). 1K product of the EPDM seal (b).

To produce the 2K seals, processing conditions for the individual components were optimised. Similarly as the rectangular 2K samples (Figure 23), the thermoplastic parts were first produced separately. Afterward, the 2K specimens were produced by injection moulding the rubber onto the thermoplastic parts. The specific injection moulding parameters are listed in Table 22. These parameters were selected based on recommendations provided by Bex [3]. The volumetric injection rate for the rubber was set low to ensure complete filling and to prevent heat build-up in the rubber cavity. The injection time remains below the induction time/scorch time of each rubber compound. For the thermoplastic part, injection rate was set low to prevent burn marks at the end of the flow length. Too high injection rates caused a diesel effect (burn marks) due to the absence of air venting. Holding pressure for both the EPDM and thermoplastic part was set high enough to ensure optimal product dimensions. For EPDM, the vulcanisation temperature was set at 180°C. The mould temperature of the thermoplastic cavity during adhesion with the rubber was limited by thermoplastic part deformation which led to an interface temperature of 163°C for EPDM-PC and EPDM-PP. This interface temperature was experimentally determined with an infrared camera (OPTRIS PI400).

The required EPDM vulcanisation time was determined by producing subsequent EPDM-PP 2K samples with vulcanisation times ranging from 100 s to 1100 s with increments of 100 s. The measurement of the vulcanisation degree is elaborated in Section 4.3.1.3.

Table 22: Individual injection moulding parameters for the 2K sealing product

Process parameters	PP	PC	EPDM
Injection temperature (°C)	230	300	80
Mould temperature (°C)	20	100	180
Injection rate (cm <sup>3</sup> /s)	19	5	2/5 <sup>a</sup>
Holding pressure (bar)	692	494	396

#### 4.3.1.3 Rubber characterisation

Cure characteristics of EPDM compounds with varying oil concentrations and filler types were evaluated with a Monsanto moving die rheometer (MDR2000E). Cure time ( $t_{90}$ ), scorch time ( $t_{s1}$ ), minimum torque ( $S'_{min}$ ), maximum torque ( $S'_{max}$ ), delta torque ( $\Delta S'$ ) and cure rate index (CRI) were obtained at 180°C and 160°C. Measuring times at these temperatures were respectively 20 min and 45 min. Additionally, vulcanisation degree of 2K injection moulded samples was determined by hardness measurements as 90 % vulcanisation needs to be assured at the interface. Five Shore A hardness measurements were performed according to ISO 7619 with a measuring time of 15 s and the vulcanisation degree near the interface was calculated according to Eq.(24).

Mechanical properties of each EPDM compound were determined on the outer rubber seal of the 2K products. The region with the weld line was excluded from the measurements. By applying aluminium tape on the complete surface of the PP inner wheel, adhesion was inhibited during the injection moulding process [3]. Then, the rubber seal could be removed and used for mechanical testing. All samples were conditioned at 23 °C for 3 days. A Zwick Z050 equipped with a 1 kN load cell was used at room temperature, a crosshead speed of 200 mm/min and a gauge length of 13.5 mm to determine tensile properties. The samples for tensile testing had a length of 35 mm. The thickness and width of the rubber are indicated in Figure 53 but were determined for each sample individually. The hardness was measured using a CV Shore A hardness durometer according to ISO 7619. Compression set tests were performed at 23°C for 24 h according to ISO 815. Three rubber pieces were laminated to result in a sample thickness of  $5.9 \pm 0.1$  mm. The sample diameter was 13 mm. Average values of three samples for tensile strength and compression set, and of five samples for hardness with their 95 % confidence intervals are reported.

---

<sup>a</sup> Injection rate of 5 cm<sup>3</sup>/s for UNF, K-O30 and R-O30, and of 2 cm<sup>3</sup>/s for K-O15 and K-O0.

#### 4.3.1.4 Adhesion characterisation

##### Compatibility measurements

Differences in compatibility due to changes in filler and oil composition were assessed by contact angle measurements as described in detail in Chapter 3, section 3.2.6. Thus, vulcanised substrates were taken of each compound and a PP or PC granule was placed on the substrates at temperatures of 200°C and 230°C respectively. Contact angles were monitored every minute during 15 minutes. Three measurements were made for each combination of thermoplastic with EPDM rubber and average values with their 95 % confidence intervals are reported.

##### Peel test

To define the adhesion strength, peel tests were executed on a custom-made set-up as described by Six et al. [120]. For this peel test, a piece of aluminium tape was put on the surface of the thermoplastic internal wheel as shown in Figure 54a. Afterwards, the thermoplastic wheel was overmoulded with rubber. Peel tests were not executed in the region of the weld line. At the location of the aluminium tape, no adhesion can be created at the interface. Then, the rubber was cut at the beginning of the aluminium tape (cutting zone in Figure 54a). This enabled the fixation in the clamps during peel testing on a tensile testing machine (Zwick Z050 equipped with 1 kN loading cell) as shown in Figure 54b. Testing speed was 200 mm/min. For peel testing, the 2K sample wheel was mounted in the centre on a free rotating axis. Afterwards, the rubber seal was peeled off creating a loaded area as shown Figure 54b which enables measurement of a peel force. Due to the free rotation in the centre of the 2K sample, a constant peel angle is reached. Five measurements were taken of each material combination and 95 % confidence intervals are reported.

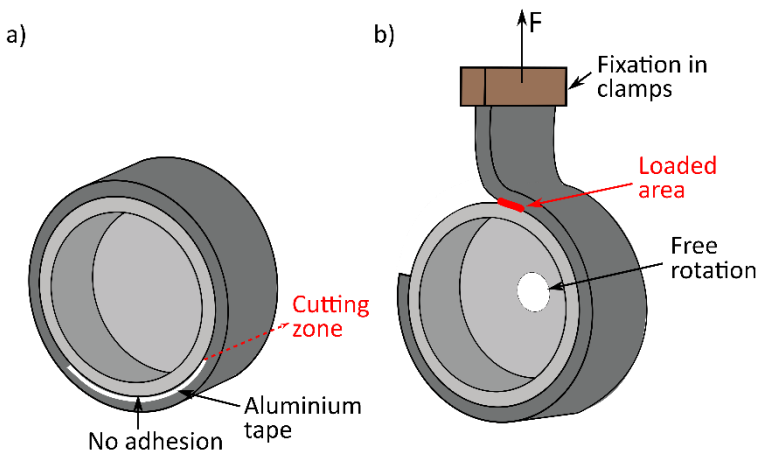


Figure 54: Peel test sample preparation. 2K thermoplastic internal wheel partially covered with aluminium tape (a) and positioning of 2K sample during testing (b).

To compare results of adhesion strength between PP and the different EPDM compounds, an equivalent adhesion width was defined by relating the peel strength to the total tensile strength as the peel strength for cohesive failure will not exceed the

rubber strength. The SI unit for tensile strength of vulcanised rubber (ISO 37) is MPa. For a peel test, the SI unit is N/mm. Thus, the equivalent adhesion width is calculated by dividing the peel force per unit width ( $P$ ) at the interface by the tensile strength of the rubber ( $\sigma_t$ ) (Eq. (28)) which results in an equivalent adhesion width expressed in mm:

$$\text{Equivalent adhesion width (mm)} = \frac{P}{\sigma_t} \quad (28)$$

### Shear test

A custom-made set-up was used to measure adhesion strength under shear conditions. The presented 2K seal sample consists of an inner thermoplastic wheel and an outer rubber seal. Therefore, a more accurate method of adhesion evaluation would be to disjoint the complete seal from the thermoplastic wheel by pushing the inner thermoplastic wheel downwards while maintaining the rubber seal at a fixed position. This custom shear test resembles the pin-and collar test from ISO 10123. In Figure 55, the shear test set-up is represented. This entails mounting the 2K sample on the upper solid core. Afterwards, this upper solid core is moved downwards until contact with the bottom support cylinder. Here, the rubber outer seal is prevented to move in the axial direction, while the inner thermoplastic wheel is pushed in the opening of the support cylinder. The clearance between the opening and the thermoplastic wheel is 0.25 mm. Due to the shear forces, the rubber seal will detach from the thermoplastic wheel either, cohesively or adhesively.

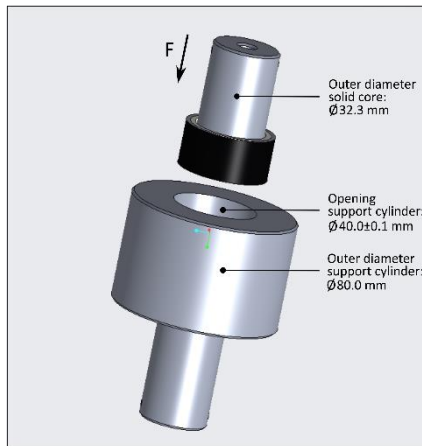


Figure 55: Set-up of custom-made shear test.

A Zwick Z050 tensile testing machine equipped with a 50 kN loading cell was used. The solid core was axially aligned with the opening of the support cylinder to reach an equal clearance between the solid core and the support cylinder when moving through the opening. The testing speed was 1 mm/min. The measurement started upon contact between the 2K sample and the support cylinder. Shear forces were measured in function of the crosshead distance. The crosshead distance represents the distance of the upper solid core travels after reaching an onset load of 10 N upon contact between the rubber seal and the support cylinder.

### 4.3.2 Results and discussion

#### 4.3.2.1 Influence of fillers and oil concentration on EPDM cure characteristics

Cure characteristics of EPDM without filler and oils (UNF), kaolin-filled EPDM with varying oil concentration (K-O30, K-O15 and K-O0), and carbon-black-filled EPDM with oil (R-O30) are listed in Table 23. Furthermore, in Figure 56a torque-time curves are represented and in Figure 56b scorch time ( $t_{s1}$ ), vulcanisation time ( $t_{90}$ ) and CRI of each sample is shown.

Table 23: Cure characteristics of EPDM compounds with varying filler and oil concentration at 180°C and 160°C.

Characteristic	UNF	K-O0	K-O15	K-O30	R-O30
$S'_{min}$ at 160°C	0.22	0.68	0.45	0.35	0.43
$S'_{max}$ at 160°C	5.95	13.26	6.37	4.70	3.98
$\Delta S'$ at 160°C	5.73	12.58	5.92	4.35	3.55
$t_{90}$ (min) at 180°C	3.86	3.45	3.35	3.19	2.88
$t_{90}$ (min) at 160°C	21.69	21.96	21.89	22.63	19.38
$t_{s1}$ (min) at 180°C	0.77	0.54	0.66	0.67	0.39
$t_{s1}$ (min) at 160°C	2.32	1.37	2.13	2.68	2.96
CRI ( $\text{min}^{-1}$ ) at 180°C	32.36	34.36	37.17	39.68	50.00
CRI ( $\text{min}^{-1}$ ) at 160°C	5.16	4.86	5.06	5.01	6.09

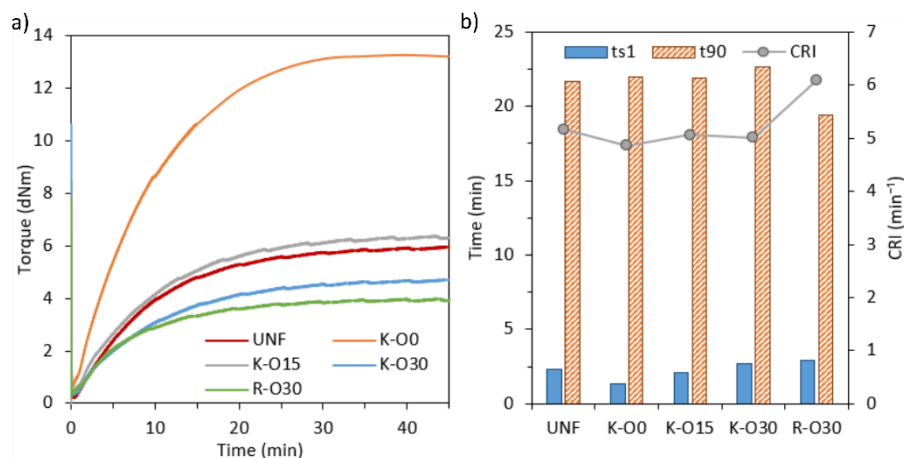


Figure 56: Cure characteristics of EPDM at 160°C with varying filler and oil concentration: torque in function of time (a) and scorch time ( $t_{s1}$ ), vulcanisation time ( $t_{90}$ ) and CRI (b).

Cure characteristics at 160°C (Figure 56a and Table 23) indicate major differences in delta torque ( $\Delta S'$ ). This torque difference relates to the crosslink density [75]. A higher  $\Delta S'$  corresponds to a higher crosslink density. Compared to the control sample without any fillers or oils (UNF), a clear increase in torque difference is seen when adding solely a calcined kaolin filler (K-O0). This EPDM compound also has a higher minimum torque value. The minimum torque relates to the rubber compound viscosity. When fillers are added, physical crosslinks may form, limiting rubber chain mobility which enhances  $S'_{min}$  [79]. Li et al. [79] mentions minimum torque as being an indicator for the degree of

physical crosslinks and delta torque as indicator for the degree of chemical crosslinks. Ahmed et al. [83] also found an increase in minimum torque when adding kaolin due to the macromolecules being restricted in terms of motion. Thus, adding the kaolin filler, increased compound viscosity (physical crosslinks) and crosslink density (chemical crosslinks). Furthermore, higher oil concentrations (K-O0 = 0 phr oil; K-O15 = 15 phr oil; K-O30 = 30 phr oil) significantly reduced viscosity and crosslink density for both compounds. The maximum torque also decreases with higher paraffinic oil concentration. This was also found by Wang et al. [136] when examining the influence of process oil content in peroxide-based EPDM. The authors related this phenomenon to the reduced interaction between the polymer chains as free volume is increased by the presence of oil hydrocarbons between the EPDM chains. This was referred to as a 'dilution effect'. Moreover, the peroxide free radicals, created during the vulcanisation reaction, might be consumed by the oil which reduced the amount of free radicals for crosslinking. This was referred to as the 'chemical effect'. Furthermore, when comparing the kaolin-filled compound (K-O30) with the carbon-black-filled compound (R-O30),  $\Delta S'$  is higher for the kaolin-filled compounds indicating a higher crosslink density while minimum torque is lower referring to a lower compound viscosity. Important to keep in mind is the difference in filler concentration for both compounds, i.e. 110 phr for calcined kaolin and 70 phr for carbon black N550.

In terms of cure time, scorch time and cure rate, differences are observed due to the presence of fillers and oils. At the interface during 2K injection moulding, the temperature of EPDM is around 160°C. Compared to control sample (UNF), adding a calcined kaolin filler causes a reduction in scorch time which could be due to the participation of kaolin during the curing reaction [83]. Then, adding higher concentrations of oil to the kaolin filled compound increases the scorch time improving processing safety as was also found by Wang et al. [136]. The authors in that study also ascribed the delayed curing reaction to the dilution and chemical effect reducing the effective peroxide concentration [136]. The CRI increases slightly by adding paraffinic oil, possibly due to a better dispersion of peroxides, but a further increase in oil concentration does not have an influence. Finally, when comparing K-O30 with R-O30, a clear reduction in vulcanisation time ( $t_{90}$ ) and higher cure rate was found when interchanging kaolin with a carbon black filler. Literature indicates cure characteristics being dependent on the surface area of the filler as chemical and physical interaction can occur on the filler surface [79], [137]. The calcined kaolin filler in K-O30 has a much lower surface area (8.5 m<sup>2</sup>/g) compared to the carbon black N550 in R-O30 (40 m<sup>2</sup>/g). Possibly, this high surface area of N550 improved curing properties.

After determining cure characteristics of the EPDM compounds with varying filler and oil content, vulcanisation degree in function of time was evaluated at the interface of K-O30. This EPDM compound had the highest  $t_{90}$  at 160°C and was therefore selected to determine the required vulcanisation time during injection moulding.

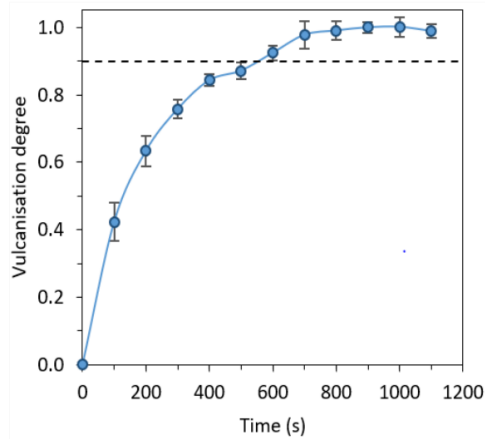


Figure 57: Vulcanisation curve of injection moulded K-O30 based on hardness measurements. The dashed line represents 90 % vulcanisation degree. Error bars represent 95 % confidence intervals.

As shown in Figure 57, 90 % vulcanisation degree can be reached after 500s which is significantly faster than indicated with the MDR at 160°C. Based on the temperature evaluation in the 2K mould, the interface temperature is 163°C and a temperature profile is created throughout the 2 mm rubber seal. Thus, this induces a more efficient curing reaction. However, to ensure sufficient vulcanisation degree for all samples, a vulcanisation time of 800 s was chosen. To analyse whether this 800 s vulcanisation time was sufficient for all compounds Shore A hardness measurements were executed on the 2K injection moulded samples and the vulcanisation degree was determined according to Eq. (24). Results showed that the vulcanisation degrees for the different compounds varied between 97 % and 100 % vulcanisation degree which is above the requirement of 90 %.

#### 4.3.2.2 Influence of fillers and oil concentration on EPDM properties

By changing the filler and paraffinic oil content in EPDM, differences in mechanical properties can be observed. In Figure 58, tensile strength, compression set, hardness and elongation at break are shown for each EPDM compound.

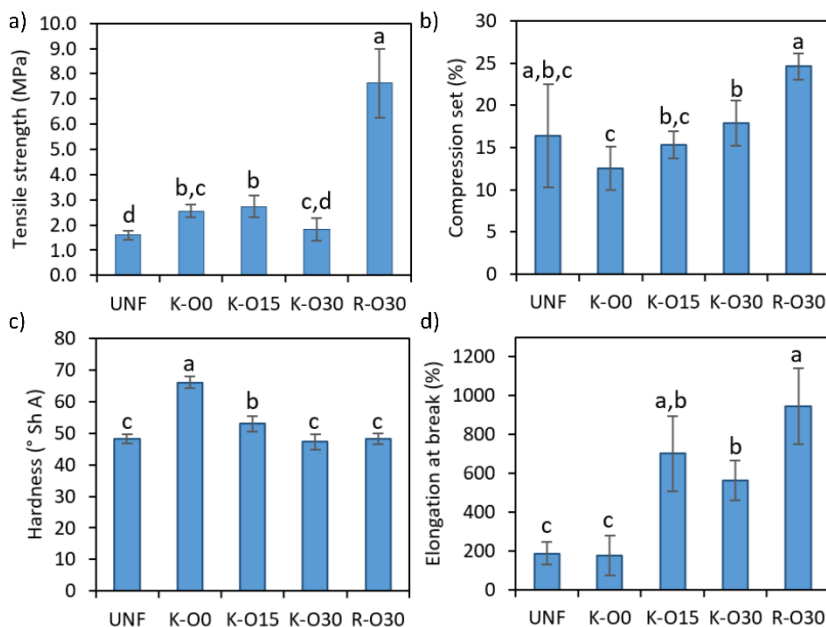


Figure 58: Mechanical properties of EPDM with varying oil and filler concentrations: tensile strength (a), compression set (b), Shore A hardness (c), and elongation at break (d). Error bars represent 95 % confidence interval. Grouping information from a one-way ANOVA is given by lower case letters.

The control sample without filler and oils shows low tensile strength, elongation at break and large variations in compression set. When adding 110 phr kaolin (K-O0), tensile strength and hardness significantly increase due to the reinforcing effect and high filler loading which causes a higher crosslink density due to more physical entanglements. Then, adding paraffinic oil improves the dispersion of the kaolin filler which decreases the distance between neighbouring EPDM chains and entanglement density [86]. This lower crosslink density causes a lower hardness and higher compression set with higher oil content. Elongation at break shows large error bars for all samples containing oil and fillers (K-O0, K-O15, K-O30 and R-O30) but the presence of oils improves the mean elongation at break due to decreased crosslink density compared to the non-oil filled compounds (UNF and K-O0) [138]. Compared to the kaolin filled EPDM (K-O30), carbon black filled EPDM (R-O30) has a higher tensile strength which might be due to the higher surface area of N550 causing a higher reinforcing effect [75].

#### 4.3.2.3 Influence of fillers and oil concentration on adhesion between EPDM and thermoplastics

First, to analyse differences in adhesion between thermoplastic PP and PC, and thermoset rubber EPDM with varying oil and filler content, peel tests were executed. Results from these measurements are indicated in terms of adhesion force as shown in Figure 59a. Furthermore, equivalent adhesion width relates the peel force to the tensile strength of each rubber compound as shown in Figure 59b.

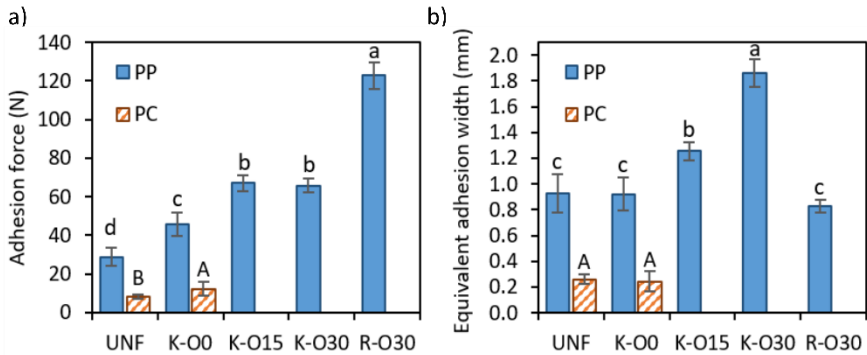


Figure 59: Peel test results between PP or PC and EPDM with varying oil an filler content: adhesion force (a), and equivalent adhesion width (b). The error bars represent 95 % confidence intervals. Grouping information from a one-way ANOVA is given by lower case letters for PP and by upper case letters for PC.

Results of adhesion force (Figure 59a) indicate a lack of adhesion between PC and EPDM compounds which contain a paraffinic oil. Specifically during 2K injection moulding, the 2K sample was demoulded by compressed air in the centre of the thermoplastic wheel. Upon ejecting the sample, the PC wheel detached from the outer rubber seal, preventing further adhesion measurements. With UNF and K-O0, peel tests were possible but adhesion remained low. Adding calcined kaolin slightly improved the adhesion force. The rubber tensile strength also improved from UNF to K-O0 and therefore the equivalent adhesion width, as shown in Figure 59b, did not significantly change upon adding calcined kaolin (K-O0) compared to the unfilled compound (UNF). To clarify the influence of paraffinic oil in EPDM on the adhesion with PC contact angle measurements were performed on UNF, K-O0 and K-O30. These results are shown in Figure 60b. EPDM without fillers and oils (UNF) seems to go to a lower mean contact angle which might indicate a better physical interaction between PC and UNF causing a certain adhesion during injection moulding. However, PC on K-O0 resulted in the highest mean contact angles which contradicts the adhesion with K-O0 compared to no adhesion with K-O30. Possibly, these contact angle measurements at high temperature do not clarify the adhesion results as they do not imitate sufficiently the conditions during processing, for example the possible migration of oils to the interface. Furthermore, the adhesion force remains extremely low ( $12 \pm 4$  N). The spreading dynamics of PC on EPDM substrates in Figure 60 cannot be compared to those of PP as viscosity values are not identical. Such comparison was, however, not the goal of these tests.

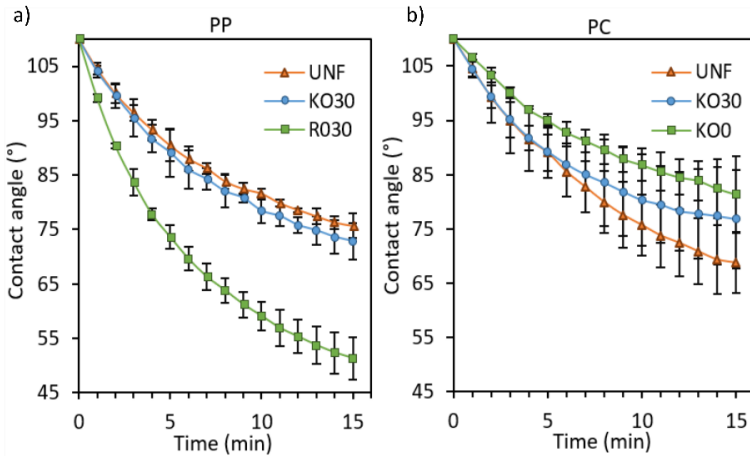


Figure 60: Contact angles of PP (at 200°C) on EPDM without oils and fillers (UNF), on EPDM with 30 phr oil and 110 phr calcined kaolin (K-O30), and on EPDM with 30 phr oil and 70 phr N550 carbon black (R-O30) (a); PC (at 230°C) on UNF, on EPDM without oil and 110 phr calcined kaolin (K-O30) on EPDM with 30 phr oil and 110 phr calcined kaolin (K-O30) (b). The error bars represent 95 % confidence intervals.

Adhesion force results of PP with EPDM (Figure 59a) were significantly influenced by the addition of paraffinic oil and fillers. Compared to K-O0, adding 15 phr or 30 phr oil improved the adhesion force with PP. However, no significant difference is found between K-O15 and K-O30. From Figure 58a, it is known that 30 phr lowered the total tensile strength of the rubber. Thus, when comparing the adhesion force with the total tensile strength of K-O15 and K-O30, it can be seen in Figure 59b that 30 phr paraffinic oil caused the highest relative strength. For EPDM, it is known that it is a highly entangled polymer with branched chains which significantly reduce chain mobility [139]. Thus, higher oil content causes a dilution of these entangled chains, improving mobility at the interface with PP. Furthermore, other components within the EPDM formulations may migrate to the interface. Specifically, for chemical bonding between EPDM and PP, dicumylperoxide initiates co-vulcanisation. Possibly, these peroxides are more accessible for PP due to the dilution effect. However, Wang et al.[136] also indicates possible consumption of peroxide radicals by the process oil, which makes it difficult to validate this assumption. Thus, multiple possible explanations arise: (1) improved interdiffusion of PP within EPDM due to lower crosslink/entanglement density in EPDM; (2) enhancement of co-vulcanisation due to more easily accessible peroxide radicals; (3) improved mobility of EPDM chains; (4) improved interdiffusion of PP into EPDM due to less entanglement and subsequent higher efficiency of co-vulcanisation.

When comparing the calcined kaolin filled EPDM (K-O30) with the carbon black filled EPDM (R-O30), a higher adhesion force with PP was found with R-O30. However, when taking into account the rubber tensile strength, equivalent adhesion width seems to be significantly higher for PP with K-O30. Furthermore, contact angle measurements at high temperature (Figure 60a) indicate the lowest contact angles of molten PP on R-O30 and thus a better interaction. This does not coincide with the equivalent adhesion width results. Probably, even though adsorption of PP onto R-O30 might be better than onto K-O30, adsorption does not dominate as adhesion mechanism. Additionally, only PP on K-O30 gave a full cohesive failure during peel test as shown in Figure 61. This

cohesive failure was not found for R-O30 with PP. Furthermore, the adhesion force of K-O30 with PP was  $66 \pm 4$  N, while the total tensile force of the K-O30 sample during tensile testing was  $73 \pm 15$  N. Thus, the adhesion force is not significantly different from the rubber tensile force. Therefore, it is believed that during peel testing of PP with K-O30, the rubber fails as this is weaker than the interfacial bond. Additionally, it needs to be questioned why calcined kaolin in combination with a paraffinic oil in EPDM results in better adhesion with PP compared to carbon black filled EPDM. According to Mark et al. [75], surface area is a morphological property that defines the interaction between the elastomer and filler surface. The high surface area causes a high accessibility of the elastomer chains to be adsorbed onto the surface. This can drastically decrease the mobility of the elastomer chains. Possibly, the rubber-filler network in carbon black filled EPDM hinders a good adhesion with PP. Another explanation for the lower adhesion strength with carbon black filled EPDM could be the higher curing efficiency when adding carbon black. Cure results showed a higher cure rate index which can again be ascribed to the higher surface area of carbon black causing chemical and physical interactions with EPDM and subsequently limiting good interdiffusion and covalent crosslinking as crosslinks within the rubber are formed more rapidly.

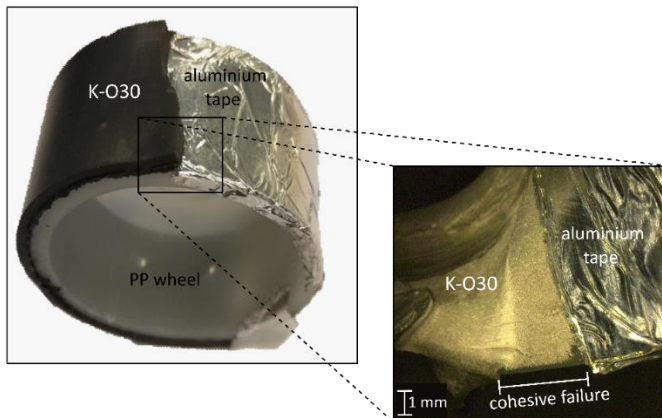


Figure 61: Cohesive failure between K-O30 and PP after a peel test.

To validate the equivalent adhesion width results, shear tests were executed on wheels combining PP with UNF, K-O30 and R-O30. For K-O0 and K-O15 a shear test was not possible as at the weld line of the rubber seal a small amount of PP gathered as these rubbers caused a high pressure build-up near the end of the flow path in the narrow rubber cavity due to the high viscosity. Thus, a small amount of molten PP was enclosed at the weld line before complete filling of the rubber cavity. Results of the shear test are shown in Figure 62.

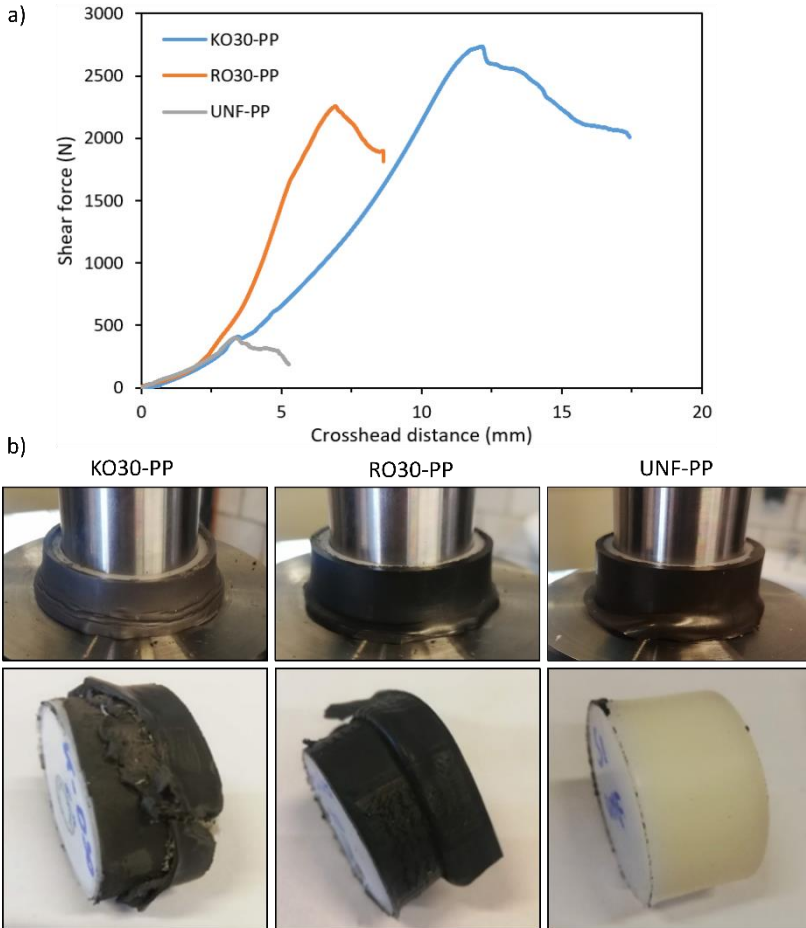


Figure 62: Shear test: (a) shear force between PP and K-O30, R-O30 and UNF over a shear distance, and (b) 2K sample during and after testing.

Similar to the peel test results, the highest shear force was reached for PP with K-O30. Thus, this confirms the assumption that calcined kaolin provides better adhesion than carbon black. In contrast to the peel test, shear test showed a cohesive failure at the interface of PP with K-O30 and R-O30. Thus, a good adhesion can be reached as well in application under shear similar to the proposed 2K sample for carbon black filled EPDM. However, when evaluating adhesion results and mechanical properties, it can be concluded that the choice of filler type will be largely application dependent. For EPDM with kaolin and a peroxide curing system a very good compression set can be provided. Especially as seen in Figure 58, K-O15 offers a good compression set when selecting an oil containing EPDM. Oil is generally necessary for optimal compound mixing and good injection moulding conditions. When adding only 15 phr of oil, it has to be taken into account that adhesion will be lower than when adding higher oil content. Carbon black is more likely to be used in application under high loading, for example rubber valves, due to its high reinforcing effect.

## 4.4 Conclusion

Results from the study on the EPDM macromolecular characteristics indicate a significant effect of the EPDM structure on the adhesion with PP during 2K injection moulding for both a sulphur and a peroxide curing system. Specifically for peroxide curing, interdiffusion and co-vulcanisation may occur simultaneously. By applying a higher propylene content, compatibility with PP improves, leading to better interdiffusion. Furthermore, co-vulcanisation benefits from a low ENB content and low EPDM molecular weight as crosslinking efficiency with PP increases. Similar to peroxide curing, adhesion during sulphur curing benefits from a higher compatibility in case of higher propylene content. The influence of Mooney viscosity or molecular weight during sulphur curing was limited which could be due to an interference by molecular weight distribution. Eventually, combining low Mooney viscosity with a low ethylene content resulted in the highest adhesion percentage for both sulphur and peroxide curing. Furthermore, results from the influence of diene content and results from the design of experiments indicated the best adhesion between EPDM and PP for the peroxide curing system. During the experimental design, high diene containing EPDMs were used, while a lower diene level would be better for adhesion during peroxide curing. However, the interaction between low diene content, Mooney viscosity and ethylene content is currently unclear and requires further investigation.

Besides the EPDM macromolecular structure, the influence of oil and filler content was evaluated. EPDM-PC adhesion could not be positively affected by oils or fillers. Probably, the co-agents concentration was too low to enable sufficient adhesion. The adhesion with PP can be improved when adding higher contents of paraffinic oil as this causes a dilution of entangled EPDM chains. Consequently, mobility at the interface with PP is enhanced. This can enable interdiffusion of PP and subsequent co-vulcanisation. However, currently it is not possible to define in which manner the paraffinic oil specifically influences the interdiffusion tendencies of PP or EPDM chains. In terms of filler type, calcined kaolin offers higher peel and shear forces at the interface between EPDM and PP compared to carbon black filled EPDM. As it was not possible to relate contact angle measurement results to the adhesions strength, wetting is believed to play an insignificant role in the final adhesion formation. Interdiffusion and subsequent co-vulcanisation are more likely to influence adhesion. In this study, carbon black N550 has a higher surface area than calcined kaolin creating higher accessibility for the elastomer chains to be adsorbed onto the filler surface and higher cure rate. This can drastically decrease the mobility of the elastomer chains and interdiffusion. However, it can be concluded that both calcined kaolin and carbon black offer promising results for adhesion in rubber-thermoplastic moulded products. Therefore, the requirements in terms of product properties need to be considered as well when selecting the filler type.

---

## Chapter 5 Adhesion mechanism analysis

---

### 5.1 Introduction

Adhesion between two polymer surfaces is a complex phenomenon related to intermolecular interactions. Depending on the specific material composition, dispersive interactions, acid-base interactions, interdiffusion, and/or chemical bonding can occur [7], [8]. In this chapter, different adhesion mechanisms for the proposed material combinations of EPDM with thermoplastics are evaluated and discussed. First, a more sophisticated wetting methodology, closer-to-processing-conditions, is represented in Section 5.2. This is a follow-up study on the work of Bex et al. [6]. The methodology, presented in this chapter, focusses on relating a thermodynamic property, the work of adhesion, to the adhesion percentage. Afterwards, chemical bonding between EPDM and thermoplastics in the current 2K process is addressed in Section 5.3. Specifically, the reaction mechanism of co-vulcanisation is clarified and a reactive wetting methodology to evaluate chemical bonding is represented. Finally, interfacial characterisation techniques were applied to analyse interdiffusion between EPDM and thermoplastics in Section 5.4.

The proposed reaction mechanism for co-vulcanisation between EPDM and thermoplastics and the prediction of co-vulcanisation based on a reactive wetting methodology have been published in two journal papers [124], [140]:

- (1) **B. Laing**, J. De Keyzer, D. Seveno, and A. Van Bael, “Adhesion between ethylene-propylene-diene monomer and thermoplastics in two-component injection molding: Effect of dicumylperoxide as curing agent,” *J. Appl. Polym. Sci.*, 49233, 2020.
- (2) **B. Laing**, D. Seveno, J. De Keyzer, and A. Van Bael, “Reactive wetting of polyethylene on ethylene-propylene-diene terpolymer,” *Colloids Interface Sci. Commun.*, Vol. 40, 100343, 2021.

### 5.2 Wetting

To predict the adhesion between thermoplastics and thermoset rubbers, Bex et al. [6] proposed a high temperature direct contact angle methodology. This high temperature contact angle measurement methodology was already discussed and applied in Chapter 3 section 3.2.6. However, this technique has its limitations. As it enables a ranking of different thermoplastics for possible adhesion with a certain thermoset rubber, the lowest contact angle would implicate the best adhesion. No minimum contact angle was defined which could lead to good adhesion. Furthermore, measurements started after reaching a contact angle of  $110^\circ$  and were executed during 15 min at a certain high temperature. No equilibrium angles were reached, thus, measurement merely focused on dynamic

spreading. Therefore, a methodology was sought after to analyse the complete wetting process going from initial contact between the thermoplastic melt up to an equilibrium state.

In this wetting study, a drop and surface analysis apparatus, composed of a high temperature dosing unit and a thermalised cell under inert atmosphere, is used to characterise wettability of the rubber substrates. As a result, the work of adhesion ( $W_a$ ) can be calculated according to Young-Dupré's equation (Eq. ((3))). The pendant drop shape analysis of the polymer melt created by the heated syringe provides the liquid/vapour surface energy at high temperature and afterwards the final stable contact angle can be measured between the molten thermoplastic and a cured rubber substrate. Time and spreading of the thermoplastic droplet is monitored until an equilibrium is reached. It will be investigated whether a correlation exists between work of adhesion  $W_a$  and the adhesion strength of the 2K injection moulded samples.

### 5.2.1 Drop and surface analysis: set-up

To evaluate wetting between thermoset rubbers and polyolefins, a fully automatic contact angle analysis instrument OCA 50 from Dataphysics was employed with an environmental control chamber TEC 700 and a needle heating device NHD 700 for pendant drop of polymer melts. Contour analysis was executed with the SCA20 software coupled to the Dataphysics device.

The contact angle measurement device is shown in Figure 63. The environmental control chamber is equipped with a twin electric resistance heater for manual and software controlled temperature settings up to 700°C and a twin PID temperature controller TC 700. The TEC 700 can be cooled with compressed air and an inert environment can be created, in this case with Argon (Ar). The temperature close to the pendant drop is measured with a thermocouple. Furthermore, the electrical needle heating device can enter the heated chamber from the top. In the needle heating device a ceramic cannula can be placed in which the thermoplastic material can be melted and dosed through a ceramic dosing tip with a graphite plunger. Furthermore, observations can be made by a video measuring system with USB 3.0 camera (2048 x 1088 pixel resolution) and a clear image is retrieved by adjusting the light source behind the heated chamber.

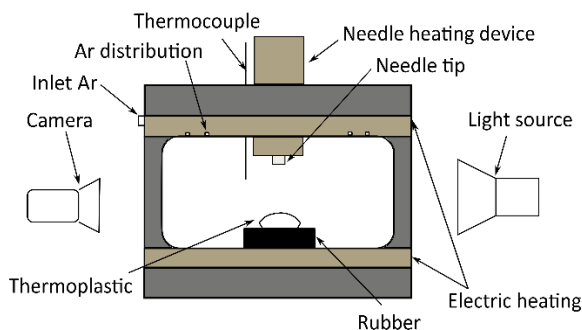


Figure 63: Environmental control chamber with heated needle device for analysis of polymer melts (pendant drop) and wetting on solid substrate.

## 5.2.2 Thermoplastic melt properties

### 5.2.2.1 Density

Constant pressure PVT measurements were executed to determine the density of PP and PE at high temperatures. Measurements were executed on a SmartRheo 2000 capillary rheometer according to ISO 17744 with pressures ranging from 10 to 60 MPa at increments of 5 MPa at 200°C, 220°C, 240°C and 260°C for PP and at 160°C, 180°C, 200°C and 220°C for PE. Afterwards, the datapoints were fitted and extrapolated to 0 MPa, i.e. pressure during contact angle measurements. Results for PE are indicated in Figure 64a and for PP in Figure 64b.

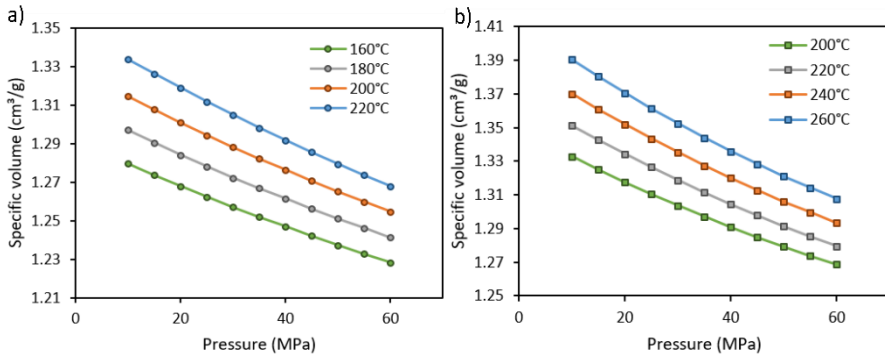


Figure 64: PVT properties of PE (a) and PP (b).

Based on the specific volumes at 0 MPa densities were determined and these results are listed in Table 24 and Table 25. With increasing temperature, the density for both thermoplastics decreases.

Table 24: Density of PE (M80064, Sabic) at 160°C, 180°C, 200°C, and 220°C.

Temperature	Specific volume (cm <sup>3</sup> /g)	Density (g/cm <sup>3</sup> )
160°C	1.274	0.785
180°C	1.292	0.774
200°C	1.310	0.763
220°C	1.329	0.753

Table 25: Density of PP (400-GA05, Ineos) at 200°C, 220°C, 240°C, and 260°C.

Temperature	Specific volume (cm <sup>3</sup> /g)	Density (g/cm <sup>3</sup> )
200°C	1.349	0.741
220°C	1.370	0.730
240°C	1.390	0.720
260°C	1.412	0.708

### 5.2.2.2 Viscosity

Rheology measurements were executed to determine the viscosity of PP and PE in function of shear rate. During wetting experiments, i.e. droplet spreading, Zhang et al.[23] indicated that shear rates are below the critical value of  $0.01 \text{ s}^{-1}$ , which corresponds to a constant zero-shear viscosity. In this study, equal zero-shear viscosity was sought after to compare wetting between different thermoplastics on rubber substrates.

For the dynamic oscillatory measurements an ARES strain-controlled rheometer (TA Instruments) was used with a parallel-plate geometry (diameter of 25 mm, and a gap of 1.5 mm). For PP, three measurements were executed at  $240^\circ\text{C}$ . The specific selection of this temperature will be further clarified in section 5.2.2.3. A frequency sweep was executed at angular frequencies ranging from 0.1 to 100 rad/s with a strain amplitude of 5 %. With a strain sweep, the strain amplitude was verified to remain in the linear viscoelastic regime. Furthermore, a rate sweep was executed from  $0.01 \text{ s}^{-1}$  to  $10 \text{ s}^{-1}$ . Afterwards, a SmartRheo 2000 capillary rheometer with a twin bore barrel was used to define the viscosity at shear rates ranging from 10 to  $10000 \text{ s}^{-1}$ . Apparent viscosities and shear rates were corrected by a Bagley correction for correct entrance pressure determination at a specific shear rate and a Rabinowitsch correction to account for the shear thinning behaviour [141]. Then, results from the rate sweep, frequency sweep and capillary rheometer were combined by applying the Cox-Merz rule. This rule states that the shear-rate dependence of the steady-state viscosity is equal to the frequency dependence of the complex viscosity [75].

To determine the temperature at which the zero-shear viscosity of PE is equal to that of PP, a steady-state rate temperature ramp test was executed from  $150^\circ\text{C}$  to  $190^\circ\text{C}$  at  $0.1 \text{ s}^{-1}$ . This measurement indicated  $160^\circ\text{C}$  as suitable temperature. Therefore, similar to the tests with PP, a rate sweep, frequency sweep and capillary rheometer measurements were taken.

In Figure 65, the viscosity of PE at  $160^\circ\text{C}$  and PP at  $240^\circ\text{C}$  in function of shear rate are represented. At these temperatures, both thermoplastics reach equal zero shear viscosity. Thus, for further wetting experiments, these proposed temperatures are applied. Furthermore, Figure 65 also shows a broader linear plateau for PE which indicates that PE has a smaller MWD compared to PP as disentanglement or shear thinning occurs at lower shear rates for PP [141]. This could also have important implications for the interdiffusion process during injection moulding. As PE reaches a similar zero shear viscosity as PP at a much lower temperature of  $160^\circ\text{C}$ , the viscosity of PP will probably be higher at equal temperatures.

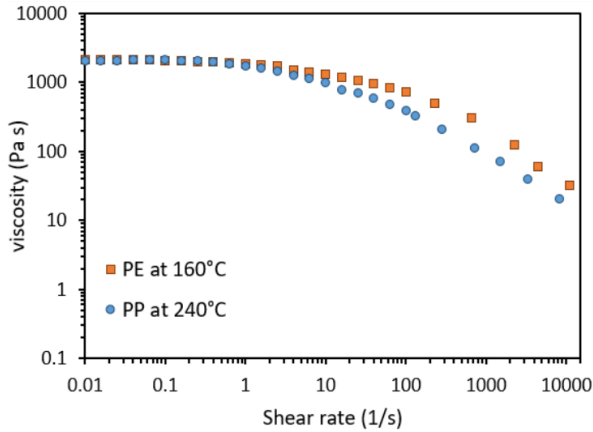


Figure 65: Viscosity in function of shear rate for PP at 240°C and PE at 160°C.

### 5.2.2.3 Surface tension

For the pendant drop measurements, pieces from the sprue of injection moulded thermoplastics samples were shaped to fit the alumina cannula. Both the needle and chamber were set at a high temperature, i.e. 240°C, 220°C and 200°C, which is similar to the selected temperature by Zhang et al. [23] for PP on glass substrates. Three pendant drops were created for each temperature. A needle tip/nozzle with an outer diameter of 3 mm and an internal diameter of 1 mm was used. After setting the temperature, the cannula was filled with the thermoplastic. The needle was then lowered into the heated chamber, Ar-flow was initiated and the chamber was stabilised during 10 min. A pendant drop was gradually created by pushing subsequent small amounts of molten polymer through the needle tip. Specifically, the interface surface tension of the droplet was monitored during each droplet volume increase until stable conditions were reached; i.e. no more polymer flow and a stable surface tension. Furthermore, the Worthington number ( $W_0$ ) (Eq. (19)) was calculated throughout each phase until a maximum value was reached. When increasing the droplet volume further than this point, the droplet started to neck, causing a drop in  $W_0$ . The polymer melt surface tension corresponding with the maximum  $W_0$  was selected as correct value at a given temperature. Images of the optimal pendant drop of PP and PE are represented in Figure 66.

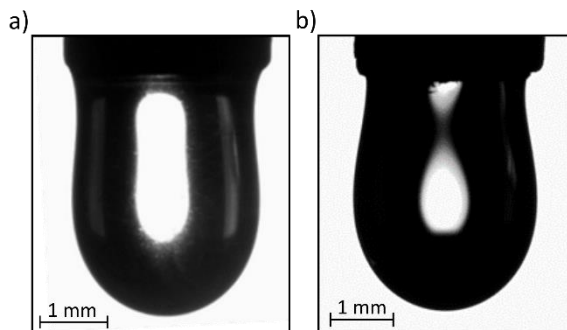


Figure 66: Pendant droplet of PP at 240°C (a), and of PE at 160°C (b).

Calculating the interface surface tension of the polymer pendant drop was done according to Laplace-Young equation (Eq. (18)). This entailed acquiring the temperature dependency of the density for each thermoplastic as addressed in 5.2.2.1. Results of the pendant drop shape analysis of PP at 200°C, 220°C and 240°C are given in Figure 67. As expected, the surface tension of PP decreases with increasing temperature. This decreasing trend was also found by Zhang et al.[23].

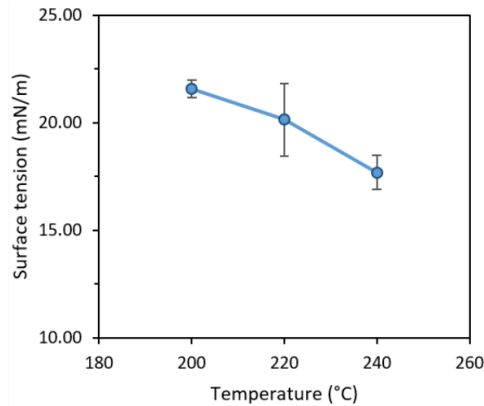


Figure 67: Temperature dependency of surface tension of PP. 95 % confidence intervals are reported.

Creating a PP pendant drop required approximately 30 min at 240°C, 50 min at 220°C, and 100 min at 200°C. Therefore, 240°C was selected for further deposition and wetting on a solid substrate which corresponded to a surface tension of  $17.7 \pm 0.8$  mN/m of the PP pendant drop with a droplet volume of  $19 \pm 1$  mm<sup>3</sup>. At this temperature, no degradation of the PP pendant drop was observed. Furthermore, at this temperature for PP, a corresponding temperature for PE could be selected, i.e. 160°C, due to equal zero-shear viscosity. At 160°C, PE had a surface tension of  $25.6 \pm 0.1$  mN/m and pendant drop volume of  $19.1 \pm 0.1$  mm<sup>3</sup>.

### 5.2.3 Wetting of thermoplastic melt on rubber substrate

After creating a pendant drop for surface tension determination, the pendant drop volume was slightly increased, surpassing the critical volume after which necking of the droplet started due to the gravitational effect, as seen in Figure 68a. After contact with the rubber solid substrate (Figure 68b), the base diameter of the sessile drop started to increase and a thin filament started to form (Figure 68c). Then, the heated syringe was slowly pulled upwards, which caused a further thinning effect of the filament and eventually a detachment from the needle tip (Figure 68d). From this point on, dynamic contact angles were monitored of the sessile drop (Figure 68e) until an equilibrium angle was reached (Figure 68f).

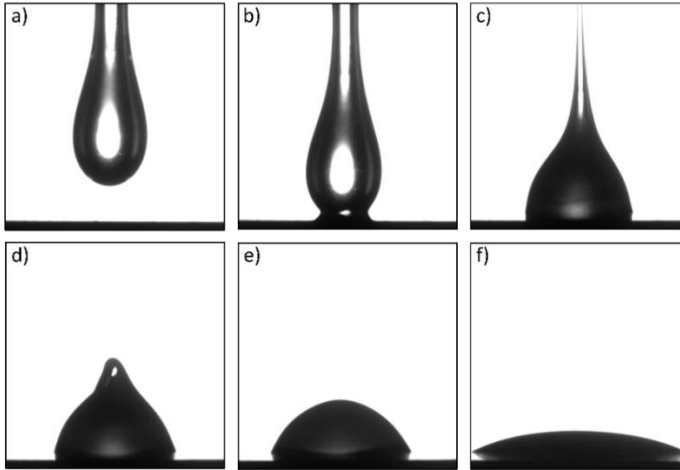


Figure 68: Deposition of PP droplet at 240°C on EPDM\_TAC3 substrate: droplet necking (a), contact between droplet and substrate (b), filament formation (c), rupture of filament (d), and droplet spreading (e) and (f).

PP droplets were deposited on five different cured rubber substrates. Four substrates were EPDM with varying composition; two of which were peroxide-based, i.e. TAC3 and TAC12, and two of which were sulphur-based, i.e. S1 and S5. Compound formulations can be found in Section 3.3.1.1 and 3.4.1. As fifth substrate, a vulcanised NBR sample (42G from Hercorub), which was sulphur-based, was selected. The average roughness values ( $R_a$ ), based on a three measurements with a Diavite Compact VHF (measuring length = 4.8 mm; cutoff = 0.8 mm), of TAC3, TAC12, S1, S5 and NBR are respectively  $0.56 \pm 0.13 \mu\text{m}$ ,  $0.69 \pm 0.15 \mu\text{m}$ ,  $0.46 \pm 0.09 \mu\text{m}$ ,  $0.50 \pm 0.06 \mu\text{m}$  and  $0.55 \pm 0.05 \mu\text{m}$ . A sessile drop fitting was done after contact with the rubber substrate. Results of successful fitting of a PP droplet in time on each substrate is given in Figure 69.

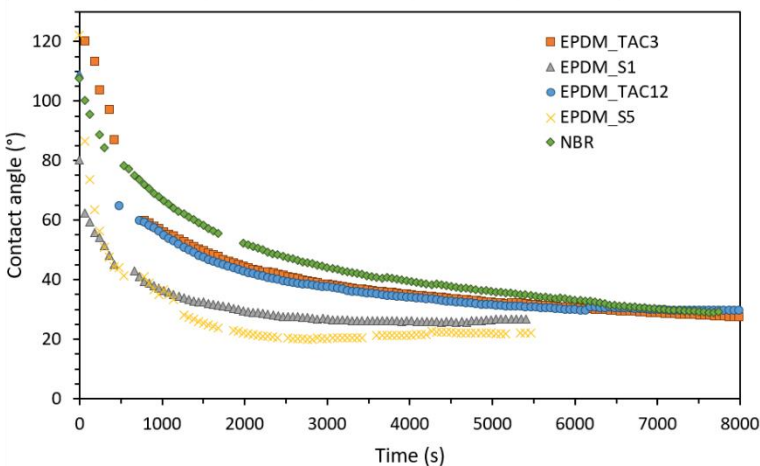


Figure 69: Contact angles of PP melt on EPDM substrates TAC3, TAC12, S1 and S5, and on an NBR substrate at 240°C.

When PP was brought in contact with sulphur-based EPDM (EPDM\_S1 and EPDM\_S5) fast spreading of the PP melt occurred as the contact angle stabilised after approximately 2500 s. However, on peroxide-based EPDM (EPDM\_TAC3 and EPDM\_TAC12) contact angle relaxation occurred much slower. Even after 8000 s, contact angles kept decreasing. Furthermore, a peculiar result was found for spreading of PP on NBR. NBR is a polar rubber and therefore limited spreading of PP was expected. However, even on NBR, PP reached low contact angles after long measuring time. Bianco et al. [142] indicated that the dynamics during spreading are initially controlled by inertia and afterwards spreading forces and viscosity dominate the dynamics. As different rubber substrates were used, differences in dynamics can be ascribed to differences in interfacial forces because a similar PP was used for all measurements, eliminating viscosity effects. DSC measurements were executed on the PP droplet after spreading on NBR to analyse possible degradation due to long exposure to high temperature, even under an inert environment, which could reduce viscosity. However, no significant differences in enthalpy of crystallisation or crystallisation temperature were found. Zhang et al. [23] also found PP to be stable during spreading measurements at high temperature on glass substrates. Thus, the droplet relaxations show that the rubber substrate does not significantly influence the equilibrium final contact angle. Only, differences in dynamic spreading were observed. Probably, the low surface tension of PP has a higher contribution to the equilibrium state than the interaction with the substrate.

A comparison was also made between wetting of PP on EPDM\_TAC3 and PE on EPDM\_TAC3. Measurements were executed at 240°C for PP and at 160°C for PE as both polymers have similar zero-shear viscosity at these temperatures. Results of spreading dynamics of PP and PE on EPDM\_TAC12 are represented in Figure 70.

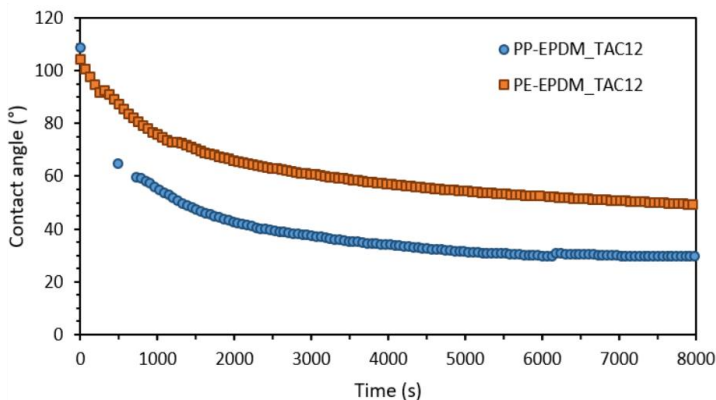


Figure 70: Contact angles of PP melt on EPDM\_TAC12 at 240°C and PE melt on EPDM\_TAC12 at 160°C.

When comparing spreading dynamics of a PE melt and a PP melt on an EPDM substrate, similar behaviours are observed. This additionally confirms that degradation of PP is limited as viscosity does not play a role when comparing results of PP and PE. However, PE remains at higher contact angles compared to PP. This was also found by Bex et al. [6] when executing direct contact angle measurements at high temperature. In contrast, an adhesion percentage of  $49 \pm 1$  % was reached for PP-EPDM\_TAC12 and

of  $64 \pm 2\%$  for PE-EPDM\_TAC12. Thus, lower contact angles do not necessarily ensure a better adhesion.

#### 5.2.4 Relation between adhesion percentage and work of adhesion

To analyse whether a correlation exists between the interface thermodynamics and the adhesion induced during 2K injection moulding, adhesion percentage was related to the work of adhesion, which was calculated according to the Young-Dupré equation (Eq. (3)). Results are shown in Figure 71.

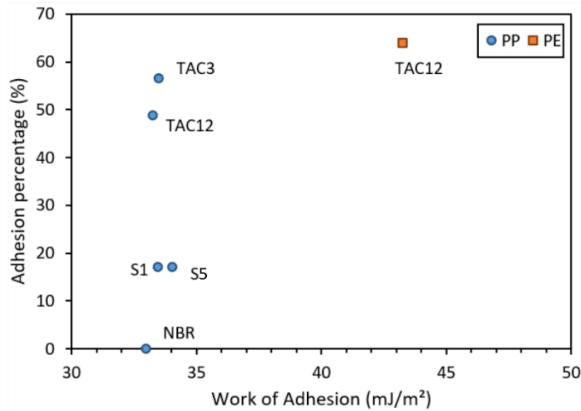


Figure 71: Adhesion percentage in function of work of adhesion ( $W_a$ ) between EPDM types TAC3, TAC12, S1 and S5 or NBR and polyolefins PP and PE.

In Figure 71, no clear correlation can be found between the adhesion percentage and work of adhesion. In terms of adhesion mechanism, based on results from previous chapters, interdiffusion is most likely between PP and sulphur-based EPDMs (S1 and S5). Between peroxide-based EPDMs and PP or PE a combination of chemical bonding and interdiffusion occurs. Between NBR and PP, no adhesion can be reached due to the differences in polarity. As no influence is found of the thermodynamic property  $W_a$ , the adhesion strength is probably dominated by adhesion mechanisms occurring after contact, i.e. interdiffusion and chemical bonding.

For PE, a higher work of adhesion was found compared to PP. Normally, higher interfacial interactions will lead to a greater work of adhesion and smaller contact angles would indicate better wetting and therefore a greater work of adhesion. However, this was not seen here. Irrespective of the higher contact angles with PE, the higher surface tension (25.50 mN/m for PE vs 17.70 mN/m for PP) seems to have a bigger influence on the work of adhesion. Thus, PE has a better interfacial interaction with EPDM. When combining this phenomenon together with the better diffusion capability due to less branched PE chains and higher efficiency of chemical bonding as no chain scission is possible, the better adhesion with peroxide-based EPDM can be clarified.

Kisslinger et al. [56] also studied the thermodynamics in multi-component injection moulding. No relation was found between surface tension ratios and the adhesion strength. Furthermore, no correlation was found between adhesion percentages and polarity ratios or work of adhesion. Therefore, Kisslinger concluded that it needs to be questioned whether wetting phenomena are responsible for adhesion in multi-

component injection moulding. More specifically, the thermodynamic theory is based on the adsorption during the initial contact. However, during multi-component injection moulding high pressures force contact between the adjoining materials and therefore possibly limit the contribution of adsorption to adhesion. Current results indicating a lack of correlation between adhesion percentage and work of adhesion for thermoset rubbers and polyolefins additionally validate this idea.

Even though wetting does not directly control the amount of adhesion, results from Chapter 3 have shown that the methodology by Bex [6] can have merit to analyse the compatibility as for PC an adhesion was induced due to an increase in co-agent concentrations. The better compatibility with high co-agent concentration in EPDM led to lower contact angles. These co-agents most likely migrate towards the EPDM-PC interface due to their higher affinity for PC which can be ascribed as well to the interdiffusion theory. Thus, when comparing wetting of one single thermoplastic on rubber substrates with different compositions, the contact angle measurement technique according to Bex et al. [6] has merit as measurements when only executed during 15 min, not reaching an equilibrium angle, which can show differences on different substrates. However, caution is still needed when interpreting results as for example high temperature contact angle measurement results from the oil and filler study (Section 4.3) did not clarify the adhesion strength result.

Overall, it is believed that a complete evaluation and combination of multiple adhesion theories is needed to give an exact correlation with the adhesion strength. Therefore, chemical bonding and interdiffusion were studied in more detail as well in the next sections.

## 5.3 Chemical bonding

### 5.3.1 EPDM-Thermoplastic co-vulcanisation: reaction mechanism

The reaction mechanism during peroxide vulcanisation of EPDM has already been extensively studied and reported [59], [71], [143]. During exposure to heat, DCP will decompose in cumyloxy radicals which in turn can rearrange to yield methyl radicals that are less sterically hindered [88], [91]. These radicals can then abstract hydrogen atoms from secondary and mainly tertiary carbons on the EPDM main chain, and the allylic hydrogen in the ENB unit, resulting in respectively alkyl and allyl macro-radicals [59]. Orza [59] provided a detailed description of peroxide crosslinking of EPDM with ENB as third monomer and based on this mechanism possible co-vulcanisation reactions between EPDM and PE, PP or ABS are proposed here. For PC, crosslinking is unlikely due to the ester oxygen.

Crosslinking unsaturated polymers, like PE and PP, can only occur through hydrogen abstraction, followed by a recombination of macro-radicals [88], [91]. However, main chain scission reactions are prone to occur in the presence of tertiary radicals, which are abundant in PP. In contrast, primary and secondary radicals are more susceptible towards combinations reactions, indicating possible successful crosslinking in PE. In ABS, styrene, butadiene, and acrylonitrile structural units are present. Thus, both hydrogen abstracting reactions and addition reactions to the double bonds are possible. Specifically, for the double bonds, addition reactions are more amendable when they are located at the end of the polymer chain or in a side chain group, while in-chain double bonds are more sterically hindered. The presence of the electron withdrawing nitrile groups in ABS

reduces the reactivity of the in-chain double bond, prevailing abstraction reactions [88]. In Figure 72, possible macro-radicals of EPDM, PE, PP and ABS are represented (ChemDraw Prime, PerkinElmer). The allyl and alkyl radicals in EPDM can form in a 1:1 ratio [88]. PE forms alkyl radicals on the  $\text{CH}_2$  positions and for PP the alkyl radical on the CH position was selected because it has the lowest bond strength (tertiary: 380 kJ/mol; secondary: 405 kJ/mol [88]). Hydrogen abstraction reactions were presumed dominant in ABS forming stable benzyl and allyl macro-radicals due to possibility of resonance stabilisation.

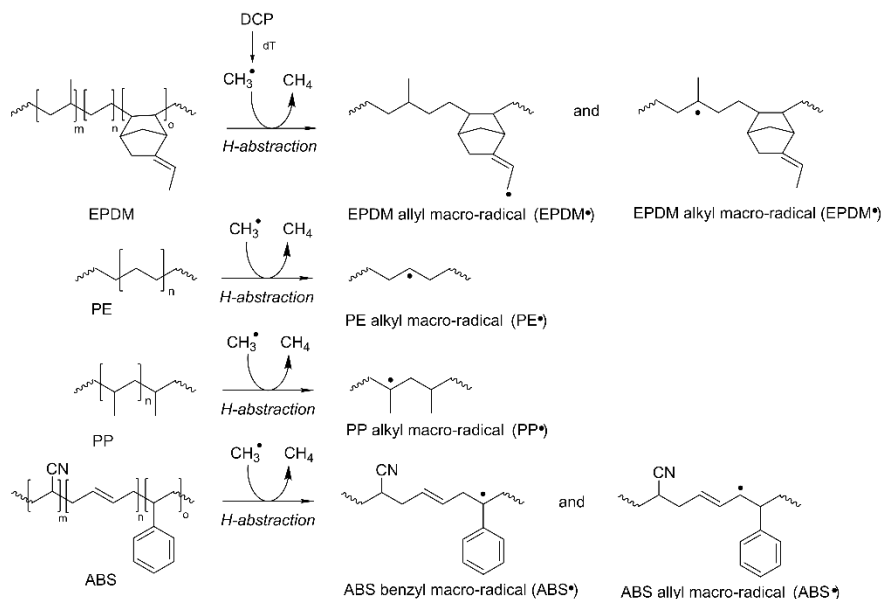


Figure 72: Hydrogen abstraction from EPDM, PE, PP and ABS chain by methyl radicals from DCP. The brackets indicate repeating units in each polymer, but these are removed in the reaction mechanism to give a clearer view.

In Figure 73, crosslinking reactions are represented that can occur between EPDM and PP, PE or ABS. Neither possible side reactions, nor the contribution of the co-agent are discussed. As Orza [59] states, EPDM yields  $\sim 25\%$  alkyl/alkyl,  $\sim 25\%$  allyl/allyl and  $\sim 50\%$  allyl/alkyl combination crosslinks. Similarly, EPDM allyl and alkyl radicals might combine with an alkyl radical from PE resulting in allyl/alkyl and alkyl/alkyl crosslink, and through an addition to the double bonds of the ENB unsaturation an alkene/alkyl crosslink may occur. For PP, it has been suggested that between a PP radical and a neighbour chain with an allyl radical crosslinking is more probable [100]. In this case, EPDM can provide the allyl radical making the allyl/alkyl crosslink most likely. However, it is important that both radicals are in close vicinity [100]. Finally, several possible carbon-carbon bonds can form between ABS and EPDM as both polymers can donate hydrogens creating stable radicals. Besides combination reactions between ABS and EPDM radicals, addition reactions to the EPDM or ABS unsaturations, followed by H-transfer might occur as well. For the addition reaction of the allyl EPDM or alkyl EPDM radical to ABS, an alkyl radical forms, due to the addition to the butadiene unsaturation. The most stable location was selected for this radical, i.e. reduced influence of electron withdrawing nitrile group.



### 5.3.2 Prediction of EPDM-thermoplastic co-vulcanisation

Regardless of the adhesion mechanisms, intimate contacts between the two polymer surfaces is a prerequisite, i.e. wetting must be ensured [21]. When a liquid wets a solid substrate, spreading usually occurs through a physical process leading to an increase of the liquid coverage area in time after droplet deposition [20]. This process is referred to as non-reactive wetting as no reaction between the liquid and substrates occurs. It has been extensively studied and reviewed in literature [16], [20], [42]. However, chemical reactions between the liquid and solid substrate can alter the solid/liquid interface and consequently the wetting process leading to reactive wetting [20], [43]. Figure 74a illustrates this reactive wetting phenomenon, while in Figure 74b the traditional wetting process based on physical interactions is represented.

During the injection of a 2K rubber/thermoplastic composite, a thermoplastic molten zone is created near the rubber/thermoplastic interface, while vulcanisation occurs in the rubber part [1], [5]. Consequently, adhesion mechanisms like chemical bonding and/or interdiffusion may be initiated. The occurrence of these mechanisms depends on the specific curing system, i.e. sulphur or peroxide curing, applied in the rubber. However, a clear characterisation of the adhesion mechanism at the interface is currently lacking. Typical techniques to evaluate chemical bonding are X-Ray Photoelectron Spectroscopy (XPS), Time-of-Flight Secondary Ion Mass Spectroscopy (ToF-SIMS), Attenuated Total Reflectance Fourier transform infrared spectroscopy (ATR-FTIR) and confocal Raman spectroscopy as they can identify chemical groups at a substrate surface [8], [18], [39]. Specifically at the interface between EPDM and PE, a co-vulcanisation reaction might lead to allyl/alkyl, alkyl/alkyl and alkene/alkyl crosslinks which are all composed of carbon-carbon (C-C) bonds [124]. As indicated by Orza et al. [59] these crosslinks are also present in EPDM, so that these techniques cannot distinguish the C-C/C-H in PE from these of EPDM and the interfacial crosslinks as both polymers contain aliphatic carbons. Therefore, an attempt was made to use contact angle measurements to characterise chemical bonding between a polymer melt and an EPDM substrate due to reactive wetting [7], [20]. Specifically, reactive wetting, i.e. simultaneous spreading and formation of covalent bonds, of a thermoplastic melt on initially unvulcanised peroxide-based EPDM is studied both from wetting and practical adhesion aspects. Wetting on peroxide-based EPDM is also compared to wetting on sulphur-based EPDM, and the influence of peroxide curing agent concentration is analysed as this can cause reactivity differences near the interface.

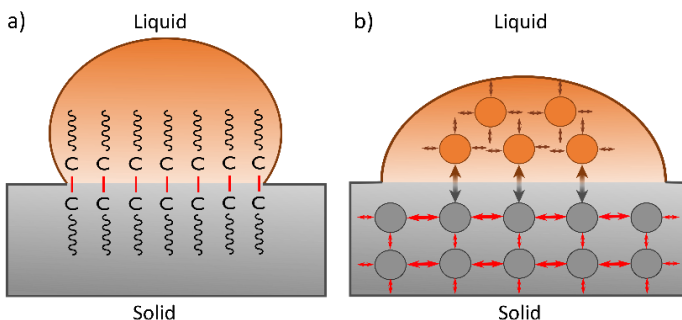


Figure 74: Reactive wetting between thermoplastic melt (liquid) and EPDM substrate (solid) (a) and thermodynamic wetting of thermoplastic melt on EPDM substrate (b).

### 5.3.2.1 Methodology

#### Materials and processing

All EPDM compounds were mixed and supplied by Hercorub NV. A peroxide-based EPDM compound was selected with DCP as curing agent. As a higher DCP concentration may cause more interfacial crosslinks [124], a comparison was made between 2 phr and 8 phr DCP with respective sample names DCP2 and DCP8. Additionally, a third compound was selected, S1, which is sulphur-based EPDM to analyse differences in spreading with peroxide-based EPDM. A detailed description of the formulations and processing conditions of EPDM compounds DCP2 and DCP8 can be found in 3.3.1.1 and of EPDM compound S1 in 3.4.1 of Chapter 3. As thermoplastic material, PE was selected to evaluate the adhesion with EPDM. Samples were produced with the 2K injection moulding process as described in 3.2.2. Unvulcanised EPDM samples were produced as well for the contact angle measurements. These were injected in the rubber cavity with the EPDM injection moulding parameters (Table 4). However, the mould cavities were set at 80°C to prevent vulcanisation. Consequently, both vulcanised and unvulcanised EPDM substrates had similar sample dimensions.

The average roughness values ( $R_a$ ) of the vulcanised rubber substrates, based on three measurements with a Diavite Compact VHF (measuring length = 4.8 mm; cutoff = 0.8 mm), were  $0.47 \pm 0.04 \mu\text{m}$  for DCP2,  $0.48 \pm 0.08 \mu\text{m}$  for DCP8 and  $0.46 \pm 0.08 \mu\text{m}$  for S1; for the unvulcanised rubber substrates the  $R_a$  values were  $0.66 \pm 0.09 \mu\text{m}$  for DCP2,  $0.83 \pm 0.16 \mu\text{m}$  for DCP8 and  $2.05 \pm 0.16 \mu\text{m}$  for S1. The roughness measurements were executed before starting the wetting experiments.

#### Wetting methodology

For the wetting experiments, a high temperature contact angle measurement device from Dataphysics (OCA 15 plus) was used. In Figure 24 (Chapter 3), the experimental setup of this device is schematically represented. The electrical heating within the chamber is controlled by a Dataphysics TEC 350 temperature control unit which enables a chamber temperature between 40°C and 350°C. The temperature within chamber, right above the PE granule, was measured and controlled with a thermocouple. During measurement, the temperature ( $T_H$ ) above the granule had a maximum deviation of  $T_H \pm 2 \text{ }^\circ\text{C}$ . Measurements were carried out under an inert atmosphere (Nitrogen gas  $\geq 99.999 \%$ , ALPHAGAZTM 1, Air Liquide) to prevent oxidative degradation of the polymers. A CCD camera was used with a resolution of 768 x 576 pixels and a frame rate of 30 frames per seconds. Furthermore, contact angles between the PE melt and EPDM substrate were calculated with Dataphysics SCA 202 analysis software. Before starting the measurements, the heated chamber was stabilised under nitrogen flow for 5 minutes. The surface of the EPDM substrate was cleaned carefully with isopropanol (99.5 %, Sigma-Aldrich) using a tissue. No differences in substrate's surface roughness  $R_a$  were measured before and after cleaning with isopropanol.

First, the vulcanisation process of the unvulcanised EPDM substrates (DCP2, DCP8 and S1) was evaluated directly in the heated chamber. Without applying pressure, bubbles may form at the surface due to released gasses, resulting from the curing decomposition products [88], and modify the topography of the surface. It is however important to select a suitable temperature which preserves a smooth substrate surface. Unvulcanised EPDM substrates (10 mm x 10 mm x 2 mm) were then exposed to 140°C, 150°C, 160°C and 170°C. At each temperature, samples were evaluated after 5, 10, 15, 20, 25 and 30 min to

analyse the substrate surface (Keyence VHX-500F digital microscope). Furthermore, vulcanisation needed to be ensured at the selected temperature. Therefore, vulcanisation degree after 30 min was assessed by Shore A hardness measurements (CV Shore A hardness durometer) according to Eq. (24) and an additional verification of the vulcanisation behaviour was executed with a moving die rheometer (MDR2000E, Monsanto).

Then, the wetting behaviours of PE on vulcanised and unvulcanised DCP2, DCP8 and S1 were compared. The vulcanised EPDM substrates were taken from EPDM bulk vulcanised at 180°C, ensuring complete vulcanisation. The EPDM substrate (10 mm x 10 mm x 2 mm) was placed in the heated chamber and immediately afterwards, the PE granule was placed on top of it with the spherical side facing down (average PE weight at  $T=25^{\circ}\text{C}$ :  $11.6 \pm 0.7$  mg), see Figure 24 (Chapter 3). Consequently, the interaction between the melting/molten PE on vulcanising EPDM from the initial start of curing could be evaluated. Contact angles were registered every minute during 30 min. The evolution from solid to molten stage lasted 3 min. From then on, contact angles could be calculated through an ellipse fitting. Figure 75 shows a fitting of a PE droplet on vulcanised and unvulcanised DCP8 after 5 min and after 30 min. Three measurements were performed for each combination of PE with EPDM and average values with their 95 % confidence intervals are reported.

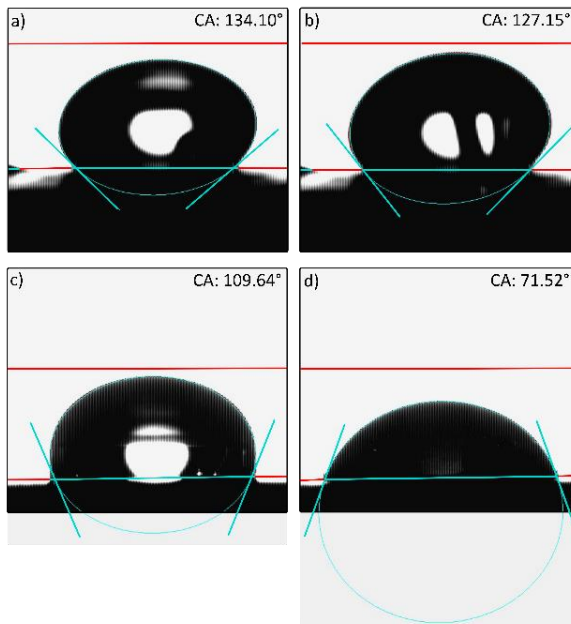


Figure 75: Ellipse fitting of PE droplets on an unvulcanised DCP8 substrate after 5 min (a), after 30 min (b) and on a vulcanised DCP8 substrate after 3 min (c), after 30 min (d). The baseline represents the contact between the PE droplet and EPDM substrate which is slightly higher than the EPDM substrate surface (in c and d) due to a reflection of the droplet on the surface.

## 5.3.2.2 Results and discussion

**Behaviour of unvulcanised EPDM substrate in a heated chamber**

First, it was necessary to identify the best trade-off temperature that ensures a stable substrate surface (no gas bubbles), vulcanisation of initially unvulcanised EPDM, and melting of PE. At 140°C, no bubbles occurred at the substrates' surfaces after 30 min. At 150°C, formation of bubbles still remained insignificant during 30 min (Figure 76a). However, at 160°C and 170°C gas bubbles started to appear even after 5 min inducing a change of the surface topography as illustrated by Figure 76b and Figure 76c. Figure 76d represents a 3D view of one of the largest detected bubbles (height of 190 μm). On DCP2 small bubbles appeared on the complete sample surface while S1 and DCP8 had less but larger bubbles at 160°C. This change in topography would influence the dynamic process of spreading of the thermoplastic melt during contact angle measurements. Therefore, a measuring temperature of 150°C was selected.

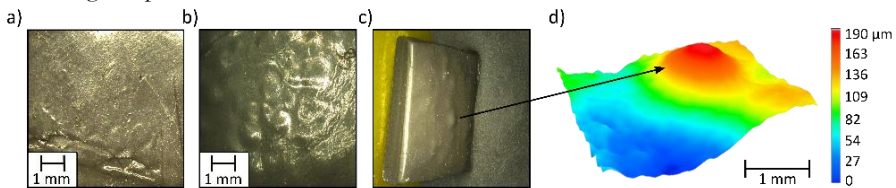


Figure 76: Microscopic images of DCP2 substrate surface after 30 min at (a) 150°C, (b) 160°C and of DCP 8 at (c) 160°C. In (c) the image represents a side view of the complete DCP8 substrate (10 x 10 x 2 mm) to illustrate the surface topography. (d) 3D image of a gas bubble from the DCP8 substrate.

In parallel, the vulcanisation degree was analysed after 30 min at 150°C using the moving die rheometer and vulcanisation degrees of 68 % , 77 % , and 97 % for respectively DCP2, DCP8, and S1 were obtained (Figure 77). For the substrates vulcanised in the heated chamber during 30 min, based on hardness measurements, slightly lower vulcanisation degrees of 58 % for DCP2, 73 % for DCP8 and 83 % for S1 were reached. Thus, in spite of the absence of pressure in the heated chamber, vulcanisation will occur simultaneously with spreading of the thermoplastic melt during contact angle measurements. Then, contact angle measurements were executed at 150°C with PE melts on vulcanised and unvulcanised substrates of DCP2, DCP8 and S1.

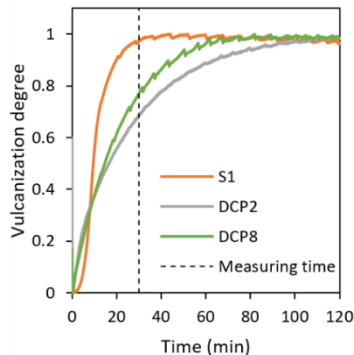


Figure 77: Vulcanisation degree in function of time for S1, DCP2 and DCP8. The dashed line indicates the measuring time of 30 min of the contact angle measurements.

### Influence of vulcanisation on wetting

Figure 78 shows melting and spreading of a PE granule on vulcanised and unvulcanised DCP2 (a) and DCP8 (b). The corresponding contact angles are represented in Figure 80. After 3 min, a PE droplet was created and contact angles could be calculated. The initially unvulcanised substrates DCP2, DCP8 and S1 tended to increase in thickness (respectively with 23 %, 7 % and 11 %) during vulcanisation. This increase in thickness did not restrict the spreading process on the peroxide-based substrates DCP2 and DCP8 or on the sulphur-based substrate S1 as can be seen in Figure 78 and Figure 79 when comparing the droplet at 1 min with the droplet at 5 min which corresponds to a decrease in contact angles as shown in Figure 80. When comparing images in Figure 78 and the spreading dynamics in Figure 80, a clear difference can be seen between vulcanised and unvulcanised peroxide-based EPDM substrates. While a significant contact angle relaxation process occurs on vulcanised DCP2 and DCP8, spreading on the unvulcanised substrates is restricted. Here, spreading is not dominated anymore by a physical process but by chemical bonding, in particular the formation of C-C bonds between EPDM and PE. Such bonds tend to retain the shape of the PE droplet as they originate from a co-vulcanisation reaction caused by combination of allyl or alkyl EPDM radicals with alkyl PE radicals, or from addition of EPDM with alkyl PE radicals. Contact angles on unvulcanised DCP2 do not significantly change anymore after 11 min ( $112 \pm 2^\circ$  at  $t=30$  min) because enough C-C bonds were formed preventing further spreading. In contrast, on vulcanised DCP2 contact angles continuously decrease in time ( $71.9 \pm 0.7^\circ$  at  $t=30$  min). Furthermore, on unvulcanised DCP8, PE is retained even more ( $130 \pm 2^\circ$  at  $t=30$  min) with a stabilisation after 6 min, while spreading on vulcanised DCP8 is similar to DCP2, evidencing that adding 2 or 8 phr DCP does not change compatibility with PE.

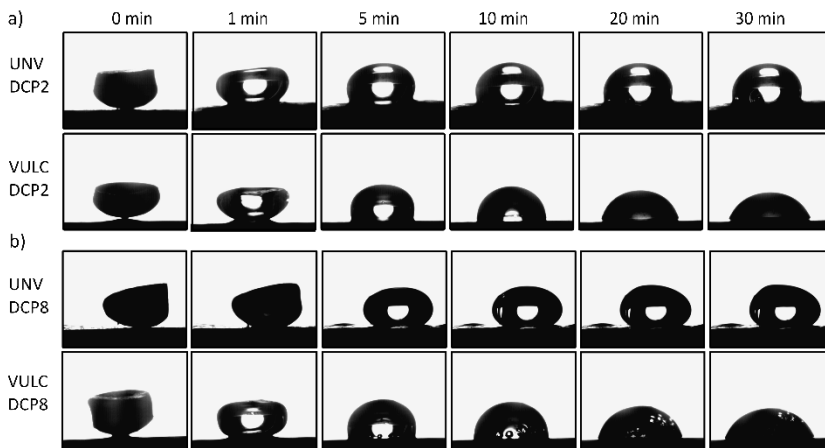


Figure 78: Spreading of PE granule on DCP2 (a) and DCP8 (b) at  $150^\circ\text{C}$ . At 0 min the PE granule is in solid state. 'UNV' refers to unvulcanised and 'VULC' refers to vulcanised.

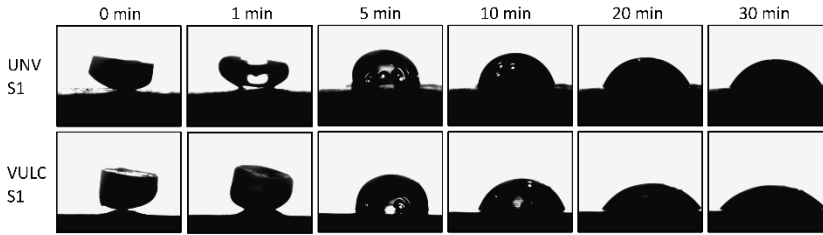


Figure 79: Spreading of PE granule on S1 at 150°C. At 0 min the PE granule is in solid state. 'UNV' refers to unvulcanised and 'VULC' refers to vulcanised.

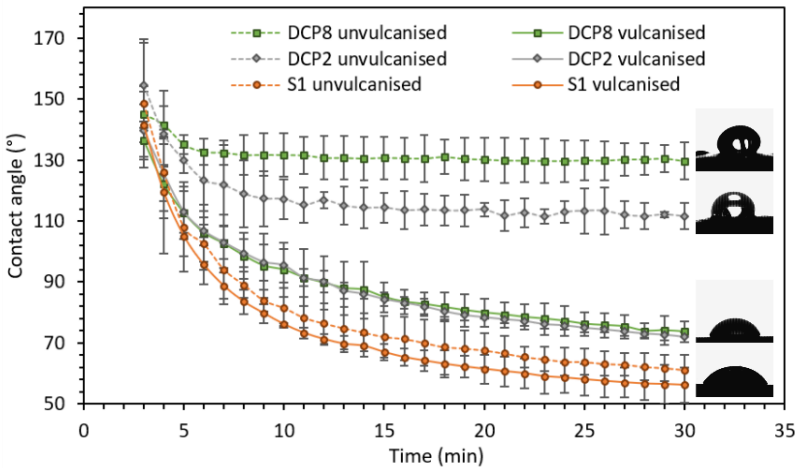


Figure 80: Contact angle measurements of PE melt (150°C) on DCP2, DCP8 and S1. Error bars represent 95 % confidence interval.

The limitation in spreading on unvulcanised DCP substrates cannot be attributed to a polarity increase at the surface as no increase in chemical functional groups at the surface were found when comparing ATR-FTIR spectra of unvulcanised with vulcanised DCP in Figure 81.

The reactive wetting results with a retained PE melt contradict findings by Grundke et al. [7], where an interfacial chemical reaction between the amino groups of poly(aminosiloxane) and the copolymer's maleic anhydride groups improved wetting at 130°C. It is surmised that the spreading of the PE melt in the current study is restricted due to the uniqueness of the material combination as the PE chains at the interface become part of the three-dimensional rubber network during vulcanisation [88]. The findings from this reactive wetting study were confirmed by the adhesion strength between EPDM and PE as already presented in section 3.3 of Chapter 3. Between DCP2 and PE an adhesion strength of  $2.01 \pm 0.06$  MPa was reached. DCP8 with PE even lead to  $4.28 \pm 0.13$  MPa. Comparing these adhesion strengths to the total strength of each rubber ( $4.47 \pm 0.05$  MPa for DCP2;  $7.59 \pm 0.06$  MPa for DCP8) shows an adhesion percentage of 45 % for DCP 2 and 57 % for DCP8. The higher adhesion percentage of EPDM-PE at 8 phr DCP was attributed to an increase in chemical bonding or formation of more carbon-carbon bonds between EPDM and PE. Thus, the higher contact angle

found on DCP8 during reactive wetting corresponds to more chemical bonding which leads to a higher adhesion percentage as well.

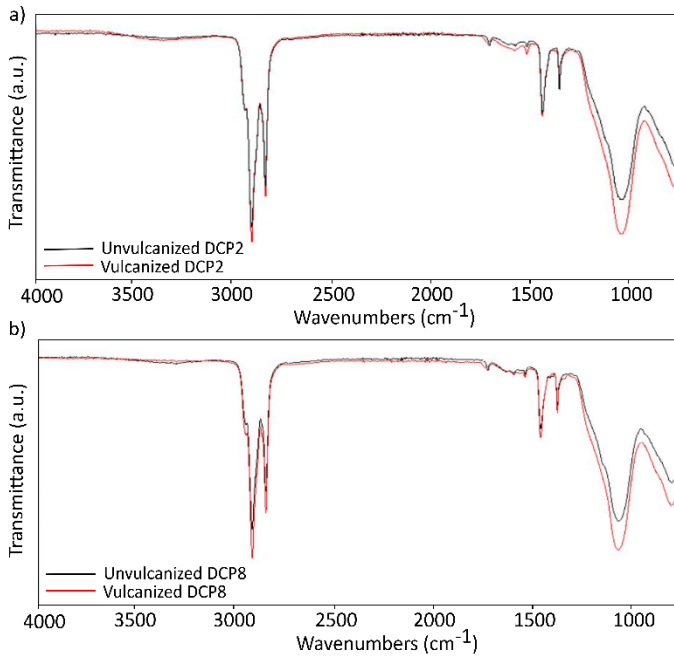


Figure 81: ATR-FTIR spectra of vulcanised and unvulcanised DCP2 (a) and DCP8 (b).

To confirm that the differences between vulcanised and unvulcanised peroxide-based EPDM can be attributed to chemical bonding, measurements were also executed on sulphur-based EPDM substrates (S1). Interestingly, Figure 79 and Figure 80 show that good wetting occurs on both unvulcanised and vulcanised S1, with contact angles after 30 min that do not differ significantly (respectively  $61 \pm 2^\circ$  and  $56 \pm 3^\circ$  at  $t=30$  min). As expected, co-vulcanisation between sulphur-curing EPDM and PE is impossible due to the absence of unsaturations in PE, and thus spreading of PE is related to a physical process. The difference in roughness  $R_a$  between vulcanised and initially unvulcanised S1 also does not seem to affect spreading as contact angles are not significantly different. Furthermore, Chen et al. [144] proposed a deformation of a soft substrate due to formation of a wetting ridge at the contact line, limiting spreading. However, Shore A hardness of unvulcanised S1 was lowest (DCP2: 17.5 Sh A; DCP8: 21.7 Sh A; S1: 14.9 Sh A) making it the softest substrates, and here no limitation in spreading was observed. Thus, wetting measurements were not affected by ridge formation. The higher cure rate of S1 (Figure 77) can also not be responsible for the different wetting behaviour as the spreading of DCP8 was already restricted after 6 min which corresponds to a vulcanisation degree of 25 % according to Figure 77. During the initial phase of curing, i.e. 0 to 30 %, S1 does not show a faster cure rate than DCP2 and DCP8.

### 5.3.2.3 Reactive wetting: influence of ethylene content in EPDM on chemical bonding with PE

To confirm the reactive wetting phenomenon, additional measurements were executed on samples from the study focussing on the influence of EPDM macromolecular structure (Section 4.2). In this study, the influence of ethylene content, Mooney viscosity and diene content on the adhesion with PP was investigated. Additionally, the rubber formulations of the different samples were equal except for the curing system and the EPDM macromolecular structure. For the ethylene content, differences in adhesion percentage were ascribed to differences in compatibility with PP, with a lower ethylene content leading to a better adhesion. For PE, contrary to PP, a high ethylene content in EPDM could improve compatibility. Changes in chemical bonding are not expected.

To analyse whether ethylene content does not affect chemical bonding with PE, the reactive wetting methodology was used. As additional confirmation, a comparison between sulphur-based samples (S) and peroxide-based (P) samples was made. Samples were taken with a low ethylene content (50 wt%, P4570 and S4570) and a high ethylene content (70 wt%, P4770 and S4770). Details of these compositions can be found in Table 14 in section 4.2.1.2.

No significant differences in surface roughness between vulcanised and unvulcanised substrates were observed. Furthermore, the surface topography of each unvulcanised substrate in the heated chamber at 150°C was evaluated and stable conditions together with a curing reaction were assured. Then, contact angle relaxation of a PE melt on each EPDM substrate was investigated. Results are represented in Figure 82.

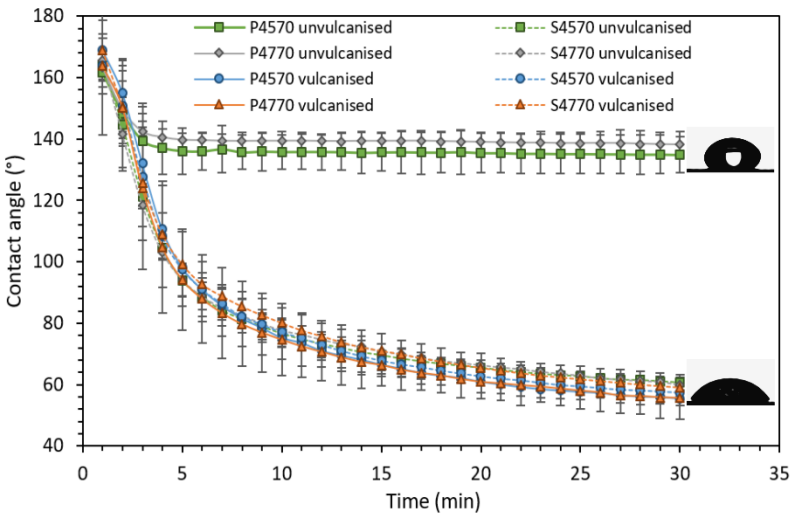


Figure 82: Contact angle measurements of PE melt (150°C) on vulcanising and vulcanised EPDM with 50 wt% ethylene content (4570) and 70 wt% ethylene content (4770). EPDM was sulphur-based (S) or peroxide-based (P). Error bars represent 95 % confidence intervals.

Figure 82 confirms that the differences in dynamic wetting of PE on EPDM can solely be ascribed to the influence of the rubber curing reaction. For example, unvulcanised EPDM with 50 wt% ethylene content and peroxide curing system (P4570)

show a clear restriction in wetting after 5 min. The contact angle is retained and no significant further decrease in contact angles is measured, causing a stable contact angle after 30 min of  $135 \pm 2^\circ$ . In contrast, on vulcanised P4570 a continuous spreading process occurs to low contact angles after 30 min ( $56 \pm 1^\circ$ ). This major difference in contact angle relaxation between vulcanised and unvulcanised samples was not found for sulphur-based samples. On sulphur-based substrates solely physical wetting was observed. Thus, the peroxide curing reaction caused a co-vulcanisation at the interface of PE with EPDM during wetting. These results confirm the reactive wetting phenomenon from the previous section, when selecting the right measuring conditions, as a tool to predict chemical bonding at a rubber-thermoplastic interface.

When comparing results of EPDM with a low (50 wt%) and a high (70 wt%) ethylene content, i.e. P4570 and P4770 unvulcanised, no significant differences are observed in spreading dynamics or final stable contact angle. This could confirm that, at an EPDM-PE interface, chemical bonding is not significantly controlled by the ethylene content. Then, differences in adhesion strength could be ascribed to the differences in compatibility/solubility. This confirms findings from the study of the influence of ethylene content in EPDM on the adhesion with PP, i.e. better adhesion with EPDM containing high propylene content due to improved compatibility.

## 5.4 Interdiffusion

### 5.4.1 Rubber-thermoplastic immersion in cyclohexane

Due to the difficulty of correctly analysing the interface between polymers with a similar molecular composition, alternative methods were sought after. Ruch et al. [29] studied the adhesion in EPDM joints. In this study, the influence of interdiffusion on the interfacial co-vulcanisation was analysed. Two partially crosslinked EPDM sheets were brought into contact during various periods of time at room temperature. After the contact period, the samples were irradiated to create additional crosslinks. Afterwards, the samples were immersed in cyclohexane, causing the rubber to swell, and samples with short contact times showed spontaneous separation. In contrast, samples with long contact times did not show any separation. It was concluded that the efficiency of the crosslinking reaction at the interface is dependent on the interpenetration depth. Thus, interdiffusion needs to be assured.

When combining EPDM with PP, both interdiffusion and co-vulcanisation can occur when using a peroxide curing system. For the co-vulcanisation it is believed, similar to findings from Ruch et al. [29], that interdiffusion needs to proceed to cause a subsequent efficient co-vulcanisation. When applying a sulphur curing only interdiffusion is possible. Therefore, solvent immersion experiments were executed. When no/limited interdiffusion occurs, a separation of EPDM from PP is expected. A comparison is made between peroxide-based EPDM with PP and sulphur-based EPDM with PP.

#### 5.4.1.1 Materials and methods

Two samples were taken from the study on the influence of EPDM macromolecular structure in Chapter 4 Section 4.2. This study showed that an optimal adhesion was reached for samples containing low ethylene content and low Mooney viscosity for both

peroxide and sulphur cured samples, i.e. P4520 and S4520. Thus, PP-P4520 and PP-S4520 were used for immersion tests.

Samples with dimensions  $2 \times 2 \times 10 \text{ mm}^3$  were cut at the interface from 2K products (Figure 23). Then, these 2K samples were immersed in 70 ml cyclohexane during 8 weeks. After 8 weeks, the immersed samples were removed from the solvent, excessive solvent was removed with filter paper and samples were weighed ( $m_{\max}$ ). Then, the samples were dried in an oven at  $60^\circ\text{C}$  for 24 h to remove all the solvent and finally reweighed ( $m_0$ ). A percentage of mass swelling was calculated according to Eq. (29):

$$\text{Mass swell (\%)} = \frac{m_{\max} - m_0}{m_0} \cdot 100 \quad (29)$$

#### 5.4.1.2 Results and discussion

The EPDM-PP samples were immersed during a period of 8 weeks. Neither PP-P4520 nor PP-S4520 showed a separation at the interface. A clear swelling of the EPDM part was visible. However, this did not diminish the adhesion. Furthermore, the fact that EPDM has swollen and the interface remains intact suggests sufficient interdiffusion together with accompanying entanglements preventing a phase separation. In Table 26, the mass swell is listed, indicating a clear swelling process due to immersion in cyclohexane.

Table 26: Mass swell percentage of PP-P4520 and PP-S4520 after immersion in cyclohexane.

	PP-P4520	PP-S4520
Mass swell (%)	118	95

After removal from the solvent, the samples were dried and re-analysed. An intriguing phenomenon was observed on the dried samples which is shown in Figure 83.

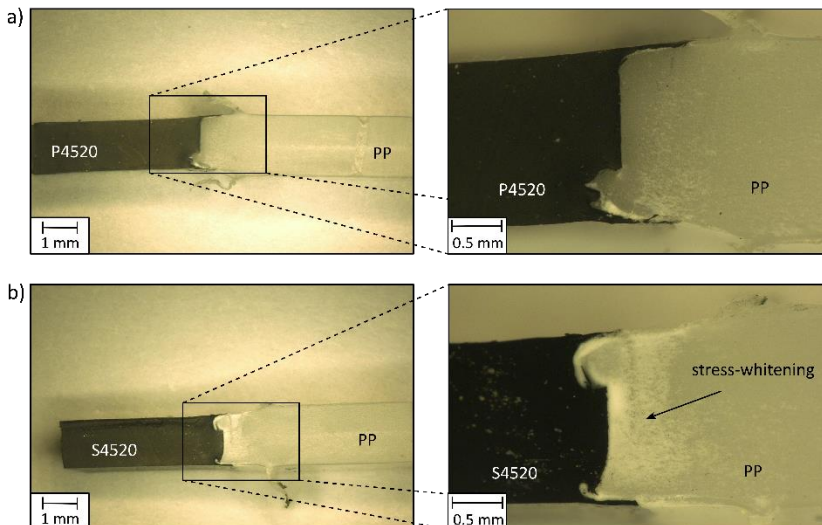


Figure 83: Microscopic images of EPDM-PP samples after swelling in cyclohexane and drying: PP-P4520 (a) and PP-S4520 (b).

In Figure 83b, sulphur-based EPDM (S4520) with PP, residual stresses or stress whitening in the PP part is observed. However, in Figure 83a, peroxide-based EPDM (P4520) with PP, this was not seen. Thus, residual stresses arise in the PP part upon removal of the solvent from PP-S4520. The adhesion in this samples is created by interdiffusion during the 2K injection moulding process. The residual stresses could be caused by a mismatch in deformation of the EPDM and PP part. After swelling, a volumetric change occurs and the polymer deforms due to the removal of the solvent. For thermoplastic composites, e.g. fibre reinforced thermoplastics, literature indicates several parameters causing residual stresses: temperature difference, shrinkage, elastic coefficients, fibre volume fractions. Furthermore, these parameters in turn depend on matrix morphology, type of fibre, fibre-matrix interface, fibre morphology, and processing conditions [145]. Similarly here, at the interface there is a contact between two dissimilar polymers which differ in morphology and elastic properties. From the swelling measurements it appears that limited stresses are present in PP near the interface when both interdiffusion and co-vulcanisation occurs (Figure 83a), while solely interdiffusion as adhesion mechanism induces residual stresses in PP near the interface (Figure 83b). Due to the chemical bonding between PP and P4520, a stress transfer might occur at the interface towards the EPDM phase during shrinkage, i.e. upon removal of the solvent. In PP-S4520, it appears that these interfacial shear stresses cannot be transferred. PP and S4520 have different viscoelastic properties and mainly the EPDM part will shrink as the crosslinks within the EPDM enable swelling when immersed in cyclohexane. The solvent elimination could cause chain slippage in the interdiffusion region creating cracks and crazes within PP, i.e. stress corrosion cracking. However, a more detailed study would be required to analyse the stress distribution at the interface. Possibly, the immersion test could additionally be used for thermoplastic-thermoset rubber samples to distinguish the adhesion mechanisms.

### 5.4.2 Material interaction

As indicated in the state of the art (Chapter 2), the interaction between mixing polymers can be described by the Flory-Huggins interaction parameter  $\chi_{AB}$ . This interaction parameter is dimensionless, temperature dependent, and can be calculated according to Eq. (15). This Eq. (15) does not allow a negative outcome. Literature states that to have mutual miscibility  $\chi_{AB}$  needs to reach low values, i.e. below 0.00277 for polymers and below 2.77 for low molecular weight materials [4], [13], [25]. The value of the interaction parameter can indicate the extent of interdiffusion, with smaller  $\chi_{AB}$  resulting in a higher interdiffusion probability.

#### 5.4.2.1 Methodology

For Eq. (15), three-dimensional solubility parameters needs to be known for a given molecule. Therefore, the group contribution procedure by Hoy is used [25], [26]. These group contributions can be consulted in 'Polymer Handbook' by Brandrup et al. [26]. Based on these group contributions, the solubility parameter ( $\delta$ ), the molecular aggregation number  $a$  and the number of repeating units per polymer chain segment  $n$  can be calculated according to Eq. (30, 31, and 32). For low molecular weight components  $n$  is equal to 1.

$$\delta = \frac{F_t + \frac{B}{n}}{v_m} \quad (30)$$

$$a^a = \frac{777 \Delta_T}{v_m} \quad \text{or } \log a^b = 3.39 \left( \frac{T_b}{T_{cr}} \right) - 0.1585 - \log v_m \quad (31)$$

$$\text{with } \left( \frac{T_b}{T_{cr}} \right) = 0.567 + \Delta_T - \Delta_T^2$$

$$n = \frac{0.5}{\Delta_T} \quad (32)$$

where  $F_t$  is a molar attraction function,  $\Delta_T$  is the Lydersen correction for polymer non-ideality, B is a dimensionless constant equal to 277, and  $v_m$  is the molar volume.  $T_b$  is the boiling temperature and  $T_{cr}$  is the critical temperature. Based on these parameters, the polar, disperse and hydrogen solubility parameters can be calculated. In Eq. (33),  $F_p$  is the polar component of the molar attraction function and this is used to calculate the polar solubility parameter. The hydrogen solubility parameter and the disperse solubility parameter can be determined with respectively Eq. (34) and Eq. (35):

$$\delta_p = \delta \left( \frac{1}{a} \frac{F_p}{F_t + B/n} \right)^{1/2} \quad (33)$$

$$\delta_h = \delta \left( \frac{a-1}{a} \right)^{1/2} \quad (34)$$

$$\delta_d = (\delta^2 - \delta_p^2 - \delta_h^2)^{1/2} \quad (35)$$

Finally, polymer miscibility can be studied with the Flory-Huggins  $\chi$  parameter (Eq. (15)) as already discussed in Chapter 2 Section 2.2.1.4.

#### 5.4.2.2 Results and discussion

When examining the interaction parameters, material compatibility can be evaluated. In the rubber formulation several components are present like co-agents and a curing agent. In Chapter 3, the influence of co-agents TAC and TMPT, and curing agent DCP was studied. During injection moulding these components may segregate and migrate to the surface due to an incompatibility with EPDM. This can enhance the adhesion mechanism at the interface, i.e. chemical bonding and interdiffusion, with a certain thermoplastic. Therefore, the interaction parameter is determined between TAC, TMPT and DCP and polymers EPDM, PP, PE, ABS and PC. A higher interaction parameter with EPDM can indicate a migration to the surface during injection moulding. TAC, TMPT and DCP are low molecular weight components. Stenert [146] indicates that low molecular weight components have very low solubility at an interaction parameter above 2.77. In Table 27, the interaction parameters are listed.

---

<sup>a</sup> For polymers

<sup>b</sup> For low molecular weight components

Table 27: Interaction parameter at room temperature for co-agents TAC and TMPT, and curing agent DCP with polymers EPDM, PP, PE, ABS and PC.

$\chi$	PP	PE	EPDM	ABS	PC
TAC	6.518	5.324	11.546	4.854	1.888
TMPT	8.020	6.853	11.147	0.294	1.063
DCP	8.083	6.891	11.221	0.249	1.003

Within EPDM, low solubility is found for TAC, TMPT and DCP. When comparing the interaction parameters with all thermoplastics, a better solubility is reached in all thermoplastics compared to EPDM. Thus, during injection moulding TAC, TMPT and DCP might segregate and migrate to the surface. Furthermore, the better interaction between TMPT, TAC or DCP and thermoplastics PP, PE, ABS or PC emphasises that these components are likely to be present at the interface. In case of PP and PE, DCP at the interface can promote co-vulcanisation and the presence of co-agents can increase the efficiency of chemical bonding. Especially for PP this is important to reduce chain scission. Compared to PP and PE, polar thermoplastic ABS and PC have lower  $\chi$  with TAC, TMPT, and DCP. These low molecular weight components have a higher affinity with ABS and PC due to their polar character. This might improve chemical bonding or cause an interphase region with a higher concentration of curing components promoting a certain diffusion between EPDM and the polar thermoplastic.

For EPDM-ABS, both co-agents TAC and TMPT, and curing agent DCP have a better solubility in ABS than in EPDM. TMPT and DCP even have an interaction parameter below 2.77. This can promote both interdiffusion and chemical bonding. Between PC and EPDM, only interdiffusion is likely and an enrichment of DCP and TMPT or TAC can enhance the compatibility ( $\chi < 2.77$ ). However, the interaction parameter of TMPT-PC seems to be lower than TAC-PC. The better solubility of TMPT in PC is probably caused by a better similarity in molecular structure and polarity. Contact angle measurements results from Figure 30 in Chapter 3 showed slightly lower angles between PC and EPDM with TMPT, but a better adhesion percentage was reached with TAC-based EPDM. Thus, the interaction parameter, based on the group contribution method indicates possible migration to the interface, but it does not clarify the better interdiffusion with higher TAC concentrations. Furthermore, caution is needed upon interpreting the results as all values are determined at room temperature, while injection moulding is done at a high temperature.

Besides components within the rubber, interaction parameters between rubbers, i.e. EPDM and NBR, and thermoplastics, i.e. PP, PE, ABS and PC, were determined. As miscibility between two polymers is studied, the interaction parameter needs to be below 0.00277 according to Stenert [146] to create mutual solubility.

Table 28: Interaction parameter at room temperature between thermoset rubbers and thermoplastics.

$\chi$	PP	PE	ABS	PC
EPDM	0.466	0.365	8.906	12.256
NBR	6.392	5.317	0.201	0.411

According to Table 28, EPDM has the lowest interaction parameter with PE. Thus, between EPDM and PE interdiffusion is most likely. However, none of the material combinations are miscible ( $\chi > 0.00277$ ). Injection moulded samples also showed better adhesion between EPDM and PE when using a sulphur curing system, i.e. solely interdiffusion as adhesion mechanism. Furthermore, the lower interaction parameter with PE compared to PP confirms findings from the contact angle measurement methodology in Section 5.2. There, a higher work of adhesion was found between PE and EPDM compared to PP and EPDM due to the higher surface tension of PE. Furthermore, contact angle measurements with PP were performed as well on NBR in Section 5.2. Results indicated spreading of PP to low angles on NBR at high temperature. However, no adhesion was reached during injection moulding. The interaction parameter in Table 28 shows a high value, i.e. insolubility, between NBR and PP which further confirms the idea of the low surface tension of PP having a higher contribution to the equilibrium state than the interaction with the substrate NBR during contact angle measurements.

### 5.4.3 SEM-EDX

As a first interdiffusion characterisation technique, SEM-EDX was used to define the interdiffusion width between EPDM and PE. This material combination provides a high adhesion strength when applying a sulphur curing system while no chemical reactions are possible, indicating the dominance of interdiffusion. During SEM-EDX analysis, chemical composition can be analysed. C-atoms are present in both PE and EPDM, therefore the focus was put on sulphur by tracking possible sulphur migration across the interface.

#### 5.4.3.1 Methodology

A Nova 600 NanoLab (FEI) equipped with an EDAX (Energy dispersive x-ray detector with an ultra-thin window) was used for SEM-EDX measurements. It was operated under high vacuum which required coating the polymer sample to make the samples conductive. Specifically, 5 nm Platinum-Paladium coating was applied. An elemental composition analysis was executed in the interface region. This EDX analysis was performed with an accelerating voltage of 15 kV. The interface region was mapped and line scans were taken perpendicular to the interface. The distance between each scan point was 0.3  $\mu\text{m}$ .

Measurements were performed on S1-PE. A detailed description of S1 can be found in Section 3.4.1 of Chapter 3. In S1-PE following chemical elements are present: S, C, N, O, P, Ca, Si, and Zn. However, the most important feature is the sulphur curing system. Thus, S1-PE adhesion is created by interdiffusion. Samples were prepared for SEM-EDX

by cryogenically (Liquid Nitrogen) cutting perpendicular to the interface to prevent smearing of EPDM at the interface. By performing line scans across the interface, the amount of sulphur can be tracked. This might enable defining the interdiffusion width.

#### 5.4.3.2 Results and discussion

SEM-EDX measurements were performed on a EPDM-PE sample. In Figure 84a, The interface is imaged using backscattered electrons (BSE) detection mode. This enables analysing the surface topography and chemical composition as the intensity of BSEs are proportional to the mean atomic number of the components [147]. Two different regions can be distinguished, i.e. EPDM and PE, and between these two regions a sharp interface is visible. Furthermore, in Figure 84b-h elemental mappings are represented and a higher intensity corresponds to a higher concentration of the element. S is present in EPDM due to its contribution to the curing reaction. In Figure 84f, a higher intensity of S is visible near the interface in the EPDM region, while the intensity of C is lower. Therefore, a line scan across the interface was taken of S and C. S is studied relative to C because, as Enganati et al. [147] indicated as well, discrepancies due to an unevenness in surface need to be taken into account.

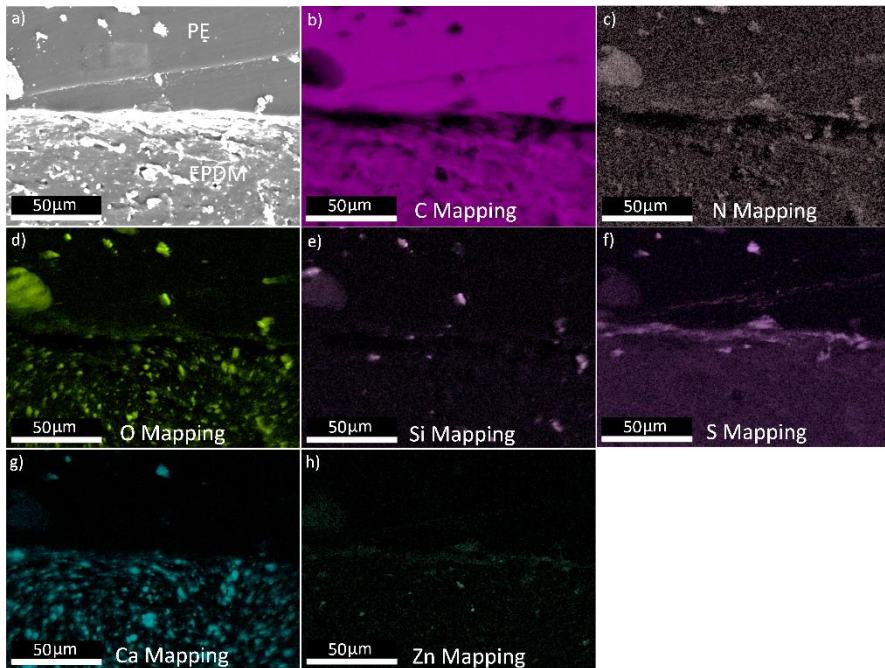


Figure 84: SEM imaging of EPDM-PE interface region in BSE mode (a), and corresponding EDX elemental mapping of carbon (b), nitrogen (c), oxygen (d), silicon (e), sulphur (f), calcium (g), and zinc (h).

In Figure 85, the relative sulphur amount ( $S/C$ ) is represented going from PE to EPDM. The distance registered during the line scan is  $25 \mu\text{m}$ . A higher relative sulphur amount was found near the interface with a gradual decrease from EPDM to PE. This higher

relative S amount was already indicated in Figure 84f. Specifically, from 11  $\mu\text{m}$  to 20  $\mu\text{m}$  the mean relative S amount is 0.039, while in the EPDM bulk this is averagely 0.016. Thus, it seems that S has migrated towards the interface. The interaction parameter between PE and elemental sulphur ( $S_8$ ), and between EPDM and elemental sulphur was calculated according to the methodology as described in Section 5.4.2.1. Results confirm SEM-EDX results as  $\chi_{\text{EPDM-S}_8}$  is higher than  $\chi_{\text{PE-S}_8}$  ( $\chi_{\text{EPDM-S}_8} = 54.806$ , and  $\chi_{\text{PE-S}_8} = 26.727$ ). Enganati et al.[147] also reported sulphur migration from rubber to an RFL dip region based on line scan measurements in SEM-EDX mode. Furthermore, the authors found a progressive transition in relative sulphur amount over a distance of 2.5  $\mu\text{m}$  which was surmised to be possibly an interphase. Similarly, here for EPDM-PE, a transition in relative sulphur amount is visible going from PE to the high concentration at the EPDM interface. This could possibly be an interphase/diffusion region with a width of 2  $\mu\text{m}$ , but it has to be taken into account that the spatial resolution, i.e. size of the interaction volume, during measurements was 1  $\mu\text{m}$ .

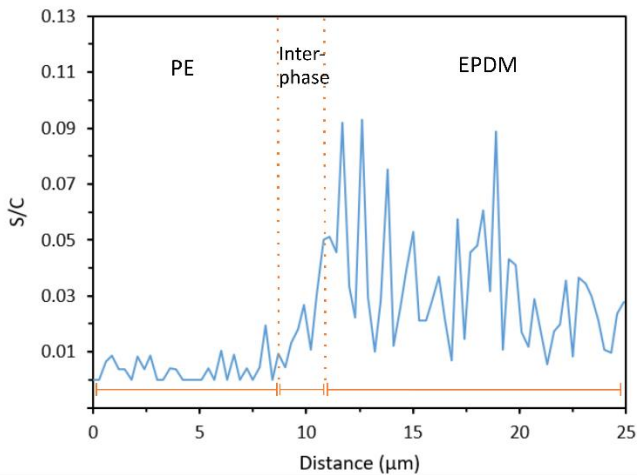


Figure 85: Relative sulphur amount (S/C) along the line scan going from PE to EPDM. The possible interphase region is confined by the dotted line.

#### 5.4.4 Nano-mechanical analysis by AFM

Besides SEM-EDX, a nano-mechanical analysis by AFM was performed to characterise the interphase between EPDM and PE. In this interphase region, intermediate mechanical properties should exist due to the presence of both EPDM and PE.

##### 5.4.4.1 Methodology

AFM measurements were performed on a PE-EPDM sample (PE-S4, Table 11). A Dimension Icon multimode AFM from Bruker was used in PeakForce Tapping mode with Quantitative Nanomechanical Mapping (PFT-QNM). The sample surface was prepared by cryo-microtomy ( $-55^{\circ}\text{C}$ ) to retrieve a flat trimmed surface. During measurements, a PFT amplitude of 75 nm and frequency of 2 kHz was used. The surface was scanned by a RTESPA-150 probe from Bruker with a calibrated spring constant of 3.85 N/m and a calibrated tip radius of 50 nm. During PeakForce tapping the vertical

position of the probe is modulated, the cantilever deflection is measured in time and the feedback on peak force captures the topography. Then, with QNM, an online reconstruction and analysis of the force-curves generates images of the modulus. The images specifically represent the modulus fitted by the Derjaguin-Muller-Toropov (DMT) model. Images were taken over a surface area of  $5 \times 5 \mu\text{m}^2$ ,  $15 \times 15 \mu\text{m}^2$ , and  $50 \times 50 \mu\text{m}^2$ .

#### 5.4.4.2 Results and discussion

In Figure 86, the topography and indentation (DMT) modulus of PE-EPDM is imaged over a surface area of  $5 \times 5 \mu\text{m}^2$ ,  $15 \times 15 \mu\text{m}^2$ , and  $50 \times 50 \mu\text{m}^2$ . These images show a globular morphology of both PE and EPDM (diameter  $\sim 200\text{-}400 \text{ nm}$ ). The indentation modulus ranges up to 1 GPa in PE which corresponds well to the Young's modulus of 1.2 GPa indicated in the datasheet of HDPE Sabic M80064 (Appendix A). The probe was calibrated to analyse these high modulus values, and therefore, caution is needed as the EPDM values will be overestimated due to the high difference with PE. Therefore, the focus is more on the visual comparison between both materials. In EPDM occasional bright spots are visible which represent carbon black particles within the rubber. The topography shows a difference in surface height for PE and EPDM creating a rather large step at the interface ( $> 1 \mu\text{m}$ ). This is probably due the larger dilation of EPDM when the sample was heated back to room temperature after surface preparation at  $-55 \text{ }^\circ\text{C}$  preventing a fine analysis of the interdiffusion at the interface. The modulus images reveal a sharp interface which was also seen during SEM measurements. SEM-EDX indicated a possible diffusion width of  $2 \mu\text{m}$ . Thus, the surface was imaged during AFM over an area of  $5 \times 5 \mu\text{m}^2$ . The red arrow in the topography image Figure 86c indicates an area where the height difference from PE to EPDM is rather limited compared to other locations. When analysing this area in the DMT modulus image (red box) an intermediate modulus is found over a width of  $\sim 1 \mu\text{m}$ . Thus, AFM measurements confirm the limited interdiffusion region between EPDM and PE. However, this interdiffusion width of approximately  $1 \mu\text{m}$  seems to be sufficient to create strong adhesion. Possibly, the interdiffusion is more in the nanometer range. Mutsuda et al. [30] reported a diffusion layer between PPE and SBR with a width of  $96 \text{ nm}$ . However, there, no melt of PPE at the interface was reached during the curing of SBR (at  $170^\circ\text{C}$ ). Thus, a larger diffusion layer between EPDM and PE is expected due to the melt phase of PE improving chain mobility at the interface. Bruckmoser et al. [39] found interdiffusion lengths from below  $1 \mu\text{m}$  up to  $3 \mu\text{m}$  for thermoplastic-thermoplastic or thermoplastic-TPE 2K injection moulding, by Raman measurements, confirming the possibility of a  $1 \mu\text{m}$  interdiffusion width for PE-EDPM. An attempt was made to perform similar Raman measurement, but the fillers in EPDM caused fluorescence within the spectra eliminating this as possible characterisation technique. AFM images do not show any voids at the interface, making a weak boundary layer due to voids unlikely. Thus, diffusion remains most probable and the good adhesion strength might additionally be reached due to the high entanglement possibility between EPDM and PE. Abbott [148] also indicates that to initiate a fracture at the interface, these entangled chains need to move and stretch first resulting in a strong adhesion. Abbott also discusses the Helfand formula as possible indication for intermingling. This formula relates the distance for intermingling to the Flory-Huggins interaction parameters as indicated in Eq. (16). For  $\chi_{EPDM-PE}=0.365$  (Table 28), this would result in a distance of only a few nanometer [149]. However, the Flory-Huggins parameter was calculated at room

temperature. The high temperature during processing, contact time and molecular weight are not taken into account. The indication of only a few nanometers also does not coincide with the characterisation by SEM-EDX and AFM. However, for future measurements, a nanoscale analysis by AFM seems to be promising when the height difference at the interface can be eliminated. So far, despite the similar molecular composition, an adhesion characterisation was possible, but, as indicated, sample preparation requires further attention. Possibly, modelling of the diffusion dynamics could further validate the expectation of entanglements dominating interdiffusion.

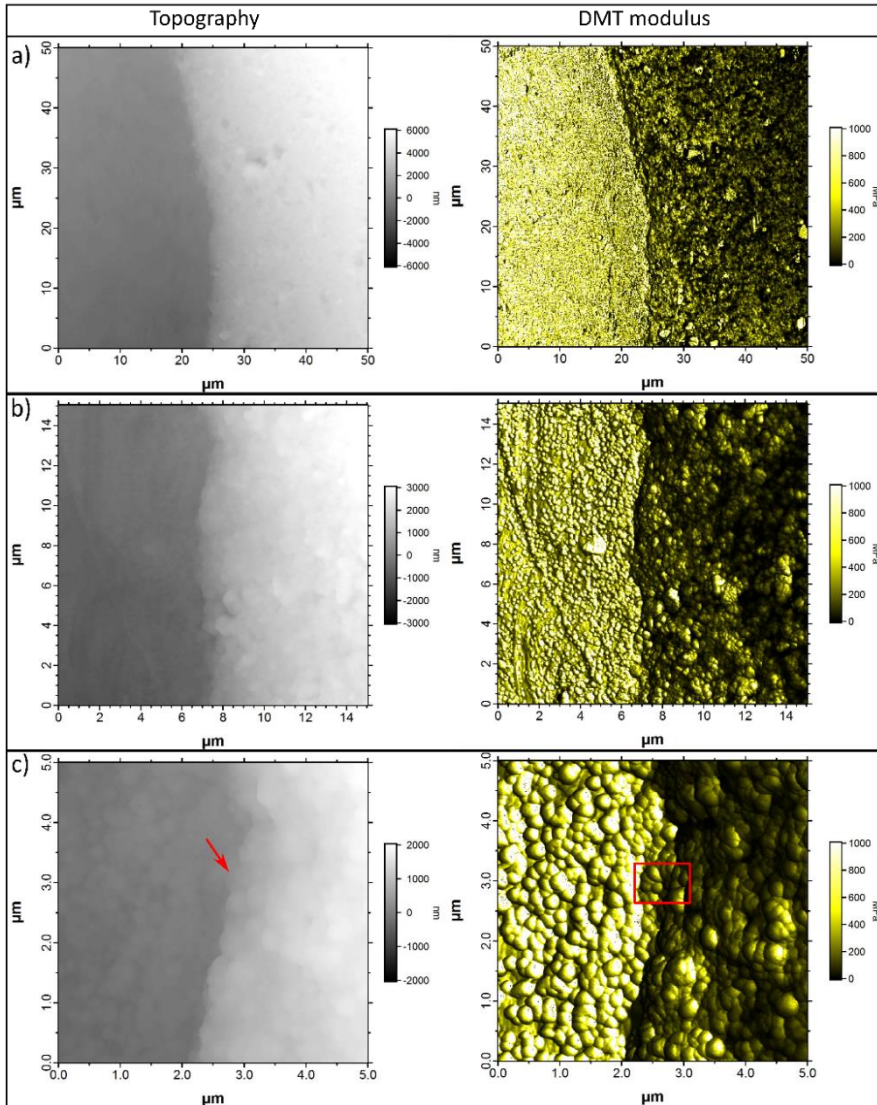


Figure 86: AFM images of PE-EPDM topography and DMT modulus for a surface area of  $50 \times 50 \mu\text{m}^2$  (a),  $15 \times 15 \mu\text{m}^2$  (b), and  $5 \times 5 \mu\text{m}^2$  (c).

## 5.5 Conclusion

During 2K injection moulding, good adhesion can be created between PP or PE and EPDM. However, characterising the adhesion mechanism proved to be very challenging. Three mechanisms were studied in detail: wetting, chemical bonding and interdiffusion.

To analyse wetting at high temperature, an attempt was made to perform high temperature contact angle measurements by depositing a molten thermoplastic droplet on a rubber substrate. Contact angles were analysed in time until an equilibrium state was reached. Then, work of adhesion was calculated from the equilibrium contact angles, but no clear correlation was found with the adhesion percentage determined after 2K injection moulding. However, when adjusting the rubber composition, compatibility measurements, as developed by Bex et al. [6], can have merit as first adhesion evaluation. Additionally, the Flory-Huggins interaction parameter can help clarify the interdiffusion probability due to differences in miscibility. This interdiffusion might range up to maximum a few micrometers, as found by AFM and SEM-EDX measurements. For future work, a more detailed analysis in the nanometer range is recommended, and element detection could be optimised for the polymer samples by performing SEM measurements under low vacuum.

To analyse the difference in adhesion mechanism between sulphur or peroxide crosslinked samples, a high temperature contact angle measurement methodology was developed. Specifically, physical wetting could be distinguished from reactive wetting. This methodology was successful for identifying the adhesion mechanism of EPDM with PE. On vulcanising EPDM, spreading of the PE melt was clearly restricted and high contact angles were obtained due to a co-vulcanisation reaction at the interface. Furthermore, higher peroxide concentration caused a higher contact angle on vulcanising EPDM, as more C-C bonds can be formed, which can be related to the higher adhesion strength as well.

Overall, a combination of multiple adhesion theories is needed to define suitable material combinations and related adhesion strength.



---

## Chapter 6 Material selection guidelines, case-study and end-of-life

---

### 6.1 Introduction

Previous chapters have indicated the significance of the rubber formulation on the adhesion with thermoplastics. However, to transfer this knowledge to the industry, a more clear rubber composition selection procedure is needed. Therefore, in this chapter, material selection guidelines are provided in the form of radar charts for EPDM-PP, EPDM-PE, EPDM-ABS and EPDM-PC. Based on the required product properties, these charts facilitate a better insight on the role of each rubber component. Furthermore, in this thesis a specific focus has been put on EPDM-PP material combination. Therefore, a more detailed material selection grade map is provided. This map visualises the effect of curing system composition, EPDM structure, and filler and oil content on the adhesion. Afterwards, an economic evaluation follows by optimising the product cost of a 2K product for several material combinations. Additionally, the industrial relevance of EPDM-PP 2K products is discussed. Then, for this EPDM-PP combination, a case study is presented to validate the influence of rubber formulation on adhesion and product properties. Finally, the end-of-life of EPDM-PP products is studied as a good adhesion complicates recyclability. In this respect, the re-use of EPDM/PP granulates in virgin PP or in a thermoplastic vulcanisate (TPV) is evaluated.

### 6.2 Material selection guidelines

Several studies were presented in this thesis to determine the influence of rubber composition on the adhesion with thermoplastics. Results indicated that the influence of each component, i.e. peroxide, co-agents, sulphur system, EPDM macromolecular structure, fillers and plasticisers, depends on the type of thermoplastic to which EPDM is adhered. Therefore, when defining guidelines an evaluation for each material combination is required.

In this work, radar charts are provided to visualise the rubber properties together with the accompanying adhesion strength. Such a method is often used in the rubber industry to enable the selection of a rubber type or rubber components based on the required rubber properties. Each chart contains information about the EPDM bulk physico-mechanical properties: tensile strength, hardness, elongation at break, and compression set. Furthermore, interface properties like the adhesion percentage and the vulcanisation rate at the interface, i.e. CRI, are indicated. Every chart enables analysis of a specific component within the rubber formulation, e.g. curing system, macromolecular structure, and fillers and oils, on these properties. Based on the complete representation of all

properties, a selection of optimal components for each applications can be made. For EPDM-PP and EPDM-PE a subdivision is made based on the applied curing system.

## 6.2.1 EPDM – PP

### 6.2.1.1 Peroxide-based EPDM-PP

In Figure 87, Figure 88 and Figure 89 radar charts are given for peroxide-based EPDM-PP with varying EPDM compositions.

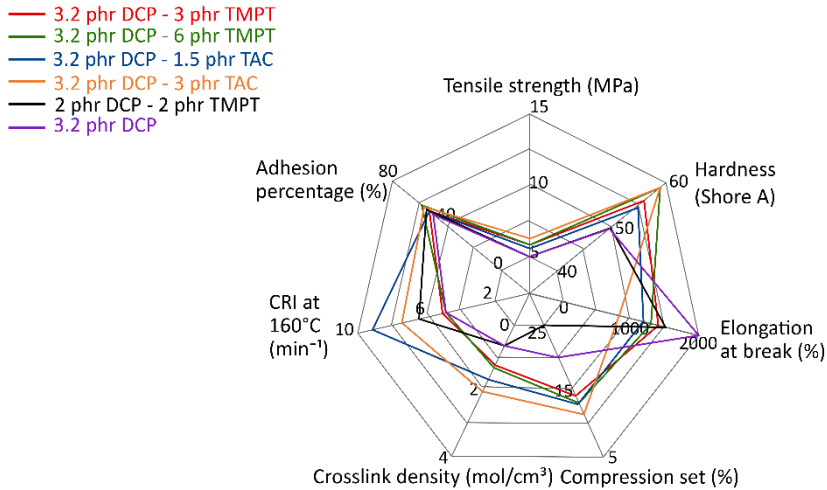


Figure 87: Radar chart illustrating adhesion strength and rubber properties of peroxide-based EPDM-PP with varying peroxide and co-agent concentrations.

In Figure 87, a radar chart is represented which illustrates the influence of DCP and co-agents concentration. The complete rubber formulation can be found in Sections 3.3.1.1 and 3.3.2.1. The EPDM in this radar chart is kaolin loaded with high oil content, low Mooney viscosity, average ethylene content and medium ENB content. Without co-agents an average adhesion strength is reached with accompanying high elongation at break and low vulcanisation speed at the interface. When adding TAC or TMPT as co-agents, the adhesions percentage and compression set improve. In terms of rubber properties, TAC provides a higher cure rate than TMPT. Furthermore, TMPT requires nearly double the concentration of DCP for optimal adhesion (58 % adhesion for 6 phr TMPT at 3.2 phr DCP) while for TAC an equal concentration to that of DCP seems to suffice (57 % adhesion for 3 phr TAC at 3.2 phr DCP). From the DCP concentration study, the lowest concentration was optimal for adhesion with PP due to a lower chain scission possibility. Possibly changing the concentration at 2 phr DCP from 2 phr TMPT to 2 phr TAC could improve the adhesion mechanism as TAC is more effective for adhesion with PP at low concentrations, and it provides better compression set and vulcanisation speed than TMPT.

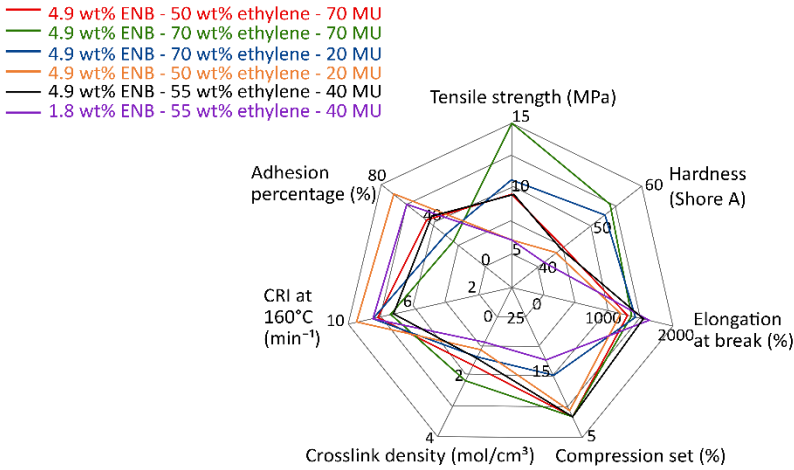


Figure 88: Radar chart illustrating adhesion strength and rubber properties of peroxide-based EPDM-PP with varying EPDM macromolecular structures. Compression set results are based on the EPDM NORDEL™ grade datasheet as listed in Appendix A.

In Figure 88, the influence of Mooney viscosity, ethylene content and ENB content is represented. The complete rubber composition is given in Section 4.2.1. The optimal adhesion with PP was found for EPDM with low ethylene content and Mooney viscosity at an average ENB level. This is a soft compound as indicated by the hardness. Physical properties are rather low, but it gives superior compression set, while providing an efficient cure at the interface. For applications requiring these properties, e.g. sealing products, product cost will be lower due to the faster cure at the interface compared to EPDM with high Mooney viscosity and ethylene content. The dependence of product cost on curing efficiency will be further explained in Section 6.3.

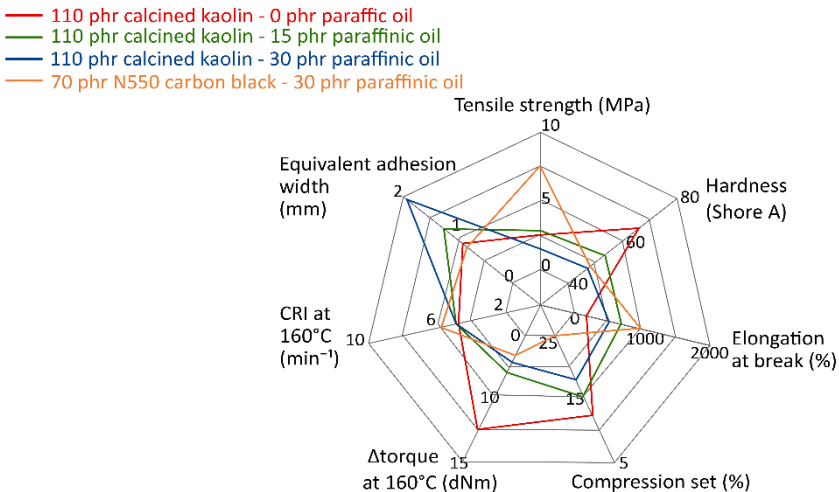


Figure 89: Radar chart illustrating adhesion strength and rubber properties of peroxide-based EPDM-PP with varying oil and filler content.

Finally, in Figure 89, the influence of fillers and oils is illustrated. The complete rubber composition is given in Section 4.3.1. Furthermore, the adhesion is expressed in equivalent adhesion width as explained in Section 4.3.1.4 (Eq. (28)) due to the wheel geometry. While EPDM with calcined kaolin and high oil content provides very good adhesion, products containing this rubber will provide average compression set and low physical properties. Lowering the oil content compromises the adhesion partially, but better rubber properties will be reached. Furthermore, carbon black and high oil content improve the physical properties considerably, but these benefits are accompanied by poorer compression set and adhesion.

### 6.2.1.2 Sulphur-based EPDM-PP

Besides peroxide curing, sulphur curing was studied for the combination of EPDM with PP. In Figure 90, the variation in accelerator composition is given and in Figure 91 the influence of EPDM macromolecular structure combined with sulphur curing is illustrated.

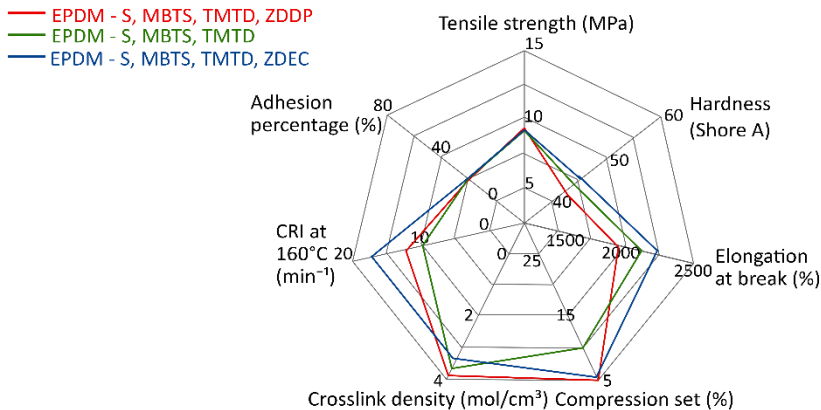


Figure 90: Radar charts illustrating adhesion strength and rubber properties of sulphur-based EPDM-PP with varying sulphur system composition.

In contrast to peroxide curing, sulphur curing causes a lower adhesion for EPDM-PP. As no chemical bonding is possible, interdiffusion dominates. When studying the influence of the accelerator composition, as shown in Figure 90, an optimisation of the curing time due to higher CRI does not alter the adhesion percentage. The EPDM compounds in Figure 90 all contain a raw EPDM polymer with 43 MU, 68 wt% ethylene, and 8 wt% ENB. The complete rubber composition is given in Section 3.4.1. Possibly, the high ethylene content inhibits sufficient interdiffusion due to a lower compatibility with PP.

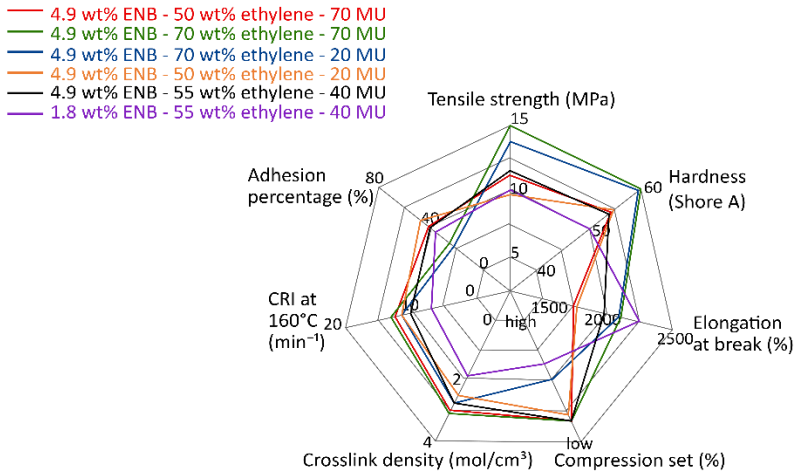


Figure 91: Radar charts illustrating adhesion strength and rubber properties of sulphur-based EPDM-PP with varying EPDM macromolecular structure. Compression set results are based on the EPDM NORDEL™ grade datasheet as listed in Appendix A.

Altering the EPDM macromolecular parameters, as shown in Figure 91, confirms that high ethylene content has an adverse effect on the adhesion. The complete rubber composition is given in Section 4.2.14.3.1. 70 wt% ethylene in EPDM results in high strength, hardness and elongation at break. Compression sets in this chart are based on results from the EPDM NORDEL™ grade datasheet as listed in Appendix A. In this datasheet compression set results are given for a peroxide based compound. Thus, exact values in combination with sulphur curing are unknown. Lowering the ethylene content clearly improves the adhesion. These compounds give good physical properties to the product, but are accompanied by average adhesion. Thus, it is possible to produce sulphur-based EPDM-PP products with average adhesion (48 %), but peroxide curing gives a better adhesion as 70 % adhesion can be reached (Figure 88). Eventually, for a specific application, a detailed analysis of the product requirements is needed and then within the acceptable property ranges the optimal composition for good adhesion needs to be selected. For example sulphur curing will be better for dynamic applications, but peroxide curing offers better temperature resistance and compression set.

## 6.2.2 EPDM – PE

For EPDM-PE, the focus in this PhD research has been on the influence of the curing system composition. Previous work by Bex et al. [1] already indicated that an efficient adhesion could be reached between EPDM and PE. However, the cycle time was high making it an inefficient process. Furthermore, a detailed study of the adhesion mechanism was needed. Therefore, sulphur curing was compared to peroxide curing. In Figure 92, a radar chart of the peroxide curing system composition is given and in Figure 93, varying sulphur system compositions are illustrated. The complete rubber composition of each radar chart is given in Section 3.3.1.1 and 3.3.2.1 for the peroxide system and in Section 3.4.1 for the sulphur system.

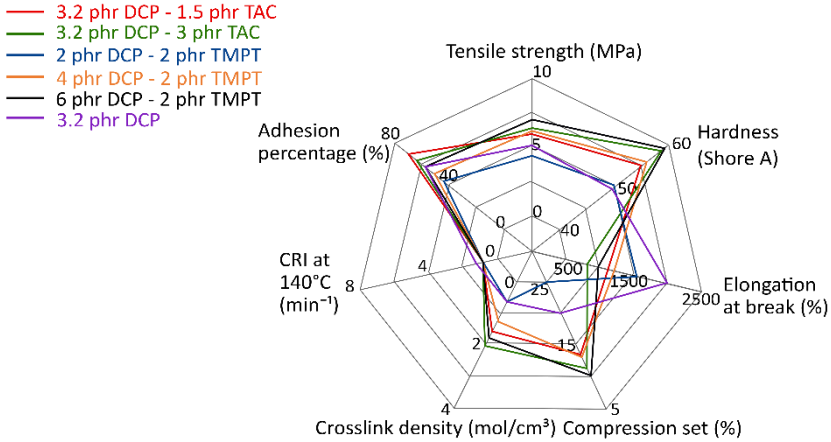


Figure 92: Radar charts illustrating adhesion strength and rubber properties of EPDM-PE with varying peroxide system composition.

When applying a peroxide curing system in EPDM-PE, variations in the curing agent and co-agent concentration significantly influence the adhesion percentage. Optimal adhesion seems to be reached when 1.5 phr TAC is added as co-agent. Only half the concentration of DCP needs to be added of TAC for the highest adhesion percentage. Furthermore, due to the low chain scission yield, high concentrations of DCP could be added. The optimal concentration of DCP was 6 phr. Possibly adding 3 phr TAC could further improve the adhesion. Large variations can be observed in Shore A hardness and compression set upon changing the curing system. However, the biggest downside of peroxide cured EPDM-PE are the extremely low vulcanisation rates (CRI) at the interface. This even worsens the product cycle time compared to the result from Bex et al. [3], who used sulphur curing. Therefore, the sulphur curing system was studied in more detail. Higher cure rates can be achieved by altering the accelerator composition. However, this can compromise the adhesion strength as shown in Figure 93.

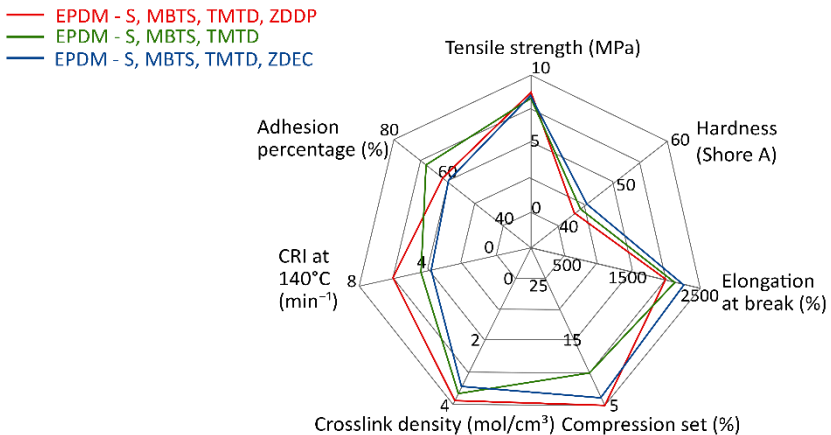


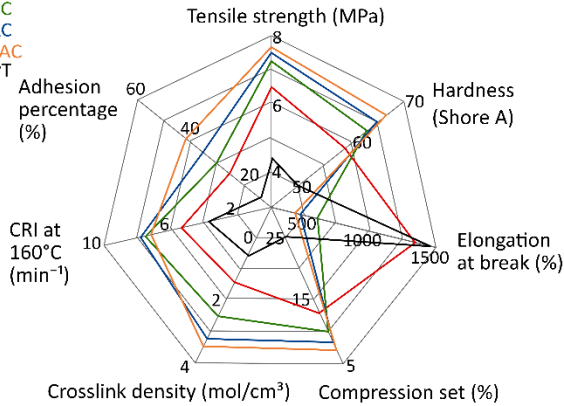
Figure 93: Radar charts illustrating adhesion strength and rubber properties of EPDM-PE with varying sulphur system composition.

### 6.2.3 EPDM – polar thermoplastics

Besides with polyolefin thermoplastics, EPDM was combined as well with polar thermoplastics like PC and ABS. Due to the polar characteristics, adhesion with EPDM seems unlikely. However, the compatibility can be influenced by changing the rubber composition. When using a sulphur curing systems, adhesion could not be initiated. However, a shift to peroxide curing caused major differences in adhesion strength. In Figure 94a, a radar chart of peroxide-based EPDM-PC is shown and in Figure 94b peroxide-based EPDM-ABS is illustrated.

#### a) EPDM-PC

- 3.2 phr DCP - 9 phr TMPT
- 3.2 phr DCP - 6 phr TAC
- 3.2 phr DCP - 9 phr TAC
- 3.2 phr DCP - 12 phr TAC
- 4 phr DCP - 2 phr TMPT



#### b) EPDM-ABS

- 3.2 phr DCP - 3 phr TMPT
- 3.2 phr DCP - 9 phr TMPT
- 3.2 phr DCP - 6 phr TAC
- 3.2 phr DCP - 9 phr TAC
- 3.2 phr DCP - 12 phr TAC
- 2 phr DCP - 2 phr TMPT
- 4 phr DCP - 2 phr TMPT

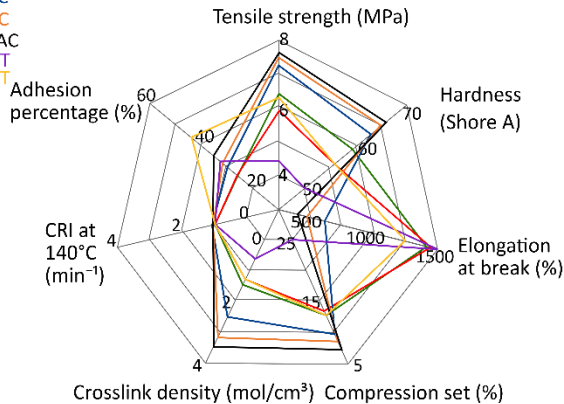


Figure 94: Radar charts illustrating the influence of peroxide curing on adhesion strength and rubber properties (a) EPDM-PC, and (b) EPDM-ABS.

Changing the composition of the peroxide curing system severely influences rubber properties and adhesion with polar thermoplastics. Furthermore, the influence of co-agents and peroxide curing agents on the adhesion depends on the specific type of thermoplastics. For EPDM-PC, adhesion is mainly improved by changing co-agent concentrations with higher concentrations causing a better adhesion. When varying only

DCP concentration, and with TMPT fixed at 2 phr, the highest possible adhesion was found for 4 phr DCP but this adhesion is still poor. In contrast, for EPDM-ABS, at low co-agent concentration and increasing DCP concentration adhesion significantly improves. This difference between EPDM-PC and EPDM-ABS can be ascribed to a difference in adhesion mechanism. As chemical bonding is unlikely for EPDM-PC, higher co-agent concentrations are important to improve compatibility. EPDM-ABS can exhibit co-vulcanisation and here higher DCP concentration can promote co-vulcanisation as more peroxide radicals can initiate bonding between EPDM and ABS.

For the polar thermoplastics, peroxide curing is needed to enable adhesion with EPDM. However, this remains only economically feasible for EPDM-PC as the cure rate at the interface between EPDM and ABS is extremely low. Therefore, only EPDM-PC was studied in further detail concerning the influence of fillers and oils to analyse whether this influences the compatibility. Results are illustrated in Figure 95.

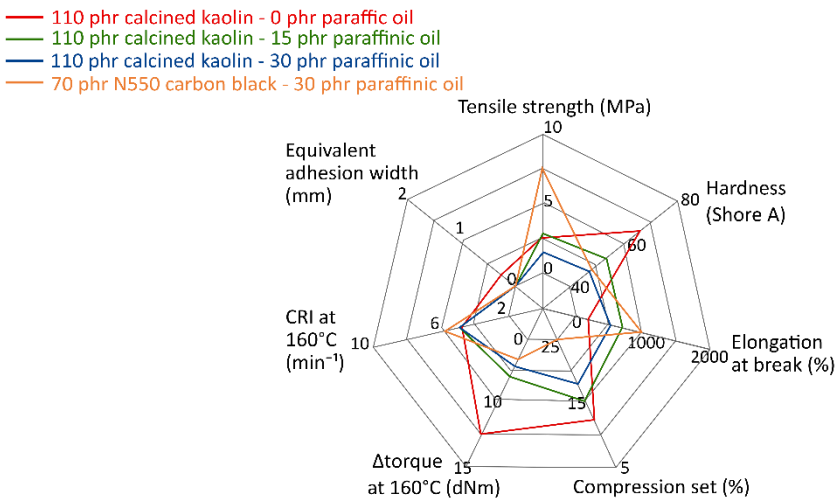


Figure 95: Radar charts illustrating the influence of fillers and oils on adhesion strength and rubber properties of EPDM-PC.

Results showed limited adhesion at high kaolin content. This adhesion is expressed in equivalent adhesion width as explained in Section 4.3.1.4 (Eq. (28)) due to the wheel geometry. Adding oils inhibits adhesion as this might prevent interdiffusion due to lower compatibility. Furthermore, compounds in Figure 95 contained 3.2 phr DCP and 2 phr TMPT which is known to be too low for adhesion with PC. Thus, it remains important to select a high co-agent concentration when adhering EPDM to PC.

#### 6.2.4 Material selection map

Based on the previous radar charts, a better understanding of the rubber compositional influence on the adhesion with PP, PE, PC and ABS is achieved. A major focus was put on the rubber curing system as this defines the specific adhesion mechanism at the interface. For EPDM-PE, sulphur curing is most beneficial due to its faster cure at the interface. For EPDM-PC, peroxide curing with high co-agent

concentration is required. EPDM-ABS is currently economically unfeasible when using peroxide curing and sulphur curing does not enable adhesion.

Besides these material combinations, a more in depth study was performed for EPDM-PP because of its high applicability, low material cost and good product properties. Therefore, for future evaluations when selecting a rubber composition for EPDM-PP, a material selection map was set up as shown in Figure 96. This enables optimal selection of a rubber formulation taking both rubber properties and adhesion into account. In Figure 96, EPDM-PP adhesion is ranked from low to high for both peroxide and sulphur containing compounds. Each box in this figure represents a certain rubber composition as indicated in the white box in the bottom corner. Boxes that are linked contain the same general composition except the component indicated in bold. Furthermore, associated rubber properties are listed below each box.

Further on in Section 6.4, this material selection map is used to define an optimal EPDM composition for the case study as represented in Section 6.4. Furthermore, adhesion percentages are used to rank adhesion from low to high. These percentages depend on the tensile strength of the rubber compound. Thus, for a certain application, first the requirements in product properties and, more specifically, rubber properties need to be defined. Afterwards, these requirements need to be combined with knowledge of good adhesion to determine the optimal composition. A practical example is given in Section 6.4.

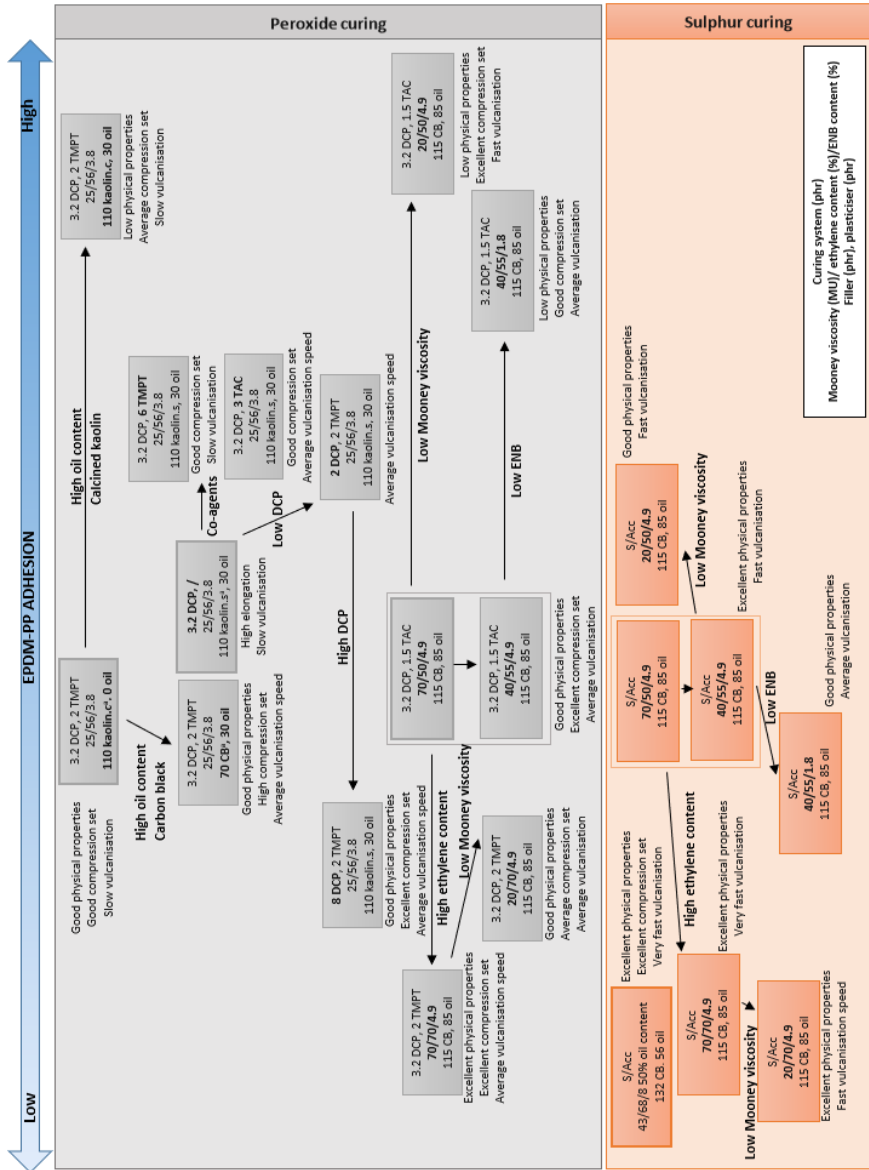


Figure 96: Material selection grade map of EPDM-PP.

## 6.3 Economic evaluation

When selecting a material combination for a specific application, the economic feasibility has to be evaluated as well. Bex [3] performed a complete economic evaluation to compare 1K injection moulding with 2K injection moulding of ABS with NBR. In particular, 1K manual, 1K automatic, full 2K, and semi 2K were distinguished as possible alternatives. With 1K manual, the thermoplastic and rubber part are glued together in a separate manual production step, and the 1K automatic is used when this step is carried out in an automated manner. A full 2K process entails a pre-form transfer moulding process with two cavities on one 2K injection moulding machine. For semi 2K, the thermoplastic part is produced separately in a 1K machine and afterwards, the thermoplastic part is overmoulded with rubber in a rubber injection moulding machine with a mould equipped with thermally separated cavities. A detailed description of material cost, mould cost and production cost is discussed by Bex [3]. Bex concluded that a semi 2K process is economically favourable over a full 2K process. For a batch of 50000 products, 1K manual was also more competitive than the automatic 1K process. For this batch size it was eventually found that by optimising the number of cavities in the mould optimal product cost could be achieved. However, the 1K process remained more beneficial in terms of cost. Despite the higher cost, the 2K process does result in a much better adhesion as with polyolefins, which are difficult to glue to other substrates due to their low surface tension, adhesion can be improved by 500 % [3].

In this chapter, the methodology for economic evaluation by Bex is applied to analyse the influence of rubber material composition and the specific rubber-thermoplastic combination. A comparison is also made between the manual 1K process and semi 2K process by selecting a good rubber composition for adhesion. Furthermore, the industrial relevance of EPDM-PP is discussed in more detail by comparing the adhesion in 2K injection moulding with the adhesion by glue in the 1K process.

### 6.3.1 Product cost optimisation: Thermoplastic-rubber 2K seal

For each thermoplastic an optimal EPDM composition can be produced. For PE, this involves choosing an appropriate EPDM composition with a sulphur curing system as this has the highest curing efficiency at the low interface temperature. For PP-EPDM, a peroxide curing system would lead to the highest adhesion strength. Successful combination of ABS with EPDM is currently unlikely. No ABS-EPDM adhesion can be obtained with a sulphur curing system. Peroxide curing with modest peroxide curing agent concentration and high co-agents concentration improves bonding but the peroxide curing efficiency is too low at the interface leading to extremely high processing times. Instead, the combination of ABS with NBR is included here as comparison with the EPDM-thermoplastic material combinations. PC could be combined with EPDM when high co-agent concentrations are used to improve compatibility.

For economic evaluation, the 2K seal product from Figure 53 is studied. In particular, the manual 1K is compared with the semi 2K injection moulding process as these are more competitive at a batch size of 50000 products compared to automatic 1K and full 2K respectively [3]. Varying the rubber composition influences the material cost. The rubber-thermoplastic material combination influences production cost as each thermoplastic has different temperature requirements at the interface for adhesion which in turn influences the required vulcanisation and cycle time.

Table 29: Material cost of rubber and thermoplastic part in a 2K seal.

Material cost	Mass (g)		Price (€) per piece	
	Rubber	Thermoplastic	Rubber	Thermoplastic
PP-EPDM	6.386	7.850	0.011	0.016
PE-EPDM	6.122	8.229	0.007	0.008
PC-EPDM	6.439	10.516	0.014	0.026
ABS-NBR	5.911	9.388	0.009	0.018

Table 30: Rubber vulcanisation time of a PP-EPDM, PE-EPDM, PC-EPDM or ABS-NBR 2K seal when applying a 2K or 1K injection moulding process.

Rubber vulcanisation	2K vulcanisation time (s)	1K vulcanisation time (s)
PP-EPDM	500	235
PE-EPDM	1500 <sup>a</sup>	230
PC-EPDM	500	230
ABS-NBR <sup>b</sup>	700	120

In Table 29, the material cost of several thermoplastic-rubber combinations are represented. The rubber cost is highest when combining EPDM with PC as a higher co-agents concentration was taken to improve adhesion with PC. This increases the price due to the general high cost of co-agents, e.g. €10.16/kg, which increased the rubber cost in the 2K seal by 27 %. Furthermore, the thermoplastic part price is highest for PC and lowest for PE. In Table 30, the required vulcanisation times show a major difference for PE in combination with EPDM due to the low interface temperature causing a low cure rate. The most efficient vulcanisation was found for EPDM with PP or PC as the interface temperature is approximately 160°C. The 1K vulcanisation time represents the times required to reach 90 % vulcanisation at 180°C of the outer rubber seal when produced separately. This corresponds with a high cure rate but often lower temperatures, i.e. 160°C-175°C, are taken by manufacturers for processing safety. For EPDM-PE, high vulcanisation times were needed to cure EPDM at the interface in the 2K process due to the low interface temperature.

After determining the material cost and vulcanisation times, product prices could be calculated. In Figure 97a, the price per piece for the manual 1K process is given for PP-EPDM, ABS-NBR, PP-EPDM and PC-EPDM 2K samples. Clearly, the highest cost goes to the production of the pieces. This is also the case for the semi 2K injection moulded products as shown in Figure 97b. In this figure, it is also remarkable how high the product cost is for PE-EPDM samples. Even though this material combination has the lowest material cost, the long required vulcanisation time results in a product price (€ 3.01) that is 87 % higher than PP-EPDM (€ 1.61). Furthermore, PC-EPDM and PP-EPDM have a similar 2K vulcanisation time, but PC-EPDM has material cost that are 43 % higher than that of PP-EPDM. However, this barely influences the total product cost. Thus, varying the rubber composition for optimal adhesion does not significantly affect the product price.

<sup>a</sup> Optimal vulcanisation time for 2K seal with PE in combination with sulphur-based EPDM as defined by Six et al. [120].

<sup>b</sup> Vulcanisation times of NBR in 2K and 1K process are based on results from Bex et al. [3].

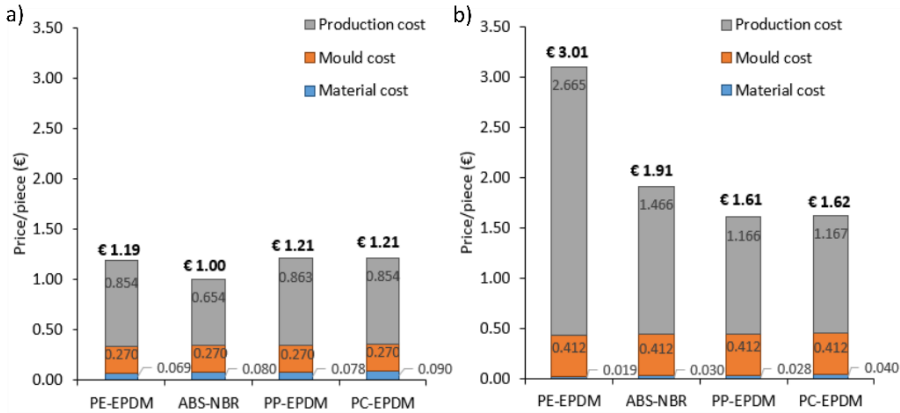


Figure 97: Product price of a PE-EPDM, ABS-NBR, PP-EPDM and PC-EPDM 2K seal for a batch size of 50000 products in case of the manual 1K process (a), and the semi 2K process (b).

After determining the product cost at a batch size of 50000 products, the number of cavities in the mould were optimised according to the calculations by Bex [3]. During injection moulding, a higher number of cavities in the mould can reduce product cost and number of production days for a certain batch size. In Figure 98, the product price in function of number of cavities is shown for each material combination and type of production process. A higher number of cavities increases the mould cost as more work is required, but reduces the production cost as every cycle more products can be produced [3]. For the 1K processes, the use of two cavities reduces the product cost whereas for the semi 2K process the optimal number of cavities is material dependent. Specifically, the use of three cavities is most optimal for PP-EPDM, PC-EPDM and ABS-NBR, but PE-EPDM cost is optimal at four cavities. Possibly an injection moulding machine with a higher clamping force is required when implementing more cavities. However, this has no significant effect on the product cost when going for example from a 50 ton to 80 ton injection moulding machines for the semi 2K process.

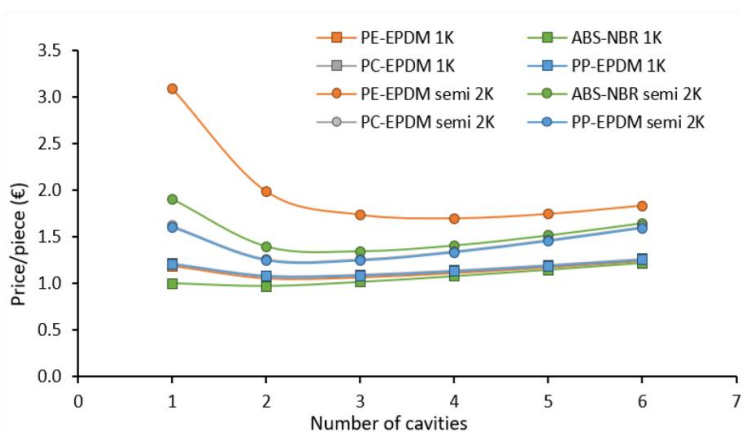


Figure 98: Total product cost based on material cost, mould cost and production cost.

Taking into account the optimal number of cavities for each material combination and type of process, a new evaluation can be made of the product cost for 50000 products. These results are represented in Figure 99. When comparing the manual 1K process (Figure 99a) with the semi 2K process (Figure 99b), the semi 2K process remains more expensive. However, the semi 2K PP-EPDM product costs only € 0.17 more than the 1K product. This difference is less than originally found for one cavity in Figure 97 (€ 0.40). As already indicated by Bex [3], the 1K process benefits less from high cavity numbers because it already has much lower cycle times. Furthermore, the optimal cost for the 2K produced PE-EPDM product is 44 % lower than originally found in Figure 97b. Despite this lower cost, 2K injection moulding of PE-EPDM remains much more costly compared to the manual assembly of the individual parts. The lowest cost for 2K injection moulding was found for PP-EPDM and, additionally, EPDM-PP can exhibit very good adhesion. Therefore, the relevance of this material combination is discussed in the next section.

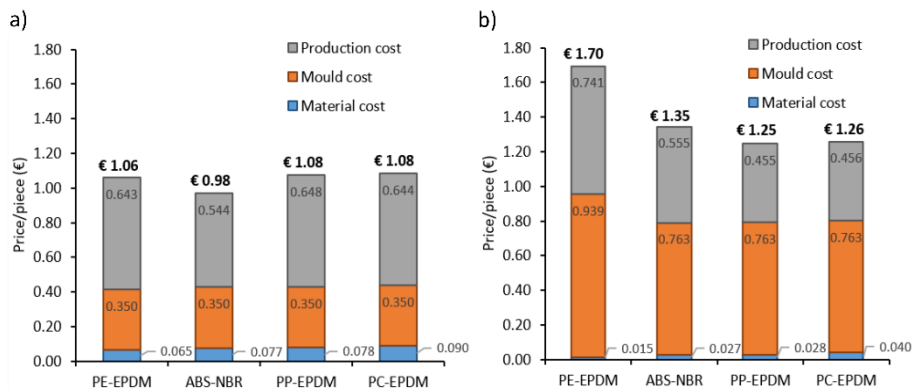


Figure 99: Optimal product price of a PE-EPDM, ABS-NBR, PP-EPDM and PC-EPDM 2K seal for a batch size of 50000 products in case of the manual 1K process (a), and the semi 2K process (b).

### 6.3.2 Industrial relevance of 2K injection moulding of PP with EPDM

The economic evaluation in the previous section showed that of all studied material combinations PP-EPDM comes closest to the 1K process in terms of product cost. For this evaluation, the vulcanisation time of the rubber part in the 1K process was determined for a mould temperature of 180°C. However, manufacturers often injection mould EPDM at lower temperatures for good process repeatability and safety. Therefore, an additional comparison is made between the semi 2K process and the manual 1K process when vulcanising the rubber part at 170°C. The required vulcanisation time at this temperature is 480 s. Results of the optimal product cost are shown in Figure 100.

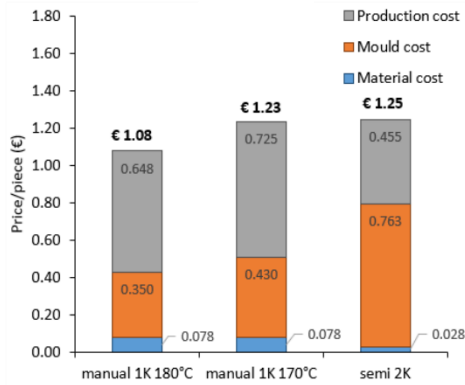


Figure 100: Optimal product cost of PP-EPDM for manual 1K at 180°C or 170°C and semi 2K.

When optimising the manual 1K process at this temperature, minimal product cost of € 1.23 are found. At 170°C, the mould cost are higher as the optimal cavity number is three instead of two (manual 1K 180°C). Furthermore, the production cost are higher due to the longer vulcanisation time. This variation of 10°C in mould temperature in the 1K process significantly influences the product cost. When comparing this now with the semi 2K process, almost equal product cost are found. Of all the studied material combinations, PP-EPDM has the highest industrial potential when applying the 2K injection moulding process due to its more efficient cure and high adhesion quality. The 2K process now offers a competitive price as it provides a much higher quality compared to individually injection moulded and glued samples. In particular, when PP-EPDM (K-O30 for EPDM) is adhered by glue a shear strength of 399 N is reached compared to 2919 N for 2K injection moulded PP-EPDM. Thus, 2K injection moulded EPDM-PP products are much more suited for application exposed to higher loads. Glued samples will fail more easily under higher loads and this might require sample replacement during the life-time of the product part in a certain application. Furthermore, as already indicated by Bex [3], 2K injection moulding offers other advantages like the possibility of a re-design which together with the elimination of glue can lead to savings in material cost, correct positioning, and less dimensional errors. For future implementation of the 2K injection moulding process it is recommended to optimise the mould design to avoid leakages due to the variotherm process, i.e. switching from vulcanisation to cooling temperature. This entails selecting a better type of mould steel (e.g. Stavax, to reduce corrosion), a better design and positioning of rubber seals within the mould, and preventing inserts in a mould.

## 6.4 Case study: EPDM-PP 2K automotive sealing applications

When combining EPDM with PP in 2K injection moulding several opportunities arise in terms of possible applications. The focus in this section is on automotive applications where thermal and chemical resistance are required together with good compression set.

Currently, eMobility is booming and polymers like PP and EPDM can play a major role in this thriving industry. Combining this with the demand for reducing assembly times and weight together with high quality, the novel 2K process comes to mind.

Especially, weight reduction is key to fulfil the emission norms of electrical vehicles. Based on a forecast, global plastics turnover for electrical vehicles is targeted to reach USD 2620 million by 2025. Of these plastics, PP is believed to hold the majority share due to its low cost, low weight and good moldability [150]. Furthermore, the automotive industry is one of the biggest markets for EPDM as this rubber provides vibration resistance, heat resistance, sealing properties, durability, high tensile strength, and resistance to diluted acids and alkalis [151]. Specific automotive applications of EPDM include seals in coolant circuits, O-rings in air conditioning or heating systems, brake systems or housings for high voltage batteries.

When exploring possible applications of EPDM-PP 2K seals, a plug & seal connector, as developed by Freudenberg and shown in Figure 101, comes to mind.



Figure 101: Plug & seal connector for electrical vehicle cooling system [152].

Electrical vehicles are operated by a battery pack, like lithium ion (Li-ion) batteries. The battery cells within the pack generate heat during charge and discharge. To avoid thermal deterioration of the battery and guarantee safety and charging efficiency, operating temperatures need to remain below 50°C. The optimal temperature range for Li-ion batteries is between 25°C and 40°C [153]. Thus, battery systems require good thermal management to prevent the battery from overheating. The most common technology for battery cooling is with a water-glycol coolant mixture. This liquid-cooling system has a high heat exchanging efficiency. Chu et al. [153] determined that the battery temperature remained below 45°C with an inlet coolant temperature of 30°C at a coolant flow above 5 L./min. Furthermore, due to the large size of the battery, modular cooling is required and then many connectors are needed. These connectors require resistance to water and water-glycol, stable product dimensions, secured positioning and low leakage potential [152], [154].

Furthermore, EPDM is often used as seal in a glycol-based brake fluid system due to its accompanying fluid resistance. Thus, EPDM-PP connectors would be applicable here as well. Within this brake system, polypropylene reservoirs are also used to store the brake fluid. Here, another possible application would be the brake fluid reservoir cap. Incorrect positioning or failure of the rubber seal can cause malfunctions of the brake system due to air intake and fouling. The need for correct positioning emphasises the applicability of 2K injection moulding. Then, proper adhesion and system safety would be assured.

In this case study, a commercially available EPDM was selected from Hercorub based on the material selection map (6.2.4). This includes combining good adhesion with PP

and assuring good product properties. For the automotive EPDM-PP 2K seal connector in the battery system, resistance to water, coolant, and resistance to heat aging is needed while providing good strength and compression set between 25 and 40°C. Furthermore, in the brake system, e.g. brake fluid container, the interface must not deteriorate due to exposure to brake fluid. Thus, 2K seals are produced with sample dimensions as shown in Figure 53 as this resembles the plug & seal connector from Freudenberg. Within the application, the EPDM seal is mainly exposed to shear forces. Therefore, the custom-made shear test is used to evaluate the adhesion strength. Afterwards, heat aging, resistance to water, coolant and brake fluid, and shear strength at high temperature are determined. Furthermore, rubber properties like tensile strength, elongation at break, hardness, and compression set are analysed. Eventually, the applicability of the proposed EPDM-PP seal can be evaluated.

### 6.4.1 Materials and methods

#### 6.4.1.1 EPDM and PP grade

The standard PP, used throughout this PhD, was combined with an EPDM grade selected for a sealing application in an electrical vehicle. Product requirements were defined and where possible these requirements were quantified:

- (1) Good compression set: for good sealing properties;
- (2) Thermal stability: expected temperature range is between 25°C and 45°C and aging in time needs to be minimised;
- (3) Good dynamic compression: difference in flow and pressure might influence compression;
- (4) Efficient vulcanisation: for optimal product cost, cycle time needs to be minimal;
- (5) Electrical insulation: due to usage in the battery system;
- (6) Good adhesion: EPDM-PP adhesion above 0.13 MPa. This simulates the pressure in the coolant system according to Wang et al. [155].

To meet the requirements, as listed above, a rubber composition for adhesion with PP was pre-defined based on the material selection map (6.2.4):

Table 31: Rubber composition requirement for EPDM-PP connector.

Rubber component	Type	Property
EPDM grade	Low Mooney Low ethylene content 2-5 wt% ENB	Very good adhesion Excellent compression set Fast curing at interface
Curing system	Peroxide curing	Thermal stability Excellent compression set Good adhesion
Filler	Kaolin	Excellent compression set Electrical insulation Good adhesion
Oil content	Low	Good compression set

In Table 31, a possible EPDM composition was pre-defined. Overall, combining EPDM with a peroxide curing system and a kaolin filler offers very good compression set and thermal aging resistance. Based on all these requirements one available EPDM composition from Hercorub was selected containing following EPDM grade, curing system, filler, and oil:

- (1) EPDM grade (100 phr): KEP2320, Kuhmo Polychem with Mooney Viscosity ML 1+4, 125°C = 25 Mooney units (MU), ethylene content = 58.0 wt%, ethylene norbornene (ENB) content = 4.7 wt%;
- (2) DCP (3.6 phr): Perkadox BC-40MB-gr, AzkoNobel, 40 % active peroxide content;
- (3) Silane treated calcined kaolin filler (110 phr): Polarite 103A, Imerys;
- (4) Paraffinic oil (17 phr): Sunpar 2280, Petronas.

The EPDM grade is indicated as being ideal for electrical insulation, brake parts, gaskets and moulded goods. Furthermore, a surface treated kaolin offers superior electrical stability and moisture resistance. The downside of the selected EPDM compound is the absence of co-agents and the high peroxide concentration. This will probably reduce adhesion with PP as more chain scission is possible. In the following sections this EPDM compound from Hercorub is named EPDM.c with ‘c’ referring to case-study

#### 6.4.1.2 2K injection moulding

EPDM.c-PP samples were injection moulded according to the parameter listed in Table 32. For EPDM, the vulcanisation temperature was set at 180°C. The mould temperature of the thermoplastic cavity during adhesion with the rubber was limited by thermoplastic part deformation which led to an interface temperature of 163°C for EPDM-PP. This interface temperature was experimentally determined with an infrared camera (OPTRIS PI400). The required EPDM vulcanisation time was determined by producing subsequent EPDM-PP 2K samples with vulcanisation times ranging from 100 s to 800 s with increments of 100 s.

Table 32: Injection moulding parameters of PP and EPDM.c for production of a 2K seal.

Process parameters	PP	EPDM.c
Injection temperature (°C)	230	80
Mould temperature (°C)	20	180
Injection rate (cm <sup>3</sup> /s)	19	2
Holding pressure (bar)	692	396

### 6.4.1.3 Characterisation of rubber properties

#### Vulcanisation behaviour during injection moulding

As the vulcanisation degree in time needs to be known to define the proper vulcanisation and cycle time during injection moulding, Shore A hardness measurements were executed on injection moulded samples. Five Shore A hardness measurements were performed according to ISO 7619 with a measuring time of 15 s and the vulcanisation degree near the interface was calculated according to Eq.(24). The vulcanisation degree was determined on samples with vulcanisation times varying from 100 to 800 s. Average vulcanisation degrees are reported in time along with the 95 % confidence interval.

#### Mechanical properties

Mechanical properties of EPDM.c were determined on the outer rubber seal of the 2K products. Since the selected EPDM.c contains no co-agents, there should be no adhesion to PC. Therefore, the rubber could be moulded onto and peeled of a PC wheel, preserving a smooth rubber surface. Then, the rubber seal could be removed and used for mechanical testing. All samples were conditioned at 23 °C for 3 days. A Zwick Z050 equipped with a 1 kN load cell was used at room temperature, 40°C, 55°C, 70°C, and 85°C. These temperatures were selected from the ISO 37 standard and 85°C was taken as maximum as this corresponds to the maximum service temperature of PP. A crosshead speed of 200 mm/min and a gauge length of 13.5 mm were applied to determine tensile properties. The samples for tensile testing had a length of 35 mm, width of 10 mm and thickness of 2 mm. Furthermore, compression stress-strain properties were determined on a Zwick Z050 (50 kN load cell) at 23°C, 40°C and 85°C according to ISO 7743 method c. Three samples were analysed with dimensions 10 x 10 x 6 mm<sup>3</sup>ok and the testing procedure consisted of 4 cycles by varying the strain from 0 to 25 % and release back to 0 % at constant speed of 10 mm/min. The compressive stresses at 25 % deformation after 4 cycles was compared. This testing procedure is for quality control of the rubber seal and is often used to study anti-vibration mountings and O-rings. The hardness was measured using a CV Shore A hardness durometer according to ISO 7619. Compression set tests were performed at 23°C for 24 h according to ISO 815. Average values of three samples for tensile strength and compression set, and of five samples for hardness with their 95 % confidence intervals are reported.

### 6.4.1.4 Adhesion characterisation

Shear tests were executed for adhesion force evaluation according to the methodology discussed in Section ‘Shear test’ of Chapter 4. Samples combining EPDM.c with PP were tested after 2K injection moulding and taken as ‘control’ samples. Then, EPDM.c-PP samples were exposed to several conditions as listed in Table 33. Values of adhesion force, i.e. shear force, are compared by calculating the retention (Eq. (36)):

$$\text{Retention (\%)} = \frac{Y_1}{Y_0} \cdot 100 \quad (36)$$

where  $Y_1$  is the shear force after exposure and  $Y_0$  is the shear force of the control sample. When only a reduction of 10 % in property is found during exposure to a certain condition, the retention is 90 %, and the resistance is indicated as ‘*satisfactory*’. A retention between 90 % and 50 % is ‘*limited*’ and below 50 % ‘*unsatisfactory*’.

Table 33: EPDM.c-PP sample and shear test conditioning.

EPDM.c-PP	Pre-test conditioning	Shear test temperature
Control	/	23°C
Aged	Aged at 100°C for 72 h	23°C
H <sub>2</sub> O	2 weeks immersion in H <sub>2</sub> O	23°C
Coolant	2 weeks immersion in coolant	23°C
Brake fluid	2 weeks immersion in brake fluid	23°C
Shear at 85°C	/	85°C
Shear at 70°C	/	70°C
Shear at 55°C	/	55°C
Shear at 40°C	/	40°C

Thus, 2K samples were conditioned by immersion in three different solvents and by heat aging before shear testing:

- (1) **Solvent immersion:** to determine chemical resistance in water, coolant and brake fluid, samples were immersed in 150 ml solvent during two weeks according to ASTM D543. The containers were swirled every day during the first seven days. After seven days, the solvent was refreshed. The samples were removed from the solvent after two weeks, rinsed with water, and dried with filter paper. Sample weight, and dimensions were analysed and adhesion was re-evaluated by shear testing at 23°C. Average values of three measurements with their 95 % confidence intervals are reported. Furthermore, retention was determined according to Eq. (36).  
The applied solvents were demineralised water (H<sub>2</sub>O), ethylene-glycol-based coolant (Protection, Service Best International B.V.), and brake fluid DOT 4 (Protection, Service Best International B.V.).
- (2) **Heat aging:** EPDM.c-PP samples were exposed to 100 °C in an air circulated oven for 72 h (ISO 188). After heat aging, adhesion force was re-evaluated. Average values of three samples of each compound with their 95 % confidence intervals are reported.

Adhesion of the 'control' samples was evaluated by shear testing at 23°C. Furthermore, the adhesion in function of temperature was studied as well by varying the temperature during shear testing from 23°C, 40°C, 55°C, 70°C, and 85°C to analyse a broad temperature range.

## 6.4.2 Results and discussion

### 6.4.2.1 Properties of EPDM.c

To determine the vulcanisation time for EPDM.c-PP during injection moulding, the vulcanisation degree in time was defined. From Figure 102, a 90 % vulcanisation time of 500 s can be deduced. Therefore, a vulcanisation time of 600 s was selected during processing.

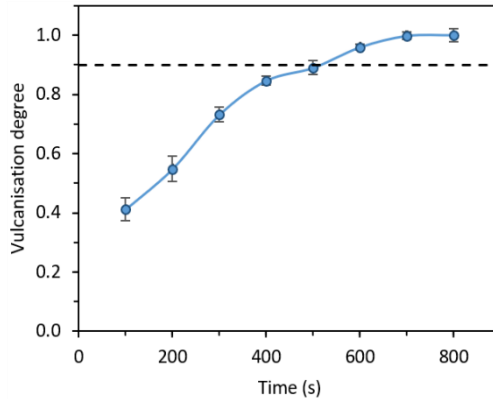


Figure 102: Vulcanisation degree of EPDM.c. The dashed line represents 90 % vulcanisation degree. Error bars represent 95 % confidence intervals.

In Table 34, mechanical properties of the EPDM.c seal are shown. Thus, the selected EPDM compound offers a good tensile strength and elongation at break, a Shore A of 60 and good compression set. However, these properties were defined at room temperature.

Table 34: EPDM.c vulcanisate mechanical properties.

Vulcanisate properties (23°C)	EPDM.c
Tensile strength (MPa)	$8.38 \pm 0.08$
Elongation at break (%)	$1320 \pm 70$
Hardness (° Sh A)	$62.4 \pm 0.8$
Compression set (%)	$13.6 \pm 0.3$

When testing the tensile strength at a temperature range between 23°C and 85°C, major differences are observed as shown in Figure 103. A clear decrease in tensile strength was found with higher temperature. This decrease in strength with temperature is due to a change in segmental mobility of the rubber chain. At 40°C, the tensile strength is retained by 70 %. Going to 85°C this reduces to 47 %. It is important to take this decrease in tensile strength into account when evaluating the adhesion at high temperature.

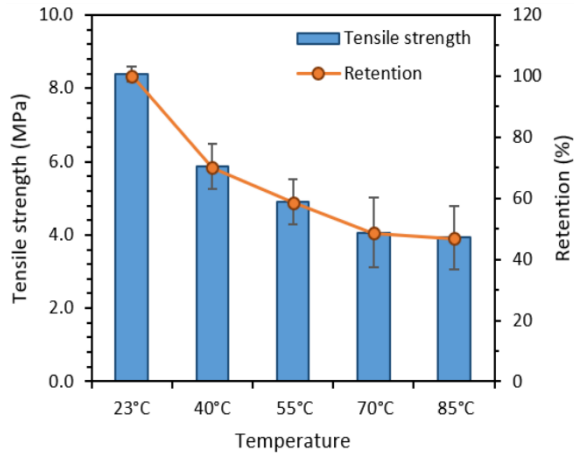


Figure 103: Tensile strength of EPDM.c at 23°C, 40°C, 55°C, 70°C, and 85°C. The retention indicates the decrease in strength compared to the strength at 23°C. Error bars represent 95 % confidence interval for the tensile strength.

As the application is mainly exposed to compression, compressive stress was determined at 25 % strain after four cycles. Tests were executed to define the influence of higher temperature. In Table 35, compressive stresses are listed and results indicate a small decrease in compressive stress of only 9 % from 23°C to 85°C. Thus, the selected EPDM composition can withstand and maintain compression in a dynamic environment. At 85°C, compressive stress is still *satisfactory* as the retention compared to 23°C is 91 %.

Table 35: Compressive stress at 25 % deformation at 23°C, 40°C and 85°C.

Temperature (°C)	Compressive stress (MPa)
23	1.29 ± 0.06
40	1.29 ± 0.05
85	1.17 ± 0.07

#### 6.4.2.2 EPDM.c-PP adhesion during in-service conditions

The EPDM.c-PP samples were exposed to in-service conditions. Thus, samples were immersed in H<sub>2</sub>O, coolant and brake fluid, and heat aged. In Figure 104, results of adhesion force are shown with the corresponding retention.

When the samples were immersed in the solvent, properties were re-evaluated after two weeks. No dimensional changes were observed, i.e. EPDM.c-PP edge thickness, diameter, height and weight remained unchanged. Thus, no solvent swelling occurred indicating a good chemical resistance to the solvent by both EPDM.c and PP. The adhesion force varied slightly after immersion. However, for all solvents the adhesion forces were retained for at least 95 % which is categorised as *satisfactory*. Adhesion force after immersion in H<sub>2</sub>O shows a large deviation which is believed to be caused by an injection moulding defect in one sample. In coolant, even an increase in adhesion force was found, but the difference with the control sample is not significant. Furthermore, stable results were found after immersion in brake fluid. Thus, chemical resistance in all

solvents is *satisfactory*. After heat aging at 100°C, a slight reduction in adhesion force is observed with a retention of 87 %. As adhesion forces of the control and heat aged sample are not significantly different, the thermal stability can still be indicated as *satisfactory*.

Within the cooling system of an electrical vehicle, the pressure of the cooling fluid can be 0.13 MPa when maintaining the battery temperature between 25 and 40°C [155]. For the 2K seal with sample dimensions as shown in Figure 53, one can calculate the required adhesion force when this pressure would be on the EPDM outer seal. Thus, the interface of the 2K seal needs to withstand these pressures. This corresponds to 318 N for an interface area of 2450 mm<sup>2</sup>. For EPDM.c-PP in coolant, an adhesion force of 2500 ± 50 N will easily withstand these pressures.

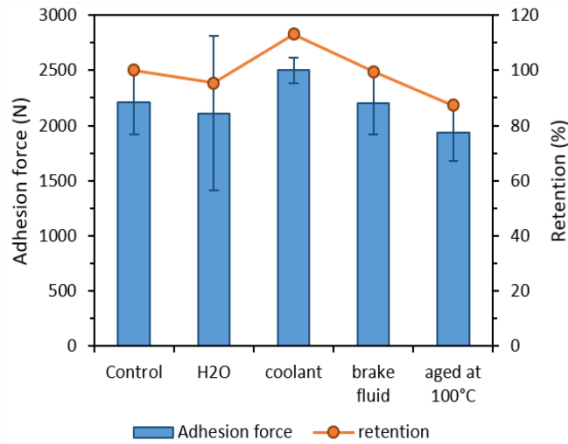


Figure 104: Adhesion force of EPDM.c-PP (control) and after immersion in H<sub>2</sub>O, coolant, brake fluid and heat aging at 100°C. The retention indicates the decrease in adhesion force compared to the control sample. Error bars represent 95 % confidence interval for the tensile strength.

As the 2K connectors are used in a cooling circuit with a temperature range between 25 and 45°C, adhesion force is defined at higher temperatures. The temperature is even increased up to 85°C, which is indicated as the maximum service temperature of PP. In Appendix A, also a heat deflection temperature (with a bending stress of 0.45 MPa) of 86°C is found. Results of EPDM.c tensile strength showed a severe reduction with higher temperature ('Mechanical properties' in Section 6.4.1.3). Therefore, adhesion at this high temperature was studied.

In Figure 105, adhesion forces based on shear test are shown in function of temperature. Clearly, a significant decrease in adhesion force is observed. During shear testing, the PP wheel is pushed through the EPDM seal by retaining the EPDM seal on the support cylinder (Figure 55). As the temperature increases, the adhesion force decreases. This decrease was also found for the tensile strength of EPDM.c. Thus, the adhesion is possibly decreasing due to a decrease in rubber properties. At 40°C only *limited* retention of 58 % is found. At 55°C and higher, the retention is *unsatisfactory* (below 50 %). Even though the adhesion force lowers, adhesion is above the required 318 N until 70°C. However, for a secured and stable application, the maximum temperature is selected to be 55°C. This ensures applicability as a coolant connector.

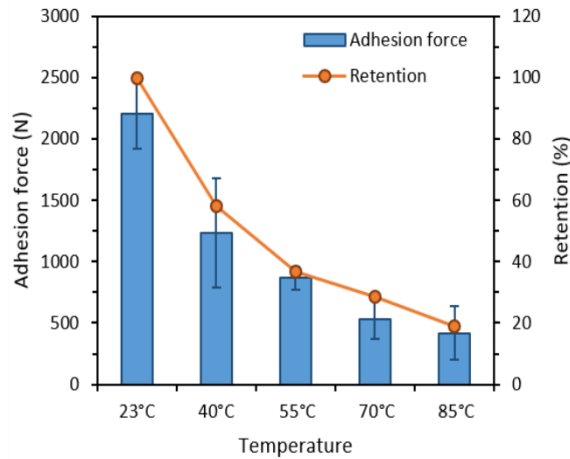


Figure 105: Adhesion force of EPDM.c-PP at 23°C, 40°C, 55°C, 70°C, and 85°C. The retention indicates the decrease in adhesion force compared to the sample at 23°C. Error bars represent 95 % confidence interval for the adhesion force.

To confirm that the reduction in adhesion force is caused by a deterioration of EPDM properties, additional measurements were done on samples KO30-PP and RO30-PP from Chapter 4. For KO30-PP adhesion force dropped to 553 N at 85°C which is only 19 % of the adhesion force at 23°C. Similarly, RO30-PP adhesion reduced to 1016 N which is 45 % of the adhesion force at 23°C. Thus, when defining a proper composition for 2K samples, characterising and analysing the rubber properties to which the product is exposed is very important. Furthermore, a custom-made shear test was used for adhesion evaluation. However, this does not exactly represent the loading conditions of the coolant connector. During the adhesion test, the force was solely applied on the EPDM seal while in application it is unlikely that the coolant pressure is solely applied on the seal. Mainly, reliable sealing and compression resistance dominate and compressive stress did not significantly decrease at higher temperature (Table 35).

## 6.5 End-of-life of PP-EPDM 2K products

When implementing the novel 2K injection moulding process, adhesion is created between a thermoset rubber and a thermoplastic. This poses a new environmental issue as these two polymers cannot be separated completely at the end of their life. Thermoset rubber wastes are already difficult to recycle due the complex crosslinked structure, making it impossible to re-process them. Therefore, in recent years, research has been focussing on the re-use of rubber waste in polymer products. This can vary from composites consisting of rubber waste granulates and synthetic rubber, to composites of thermoplastic materials and rubber waste granulates, enabling sustainable management of rubber waste [156]. To produce these rubber waste granulates a grinding process can be used (cryogenic or at ambient temperature) which together with the grain size, the used crosslinking system, and filler content influences the rubber granulate properties. For example, rubber granulates cured with sulphur can influence the curing properties when added in a rubber matrix, while curing with dicumylperoxide does not influence the vulcanisation parameters of the matrix. When merely adding the rubber granulates as

filler in thermosets, thermoplastics or virgin rubber, product properties like strength tends to decay, making it more useful as a cheap solution in low quality applications. Furthermore, grinding at ambient temperature was found to be more beneficial than cryogenic rubber granulates as they had a rougher surface creating a better contact with the rubber matrix [156].

Specifically, for 2K products of EPDM with PP recycling possibilities need to be studied. Therefore, a grinding process was applied going from large grain size to a powder as discussed in the following section. Afterwards, varying concentrations of EPDM/PP powder were added to virgin PP to analyse the effect on material properties. Then, novel 2K products with recycled EPDM/PP in the thermoplastic PP wheel are produced to study the possibility of a re-use in these products. Finally, addition of recycled EPDM/PP powder in a thermoplastic elastomer as additional recycling opportunity is studied.

### 6.5.1 Methodology

#### 6.5.1.1 Recycling process

2K samples of EPDM-PP produced throughout this PhD research were taken which have similar EPDM composition. This entails EPDM with a peroxide curing composition and a kaolin filler combined with PP 400-GA05 from Ineos. These EPDM-PP 2K samples with sample dimensions as shown in Figure 23, i.e. a plate geometry, were shredded with a Rapid Granulator 1521. This reduced the specimens to a grain size of 2 to 6 mm. Afterwards, a ZM100 centrifugal mill (Retsch) was used for ultra-fine grinding. However, when producing EPDM/PP granulates, it is difficult to define the weight percentage of EPDM and PP within the 2K recycled powder. Thus, to enable a detailed study, EPDM and PP were separated based on their differences in density, respectively  $1.18 \pm 0.05 \text{ g/cm}^3$  and  $0.98 \pm 0.03 \text{ g/cm}^3$ , in water. For post-consumer recycling, this will not be possible when the large grinded pieces (2-6 mm) contain both EPDM and PP. After ultra-fine grinding, granulates of EPDM and PP were imaged with a Keyence VH-S30 digital microscope with a maximum magnification of 200 connected to a VHX-500F monitor. Then, an ImageJ particle detection and analysis, developed by Vancleef et al. [157], was used to define the grain size distribution. A statistical analysis of the fitted grain diameter was executed on Minitab.

#### Recycled blend composition

The recycled EPDM/PP granulates were combined with virgin PP (PP 400-GA05 Ineos) to create blends with following weight percentages:

- (1) 100/0/0: 100 % virgin PP, 0 % recycled EPDM, 0 % recycled PP;
- (2) 80/10/10: 80 % virgin PP, 10 % recycled EPDM, 10 % recycled PP;
- (3) 60/20/20: 60 % virgin PP, 20 % recycled EPDM, 20 % recycled PP;
- (4) 40/30/30: 40 % virgin PP, 30 % recycled EPDM, 30 % recycled PP.

Additional blends were made of thermoplastic vulcanisate (TPV) Santoprene 111-64 from ExxonMobile and recycled EPDM/PP granulates. The TPV is a dynamically vulcanised compound consisting of cured EPDM particles enclosed in a PP matrix. Following blend compositions were made:

- (1) 100/0/0: 100 % TPV, 0 % recycled EPDM, 0 % recycled PP;
- (2) 90/5/5: 90 % TPV, 5 % recycled EPDM, 5 % recycled PP;
- (3) 80/10/10: 80 % TPV, 10 % recycled EPDM, 10 % recycled PP;

- (4) 60/20/20: 60 % TPV, 20 % recycled EPDM, 20 % recycled PP;  
 (5) 40/30/30: 40 % TPV, 30 % recycled EPDM, 30 % recycled PP.

### Blend processing

Recycled blends were compounded and tensile bars were produced, as shown in Figure 106, with a Demag IntElect 50/330-100 injection moulding machine. The maximum clamping force is 500 kN. The ratio of the screw length and the screw diameter (L/D) is 20 and the diameter of the screw is 22 mm. The injection moulding parameters to produce the tensile bars are given in Table 36.

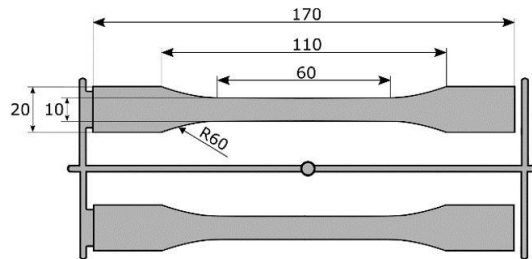


Figure 106: Geometry of ISO 527-2/1B tensile bars with dimensions. The sample thickness is 4 mm [158].

Table 36: Injection moulding parameters for tensile bars of PP-recycled EPDM/PP and TPV-recycled EPDM/PP.

Process parameters	PP-recycled EPDM/PP	TPV-recycled EPDM/PP
Injection temperature (°C)	230	220
Mould temperature (°C)	35	35
Injection rate (cm <sup>3</sup> /s)	57	76
Holding pressure (bar)	400	200

Besides tensile bars, wheels were produced of PP-recycled EPDM/PP to study the re-usability in 2K injection moulded thermoset rubber-thermoplastic products (Figure 53). Specifically, blends of virgin PP/recycled EPDM/recycled PP (80/10/10, 60/20/20, and 40/30/30) were injection moulded and afterwards overmoulded with EPDM K-O30 according to the process as described in Section 4.3.1.2. Injection moulding parameters similar as listed in Table 22 were used.

Products produced in this study were not exposed to a consumer environment, eliminating the effect of contaminations.

#### 6.5.1.2 Recycled blend properties

For all recycled blends heat flow analysis was executed with a Differential Scanning Calorimeter (DSC, 2920 TA). Samples between 10-15 mg were cut from tensile bars produced by injection moulding. To eliminate the effects of thermal history, samples were heated to 250°C at 10°C/min and cooled to 25°C at 10°C/min. Afterwards, samples were heated from 25°C to 250°C at 10°C/min. All measurements were executed under nitrogen environment (30 mL/min). The degree of crystallinity of all samples was

estimated from the peak area according to Eq. (27), where  $x$  is the weight fraction of PP in the blend,  $\Delta h$  is the specific enthalpy of fusion (in J/g) retrieved from the peak area, and  $\Delta h_c$  is the enthalpy of fusion of 100 % crystalline polypropylene (207 J/g). In EPDM, only the ethylene sequences are able to crystallise if their length is sufficiently high. However, none of the blends show EPDM crystallisation, making this negligible.

### **Properties of PP with recycled EPDM/PP granulates**

Mechanical properties of PP-recycled EPDM/PP were determined by first executing tensile tests on a Galdabini Quasar 50 with a 50 kN load cell according to ISO 527-2/1B/50. A crosshead speed of 50 mm/min was used. Furthermore, the impact strength was determined on a Zwick 5113 pendulum impact tester with a 7.5 J impact hammer according to ISO 179. Samples were prepared for impact testing by implementing a notch according to ISO 179/1eA. Next, Shore D hardness measurements were performed with a Zwick 3100 durometer according to ISO 868. For each test procedure, five measurements were taken and 95 % confidence intervals are reported.

For the 2K samples, consisting of a PP inner wheel with varying concentrations of EPDM/PP granulates and an EPDM outer seal, adhesion was evaluated by the custom shear test as reported in Section 4.3.1.4. The adhesion force of these recycled samples is compared to the original PP-KO30 adhesion force (Section 4.3).

### **Properties of TPV with recycled EPDM/PP granulates**

Tensile properties of the TPV tensile bars with recycled EPDM/PP granulates were determined on a Zwick Z050 equipped with a 1 kN load cell. Measurements were at a crosshead speed of 200 mm/min. Shore A hardness was determined with a CV durometer according to ISO 7619. For each test procedure, five measurements were taken and 95 % confidence intervals are reported.

## **6.5.2 Results and discussion**

### **6.5.2.1 EPDM-PP granulates**

After a first grinding step, reducing the grain size to 2-6 mm, grains of EPDM and PP were separated based on their different density in water. For a commercial recycling process, the ease of separating these polymers facilitates a more efficient re-use in other products. However, those pieces containing both EPDM and PP, require an in-depth study. Thus, EPDM and PP grain size were further reduced to an ultra-fine grain size. In Figure 107, microscopic images are represented of PP and EPDM grains together with their grain diameter distribution. For EPDM, mostly particles between 10-30  $\mu\text{m}$  were obtained. From literature it is known that mechanical properties can be improved by reducing grain size and a grinding process is preferred to create a larger specific surface area [156]. For PP, the fine grinding process at ambient temperature caused larger variation in grain diameter. During grinding, heat build-up is created which reduces the ease of grinding. This causes particles with a string shape rather than spherical particles due to occasional melting upon grinding in time. Thus, upon evaluating product properties, a possible degradation of the PP grains within the matrix needs to be taken into account. To reduce the temperature in the mill, a cryogenic spray (Cryolab freezing aerosol, Q Patch, VWR) was used.

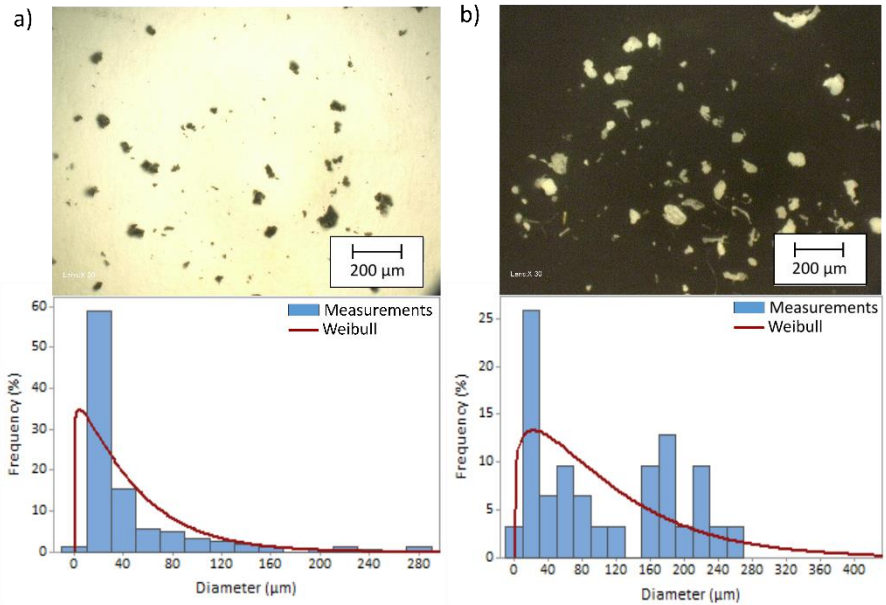


Figure 107: Microscopic image with related grain diameter distribution for EPDM (a) and PP (b). A fitted Weibull distribution is shown in each graph.

### 6.5.2.2 Virgin PP blended with recycled EPDM/PP

After producing tensile bars of different blend compositions with virgin PP and recycled EPDM/PP, DSC parameters were determined. Results are listed in Table 37. In this table  $\Delta H_m$  is the melting enthalpy,  $T_m$  is the melting peak temperature,  $T_{mo}$  is the onset melting temperature,  $\Delta H_c$  is the crystallisation enthalpy,  $T_c$  is the crystallisation peak temperature,  $T_{co}$  is the onset crystallisation temperature, and  $\alpha$  is the crystallinity.

Table 37: DSC parameters of blend compositions Virgin PP/ recycled EPDM/ recycled PP.

Blend composition	$\Delta H_m$ (J/g)	$T_m$ (°C)	$T_{mo}$ (°C)	$\Delta H_c$ (J/g)	$T_c$ (°C)	$T_{co}$ (J/g)	$\alpha$ (%)
100/0/0	75.46	169.02	158.10	78.42	113.37	117.99	36.45
80/10/10	66.01	168.33	160.00	68.14	115.31	119.88	35.43
60/20/20	65.43	168.21	159.00	66.38	115.27	119.77	39.51
40/30/30	40.21	165.70	157.37	40.68	116.58	120.42	27.75

Heat analysis results indicate a slight decrease in  $T_m$  when recycled EPDM granulates are added. This is an indication of imperfections in the formed crystallites. Furthermore, recycling PP can lower the molecular mass and increase stereo-irregularities leading to lower  $T_m$  as well [159]. Lima et al. [160] studied the crystallisation behaviour in thermoplastic elastomer blends with ground tire rubber (GTR) and EPDM. The authors found higher  $T_c$  for binary blends PP/EPDM and PP/GTR which was explained to be caused by heterogeneous nucleation process due to the presence of EPDM or GTR. Similarly, when recycling EPDM/PP in virgin PP, EPDM might initiate a nucleation

mechanism. Furthermore, crystallisation percentage decreases with higher concentration of recycled EPDM/PP. This might be due to the presence of recycled PP increasing the amorphous PP phase in the blend.

Mechanical properties for all blend concentrations were defined as well. In Figure 108, tensile properties, hardness and impact strength are represented. As expected, virgin PP (100/0/0) has a relative high tensile strength, elongation at break and toughness. When adding a higher weight percentage of recycled EPDM and PP, the tensile strength and Young's modulus linearly decrease (tensile strength:  $R^2 = 0.9978$ ; Young's modulus:  $R^2 = 0.9602$ ). This can be related to a reduction in molecular weight of PP and less molecular entanglements. Elongation at break severely deteriorated with the addition of recycled content. Thus, with the addition of recycled PP/EPDM a transition to a more brittle fracture occurs [161]. Furthermore, softer domains arise due to the recycled content causing a lower hardness as seen in Figure 108d. Impact strength decreases up to 60/20/20. However, with 30 % recycled EPDM and 30 % recycled PP, impact strength increases again. Possibly at this concentration, EPDM starts to act as a filler and impact modifier. However, the impact strength is still lower than that of the virgin PP.

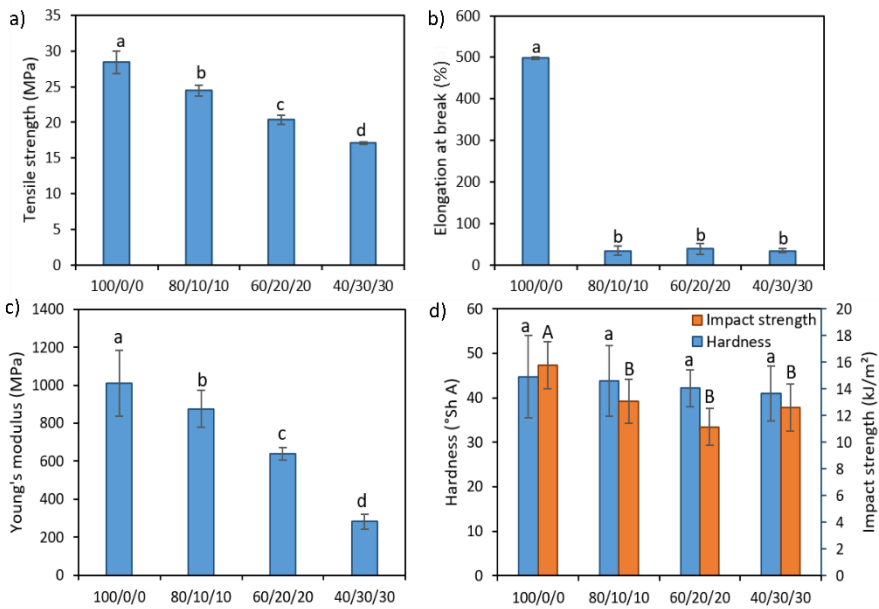


Figure 108: Mechanical properties of virgin PP/recycled EPDM/recycled PP blends: tensile strength (a), elongation at break (b), Young's modulus (c), and hardness and impacts strength (d). Error bars represent 95 % confidence intervals. Grouping information from a one-way ANOVA is given by lower case letters and by upper case letters for impact strength.

Based on mechanical properties of the blends, a clear deterioration in properties is found. Therefore, the applicability of recycled EPDM/PP granulates in virgin PP is rather limited. However, the different blends were 2K injection moulded into wheels with an outer EPDM seal to see how it would affect the adhesion. Originally, virgin PP with EPDM K-O30 resulted in an adhesion force of  $2920 \pm 180$  N. When adding recycled EPDM/PP granulates into the inner thermoplastic wheel, adhesion reduced from 1040

$\pm 160$  N, to  $790 \pm 150$  N, and  $530 \pm 60$  N for respectively 10, 20 and 30 % recycled EPDM and PP. These granulates reduced the extent of adhesion, most likely due to a reduction in molecular weight of PP and EPDM granulates limiting the entanglement possibility.

To improve the applicability of EPDM/PP recycled granulates in virgin PP, addition of compatibilisers is recommended for further research to improve the compatibility and mechanical properties of these granulates with the PP matrix.

### 6.5.2.3 Thermoplastic vulcanisate with recycled EPDM/PP

A TPV of PP and EPDM was combined with recycled EPDM and PP granulates from 2K products. DSC parameters were determined and results are listed in Table 38.

Table 38: DSC parameters of blend compositions TPV/ recycled EPDM/ recycled PP.

Blend composition	$\Delta H_m$ (J/g)	$T_m$ (°C)	$T_{mo}$ (°C)	$\Delta H_c$ (J/g)	$T_c$ (°C)	$T_{co}$ (J/g)	$\alpha$ (%)
100/0/0	11.87	154.24	144.83	12.95	105.43	109.63	14.34
90/5/5	13.86	156.35	146.17	14.32	105.93	110.31	16.33
80/10/10	16.74	158.78	147.65	18.77	106.56	111.52	19.25
60/20/20	19.29	163.52	150.99	21.48	109.49	114.6	21.18
40/30/30	21.68	164.15	151.83	24.65	112.07	116.78	22.77

The TPV, as used here, consists of EPDM and PP. However, the specific content of PP and EPDM within the TPV is unknown. As hardness is reported for this TPV in Shore A, a high content of EPDM is assumed. Specifically, 60/40 for EPDM/PP content was used to calculate the crystallinity of PP in the blends, thus these values need to be interpreted as a trend and not as absolute values. In Table 38, an increasing PP crystallinity is found when adding high content of EPDM/PP granulates which is also seen with the increase in melt enthalpy. It appears that in this TPV mainly the addition of recycled PP influences properties as a shift for both the melt onset and melt temperature is found as well.

The produced tensile bars showed a high flexibility indicating the clear presence of EPDM. Therefore, mechanical properties could be determined similar to the thermoset rubbers. The focus has been put on hardness, tensile strength and elongation at break. In Figure 109, it can be seen that for the blend composition 90/5/5, no significant differences are found in hardness, tensile strength and elongation at break. Afterwards, all properties significantly change due to the higher concentration of PP. Possibly, 80/10/10 could offer opportunities as well due to the higher tensile strength and the reasonable elongation at break.

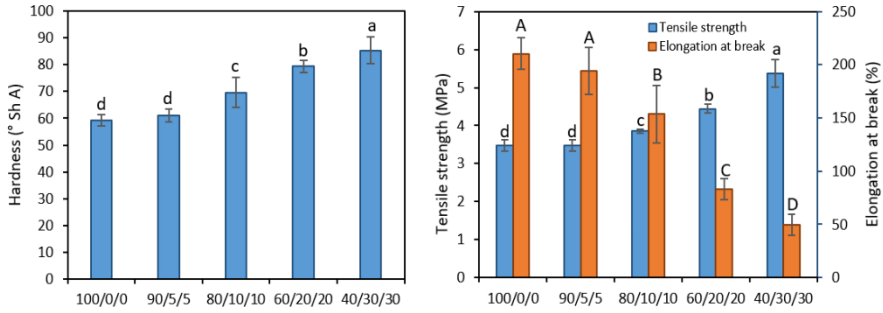


Figure 109: Mechanical properties of TPV/recycled EPDM/recycled PP blends: hardness (a), and tensile strength and elongation at break (b). Error bars represent 95 % confidence intervals. Grouping information from a one-way ANOVA is given by lower case letters and by upper case letters for elongation at break.

In terms of recyclability, adding recycled EPDM/PP to TPV is most promising. In the datasheet of Santoprene a maximum regrind of 20 % Santoprene is recommended. However, results show that recycled granulates from EPDM/PP 2K products could be added as well at low concentrations. Possibly, even higher concentration could be added when preparing the blends before the dynamic vulcanisation process of the TPV. Thus, there is a definite possibility for recycling at end-of-life.



---

## Chapter 7 Conclusions and outlook

---

### 7.1 Introduction

This thesis studied the adhesion mechanisms between thermoset rubber and thermoplastic in 2K injection moulding. Previous research enabled processing this unique material combination by the development of a versatile mould with thermally separated heat cavities. Even though adhesion between EPDM and PE was good, long processing times were required. For EPDM with PP only low adhesion was achieved, and adhesion between EPDM and polar thermoplastic was, at the start of this PhD, not yet realised. Furthermore, knowledge concerning the adhesion mechanisms was lacking. Therefore, an optimisation of the material composition and accompanying adhesion mechanism was deemed necessary. Specifically, three main goals were defined:

- (1) to optimise the adhesion strength at the thermoset rubber-thermoplastic interface by focussing on rubber formulation;
- (2) to provide insight into the adhesion mechanisms between rubbers and thermoplastics;
- (3) to increase economic feasibility of 2K injection moulding by reducing processing times.

In this concluding chapter, these three goals are re-evaluated based on results from the previous chapters. Furthermore, an outlook is provided with recommendations for further research.

### 7.2 Conclusions

By modifying the rubber composition, the adhesion with thermoplastics can be severely influenced. In particular, the rubber curing system defines the type of active adhesion mechanism between rubbers and thermoplastics. Selecting the right curing system requires taking into account the vulcanisation/cycle time, adhesion strength and rubber properties.

For EPDM-PE, a cohesive failure can be reached with peroxide curing, but unfortunately curing the interface requires long processing times making it economically less interesting. For this combination, sulphur curing is recommended as this leads to a high adhesion strength with cohesive failure at lower cycle times. An optimisation of the sulphur curing system induced faster curing rates but this also reduced the adhesion strength. Thus, a significant reduction in processing time by increasing the sulphur cure rate is not possible. Fortunately, sulphur-based EPDM-PE 2K products do offer advantages like high adhesion strength, secured positioning and dimensions, and the possibility of material savings. For EPDM-PP, efficient co-vulcanisation requires a low peroxide curing agent concentration and the presence of co-agents to reduce the chain

scission probability during peroxide curing. These co-agents provide a higher radical yield and reactivity at the interface. Furthermore, EPDM-PP adhesion benefits from an EPDM structure with low ethylene content causing better interdiffusion. Subsequent co-vulcanisation improves with lower ENB content and lower EPDM molecular weight. Furthermore, the adhesion with PP can be improved when adding higher contents of paraffinic oil. The filler type severely influences rubber properties and therefore mainly product properties need to be considered when selecting the optimal type. An economic evaluation showed that peroxide cured EPDM with PP has the highest industrial relevance. For this material combination the 2K injection moulding process can compete with the traditional 1K process due to the low cycle time resulting in low product cost and accompanying high adhesion. If needed for a certain application PP can be combined with sulphur cured EPDM. Then, an average adhesion can be reached by combining low Mooney viscosity with a low ethylene content.

Furthermore, an interaction between EPDM and polar thermoplastics ABS and PC can be induced by peroxide curing. As for EPDM-PC, chemical bonding is unlikely and higher co-agent concentrations are important to improve compatibility. However, EPDM-ABS can exhibit co-vulcanisation and therefore higher DCP concentration is beneficial.

During 2K injection moulding, two materials are brought into contact and adhesion can be controlled by several mechanisms. Wetting, chemical bonding and interdiffusion were analysed. A closer-to-processing wetting methodology was developed by depositing a molten thermoplastic droplet on a rubber substrate, but no clear correlation was found between the adhesion percentage and work of adhesion. This leads to the conclusion that during injection moulding wetting does not dominate the adhesion. To characterise the occurrence of possible co-vulcanisation reactions, a novel contact angle methodology was developed that evidenced a clear reactive wetting process during peroxide curing, whereas only physical wetting was found to occur during sulphur curing. Unfortunately, this new methodology is restricted by the melt temperature of the thermoplastic and curing reaction of the rubber. For the interdiffusion process, the Flory-Huggins interaction parameter can help clarify the interdiffusion probability, and for thermoset rubber-thermoplastic, the interdiffusion width may range up to two micrometres. Even though this low interdiffusion width was found for EPDM with PE, the adhesion strength was very good. This is probably caused by the high entanglement possibility. Eventually, a combination of multiple adhesion theories is needed to define suitable material combinations and related adhesion strength.

In this thesis, the importance of the rubber formulation on the adhesion with thermoplastics has been demonstrated. For practical application of the acquired knowledge to industry, material selection guidelines in term of radar charts were established. Starting from the required product properties, these charts facilitate insights on the role of each rubber component. Furthermore, an economic evaluation has shown limited impact of material cost, facilitating a wide range of possible rubber formulations. The industrial relevance is strongly influenced by the required vulcanisation time and the adhesion quality, and these aspects are most promising for EPDM-PP. Therefore, a detailed material grade selection map was set-up for this combination and its applicability was validated in an industrial case study. Especially, 2K sealing applications can benefit from this methodology. Finally, it was demonstrated that despite their strong adhesion, these products can even be recycled at end-of-life by blending grinded granulates in thermoplastic vulcanisates before processing.

## 7.3 Outlook

The novel 2K injection moulding process facilitates adhesion between commodity plastics and special purpose rubbers. A further optimisation was carried out specifically for EPDM with PP, PE, ABS and PC. Results showed that optimising the adhesion mechanism is extremely dependent on the material combination. Thus, other material combinations, e.g. thermoplastics with NBR, require additional research as this rubber has a completely different molecular structure, e.g. acrylonitrile (ACN), which can influence the adhesion with thermoplastics. This entails analysing how possible chemical bonding will occur, or how the material composition influences interdiffusion. Additionally, a nanoscale analysis of the interdiffusion zone and molecular dynamics modelling of the subsequent diffusion and curing of the rubber could provide more insight.

Often in thermoplastic elastomers, compatibilisers are added to optimise the interaction between the thermoplastic and the rubber phase. During 2K injection moulding, compatibiliser could promote adhesion as well. However, the presence of these adhesion promoters at the interface are required to create an interaction with the other component. To successfully implement these compatibiliser, the interaction between the compatibiliser and polymer matrix, the migration towards the interface, and a correlation with the crosslink density needs to be studied. It is believed that further research on compatibilisers in 2K injection moulding can increase the number of possible material combinations.

In polymer blends the interface can be studied by relaxation time spectra from dynamic moduli. As discussed by Ginzburg et al. [162], these spectra describe the quantity of viscoelastic properties, enabling the detection of pure components together with the interphase relaxation peaks at longer relaxation times indicating the presence of an interphase. Blends of envisaged material combinations for 2K injection moulding could be studied in this manner, and the presence of this interphase relaxation might indicate an adhesion in 2K injection moulding as well.

In this thesis, the focus was on the material optimisation of rubber. However, as adhesion is created with a thermoplastic material, additional research is needed on the influence of the thermoplastic composition. In particular for PP, an optimisation of molecular chain configuration, molecular weight and chemical composition distribution could further optimise chemical bonding and interdiffusion. Additionally, knowledge on the influence of macromolecular structure of the thermoplastic can further clarify why PE interdiffusion proceeds more efficiently than PP. Modelling the interdiffusion of these thermoplastic chains with vulcanising rubber chains could also give better insight as a characterisation remains difficult.

Finally, a study concerning the durability of the novel 2K injection moulding process is required. Due to the rapid heat cycling process, i.e. switch between vulcanising at high temperature and cooling at low temperature of the rubber cavity, problems like leakages and clogging by calcification and corrosion in the cooling channels arise. Development of more durable couplings by mould component producers, a better selection of the type of mould steel (e.g. Stavax, to reduce corrosion), a better design and positioning of rubber seals within the mould, and preventing inserts in a mould would benefit the injection moulding process. Possibly, a case-study could be set-up in collaboration with the industry focussing on mould design optimisation which could result in design guidelines, for example expressed as radar charts as presented in Chapter 6.



---

# Appendix A

---

## A.1 Datasheets of polymers

### PP Ineos 400-GA05



#### Product Technical Information

Polypropylene – Impact Copolymer

400-GA05 is a general purpose high impact copolymer for injection moulding applications. It offers a superior balance of stiffness and impact strength as compared to competitive impact copolymers of similar melt flow rate.

#### Benefits & Features

- Ultra-high impact resistance
- Superior impact/stiffness balance

#### Applications

- Appliances
- Rigid packaging
- Rigid transport packaging
- Consumer products
- Luggage

Properties	Conditions	Test Methods	Values	Units
<b>Rheological</b>				
Melt Flow Rate	230°C/2.16kg	ISO 1133-1	5	g/10min
<b>Mechanical</b>				
Flexural Modulus	23°C	ISO 178	1200	MPa
Tensile Strength at Yield	23°C	ISO 527-1,-2	25	MPa
Izod Impact Strength, notched	23°C	ISO 180/A	14	kJ/m <sup>2</sup>
Izod Impact Strength, notched	-20°C	ISO 180/A	6.5	kJ/m <sup>2</sup>
Charpy Impact Strength, notched	23°C	ISO 179-1/1eA	15	kJ/m <sup>2</sup>
Charpy Impact Strength, notched	-20°C	ISO 179-1/1eA	4.5	kJ/m <sup>2</sup>
<b>Thermal</b>				
Peak DSC melting temperature	2nd heating	ASTM D 3418	164	°C
Heat Deflection Temperature	0.45 MPa	ISO 75-2	86	°C
Vicat Softening Temperature	10N	ISO306/A50	152	°C

Data should not be used for specification work

## HDPE Sabic M80064



## SABIC® HDPE M80064

### High density polyethylene for Injection moulding

#### Description.

SABIC® HDPE M80064 is a high density polyethylene injection moulding grade with a narrow molecular weight distribution. It is intended for use in injection moulding applications where rigidity, toughness and warp resistance are required. SABIC® HDPE M80064 is available with UV stabilizer as SABIC® HDPE M80064S.

#### Typical applications.

SABIC® HDPE M80064 is designed to suit the manufacture of injection moulded cases, crates, trays, industrial pails and other similar items requiring toughness and rigidity.

#### Processing conditions.

Typical moulding conditions for SABIC® HDPE M80064 are:

Melt temperature: 230 - 275 °C (450 - 525 °F)

Mould temperature: 32 - 38 °C (90 - 100 °F)

Injection pressure: 69 - 89 MPa (10000 - 13000)

#### Typical data.

Revision 20051216

Properties	Units SI	Values	Test methods
<b>Polymer properties</b>			
Melt flow rate (MFR) at 190 °C and 2.16 kg			ASTM D 1238
Density	g/10 min kg/m <sup>3</sup>	8.0 964	ASTM D 1505
<b>Mechanical properties</b>			
Tenille test			
stress at yield	MPa	33	ASTM D 638
stress at break	MPa	15	
strain at break	%	650	
secant modulus at 1% elongation	MPa	1240	
Izod Impact notched at 23 °C	J/m	48	ASTM D 256
Hardness Shore D	-	69	ASTM D 2240
ESCR (100% Igepal), F50	h	3	ASTM D 1693B
<b>Thermal properties</b>			
Vicat softening temperature at 10 N (VST/A)	°C	128	ASTM D 1525

1) Test specimens are prepared from compression moulded sheet made according to ASTM D 1920 Procedure C.

All information supplied by or on behalf of the SABIC Europe companies in relation to its products, whether in the nature of data, recommendations or otherwise, is supported by research and believed reliable, but the relevant SABIC Europe company assumes no liability whatsoever in respect of application, processing or use made of the above-mentioned information or products, or any consequence thereof. The user undertakes all liability in respect of the application, processing or use of the above-mentioned information or product, whose quality and other properties he shall verify, or any consequence thereof. No liability whatsoever shall attach to any of the SABIC Europe companies for any infringement of the rights owned or controlled by a third party in intellectual, industrial or other property by reason of the application, processing or use of the above-mentioned information or products by the user.

## ABS Ineos Styrolution Novodur P2H-AT

**INEOS**  
**STYROLUTION**
**Novodur P2H-AT**  
 Acrylonitrile Butadiene Styrene (ABS)

**TECHNICAL**  
**DATASHEET**

## DESCRIPTION

Novodur® P2H-AT is a general purpose injection molding grade providing high flowability and contains an antistatic additive.

## FEATURES

- High flowability
- Good stiffness
- High gloss

## APPLICATIONS

- Household appliances
- Sport articles
- Oven casings

Property, Test Condition	Standard	Unit	Values
<b>Rheological Properties</b>			
Melt Volume Rate 220 °C/10 kg	ISO 1133	cm <sup>3</sup> /10 min	37
<b>Mechanical Properties</b>			
Izod Notched Impact Strength, 23 °C	ISO 180/A	kJ/m <sup>2</sup>	18
Izod Notched Impact Strength, -30 °C	ISO 180/A	kJ/m <sup>2</sup>	9
Charpy Notched Impact Strength, 23 °C	ISO 178/1eA	kJ/m <sup>2</sup>	18
Charpy Notched Impact Strength, -30 °C	ISO 178/1eA	kJ/m <sup>2</sup>	8
Charpy Unnotched, 23 °C	ISO 178/1eU	kJ/m <sup>2</sup>	100
Charpy Unnotched, -30 °C	ISO 178/1eU	kJ/m <sup>2</sup>	80
Tensile Stress at Yield, 23 °C	ISO 527	MPa	44
Tensile Strain at Yield, 23 °C	ISO 527	%	2.1
Tensile Modulus	ISO 527	MPa	2500
Flexural Strength, 23 °C	ISO 178	MPa	70
Flexural Modulus, 23 °C	ISO 178	MPa	2400
Hardness, Ball Indentation	ISO 2039-1	MPa	110
<b>Thermal Properties</b>			
Vicat Softening Temperature, VST/B/120 (50N, 120 °C/h)	ISO 308	°C	100
Vicat Softening Temperature VST/B/50 (50N, 50 °C/h)	ISO 308	°C	98
Heat Deflection Temperature A; (annealed 4 h/80 °C; 1.8 MPa)	ISO 75	°C	93

Contact us:  
 Phone +49 (2133) 9309 – 168  
 INSTY.emea@ineos.com  
 www.ineos-styrolution.com

Page 1 of 3  
 Revision Date: 2017.04.24

**Novodur P2H-AT**  
 Acrylonitrile Butadiene Styrene (ABS)

**TECHNICAL**  
**DATASHEET**

Property, Test Condition	Standard	Unit	Values
Heat Deflection Temperature B; (annealed 4 h/80 °C; 0.45 MPa)	ISO 75	°C	97
Coefficient of Linear Thermal Expansion	ISO 11359	10 <sup>-5</sup> /°C	90
<b>Electrical Properties</b>			
Dissipation Factor (100 Hz)	IEC 60250	10 <sup>-4</sup>	55
Dissipation Factor (1 MHz)	IEC 60250	10 <sup>-4</sup>	60
Dielectric Strength, Short Time, 1.0 mm	IEC 60243-1	kV/mm	34
Relative Permittivity (100 Hz)	IEC 60250	-	3
Relative Permittivity (1 MHz)	IEC 60250	-	2.9
Comparative Tracking Index	IEC 60112	V	800
Volume Resistivity	IEC 60093	Ohm*m	>10 <sup>13</sup>
Surface Resistivity	IEC 60093	Ohm	>10 <sup>15</sup>
<b>Other Properties</b>			
Density	ISO 1183	kg/m <sup>3</sup>	1050
UL94 rating at 1.5 mm thickness	IEC 60695-11-10	-	HB
Burning rate (US-FMVSS), 2.0 mm	ISO 3795	mm/min	60
Glow wire test (GWFI), 2.0 mm	IEC 60695-2-12	°C	700
<b>Processing</b>			
Linear Mold Shrinkage	ISO 294-4	%	0.4 - 0.7
Melt Temperature Range	ISO 294	°C	230 - 260
Mold Temperature Range	ISO 294	°C	60 - 80
Injection Velocity	ISO 294	mm/s	240
Drying Temperature	-	°C	80
Drying Time	-	h	2 - 4

Typical values for uncolored products

## PC Trinseo Calibre 301-15



Friday, February 15, 2019

## General Information

## Product Description

CALIBRE™ 300-15 Polycarbonate resins offer exceptional impact resistance, heat distortion resistance, and optical clarity. The CALIBRE 300-15 series products are available in 4 additive packages: CALIBRE 300: No mold release or UV Stabilizer. CALIBRE 301: Mold release. CALIBRE 302: UV stabilizer. CALIBRE 303: Mold release and UV stabilizer.

## Govt. and Industry Standards:

- CSA (Canadian Standards Association)
- Underwriters Laboratory, Inc. (UL)

## Applications:

- Automotive interiors
- Automotive exteriors
- Sheet applications
- Electrical lighting/switches
- Small & large appliances
- Beverage containers/serviceware
- Power equipment

## General

Material Status	• Commercial: Active		
Availability	• Europe	• Latin America	• North America
Additive	• Mold Release		
Features	• High Clarity	• High Impact Resistance	
Uses	• Appliances	• Automotive Interior Parts	• Lighting Applications
	• Automotive Applications	• Containers	• Sheet
	• Automotive Exterior Parts	• Electrical/Electronic Applications	
Agency Ratings	• CSA Unspecified Rating		
Forms	• Pellets		
Processing Method	• Injection Molding		

ASTM & ISO Properties <sup>1</sup>

Physical	Nominal Value	Unit	Test Method
Density	1.20	g/cm <sup>3</sup>	ISO 1183/B
Melt Mass-Flow Rate (MFR) (300°C/1.2 kg)	15	g/10 min	ISO 1133
Melt volume-flow rate (300°C/1.2 kg)	14.0	cm <sup>3</sup> /10min	ISO 1133 <sup>2</sup>
Molding Shrinkage - Flow	0.50 to 0.70	%	ISO 294-4
Water Absorption (24 hr, 23°C)	0.15	%	ISO 62
Water Absorption (Equilibrium, 23°C, 50% RH)	0.32	%	ISO 62
Mechanical	Nominal Value	Unit	Test Method
Tensile Modulus	2300	MPa	ISO 527-2/50
Tensile Stress (Yield)	60.0	MPa	ISO 527-2/50
Tensile Stress (Break)	71.0	MPa	ISO 527-2/50
Tensile Strain (Yield)	6.0	%	ISO 527-2/50
Tensile Strain (Break)	150	%	ISO 527-2/50
Flexural Modulus <sup>3</sup>	2400	MPa	ISO 178

**CALIBRE™ 301-15**  
**Trinseo - Polycarbonate Resin**

<b>Mechanical</b>		<b>Nominal Value</b>	<b>Unit</b>	<b>Test Method</b>
Flexural Stress <sup>3</sup>		97.0	MPa	ISO 178
Taber Abrasion Resistance		45	%	ISO 9352
<b>Impact</b>		<b>Nominal Value</b>	<b>Unit</b>	<b>Test Method</b>
Charpy Notched Impact Strength				ISO 179/1eA
-30°C		12	kJ/m <sup>2</sup>	
23°C		25	kJ/m <sup>2</sup>	
Notched Izod Impact Strength (23°C)		83	kJ/m <sup>2</sup>	ISO 180/A
<b>Hardness</b>		<b>Nominal Value</b>	<b>Unit</b>	<b>Test Method</b>
Rockwell Hardness				ISO 2039-2
M-Scale		73		
R-Scale		118		
<b>Thermal</b>		<b>Nominal Value</b>	<b>Unit</b>	<b>Test Method</b>
Heat Deflection Temperature (0.45 MPa, Annealed)		143	°C	ISO 75-2/B
Heat Deflection Temperature (1.8 MPa, Unannealed)		124	°C	ISO 75-2/A
Heat Deflection Temperature (1.8 MPa, Annealed)		140	°C	ISO 75-2/A
Vicat Softening Temperature		148	°C	ISO 306/B50
Ball Indentation Temperature		> 125	°C	IEC 60335-1
CLTE - Flow		7.0E-5	cm/cm°C	ISO 11359-2
<b>Electrical</b>		<b>Nominal Value</b>	<b>Unit</b>	<b>Test Method</b>
Volume Resistivity		> 1.0E+15	ohms-cm	IEC 60093
Electric Strength		17	kV/mm	IEC 60243-1
Dielectric Constant				IEC 60250
60 Hz		3.00		
1 MHz		3.00		
Relative Permittivity				IEC 60250
100 Hz		3.00		
1 MHz		3.00		
Dissipation Factor				IEC 60250
50 Hz		1.0E-3		
1 MHz		2.0E-3		
Comparative Tracking Index (2.00 mm, Solution A)		250	V	IEC 60112
<b>Flammability</b>		<b>Nominal Value</b>	<b>Unit</b>	<b>Test Method</b>
Flame Rating <sup>4</sup>				UL 94
3.0 mm		HB		
0.75 mm		V-2		
1.5 mm		V-2		
Glow Wire Flammability Index <sup>4</sup>				IEC 60695-2-12
1.0 mm		900	°C	
2.0 mm		875	°C	
3.0 mm		875	°C	
Glow Wire Ignition Temperature <sup>4</sup>				IEC 60695-2-13
1.0 mm		800	°C	
2.0 mm		775	°C	
3.0 mm		775	°C	
Oxygen Index <sup>4</sup>		26	%	ISO 4589-2
<b>Optical</b>		<b>Nominal Value</b>	<b>Unit</b>	<b>Test Method</b>
Refractive Index		1.586		ISO 489
Transmittance		89.0	%	ASTM D1003

## EPDM NORDEL™ grades

**Table 2:** Comparison of NORDEL® EPDM Grades in Peroxide-cure Test Recipe<sup>1,2,3</sup>

Property	NORDEL® EPDM Grades						
	3640	3720P	3722P	3745P	4520	4570	4640
Mooney Viscosity, ML 1 + 4, 100°C	50	25	27	59	32	72	50
Mooney Scorch at 125°C, Minutes to 5 pt. rise	>30	>30	>30	>30	>30	13	20
MDR at 175°C, 0.5° Arc, 30 min cht ML, dN.m	1.4	0.8	0.8	1.5	1.0	1.9	1.3
MH, dN.m	8.5	7.5	8.1	11.3	10.4	17.9	15.4
ts1, min	0.6	0.6	0.58	0.51	0.82	0.38	0.41
tc90, min	6.0	7.0	7.5	5.8	7.6	6.8	7.2
<b>Vulcanizate Properties, Physical Properties at R.T. Press-cured: tc95+3 min at 175°C</b>							
Tensile Strength, MPa	8.1	8.0	8.1	12.2	8.5	12.5	11.1
Elongation, %	300	324	275	307	253	245	230
Modulus at 100% Elongation, MPa	1.9	3.0	3.3	3.4	2.7	3.0	3.4
Modulus at 200% Elongation, MPa	5.1	5.6	6.3	8.7	6.6	9.1	8.9
Hardness, Shore A	53	72	71	67	58	57	61
Compression Set, Method B Pellets Cured MDR tc95+15 min 22 hr at -10°C	66	91	93	98	40	28	42
22 hr at 70°C	17	30	29	21	9	8	8
22 hr at 100°C	12	20	20	19	9	7	8
70 hr at 150°C	21	30	29	27	18	16	17
Temperature Retraction, °C							
TR-10	-39	-14	-13	-18	-43	-45	-30
TR-20	-31	-1	1	-6	-36	-38	-20
TR-50	-17	14	15	9	-24	-29	23
<b>Change in Properties Aged in Air 70 Hours at 150°C</b>							
Tensile Strength, MPa	7.9	7.7	8.1	11.4	8.3	11.0	11.9
Elongation, %	292	314	301	341	250	237	244
Elongation Change, %	2.9	-2.9	9.3	11.3	-1.3	-3.2	6.3
Modulus at 100% Elongation, MPa	2.2	3.3	3.4	3.4	2.6	3.4	3.3
Modulus Change, %	16.1	10.1	4.9	1.5	-0.8	11.7	-1.5
Hardness, Shore A	59	75	75	70	60	64	64
Hardness Change, pts	6	3	4	3	2	7	3

<sup>1</sup>Data per tests conducted by Dow. Additional information available upon request. Properties shown are typical, not to be construed as specifications. Users should confirm results by their own tests.

<sup>2</sup>Test Recipe: Polymer – 100 phr, N-650 Black – 115 phr, Paraffinic Oil – 70 phr, DCP-40% – 8 phr, TMO – 1 phr, HA #2 – 1 phr.

<sup>3</sup>All components tested per standard ASTM Method.

(continued)

**Table 2:** Comparison of NORDEL™ EPDM Grades in Peroxide-cure Test Recipe (continued)<sup>1,2,3</sup>

Property	NORDEL™ EPDM Grades					
	4725P	4760P	4770P	4785HM	4820P	5565
Mooney Viscosity, ML 1 + 4, 100°C	31	65	72	84	22	67
Mooney Scorch at 125°C, Minutes to 5 pt. rise	26	14	11	12	29	10
MDR at 175°C, 0.5° Arc, 30 min cht ML, dN.m	0.9	1.6	2.2	2.0	0.3	2.0
MH, dN.m	12.8	18.2	19.6	16.0	18.9	16.4
ts1, min	0.48	0.38	0.36	0.4	0.39	0.4
tc90, min	8.2	6.7	6.6	2.6	9.0	7.1
<b>Vulcanizate Properties, Physical Properties at R.T. Press-cured: tc95+3 min at 175°C</b>						
Tensile Strength, MPa	12.7	15.0	16.6	13.8	17.1	13.3
Elongation, %	247	254	238	296	184	214
Modulus at 100% Elongation, MPa	4.1	4.2	5.2	4.4	9.3	4.2
Modulus at 200% Elongation, MPa	9.6	11.0	13.8	9.7	–	12.7
Hardness, Shore A	72	67	71	73	90	59
Compression Set, Method B Pellets Cured MDR tc95+15 min 22 hr at -10°C	99	80	83	–	99	21
22 hr at 70°C	15	9	8	9	77	6
22 hr at 100°C	11	8	6	9	8	5
70 hr at 150°C	21	16	15	21	16	15
Temperature Retraction, °C						
TR-10	-20	-12	-4	–	–	-42
TR-20	-7	2	9	–	–	-38
TR-50	10	23	23	–	–	-28
<b>Change in Properties Aged in Air 70 Hours at 150°C</b>						
Tensile Strength, MPa	12.3	15.5	16.6	12.7	16.5	12.9
Elongation, %	247	254	235	260	181	211
Elongation Change, %	0.0	-0.1	-1.3	-12.37	-1.4	-1.3
Modulus at 100% Elongation, MPa	4.5	4.3	5.2	4.6	10.2	4.0
Modulus Change, %	8.7	2.6	1.2	4.9	9.9	-4.5
Hardness, Shore A	74	69	72	77	93	62
Hardness Change, pts	2	2	1	3	3	3

<sup>1</sup>Data per tests conducted by Dow. Additional information available upon request. Properties shown are typical, not to be construed as specifications. Users should confirm results by their own tests.

<sup>2</sup>Test Recipe: Polymer – 100 phr, N-650 Black – 115 phr, Paraffinic Oil – 70 phr, DCP-40% – 8 phr, TMQ – 1 phr, HVA#2 – 1 phr.

<sup>3</sup>All components tested per standard ASTM Method.

™Trademark of The Dow Chemical Company (Dow) or an affiliated company of Dow

---

## Bibliography

---

- [1] G. J. Bex, F. Desplentere, J. De Keyzer, and A. Van Bael, “Two-component injection moulding of thermoset rubber in combination with thermoplastics by thermally separated mould cavities and rapid heat cycling,” *Int. J. Adv. Manuf. Technol.*, vol. 92, no. 5–8, pp. 2599–2607, 2017.
- [2] A. Islam, “Two Component Injection Moulding for Moulded Interconnect Devices,” PhD thesis at Technical University of Denmark, 2008.
- [3] G.-J. Bex, “Development of 2K Injection Moulding Products and Processes of Rubber with Thermoplastics,” PhD thesis at KU Leuven, 2019.
- [4] T. Thust, “Rezeptur- und Prozesseinflüsse auf das Haftverhalten beim Mehrkomponentenspritzgießen von Thermoplast-Elastomer-Verbundbauteilen am Beispiel PA6.6 - HNBR,” PhD thesis at Martin-Luther-Universität Halle-Wittenberg, 2014.
- [5] G. J. Bex, W. Six, B. Laing, J. De Keyzer, F. Desplentere, and A. Van Bael, “Effect of process parameters on the adhesion strength in two-component injection molding of thermoset rubbers and thermoplastics,” *J. Appl. Polym. Sci.*, vol. 135, no. 29, 2018.
- [6] G. J. Bex, D. Seveno, J. De Keyzer, F. Desplentere, and A. Van Bael, “Wetting measurements as a tool to predict the thermoplastic/thermoset rubber compatibility in two-component injection molding,” *J. Appl. Polym. Sci.*, vol. 135, no. 13, pp. 12–14, 2017.
- [7] K. Grundke, S. Michel, K. J. Eichhorn, D. Beyerlein, and T. Bayer, “Influence of chemical interactions on the macroscopic spreading of a maleic anhydride copolymer melt,” *Macromol. Chem. Phys.*, vol. 203, no. 7, pp. 937–946, 2002.
- [8] F. Awaja, M. Gilbert, G. Kelly, B. Fox, and P. J. Pigram, “Adhesion of polymers,” *Prog. Polym. Sci.*, vol. 34, no. 9, pp. 948–968, 2009.
- [9] H. R. Brown, “The adhesion between polymers,” *Annu. Rev. Mater. Sci.*, vol. 21, no. 1, pp. 463–489, 1991.
- [10] A. Pizzi, *Handbook of Adhesive Technology*. New York: Marcel Dekker, Inc, 2003.
- [11] S. Ebnesaajad, *Adhesives Technology Handbook*, 2nd ed. Norwich, NY: William Andrew Inc., 2008.
- [12] K. Kendall, *Molecular Adhesion and Its Applications*. New York (N.Y.): Kluwer Academic Publishers, 2001.
- [13] L. F. M. da Silva, A. Öchsner, and R. D. Adams, *Handbook of Adhesion Technology*. Berlin, Heidelberg: Springer, 2011.
- [14] I. Rezaeian, P. Zahedi, and A. Rezaeian, “Rubber Adhesion to Different Substrates and Its Importance in Industrial Applications: A Review,” *J. Adhes. Sci. Technol.*, vol. 26, no. 6, pp. 721–744, 2012.
- [15] A. V. Pocius, *Adhesion and Adhesives Technology*, 3rd ed. München: Hanser, 2012.
- [16] Y. Yuan and T. R. Lee, “Contact Angle and Wetting Properties,” in *Springer Series in Surface Sciences*, vol. 51, no. 1, 2013, pp. 3–34.
- [17] Y. Zhang, “Wetting dynamics of liquid polymers,” PhD thesis at KU Leuven, 2019.

- [18] C. A. Fuentes *et al.*, "Predicting the adhesion strength of thermoplastic/glass interfaces from wetting measurements," *Colloids Surfaces A Physicochem. Eng. Asp.*, vol. 558, pp. 280–290, 2018.
- [19] A. Marmur, "Solid-surface characterization by wetting," *Annu. Rev. Mater. Res.*, vol. 39, pp. 473–489, 2009.
- [20] G. Kumar and K. N. Prabhu, "Review of non-reactive and reactive wetting of liquids on surfaces," *Adv. Colloid Interface Sci.*, vol. 133, no. 2, pp. 61–89, 2007.
- [21] E. Jabbari and N. A. Peppas, "Polymer-polymer interdiffusion and adhesion," *J. Macromol. Sci. Part C*, vol. 34, no. 2, pp. 205–241, 1994.
- [22] G. Zitzenbacher, Z. Huang, M. Laengauer, C. Forsich, and C. Holzer, "Wetting behavior of polymer melts on coated and uncoated tool steel surfaces," *J. Appl. Polym. Sci.*, vol. 133, no. 21, pp. 1–10, 2016.
- [23] Y. Zhang *et al.*, "Spreading Dynamics of Molten Polymer Drops on Glass Substrates," *Langmuir*, vol. 33, no. 34, pp. 8447–8454, 2017.
- [24] X. Zhang, B. Sun, N. Zhao, Q. Li, J. Hou, and W. Feng, "Experimental study on the surface characteristics of Pd-based bulk metallic glass," *Appl. Surf. Sci.*, vol. 321, pp. 420–425, 2014.
- [25] C. M. Hansen, *Hansen solubility parameters*, 2nd ed. Taylor & Francis Group, 2007.
- [26] J. Brandrup, *Polymer handbook*, 4th ed. New York (N.Y.): Wiley, 1999.
- [27] R. P. Wool, "Polymer Entanglements," *Macromolecules*, vol. 26, no. 7, pp. 1564–1569, 1993.
- [28] A. Aradian, E. Raphaël, and P.-G. de Gennes, "Strengthening of a Polymer Interface: Interdiffusion and Cross-Linking," *Macromolecules*, vol. 33, no. 25, pp. 9444–9451, 2000.
- [29] F. Ruch, M. O. David, and M. F. Vallat, "Adhesion in EPDM joints: Role of the interdiffusion mechanism on interfacial co-crosslinking," *Journal of Polymer Science, Part B: Polymer Physics*, vol. 38, no. 23, pp. 3189–3199, 2000.
- [30] M. Mutsuda and H. Komada, "Direct bonding between poly(oxy-2,6-dimethyl-1,4-phenylene) and rubber with radicals," *J. Appl. Polym. Sci.*, vol. 95, no. 1, pp. 53–59, 2005.
- [31] L. Picard, P. Phalip, E. Fleury, and F. Ganachaud, "Chemical adhesion of silicone elastomers on primed metal surfaces: A comprehensive survey of open and patent literatures," *Prog. Org. Coatings*, vol. 80, pp. 120–141, 2015.
- [32] M. Chaudhury and A. V. Pocius, *Surfaces, chemistry & applications*. Amsterdam: Elsevier science B.V., 2002.
- [33] S. Swapp, "Scanning Electron Microscopy (SEM)," *serv.carleton.edu*. [Online]. Available: [https://serc.carleton.edu/research\\_education/geochemsheets/techniques/SEM.html](https://serc.carleton.edu/research_education/geochemsheets/techniques/SEM.html). [Accessed: 17-Nov-2020].
- [34] K. Grundke, "Characterization of Polymer Surfaces by Wetting and Electrokinetic Measurements – Contact Angle, Interfacial Tension, Zeta Potential," in *Polymer Surfaces and Interfaces*, M. Stamm, Ed. Berlin, Heidelberg: Springer, 2008, pp. 103–138.
- [35] D. Son, S. re kr Cho, J. Nam, H. Lee, and M. Kim, "X-ray-based spectroscopic techniques for characterization of polymer nanocomposite materials at a molecular level," *Polymers (Basel)*, vol. 12, no. 5, 2020.
- [36] H. Miyazaki *et al.*, "Application of low-vacuum scanning electron microscopy for renal biopsy specimens," *Pathol. Res. Pract.*, vol. 208, no. 9, pp. 503–509, 2012.
- [37] S. K. Enganati, G. Mertz, F. Addiego, D. Ruch, R. Mersch, and O. Kotecky,

- “Resolving interphase structure at nanoscale in polymeric cord - rubber composites,” in *Book of papers of International Rubber Conference 2019*, 2019, pp. 10–13.
- [38] “Raman Spectroscopy,” *Mettler Toledo*. [Online]. Available: [https://www.mt.com/be/en/home/applications/L1\\_AutoChem\\_Applications/Raman-Spectroscopy.html](https://www.mt.com/be/en/home/applications/L1_AutoChem_Applications/Raman-Spectroscopy.html). [Accessed: 18-Nov-2020].
- [39] K. Bruckmoser, K. Resch, T. Kisslinger, and T. Lucyshyn, “Measurement of interdiffusion in polymeric materials by applying Raman spectroscopy,” *Polym. Test.*, vol. 46, pp. 122–133, 2015.
- [40] C. Nah *et al.*, “Effects of curing systems on the mechanical and chemical ageing resistance properties of gasket compounds based on ethylene-propylene-diene-termonomer rubber in a simulated fuel cell environment,” *Int. J. Hydrogen Energy*, vol. 40, no. 33, pp. 10627–10635, 2015.
- [41] L. Barbes, C. Radulescu, and C. Stihl, “ATR-FTIR spectrometry characterisation of polymeric materials,” *Rom. Reports Phys.*, vol. 66, no. 3, pp. 765–777, 2014.
- [42] D. Bonn, J. Eggers, J. Indekeu, J. Meunier, and E. Rolley, “Wetting and spreading,” *Rev. Mod. Phys.*, vol. 81, no. 2, pp. 739–805, 2009.
- [43] M. Vuckovac, M. Latikka, K. Liu, T. Huhtamäki, and R. H. A. Ras, “Uncertainties in contact angle goniometry,” *Soft Matter*, vol. 15, no. 35, pp. 7089–7096, 2019.
- [44] C. W. Karl and M. Klüppel, “Characterization of elastomers by wetting: Roughness and chemical heterogeneity,” *Chem. List.*, vol. 105, pp. 7–9, 2011.
- [45] C. W. Karl, W. Rahimi, A. Lang, U. Giese, M. Klüppel, and H. Geisler, “Review - Characterization of modified elastomer surfaces by wetting,” *KGK Kautschuk Gummi Kunststoffe*, vol. 71, no. 8, pp. 19–31, 2018.
- [46] E. Kraus *et al.*, “Relevance of the acid-base approach in prediction of adhesion properties in two-component injection moulding,” *J. Appl. Polym. Sci.*, vol. 133, no. 8, 2016.
- [47] C. J. van Oss and I. H. J. Busscher, “Applied surface thermodynamics,” *Colloids Surfaces B Biointerfaces*, vol. 9, no. 1–2, p. 121, 1997.
- [48] E. Yakhshi-Tafti, R. Kumar, and H. J. Cho, “Measurement of Surface Interfacial Tension as a Function of Temperature Using Pendant Drop Images,” *Int. J. Optomechatronics*, vol. 5, no. 4, pp. 393–403, 2011.
- [49] J. D. Berry, M. J. Neeson, R. R. Dagastine, D. Y. C. Chan, and R. F. Tabor, “Measurement of surface and interfacial tension using pendant drop tensiometry,” *J. Colloid Interface Sci.*, vol. 454, pp. 226–237, 2015.
- [50] J. Vera, E. Contraires, A. C. Brulez, M. Larochette, S. Valette, and S. Benayoun, “Wetting of polymer melts on coated and uncoated steel surfaces,” *Appl. Surf. Sci.*, vol. 410, pp. 87–98, 2017.
- [51] P.-G. de Gennes, “The dynamics of reactive wetting on solid surfaces,” *Physica A*, vol. 249, pp. 196–205, 1998.
- [52] B. Komolafe and M. Medraj, “Progress in Wettability Study of Reactive Systems,” *J. Metall.*, pp. 1–14, 2014.
- [53] L. Yin *et al.*, “Reactive wetting in metal–metal systems,” *J. Phys. Condens. Matter*, vol. 21, no. 46, p. 464130, 2009.
- [54] N. Eustathopoulos and R. Voytovych, “The role of reactivity in wetting by liquid metals: a review,” *J. Mater. Sci.*, vol. 51, no. 1, pp. 425–437, 2016.
- [55] K. Grundke, P. Uhlmann, T. Gietzelt, and B. Redlich, “Studies on the wetting behaviour of polymer melts on solid surfaces using the Wilhelmy balance

- method,” *Colloids Surfaces A Physicochem. Eng. Asp.*, vol. 116, pp. 93–104, 1996.
- [56] T. Kisslinger, “Untersuchung der Haftfestigkeit von Kunststoffmaterialpaarungen im Mehrkomponentenspritzguss,” PhD thesis at Montanuniversitaet Leoben, 2013.
- [57] T. Kisslinger, K. Bruckmoser, T. Lucyshyn, G. R. Langecker, K. Resch, and C. Holzer, “Interface conditions of two-shot molded parts,” *AIP Conf. Proc.*, vol. 1593, pp. 170–174, 2014.
- [58] R. Chandran, C. J. G. Plummer, P. E. Bourban, and J. A. E. Manson, “Morphology and interfacial strength of nonisothermally fusion bonded hard and soft thermoplastics,” *Polym. Eng. Sci.*, vol. 58, pp. 82–92, 2018.
- [59] R. Orza, “Investigation of peroxide crosslinking of EPDM rubber by solid-state NMR,” PhD thesis at Eindhoven University of Technology, 2008.
- [60] R. R. Babu, N. K. Singha, and K. Naskar, “Dynamically vulcanized blends of polypropylene and ethylene octene copolymer: Influence of various coagents on thermal and rheological characteristics,” *J. Appl. Polym. Sci.*, vol. 117, pp. 1578–1590, 2010.
- [61] J. S. Dick, *Rubber Technology: Compounding and Testing for Performance*, 1st ed. Munich: Hanser, 2001.
- [62] J. White and K. Naskar, *Rubber Technologist’s Handbook Volume 2*. Shawbury, Shrewsbury, Shropshire, UK: Smithers Rapra Technology Limited, 2009.
- [63] J. W. M. Noordermeer, “Ethylene-Propylene Elastomers,” in *Encyclopedia of Polymer Science and Technology*, Hoboken, NJ, USA: John Wiley & Sons, Inc., 2002.
- [64] S. Samaržija-Jovanović, V. Jovanović, G. Marković, M. Marinović-Cincović, J. Budinski-Simendić, and B. Janković, “Ethylene–Propylene–Diene Rubber-Based Nanoblends: Preparation, Characterization and Applications,” in *Rubber Nano Blends*, Springer Series on Polymer and Composite Materials, 2017, pp. 281–349.
- [65] K. Naskar, U. Gohs, and G. Heinrich, “Influence of molecular structure of blend components on the performance of thermoplastic vulcanisates prepared by electron induced reactive processing,” *Polymer (Guildf.)*, vol. 91, pp. 203–210, 2016.
- [66] Avalos, P. Mendoza, C. Ortiz, and V. Ramos, “Effect of the Ethylene Content on the Properties m-Polypropylene/EPDM Blends,” *MOJ Polym. Sci.*, vol. 1, no. 1, pp. 5–9, 2017.
- [67] A. A. Al-Juhani and M. A. Suleiman, “Study of the Effect of EPDM Structure on the Compatibility of PP/LDPE Blends,” *Arab. J. Sci. Eng.*, vol. 37, no. 4, pp. 863–875, 2012.
- [68] H. W. Xiao, S. Q. Huang, T. Jiang, and S. Y. Cheng, “Miscibility of blends of ethylene-propylene-diene terpolymer and polypropylene,” *J. Appl. Polym. Sci.*, vol. 83, no. 2, pp. 315–322, 2002.
- [69] Y. Ma, Y. P. Wu, Y. Q. Wang, and L. Q. Zhang, “Structure and properties of organoclay/EPDM nanocomposites: Influence of ethylene contents,” *J. Appl. Polym. Sci.*, vol. 99, no. 3, pp. 914–919, 2006.
- [70] N. M. Livanova, “Formation of an interfacial layer in blends of elastomers with different polarities,” *Polym. Sci. - Ser. A*, vol. 48, no. 8, pp. 821–826, 2006.
- [71] M. Van Duin, R. Orza, R. Peters, and V. Chechik, “Mechanism of peroxide cross-linking of EPDM rubber,” *Macromol. Symp.*, vol. 291–292, no. 1, pp. 66–74, 2010.
- [72] J. Radosavljević and L. Nikolić, “The effect of organic peroxides on the curing

- behavior of EPDM isolation medium voltage cables,” *Adv. Technol.*, vol. 7, no. 1, pp. 56–63, 2018.
- [73] C. Gamlin, N. Dutta, N. Roy-Choudhury, D. Kehoe, and J. Matisons, “Influence of ethylene-propylene ratio on the thermal degradation behaviour of EPDM elastomers,” *Thermochim. Acta*, vol. 367–368, pp. 185–193, 2001.
- [74] B. Crowther, *Handbook Of Rubber Bonding*. Shawbury, Shrewsbury, Shropshire, UK: Rapra Technology Limited, 2001.
- [75] J. E. Mark, B. Erman, and M. Roland, *The science and technology of rubber*, 4th ed. Waltham, USA: Elsevier, 2013.
- [76] C. G. Robertson and N. J. Hardman, “Nature of Carbon Black Reinforcement of Rubber: Perspective on the Original Polymer Nanocomposite,” *Polymers (Basel)*, vol. 13, no. 4, p. 538, 2021.
- [77] Y. Fan, G. D. Fowler, and M. Zhao, “The past, present and future of carbon black as a rubber reinforcing filler – A review,” *J. Clean. Prod.*, vol. 247, p. 119115, 2020.
- [78] J. López-de-Uralde *et al.*, “Automatic Morphological Categorisation of Carbon Black Nano-aggregates,” in *Database and Expert Systems Applications*, vol. 6262, Springer, Berlin, Heidelberg, 2010, pp. 185–193.
- [79] Z. H. Li, J. Zhang, and S. J. Chen, “Effects of carbon blacks with various structures on vulcanization and reinforcement of filled ethylene-propylene-diene rubber,” *Express Polym. Lett.*, vol. 2, no. 10, pp. 695–704, 2008.
- [80] M. Kardan, “Carbon black reinforcement in natural rubber-based adhesives and sealants,” *Int. Polym. Sci. Technol.*, vol. 31, no. 1, pp. 520–523, 2004.
- [81] K. S. Katti and M. W. Urban, “Effect of carbon black on adhesion to plastics in solventborne 2K polyurethanes,” *J. Coatings Technol.*, vol. 72, no. 903, pp. 35–44, 2000.
- [82] W. Chookaew, J. Mingbunjurdsuk, P. Jittham, N. N. Ranong, and S. Patcharaphun, “An investigation of weldline strength in injection molded rubber parts,” *Energy Procedia*, vol. 34, pp. 767–774, 2013.
- [83] N. M. Ahmed and S. H. El-Sabbagh, “The influence of kaolin and calcined kaolin on SBR composite properties,” *Polym. Compos.*, vol. 35, no. 3, pp. 570–580, 2014.
- [84] S. H. Sheikh, X. Yin, A. Ansarifar, and K. Yendall, “The potential of kaolin as a reinforcing filler for rubber composites with new sulfur cure systems,” *J. Reinf. Plast. Compos.*, vol. 36, no. 16, pp. 1132–1145, 2017.
- [85] A. Ciesielski, *An Introduction to Rubber Technology*. Shawsbury, Shrewsbury, Shropshire, UK: Rapra Technology Limited, 1999.
- [86] V. M. Litvinov, “EPDM/PP thermoplastic vulcanizates as studied by proton NMR relaxation: Phase composition, molecular mobility, network structure in the rubbery phase, and network heterogeneity,” *Macromolecules*, vol. 39, no. 25, pp. 8727–8741, 2006.
- [87] N. Ning *et al.*, “Preparation, microstructure, and microstructure-properties relationship of thermoplastic vulcanizates (TPVs): A review,” *Prog. Polym. Sci.*, vol. 79, pp. 61–97, 2018.
- [88] J. Kruželák, R. Sýkora, and I. Hudec, “Vulcanization of Rubber Compounds With Peroxide Curing Systems,” *Rubber Chem. Technol.*, vol. 90, no. 1, pp. 60–88, 2017.
- [89] J. Kruželák, R. Sýkora, and I. Hudec, “Sulphur and peroxide vulcanisation of rubber compounds-overview,” *Chem. Pap.*, vol. 70, no. 12, pp. 1533–1555, 2016.
- [90] M. Alvarez Grima, “Novel co-agents for improved properties in peroxide cure

- of saturated elastomers,” PhD thesis at University of Twente, 2007.
- [91] P. R. Dlużneski, “Peroxide Vulcanization of Elastomers,” *Rubber Chem. Technol.*, vol. 74, no. 3, pp. 451–492, 2001.
- [92] R. R. Babu, N. K. Singha, and K. Naskar, “Studies on the influence of structurally different peroxides in polypropylene / ethylene alpha olefin thermoplastic vulcanizates (TPVs),” *Express Polym. Lett.*, vol. 2, no. 3, pp. 226–236, 2008.
- [93] T. Saleesung, D. Reichert, K. Saalwächter, and C. Sirisinha, “Correlation of crosslink densities using solid state NMR and conventional techniques in peroxide-crosslinked EPDM rubber,” *Polymer (Guildf.)*, vol. 56, pp. 309–317, 2015.
- [94] H. Wang, S. Zhao, and C. Wrana, “Investigation of Network Structure and Dynamic Mechanical Properties of Peroxide-Cured Ethylene Propylene Diene Rubber,” *J. Macromol. Sci. Part B*, vol. 56, no. 1, pp. 39–52, 2017.
- [95] R. I. N. Céspedes *et al.*, “Thermoplastic elastomers based on high-density polyethylene, ethylene-propylene-diene terpolymer, and ground tire rubber dynamically vulcanized with dicumyl peroxide,” *J. Appl. Polym. Sci.*, vol. 131, no. 4, 2014.
- [96] S. Q. Liu, W. G. Gong, and B. C. Zheng, “The effect of peroxide cross-linking on the properties of low-density polyethylene,” *J. Macromol. Sci. Part B Phys.*, vol. 53, no. 1, pp. 67–77, 2014.
- [97] R. Anbarasan, O. Babot, and B. Maillard, “Crosslinking of high-density polyethylene in the presence of organic peroxides,” *J. Appl. Polym. Sci.*, vol. 93, no. 1, pp. 75–81, 2004.
- [98] K. Naskar and J. W. M. Noordermeer, “Influence of various peroxides in PP/EPDM thermoplastic vulcanizates at varied blend ratios,” *J. Elastomers Plast.*, vol. 38, no. 2, pp. 163–180, 2006.
- [99] W. Brostow, T. Datashvili, and K. P. Hackenberg, “Effect of Different Types of Peroxides on Properties of Vulcanized EPDM + PP Blends,” *Polym. Compos.*, vol. 31, no. 10, pp. 1678–1691, 2010.
- [100] M. Ratzsch, M. Arnold, E. Borsig, H. Bucka, and N. Reichelt, “Radical reactions on polypropylene in the solid state,” *Prog. Polym. Sci.*, vol. 27, pp. 1195–1282, 2002.
- [101] M. Shi, D. Zhang, J. Zhu, Y. Shi, J. Sun, and Y. Ji, “Morphology, crystallization, and thermal and mechanical properties of dynamic vulcanization EPDM/PP thermoplastic elastomer,” *J. Thermoplast. Compos. Mater.*, vol. 32, no. 7, pp. 922–935, 2019.
- [102] K. Naskar, “Dynamically vulcanized PP/EPDM thermoplastic elastomers. Exploring novel routes for crosslinking with peroxides,” PhD thesis at University of Twente, 2004.
- [103] Ján Kruželák, Z. Dugasová, A. Kvasničáková, K. Tomanová, and I. Hudec, “Cross-Linking of Rubber Matrices with Dicumyl Peroxide and Zinc Dimethacrylate. Part I: Effect of Co-Agent Content,” *Polym. Sci. - Ser. B*, vol. 62, no. 6, pp. 706–716, 2020.
- [104] J. Kruželák, R. Sýkora, and I. Hudec, “Sulfur and peroxide curing of Rubber Compounds based on NR and NBR. Part II: Thermooxidative Ageing,” *KGK Kautschuk Gummi Kunststoffe*, vol. 70, no. 3, pp. 41–47, 2017.
- [105] S. K. Henning and R. Costin, “Fundamentals of curing elastomers with peroxides and coagents,” *Rubber World*, vol. 233, no. 5, pp. 28–35, 2006.
- [106] F. R. De Risi and J. W. M. Noordermeer, “Effect of methacrylate co-agents on

- peroxide cured PP/EPDM thermoplastic vulcanizates,” *Rubber Chem. Technol.*, vol. 80, no. 1, pp. 83–99, 2007.
- [107] Nocil, “Vulcanization & Accelerators,” 2014. [Online]. Available: <http://www.nocil.com/detail/technical/technical-notes/64>.
- [108] M. Van Duin, “Chemistry of EPDM cross-linking,” *KGK-Kautschuk und Gummi Kunststoffe*, vol. 55, no. 4, pp. 150–156, 2002.
- [109] Q. Voleppe, T. Pardoën, and C. Bailly, “Interdiffusion and phase separation upon curing in thermoset-thermoplastic interphases unravelled by the characterization of partially cured systems,” *Polymer (Guildf)*, vol. 106, pp. 120–127, 2016.
- [110] S. Schlögl, M. L. Trutschel, W. Chassé, G. Riess, and K. Saalwächter, “Entanglement effects in elastomers: Macroscopic vs microscopic properties,” *Macromolecules*, vol. 47, no. 9, pp. 2759–2773, 2014.
- [111] M. Ashby, “GRANTA EduPack 2020.” Granta Design Limited, Cambridge, 2020.
- [112] A. Islam, H. N. Hansen, and M. Bondo, “Experimental investigation of the factors influencing the polymer-polymer bond strength during two-component injection moulding,” *Int. J. Adv. Manuf. Technol.*, vol. 50, no. 1–4, pp. 101–111, 2010.
- [113] S. Nguyen, C. J. Perez, M. Desimone, J. M. Pastor, J. P. Tomba, and J. M. Carella, “Adhesion control for injection overmolding of elastomeric propylene copolymers on polypropylene. Effects of block and random microstructures,” *Int. J. Adhes. Adhes.*, vol. 46, pp. 44–55, 2013.
- [114] E. Haberstroh and C. Lettowsky, “Multi-component injection moulding of liquid silicone rubber/thermoplastic-combinations,” *J. Polym. Eng.*, vol. 24, no. 1–3, pp. 203–214, 2004.
- [115] D. Y. Huang and R. S. Chen, “Bonding strength at solid-melt interface for polystyrene in a sequential two-staged injection molding process,” *Polym. Eng. Sci.*, vol. 39, no. 11, pp. 2159–2171, 1999.
- [116] Degussa, “High performance polymers,” *High Performance Polymers in plastic-rubber composites*. Marl, Germany.
- [117] D. Schneegans, R. Gattringer, and R. Bauer, “Neue Kunststoff-Kautschuk-Verbunde mit großem Innovationspotenzial,” *GAK Gummi Fasern Kunststoffe*, vol. 8, no. 60, pp. 494–499, 2007.
- [118] R. Schneegans, D. Gattringer, “Mehrkomponenten-Spritzguss,” *KGK Kautschuk Gummi Kunststoffe*, vol. 58, no. 1, pp. 16–21, 2005.
- [119] G.-J. Bex, W. Six, B. Laing, J. De Keyzer, F. Desplentere, and A. Van Bael, “Effect of process parameters on the adhesion strength in two-component injection molding of thermoset rubbers and thermoplastics,” *J. Appl. Polym. Sci.*, vol. 135, no. 29, 2018.
- [120] W. Six, “Prediction of interface strength in 2K injection molding of thermoset rubbers and thermoplastics,” PhD thesis at KU Leuven, 2020.
- [121] W. Six, G. Bex, A. Van Bael, J. De Keyzer, and F. Desplentere, “Prediction of interfacial strength of HDPE overmolded with EPDM,” *Polym. Eng. Sci.*, vol. 59, no. 7, pp. 1489–1498, 2019.
- [122] E. Raphaël and P. G. De Gennes, “Rubber-rubber adhesion with connector molecules,” *J. Phys. Chem.*, vol. 96, no. 10, pp. 4002–4007, 1992.
- [123] B. Laing, J. De Keyzer, D. Seveno, and A. Van Bael, “Effect of co-agents on adhesion between peroxide cured ethylene-propylene–diene monomer and

- thermoplastics in two-component injection molding,” *J. Appl. Polym. Sci.*, vol. 137, no. 9, p. 48414, 2020.
- [124] B. Laing, J. De Keyzer, D. Seveno, and A. Van Bael, “Adhesion between ethylene-propylene-diene monomer and thermoplastics in two-component injection molding: Effect of dicumylperoxide as curing agent,” *J. Appl. Polym. Sci.*, vol. 137, no. 41, p. 49233, 2020.
- [125] B. Laing, G.-J. Bex, J. De Keyzer, D. Seveno, and A. Van Bael, “Influence of peroxide curing on adhesion between thermoplastics and thermoset rubbers in two-component injection moulding,” in *8th Bi-annual International Conference on Polymer and Mould Innovations*, 2018, p. 111.
- [126] B. Laing, J. De Keyzer, D. Seveno, and A. Van Bael, “Effect of co-agents on the adhesion between peroxide cured EPDM and thermoplastics in two-component injection moulding,” in *Book of papers of International Rubber Conference 2019*, 2019.
- [127] S. Kulkarni, “The 6-step study.” FimmTech, Carlsbad CA.
- [128] D. Zaimova, E. Bayraktar, and N. Dishovsky, “State of cure evaluation by different experimental methods in thick rubber parts,” *J. Achiev. Mater. Manuf. Eng.*, vol. 44, no. 2, pp. 161–167, 2011.
- [129] H. Wang, Y. Ding, and S. Zhao, “Effects of Co-Agents on the Properties of Peroxide-Cured Ethylene-Propylene Diene Rubber (EPDM),” *J. Macromol. Sci. Part B*, vol. 55, no. 5, pp. 433–444, 2016.
- [130] J. Kruželák *et al.*, “Peroxide vulcanization of natural rubber. Part I: Effect of temperature and peroxide concentration,” *J. Polym. Eng.*, vol. 34, no. 7, pp. 617–624, 2014.
- [131] K. Yokomizo, Y. Banno, T. Yoshikawa, and M. Kotaki, “Effect of molecular weight and molecular weight distribution on weld-line interface in injection-molded polypropylene,” *Polym. Eng. Sci.*, vol. 53, no. 11, pp. 2336–2344, 2013.
- [132] T. Gao, R. Xie, L. Zhang, H. Gui, and M. Huang, “Use of Rubber Process Analyzer for Characterizing the Molecular Weight Parameters of Natural Rubber,” *Int. J. Polym. Sci.*, pp. 1–6, 2015.
- [133] Dow, “NORDEL EPDM - Product Selection Guide,” 2014.
- [134] H. Wang, Y. Ding, S. Zhao, and C. Wrana, “Peroxide cross-linking of EPDM using moving die rheometer measurements. I: Effects of the third monomer concentration and peroxide content,” *Rubber Chem. Technol.*, vol. 88, pp. 40–52, 2015.
- [135] G. Bex, B. Laing, A. Van Bael, W. Six, and F. Desplentere, “Two-component injection moulding of thermoset rubber and thermoplastics : from concept to industrial products,” in *International Conference on Polymer and Moulds Innovations*, 2018.
- [136] H. Wang, T. Zhuang, S. H. I. Xinyan, M. V. A. N. Duin, and S. Zhao, “Peroxide cross-linking of EPDM using moving die rheometer measurements. II: Effects of the process oils,” *Rubber Chem. Technol.*, vol. 91, no. 3, pp. 561–576, 2018.
- [137] A. A. El-gamal, “Effect of reinforcement filler on vulcanization, diffusion, mechanical, and electrical properties of natural rubber,” *J. Elastomers Plast.*, vol. 51, no. 6, pp. 512–526, 2019.
- [138] Y. Ren, S. Zhao, Q. Yao, Q. Li, X. Zhang, and L. Zhang, “Effects of plasticizers on the strain-induced crystallization and mechanical properties of natural rubber and synthetic polyisoprene,” *RSC Adv.*, vol. 5, no. 15, pp. 11317–11324, 2015.
- [139] G. C. Basak, K. D. Kumar, A. Bandyopadhyay, and A. K. Bhowmick, “Elegant

- way of strengthening polymer-polymer interface using nanoclay,” *ACS Applied Materials and Interfaces*, vol. 2, no. 10. pp. 2933–2943, 2010.
- [140] B. Laing, D. Seveno, J. De Keyzer, and A. Van Bael, “Reactive wetting of polyethylene on ethylene-propylene-diene terpolymer,” *Colloid Interface Sci. Commun.*, vol. 40, p. 100343, 2021.
- [141] T. Osswald and N. Rudolph, “Rheometry,” in *Polymer Rheology*, München: Carl Hanser Verlag GmbH & Co. KG, 2014, pp. 187–220.
- [142] A. L. Biance, C. Clanet, and D. Quéré, “First steps in the spreading of a liquid droplet,” *Phys. Rev. E - Stat. Physics, Plasmas, Fluids, Relat. Interdiscip. Top.*, vol. 69, p. 016301, 2004.
- [143] R. A. Orza, P. C. M. M. Magusin, V. M. Litvinov, M. Van Duin, and M. A. J. Michel, “Mechanism for peroxide cross-linking of EPDM rubber from MAS13C NMR spectroscopy,” *Macromolecules*, vol. 42, no. 22, pp. 8914–8924, 2009.
- [144] L. Chen, E. Bonaccorso, T. Gambaryan-Roisman, V. Starov, N. Koursari, and Y. Zhao, “Static and dynamic wetting of soft substrates,” *Curr. Opin. Colloid Interface Sci.*, vol. 36, pp. 46–57, 2018.
- [145] P. P. Parlevliet, H. E. N. Bersee, and A. Beukers, “Residual stresses in thermoplastic composites-A study of the literature-Part II: Experimental techniques,” *Compos. Part A Appl. Sci. Manuf.*, vol. 38, no. 3, pp. 651–665, 2007.
- [146] M. Stenert, “Entwicklung binärer und ternärer Polymerblends auf der basis von Polymethylmethacrylat, Poly(n-butylacrylat), Polystyrol und deren Diblockcopolymeren,” PhD thesis at Universität GH Essen, 2000.
- [147] S. K. Enganati *et al.*, “Multiscale characterization of the interfacial region in flexible rubber composites: Initial structure and evolution upon thermal treatment,” *Polym. Test.*, vol. 98, p. 107203, 2021.
- [148] S. Abbott, “Dissipation,” 2021. [Online]. Available: <https://www.stevenabbott.co.uk/practical-adhesion/dissipation.php>. [Accessed: 22-May-2021].
- [149] S. Abbott, “Polymers across Boundaries,” 2021. [Online]. Available: <https://www.stevenabbott.co.uk/practical-solubility/polymers-across-boundaries.php>. [Accessed: 01-Jul-2021].
- [150] ResearchAndMarkets.com, “Plastics for the Electric Vehicle Market by Plastic Type, Application & Component, EV Type and Region,” 2020. [Online]. Available: <https://www.businesswire.com/news/home/20200810005599/en/Plastics-for-the-Electric-Vehicle-Market-by-Plastic-Type-Application-and-Region---Global-Forecast-to-2025---ResearchAndMarkets.com>. [Accessed: 20-Apr-2021].
- [151] ReportLinker, “Automotive Rubber-Molded Components Market - Growth, Trends, and Forecast (2020 - 2025),” 2020. [Online]. Available: <https://www.globenewswire.com/news-release/2020/08/27/2084976/0/en/Automotive-Rubber-Molded-Components-Market-Growth-Trends-and-Forecast-2020-2025.html>. [Accessed: 20-Apr-2021].
- [152] Freudenberg, “E-MOBILITY PLUG & SEAL CONNECTORS,” 2018. [Online]. Available: [https://www.fst.com/-/media/files/sales\\_sheets/fst\\_plug\\_and\\_seal\\_e-mobility\\_salessheet\\_en.pdf](https://www.fst.com/-/media/files/sales_sheets/fst_plug_and_seal_e-mobility_salessheet_en.pdf). [Accessed: 20-Apr-2021].
- [153] A. Chu, Y. Yuan, J. Zhu, X. Lu, and C. Zhou, “The design and investigation of

- a cooling system for a high power Ni-MH battery pack in hybrid electric vehicles,” *Appl. Sci.*, vol. 10, no. 5, 2020.
- [154] R. Korthauer, *Lithium-Ion Batteries: Basics and Applications*. Berlin, Heidelberg: Springer, 2018.
- [155] J. Wang, H. Xu, X. Xu, and C. Pan, “Design and simulation of liquid cooled system for power battery of PHEV,” *IOP Conf. Ser. Mater. Sci. Eng.*, vol. 231, no. 1, 2017.
- [156] M. Sienkiewicz, H. Janik, K. Borzędowska-Labuda, and J. Kucińska-Lipka, “Environmentally friendly polymer-rubber composites obtained from waste tyres: A review,” *J. Clean. Prod.*, vol. 147, pp. 560–571, 2017.
- [157] A. Vancleef, D. Maes, T. Van Gerven, L. C. J. Thomassen, and L. Braeken, “Flow-through microscopy and image analysis for crystallization processes,” *Chem. Eng. Sci.*, vol. 248, p. 117067, 2022.
- [158] T. Evens, G. J. Bex, M. Yigit, J. De Keyzer, F. Desplentere, and A. Van Bael, “The influence of mechanical recycling on properties in injection molding of fiber-reinforced polypropylene,” *Int. Polym. Process.*, vol. 34, no. 4, pp. 398–407, 2019.
- [159] L. Yang, J. L. Thomason, and W. Zhu, “The influence of thermo-oxidative degradation on the measured interface strength of glass fibre-polypropylene,” *Compos. Part A Appl. Sci. Manuf.*, vol. 42, no. 10, pp. 1293–1300, 2011.
- [160] P. S. Lima, J. M. Oliveira, and V. A. F. Costa, “Crystallization kinetics of thermoplastic elastomeric blends based on ground tyre rubber,” *J. Appl. Polym. Sci.*, vol. 132, no. 40, pp. 1–11, 2015.
- [161] I. Reinholds, V. Kalkis, J. Zicans, R. Merijs Meri, and A. Grigalovica, “Thermal and Mechanical Properties of Unvulcanized Polypropylene Blends with Different Elastomers: Ethylene-Propylene-Diene Terpolymer, Nitrile-Butadiene Copolymer and Chlorinated Polyethylene,” *Key Eng. Mater.*, vol. 559, pp. 93–98, 2013.
- [162] A. Ginzburg *et al.*, “The influence of polypropylene-block/graft-polycaprolactone copolymers on melt rheology, morphology, and dielectric properties of polypropylene/polycarbonate blends,” *Rheol. Acta*, vol. 59, no. 9, pp. 601–619, 2020.

---

# List of Publications

---

## Publications in international journals

- (1) Laing, B., Seveno, D., De Keyzer, J., Van Bael, A. (2020). Reactive wetting of polyethylene on ethylene-propylene-diene terpolymer. *Colloid And Interface Science Communications*, 40, Art.No. 100343. doi: 10.1016/j.colcom.2020.100343.
- (2) Laing, B., De Keyzer, J., Seveno, D., Van Bael, A. (2020). Adhesion between ethylene-propylene-diene monomer and thermoplastics in two-component injection molding: Effect of dicumylperoxide as curing agent. *Journal Of Applied Polymer Science*, Art.No. 49233. doi: 10.1002/app.49233.
- (3) Laing, B., De Keyzer, J., Seveno, D., Van Bael, A. (2019). Effect of co-agents on adhesion between peroxide cured ethylene–propylene–diene monomer and thermoplastics in two-component injection molding. *Journal Of Applied Polymer Science*, Art.No. 48414. doi: 10.1002/APP.48414.
- (4) Bex, G-J., Six, W., Laing, B., De Keyzer, J., Desplentere, F., Van Bael, A. (2018). Effect of process parameters on the adhesion strength in two-component injection molding of thermoset rubbers and thermoplastics. *Journal of Applied Polymer Science*, 135, Art.No. 46495, 1-8. doi: 10.1002/app.46495.

## Conference proceedings

- (1) Laing, B., De Keyzer, J., Seveno, D., Van Bael, A. (2019). Effect of co-agents on adhesion between peroxide cured EPDM and thermoplastics in two-component injection molding. *Book of papers, British Library, UK. International Rubber Conference 2019, Londen, UK, 3 Sep 2019- 5 Sep 2019. ISBN 1-86125-186-6.*
- (2) Laing, B., Bex, G-J., De Keyzer, J., Seveno, D., Van Bael, A. (2018). Influence of peroxide curing on adhesion between thermoplastics and thermoset rubbers in two-component injection moulding. *PMI 2018 Conference Proceedings, (Paper No. 111), (1-6). International Conference on Polymers and Mould Innovations, Guimarães, Portugal, 19 Sep 2018-21 Sep 2018. ISBN: 978-989-20-8809-9.*
- (3) Bex, G-J., Laing, B., Six, W., De Keyzer, J., Desplentere, F., Van Bael, A. (2018). Two-component injection moulding of thermoplastics with thermoset rubbers: from concept to industrial products. *PMI 2018 Conference Proceedings, (Paper No. 110), (1-5). Presented at the International Conference on Polymers and Moulds Innovations 2018, Guimarães, Portugal, 19 Sep 2018-21 Sep 2018. ISBN: 978-989-20-8809-9.*



---

# Curriculum Vitae

---

## Personal data

Brittany Laing  
° June 18, 1994 in Genk, Belgium

## Education

2017-2021

PhD student in Engineering Technology  
KU Leuven, Department of Materials Engineering, Diepenbeek Campus, Belgium  
Thesis: Development and optimisation of adhesion mechanisms between rubber and thermoplastic materials for 2K injection moulding

2016-2017

Master of Science in Chemical Engineering Technology  
KU Leuven, Diepenbeek Campus, Belgium  
UHasselt, Diepenbeek, Belgium  
Thesis: Metal mobility for the application of biochar amendments in acidic and neutral pH mine tailing soils under variable moisture conditions (Polytechnic University of Cartagena, Spain)  
Graduated Magna Cum Laude

2012-2016

Bachelor of Science in Chemical Engineering Technology  
KU Leuven, Diepenbeek campus, Belgium  
UHasselt, Diepenbeek, Belgium  
Graduated Cum Laude

2006-2012

Mathematics – Sciences  
O.L.V. Lyceum, Genk, Belgium  
Graduated Magna Cum Laude